
JSCSEN 79(10)1199–1335(2014)

ISSN 1820-7421(Online)

Journal of the Serbian Chemical Society

e
Version
electronic

VOLUME 79

No 10

BELGRADE 2014

Available on line at



www.shd.org.rs/JSCS/

The full search of JSCS

is available through

DOAJ DIRECTORY OF

OPEN ACCESS

JOURNALS

www.doaj.org



CONTENTS

Organic Chemistry

- Lj. E. Mihajlović-Lalić, A. Savić, G. Brađan, T. J. Sabo and S. Grgurić-Šipka: Novel methylene bridged ethylenediamine-type ligands: synthesis and spectral characterization 1199
Y.-W. Li and C.-L. Ma: Improved synthesis of gastrodin, a bioactive component of a traditional Chinese medicine 1205

Biochemistry and Biotechnology

- H. P. Chen, K. Yang, C. X. You, S. S. Du, Q. Cai, Q. He, Z. F. Geng and Z. W. Deng: Chemical constituents and biological activities against *Tribolium castaneum* (Herbst) of the essential oil from *Citrus wilsonii* leaves 1213
I. Urošević, N. Nikićević, Lj. Stanković, B. Andelković, T. Urošević, G. Krstić and V. Tešević: Influence of yeast and nutrients on the quality of apricot brandy 1223

Inorganic Chemistry

- S. B. Tanasković, M. Antonijević-Nikolić, B. Barta Holló, B. Dražić, T. Stanojković, K. Mészáros Szécsényi and G. Vučković: Correlations between the *in vitro* antiproliferative activity, structure and thermal stability of some macrocyclic dinuclear Cu(II) complexes 1235

Physical Chemistry

- S. R. Marinović, A. D. Milutinović-Nikolić, A. B. Nastasović, M. J. Žunić, Z. M. Vuković, D. G. Antonović and D. M. Jovanović: Sorption of different phenol derivatives on a functionalized macroporous nanocomposite of poly(glycidyl methacrylate-*co*-ethylene glycol dimethacrylate) and acid modified bentonite 1249
R. Biswas, D. Brahman and B. Sinha: Spectrophotometric and conductometric study of the complexation of *N*-salicylidene-2-aminophenol with Cu²⁺ in methanol + 1,4-dioxane binary solutions 1263

Analytical Chemistry

- A. D. Pavlović, Lj. M. Ignjatović, S. Z. Popov, A. R. Mladenović and I. N. Stanković: Application of gas chromatography analysis to quality control of residual organic solvents in clopidogrel bisulfate 1279

Polymers

- S. A. Ben Hasan, M. M. Dimitrijević, A. Kojović, D. B. Stojanović, K. Obradović-Durić, R. M. Jančić Heinemann and R. Aleksić: The effect of the size and shape of alumina nanofillers on the mechanical behavior of PMMA matrix composites 1295

Environmental

- J. B. Pavlović, J. K. Milenković and N. Z. Rajić: Modification of natural clinoptilolite for nitrate removal from aqueous media 1309
M. Savić, I. Mihajlović, M. Arsić and Ž. Živković: Adaptive-network-based fuzzy inference system (ANFIS) model-based prediction of the surface ozone concentration 1323
Erratum 1335

Published by the Serbian Chemical Society
Karnegijeva 4/III, P. O. Box 36, 11120 Belgrade 35, Serbia
Printed by the Faculty of Technology and Metallurgy
Karnegijeva 4, P. O. Box 35-03, 11120 Belgrade, Serbia



Novel methylene bridged ethylenediamine-type ligands: synthesis and spectral characterization

LJILJANA E. MIHAJLOVIĆ-LALIĆ, ALEKSANDAR SAVIĆ#, GABRIJELA BRAĐAN,
TIBOR J. SABO# and SANJA GRGURIĆ-ŠIPKA**

Faculty of Chemistry, University of Belgrade, Studentski trg 12–16, 11000 Belgrade, Serbia

(Received 12 February, revised 11 April, accepted 11 April 2014)

Abstract: The synthesis of two new organic compounds, diisobutyl- and diisopentyl (*S,S*)- α^1,α^3 -bis(cyclohexylmethyl-1,3-imidazolidinediacetate is reported herein. The one-pot procedure was realized by the addition of the reducing agent and carbonyl compound into a methanolic solution of the parent compounds (isobutyl and isopentyl esters of (*S,S*)- α,α' -(1,2-ethanediylidimino)bis[cyclohexanepropanoic acid] in appropriate stoichiometric ratios. The compounds were fully characterized by infrared, ESI-MS, 1D (^1H and ^{13}C) and 2D (COSY, HSQC and HMBC) NMR spectroscopy and elemental analysis. The spectral data confirmed the presence of the –CH₂– group introduced between the nitrogen atoms of the ethylenediamine moiety, revealing a neutral form of the potential bidentate ligand.

Keywords: cyclohexyl derivatives; ethylenediamine; amine ligands; potential drugs.

INTRODUCTION

The chemistry of anticancer agents generally refers to pure organic species¹ and metal containing compounds.² After the promising discovery of cisplatin by Rosenberg in 1965,³ the subsequent intensive research in the field of bioinorganic chemistry has resulted in the achievement of only slight progress.⁴ Nowadays, the use of metal-based drugs is limited to cisplatin and its analogs, carboplatin and oxaliplatin.⁵ It is also noteworthy to mention the Ru(III) complexes, NAMI-A (imidazolium *trans*-[tetrachloro(*S*-dimethyl sulfoxide)(1*H*-imidazole)ruthenate(III)]) and KP1019 (indazolium [*trans*-tetrachlorobis(1*H*-indazole)ruthenate(III)])⁶ that have both entered phase II of clinical trials. Therefore, an ideal drug in terms of being extremely toxic and simultaneously highly selective is yet to be developed.

* Corresponding author. E-mail: sanjag@chem.bg.ac.rs

Serbian Chemical Society member.

doi: 10.2298/JSC140212042M

Although a major part of pharmaceutical industry is based on organic and biologically derived species, the synthetic routes still precede over natural products.^{7,8} The main reason is found in the opportunity to create a potential drug with the desired profile of biologic activity. Moreover, it is also possible to functionalize parent compounds by various structural modifications in order to utilize or expand their primary use. The structures of recently synthesized compounds with confirmed antitumor activity are given in Fig. S-1 of the Supplementary material to this paper.

Based on the above-mentioned concept, the synthesis and cytotoxic studies of (*S,S*)- α,α' -(1,2-ethanediylidimino)bis[cyclohexanepropanoic acid] and (*S,S*)- α,α' -(1,3-propanediylidimino)bis[cyclohexanepropanoic acid] joined with their corresponding esters and Pt(IV) and Ru(II) complexes were previously reported.^{9–13} The obtained results demonstrated strong antitumor potential and, in some cases, even better activity compared to that of the conventional cisplatin. The mechanism of cytotoxic activity for (*S,S*)- α,α' -(1,2-ethanediylidimino)bis[cyclohexanepropanoate] was particularly investigated, revealing induced apoptosis associated with oxidative stress, mitochondrial depolarization and nuclear translocation of the apoptosis-inducing factor.¹⁴

Since each study confirmed the positive influence of the variable length of the alkyl side chain on biological features (the longer the alkyl chain, the more active the compound),¹¹ two derivatives with the bulky alkyl chain of (*S,S*)- α,α' -(1,2-ethanediylidimino)bis[cyclohexanepropanoic acid] were additionally synthesized and fully characterized. Hence, the synthesis and characterization of diisobutyl- and diisopentyl (*S,S*)- α^1,α^3 -bis(cyclohexylmethyl-1,3-imidazolidinediacetate are reported herein. The structures of these two compounds are given in Fig. 1.

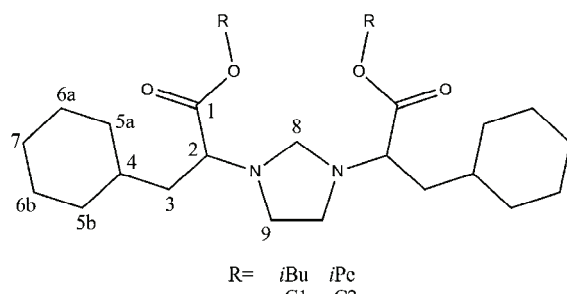


Fig. 1. The structure of the synthesized compounds, **C1** and **C2**.

EXPERIMENTAL

Reagents and instruments

The reagents and solvents were purchased from commercial suppliers and used without further purification. The precursor substances, isobutyl and isopentyl esters of (*S,S*)- α,α' -(1,2-ethanediylidimino)bis[cyclohexanepropanoate] were synthesized starting from (*S*)-2-amino-

-3-cyclohexylpropanoic acid hydrochloride purchased from Senn Chemicals (Dielsdorf, Switzerland). The preparation method was previously described and published.^{9,12}

Elemental analyses were performed on an Elemental Vario EL III microanalyzer. A Nicolet 6700 FT-IR spectrometer and the ATR technique were used for recording the infrared spectra. 1D (¹H and ¹³C), 2D COSY (correlation spectroscopy) and 2D ¹H-¹³C heteronuclear correlation spectra were recorded using a Bruker Avance III 500 spectrometer in CDCl₃ with TMS as the reference. The mass spectra were obtained with an Orbitrap LTQ XL instrument (Thermo Scientific, Bremen, Germany) in methanol.

Synthetic procedures

Synthesis of the diisobutyl (S,S)- α^l,α^d -bis(cyclohexylmethyl-1,3-imidazolidinediacetate, C1. A suspension of the precursor, diisobutyl (S,S)- α,α' -(1,2-ethanediylidiimino)bis[cyclohexanepropanoate] dihydrochloride (0.2 g, 0.36 mmol) in methanol (10 mL) was mixed and heated up to 40 °C for 20 min on a steam bath until the mixture was well homogenized. The methylation mixture was made by dissolving sodium triacetoxyborohydride (0.23 g, 1.08 mmol) in methanol (10 mL) followed by the addition of 36 % aqueous formaldehyde (0.10 mL, 3.61 mmol). The obtained methylation solution was poured dropwise into the previously made suspension. In order to adjust the pH value to 4–5, glacial acetic acid (0.25 mL) was slowly added to the reaction mixture. The next portion of the same volume was added after 2 h and stirring was continued for the following 30 min. The whole reaction solution was washed out with diethyl ether (40 mL) followed by rinsing the ether extract with three equal portions of KOH solution (10 mL, 1 M) and a portion of brine (10 mL). The combined ether solutions were dried overnight using anhydrous K₂CO₃ and evaporated *in vacuo* to obtain a colorless oil.

Synthesis of diisopentyl (S,S)- α^l,α^d -bis(cyclohexylmethyl-1,3-imidazolidinediacetate, C2. A suspension of the precursor, diisopentyl (S,S)- α,α' -(1,2-ethanediylidiimino)bis[cyclohexanepropanoate] dihydrochloride (0.2 g, 0.34 mmol) in methanol (10 mL) was mixed and heated at 40 °C for 20 min on a steam bath until the mixture was well homogenized. The methylation mixture was made by dissolving sodium triacetoxyborohydride (0.22 g, 1.03 mmol) in methanol (10 mL) followed by the addition of 36 % aqueous formaldehyde (0.09 mL, 3.44 mmol). The further procedure involved the same treatment as for C1.

The analytic and spectral data for C1 and C2 are given in the Supplementary material to this paper.

RESULTS AND DISCUSSION

Synthesis. The reductive methylation of diisobutyl- and diisopentyl esters of (S,S)- α,α' -(1,2-ethanediylidiimino)bis[cyclohexanepropanoic acid] was typical^{15,16} with slight modifications. The precursor ester was well homogenized in methanol. The mixture for methylation containing 36 % aqueous formaldehyde and sodium triacetoxyborohydride dissolved in methanol was slowly added to the ligand solution, which was then stirred for the following 2 h. The pH value was adjusted using glacial acetic acid. The obtained solution was treated with appropriate amounts of diethyl ether, 1 M KOH and brine. After drying the ether solutions overnight, the compounds were obtained by evaporation *in vacuo*. The synthesized compounds were soluble in common organic solvents (ethanol, dimethyl



sulfoxide, diethyl ether, acetone, dichloromethane and chloroform) but insoluble in water.

Spectroscopic studies. The new compounds, **C1** and **C2**, were characterized by mass spectrometry, infrared spectroscopy and one- (^1H and ^{13}C) and two-dimensional homo and heteronuclear ($^1\text{H}/^1\text{H}$ -COSY, HSQC and HMBC) NMR spectroscopy. Elemental analyses data were in a good agreement with the corresponding composition of the synthesized compounds.

The IR spectra of **C1** and **C2** showed strong bands at $\approx 1730 \text{ cm}^{-1}$ assigned to the vibrations of the carbonyl group.¹⁷ Two strong bands originating from asymmetric C–H stretching vibrations were found at ≈ 2930 and $\approx 2850 \text{ cm}^{-1}$. In addition, C–O stretching vibrations occurred around 1250 cm^{-1} , while the C–N group exhibited a weak absorption at around 1165 cm^{-1} .

The proposed structures of compounds **C1** and **C2** were also confirmed by their mass spectra, which indicated to a $[\text{M}+\text{H}]^+$ peak matched with the calculated molecular mass and proper isotope pattern. Furthermore, high intensities were also observed for peaks assigned to the $[\text{M}-\text{CH}_2+3\text{H}]^+$ fragment.

The ^1H -NMR spectrum of the products (given in the Supplementary material to this paper) indicated on the presence of cyclohexyl moiety arising in the area between 0.7–1.9 ppm with the exception of protons bonded to C5. Specifically, they appeared in a form of two separate sets of signals as their diastereotopic nature originates from the chiral C atom. Ethylenediamine protons were detected between 2.84 and 2.98 ppm in a form of two multiplets, as can be seen in Fig. 2,

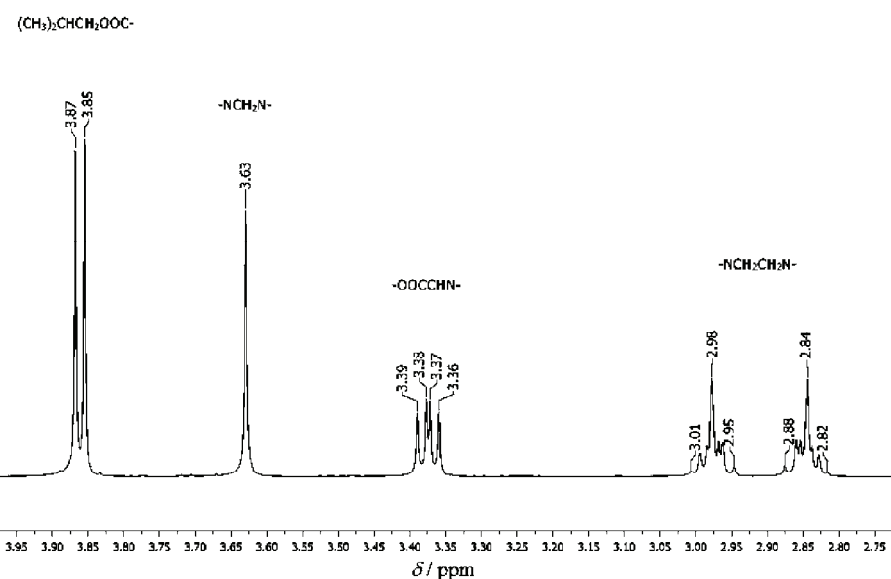


Fig. 2. ^1H -NMR spectrum of compound **C1** in the region 2.70–4.00 ppm recorded in CDCl_3 .

which shows the ^1H -NMR spectrum of compound **C1** in the region 2.70–4.00 ppm. The multiplet located at \approx 3.40 ppm was assigned to $(\text{ROOC})\text{CH}-$ protons. The presence of methylene bridged protons ($-\text{NCH}_2\text{N}-$) was confirmed in the form of a singlet (3.63 ppm) that showed negative correlation with the carbon resonance at 69.55 ppm in the edited HSQC spectrum. The same signal was correlated to carbons at 48.23 ($-\text{NCH}_2\text{CH}_2\text{N}-$) and 62.05 ppm ($-\text{OOCCHN}-$) in the HMBC spectrum, additionally confirming the newly formed imidazolidine ring. The ^{13}C -NMR spectra of **C1** and **C2**, the HSQC NMR spectrum of **C1** and the COSY spectrum of **C2** are given in the Supplementary material to this paper.

CONCLUSIONS

The primary structure of the compounds derived from cyclohexyl edda derivatives enables various structural modifications in ethylenediamine and alkyl chain moiety. In this sense, novel methylated forms of (S,S) - α,α' -(1,2-ethanediyldiimino)bis[cyclohexanepropanoic acid] which contained isobutyl and isopentyl groups were synthesized. The main reason for extending the alkyl side chain we found in the fact that more bulky molecules show significantly better antitumor activity which is planned to be investigated.

SUPPLEMENTARY MATERIAL

Analytic and spectral data for **C1** and **C2** and Figs. S-1–S-7 are available electronically from <http://www.shd.org.rs/JSCS/>, or from the corresponding author on request.

Acknowledgments. This research was supported by Ministry of Education, Science and Technological Development of the Republic of Serbia, Grant No. 172035. The authors also acknowledge the support of the FP7 RegPot project FCUB ERA GA No. 256716. The EC does not share responsibility for the content of this article.

ИЗВОД

НОВИ МЕТИЛОВАНИ ЛИГАНДИ ЕТИЛЕНДИАМИНСКОГ ТИПА: СИНТЕЗА И КАРАКТЕРИЗАЦИЈА

ЉИЉАНА Е. МИХАЈЛОВИЋ-ЛАЛИЋ, АЛЕКСАНДАР САВИЋ, ГАБРИЈЕЛА БРАЂАН, ТИВОР Ј. САБО и САЊА ГРГУРИЋ-ШИПКА

Хемијски факултет Универзитета у Београду, Студентски трг 12–16, 11000 Београд

Описана је синтеза два нова органска једињења, диизобутил- и диизопентил- (S,S) - α^1,α^3 -бис(циклохексилметил-1,3-имидазолидиндијацетат, која су добијена у реакцији изобутил и изопентил естара (S,S) - α,α' -(1,2-етандијилдиимино)бис[циклохексанпропанске киселине] са погодним метилујућим агенсом и формалдехидом у одговарајућем стехиометријском односу. Синтетисана једињења су потпуно окарактерисана инфрацрвеном, ESI-MS, 1D (^1H и ^{13}C) and 2D (COSY, HSQC и HMBC) NMR спектроскопијом и елементалном анализом. Спектрални подаци су потврдили присуство $-\text{CH}_2-$ групе уведене између два атома азота етилендиаминског дела, представљајући потенцијалне бидентатне лиганде.

(Примљено 12. фебруара, ревидирано 11. априла, прихваћено 11. априла 2014)



REFERENCES

1. W. B. Pratt, R. W. Ruddon, W. D. Ensminger, J. Maybaum, *The Anticancer Drugs*, Oxford University Press, New York, 1994, p. 69–182
2. H. M. Pinedo, J. H. Schornagel, *Platinum and Other Metal Coordination Compounds in Cancer Chemotherapy 2*, Plenum Press, New York, 1996, pp. 1–52, 253–268
3. B. Rosenberg, L. V. Camp, *Nature* **205** (1965) 698
4. G. Sava, A. Bergamo, P. J. Dyson, *Dalton Trans.* **40** (2011) 9069
5. F. Kratz, P. Senter, H. Steinhagen, *Drug Delivery in Oncology: From Basic Research to Cancer Therapy*, Wiley–VCH, Weinheim, 2012, pp. 1605–1630
6. A. Bergamo, C. Gaiddon, J. H. M. Schellens, J. H. Beijnen, G. Sava, *J. Inorg. Biochem.* **106** (2012) 90
7. B. C. Baguley, D. J. Kerr, *Anticancer Drug Development*, Academic Press, San Diego, CA, 2002, pp. 187–199
8. W. Kandioller, A. Kurzwernhart, M. Hanif, S. M. Meier, H. Henkea, B. K. Keppler, C. G. Hartinger, *J. Organomet. Chem.* **696** (2011) 999
9. J. M. Lazić, Lj. Vučićević, S. Grgurić-Šipka, K. Janjetović, G. N. Kaluđerović, M. Misirlić, M. Gruden-Pavlović, D. Popadić, R. Paschke, V. Trajković, T. Sabo, *ChemMedChem* **5** (2010) 881
10. A. Savić, M. Dulović, J. Poljarević, S. Misirlić-Denčić, M. Jovanović, A. Bogdanović, V. Trajković, T. J. Sabo, S. Grgurić-Šipka, I. Marković, *ChemMedChem* **6** (2011) 1884
11. Lj. E. Mihajlović, A. Savić, J. Poljarević, I. Vučković, M. Mojić, M. Bulatović, D. Maksimović-Ivanić, S. Mijatović, G. N. Kaluđerović, S. Stošić-Grujićić, Đ. Miljković, S. Grgurić-Šipka, T. J. Sabo, *J. Inorg. Biochem.* **109** (2012) 40
12. M. Mojić, A. Savić, V. B. Arion, M. Bulatović, J. M. Poljarević, Dj. Miljković, T. J. Sabo, S. Mijatović, D. Maksimović-Ivanić, S. Grgurić-Šipka, *J. Organomet. Chem.* **749** (2014) 142
13. A. Savić, S. Misirlić-Dencic, M. Dulovic, Lj. E. Mihajlović, M. Jovanovic, S. Grgurić-Šipka, I. Markovic, T. J. Sabo, *Bioorg. Chem.* **54** (2014) 73
14. S. Misirlić Dencic, J. Poljarevic, U. Vilimanovich, A. Bogdanovic, A. J. Isakovic, T. Kravic Stevovic, M. Dulovic, N. Zogovic, A. M. Isakovic, S. Grguric-Sipka, V. Bumbasirevic, T. Sabo, V. Trajkovic, I. Markovic, *Chem. Res. Toxicol.* **25** (2012) 931
15. R. F. Borch, A. I. Hassid, *J. Org. Chem.* **37** (1972) 1674
16. A. F. Abdel-Magid, K. G. Carson, B. D. Harris, C. A. Maryanoff, R. D. Shah, *J. Org. Chem.* **61** (1996) 3849
17. L. D. Field, S. Sternhell, J. R. Kalman, *Organic Structures from Spectra*, Wiley, Chichester, 2008, p. 15.

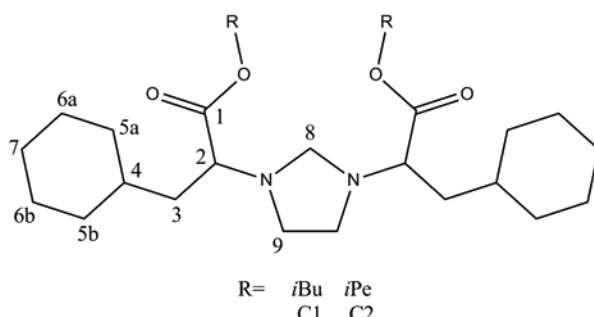


SUPPLEMENTARY MATERIAL TO
**Novel methylene bridged ethylenediamine-type ligands:
synthesis and spectral characterization**

LJILJANA E. MIHAJLOVIĆ-LALIĆ, ALEKSANDAR SAVIĆ, GABRIJELA BRAĐAN,
TIBOR J. SABO and SANJA GRGURIĆ-ŠIPKA*

Faculty of Chemistry, University of Belgrade, Studentski trg 12–16, 11000 Belgrade, Serbia

J. Serb. Chem. Soc. 79 (10) (2014) 1199–1204



Structures of **C1** and **C2** with atomic numbering.

ANALYTIC AND SPECTRAL DATA FOR **C1** AND **C2**

Compound C1. Yield: 83 %; Anal. Calcd. for $C_{29}H_{52}N_2O_4$: C, 70.69, H, 10.64, N, 5.69 %. Found: C, 70.38; H, 10.36; N, 5.76 %; IR (ATR, cm^{-1}): 2928, 2852, 1734, 1468, 1451, 1375, 1252, 1165, 994; $^1\text{H-NMR}$ (500 MHz, CDCl_3 , δ / ppm): 0.82–0.90 (4H, *m*, H_{5a'}, H_{5b'}), 0.92 (12H, *d*, *J* = 7.0 Hz, $(\text{CH}_3)_2\text{CH}$), 1.07–1.31 (8H, *m*, H₄, H_{7'}, H_{6b}), 1.47–1.52 (2H, *m*, $\text{CH}_2'\text{Cy}$), 1.60–1.66 (10H, *m*, H_{6a}, H_{5a}, H₇, CH_2Cy), 1.76 (2H, *d*, *J* = 12.5 Hz, H_{5b}), 1.92 (2H, *m*, $(\text{CH}_3)_2\text{CHCH}_2\text{O}$), 2.82–2.88 (2H, *m*, $\text{NCH}_2\text{CH}_2\text{N}$), 2.95–3.01 (2H, *m*, $\text{NCH}_2\text{CH}_2\text{N}$), 3.36–3.39 (2H, *m*, OCCHN), 3.63 (2H, *s*, NCH_2N), 3.86 (4H, *d*, *J* = 6.5 Hz, CH_2OOC); $^{13}\text{C-NMR}$ (125 MHz, CDCl_3 , δ / ppm): 19.29 ($(\text{CH}_3)_2\text{CH}$), 26.25 (C_{6a}), 26.28 (C_{6b}), 26.59 (C₇), 27.80 ($(\text{CH}_3)_2\text{CH}$), 33.20 (C_{5b}), 33.74 (C_{5a}), 34.50 (C₄), 38.89 (CH_2Cy), 48.23 ($\text{NCH}_2\text{CH}_2\text{N}$), 62.05 (OCCHN), 69.55 (NCH_2N), 70.59 (CH_2OOC), 173.31 (C1). ESI-MS (*m/z*, (relative abundance, %)): 481.58 ($\text{M}-\text{CH}_2+3\text{H}^+$, 100), 493.40 (M^+ , 37.16).

*Corresponding author. E-mail: sanjag@chem.bg.ac.rs

Compound C2. Yield: 71 %; Anal. Calcd. for $C_{31}H_{56}N_2O_4$: C, 71.49, H, 10.84, N, 5.38 %. Found: C, 71.10; H, 10.44; N, 5.49 %; IR (ATR, cm^{-1}): 2924, 2851, 1732, 1683, 1449, 1367, 1306, 1252, 1164, 971; $^1\text{H-NMR}$ (500 MHz, CDCl_3 , δ / ppm) 0.82–0.88 (4H, *m*, H_{5a'}, H_{5b'}), 0.90 (12H, *d*, *J* = 6.5 Hz, $(\text{CH}_3)_2\text{CH}$), 1.06–1.31 (8H, *m*, H₄, H_{7'}, H_{6b}), 1.46–1.53 (2H, *m*, $\text{CH}_2'\text{Cy}$), 1.59–1.70 (10H, *m*, H_{6a}, H_{5a}, H₇, CH_2Cy), 1.75 (2H, *d*, *J* = 13.0 Hz, H_{5b}), 2.80–2.86 (2H, *m*, $\text{NCH}_2\text{CH}_2\text{N}$), 2.94–3.00 (2H, *m*, $\text{NCH}_2\text{CH}_2\text{N}$), 3.33–3.35 (2H, *m*, OCCHN), 3.61 (2H, *s*, NCH_2N), 4.11 (4H, *m*, $\text{CH}_2\text{CH}_2\text{OOC}$); $^{13}\text{C-NMR}$ (50 MHz, CDCl_3 , δ / ppm): 11.32 and 16.61 ($(\text{CH}_3)_2\text{CH}$), 22.56 ($(\text{CH}_3)_2\text{CH}$), 25.16 (C_{6a}), 26.27 (C_{6b}), 26.60 (C₇), 33.19 (C_{5b}), 33.77 (C_{5a}), 34.52 (C₄), 37.50 ($(\text{CH}_3)_2\text{CHCH}_2$), 38.87 (CH_2Cy), 48.30 ($\text{NCH}_2\text{CH}_2\text{N}$), 62.16 (OCCHN), 63.04 (CH_2OOC), 69.60 (NCH_2N), 173.47 (C₁); ESI-MS (*m/z*, (relative abundance, %)): 509.43 ($\text{M}-\text{CH}_2+3\text{H}^+$, 49), 521.43 (M^+ , 100).

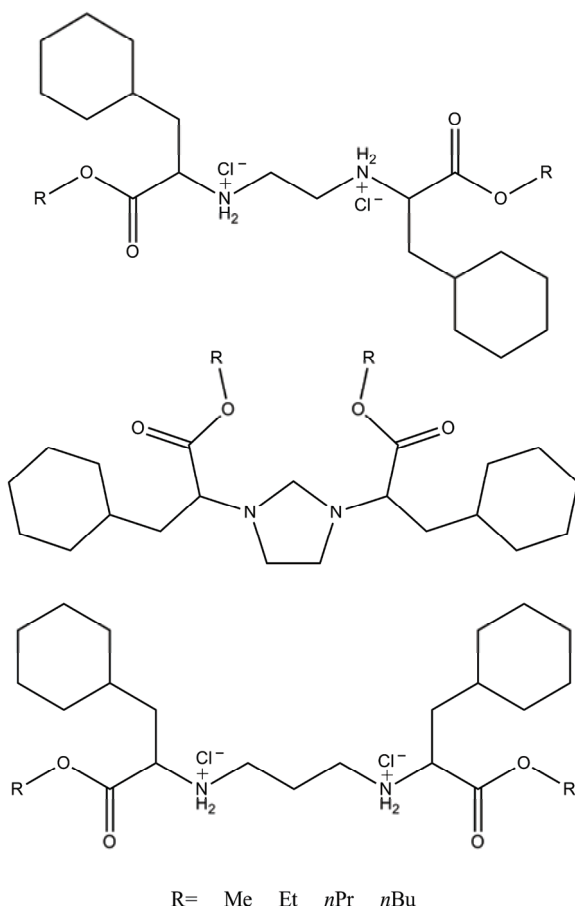
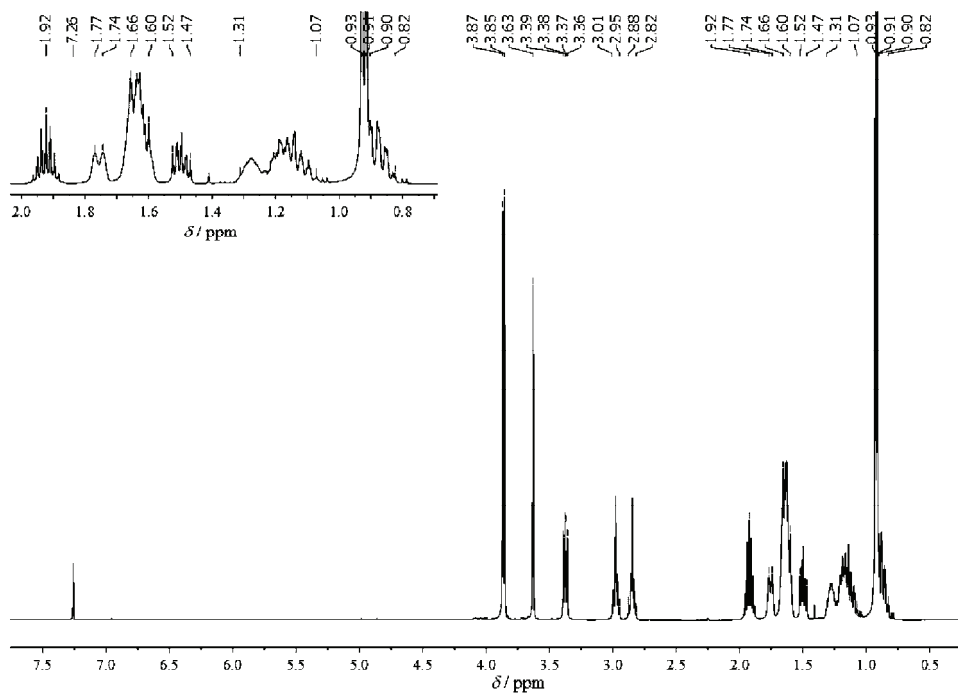
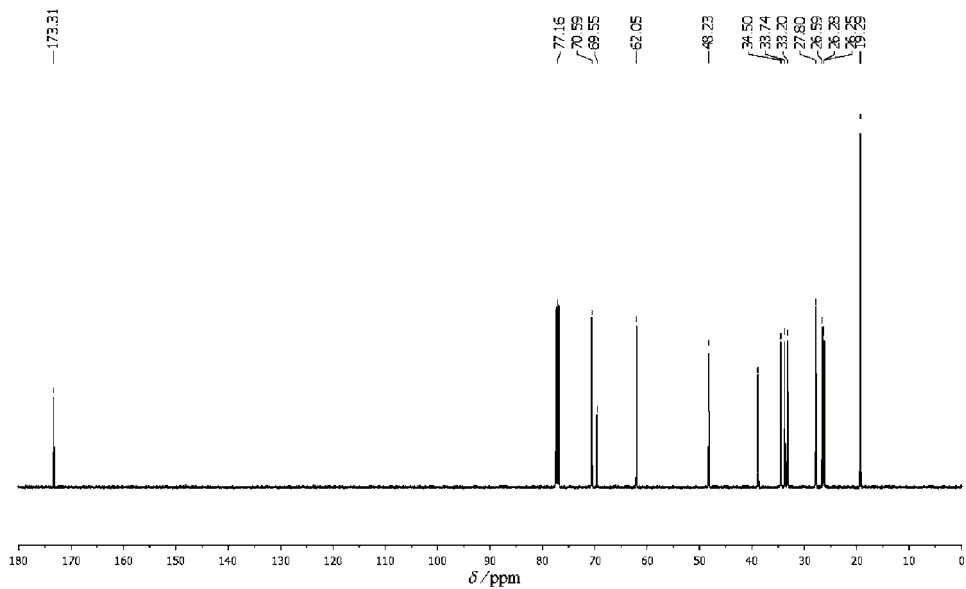
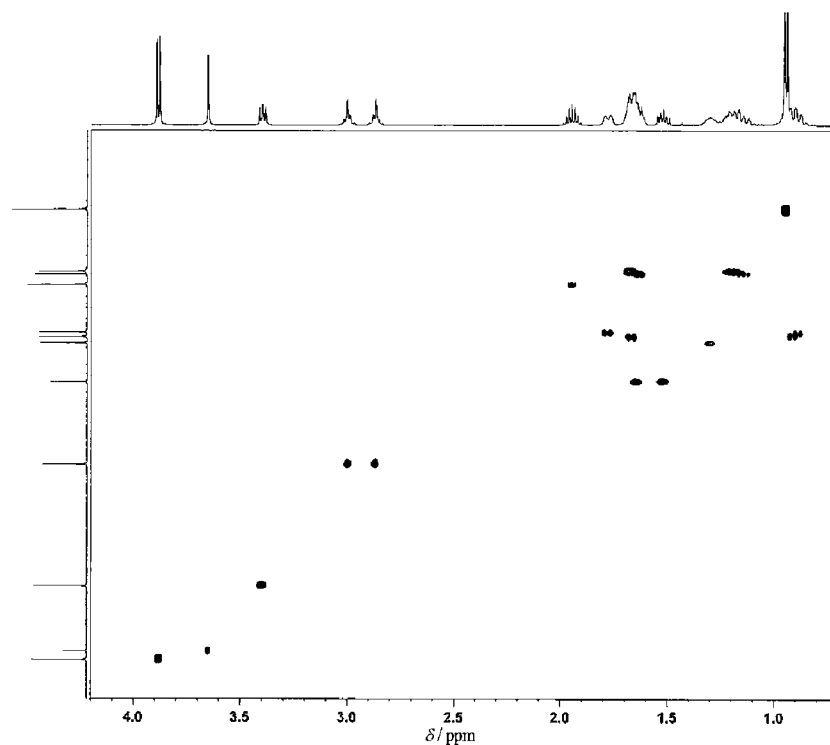
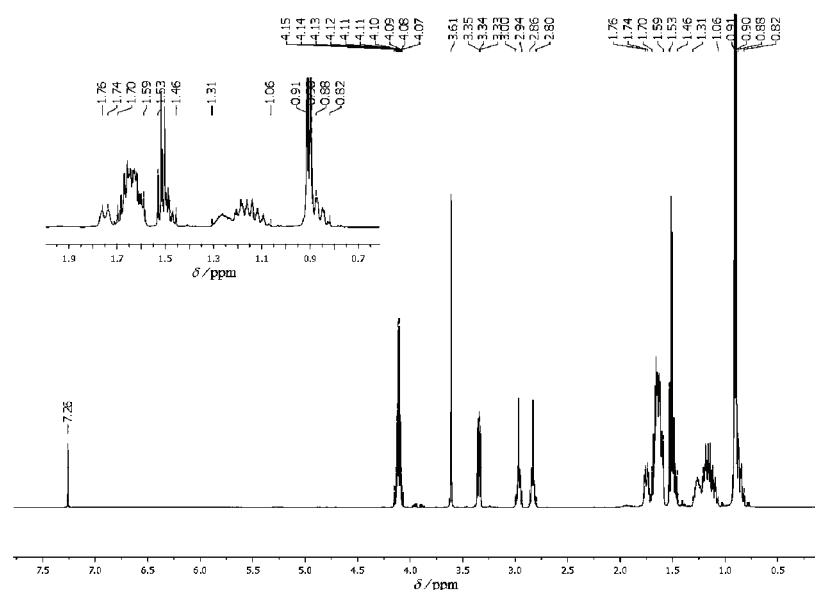


Fig. S-1. Recently synthesized compounds with confirmed antitumor activity.

Fig. S-2. ^1H -NMR spectrum of **C1** recorded in CDCl_3 Fig. S-3. ^{13}C -NMR spectrum of **C1** recorded in CDCl_3 .

Fig. S-4. HSQC NMR spectrum of **C1** recorded in CDCl_3 .Fig. S-5. ^1H -NMR spectrum of **C2** recorded in CDCl_3 .

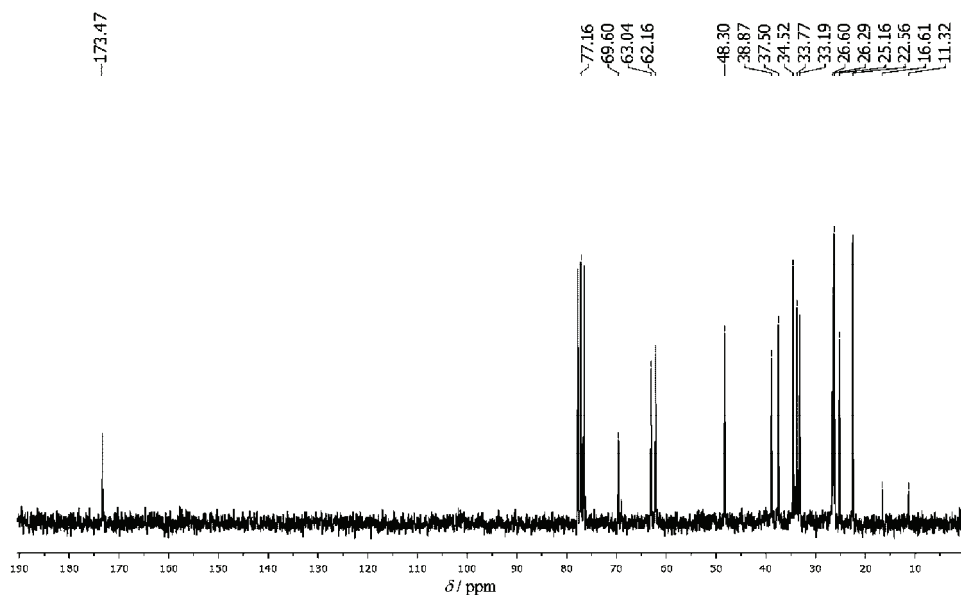


Fig. S-6. ¹³C-NMR spectrum of **C2** recorded in CDCl_3 .

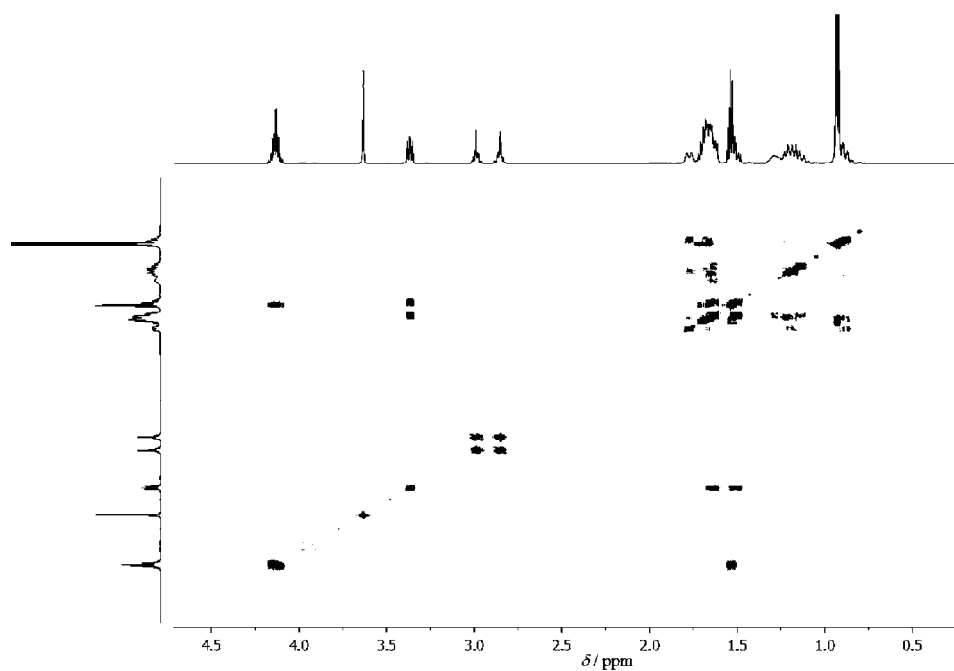


Fig. S-7. COSY NMR spectrum of **C2** recorded in CDCl_3 .



Improved synthesis of gastrodin, a bioactive component of a traditional Chinese medicine

YU-WEN LI^{1*} and CUI-LI MA²

¹School of Chemistry and Pharmacy, Qingdao Agricultural University, Qingdao 266109, China and ²Affiliated Hospital, Qingdao Agricultural University, Qingdao 266109, China

(Received 11 October 2013, revised 23 March, accepted 24 March 2014)

Abstract: Highly practical, four-step synthesis of gastrodin was developed using penta-*O*-acetyl- β -D-glucopyranose and *p*-cresol as glycosyl donor and glycosyl acceptor, respectively, in 58.1 % overall yield. As the initial step, the penta-*O*-acetyl- β -D-glucopyranose was treated with *p*-cresol in the presence of $\text{BF}_3 \cdot \text{Et}_2\text{O}$ as catalyst to generate 4-methylphenyl 2,3,4,6-tetra-*O*-acetyl- β -D-glucopyranoside in 76.3 % yield. Further, this product was subjected to radical bromination with *N*-bromosuccinimide (NBS) to provide 4-(bromomethyl)phenyl 2,3,4,6-tetra-*O*-acetyl- β -D-glucopyranoside in 91 % yield. Subsequently, reaction of 4-(bromomethyl)phenyl 2,3,4,6-tetra-*O*-acetyl- β -D-glucopyranoside with a solution of acetone and saturated aqueous sodium bicarbonate led to 4-(hydroxymethyl)phenyl 2,3,4,6-tetra-*O*-acetyl- β -D-glucopyranoside in 93 % yield. Finally, global deprotection of 4-(hydroxymethyl)phenyl 2,3,4,6-tetra-*O*-acetyl- β -D-glucopyranoside under Zemplen conditions furnished gastrodin in 90 % yield. Compared to the previously reported methods, this protocol has the advantages of operational simplicity, chromatography-free separation, high overall yield, inexpensive and common reagents as well as less waste pollutants, rendering it an alternative suitable for industrial production.

Keyword: gastrodin; glycosylation; penta-*O*-acetyl- β -D-glucopyranose; radical bromination.

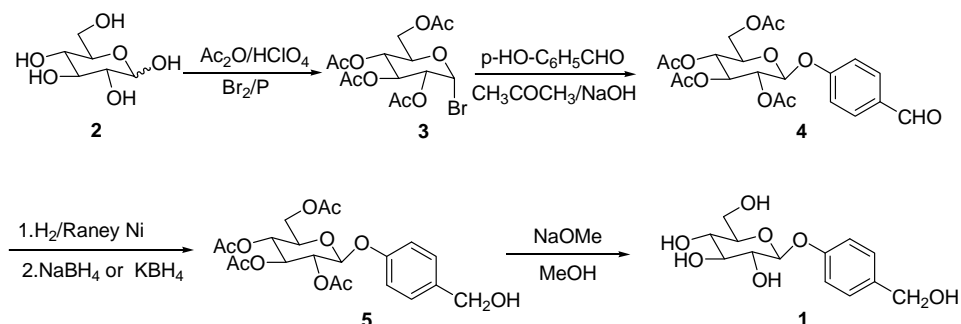
INTRODUCTION

Chemically known as 4-(hydroxymethyl)phenyl β -D-glucopyranoside, gastrodin is believed to be an important bioactive component of the famous Chinese herb *Gastrodia elata* B1, a well-known natural calcium channel blocker. Therapeutically, it has long been extensively used in China for the treatment of cardiovascular and cerebrovascular diseases, such as hypertension, stroke, migraine, dementia and hemiplegia.^{1,2} In addition to its therapeutic functions in cardiovascular and cerebrovascular diseases, gastrodin has comprehensive pharmacological effects.

* Corresponding author. E-mail: ywli@qau.edu.cn
doi: 10.2298/JSC131011026L

logical profiles, including hypoxia tolerance, neuroprotective and anticonvulsant effect,^{3–5} antioxidant and radical scavenger,⁶ protection against cardiac hypertrophy and fibrosis⁷ as well as an anti-myocardial ischemia effect in MI rabbits.⁸ Recent studies have linked gastrodin with suppressing the inflammatory response in septic cardiac dysfunction⁹ and stimulating anticancer immune response as well as repressing transplanted H22 hepatic ascetic tumour cell growth.¹⁰

Conventionally, gastrodin was extracted from *G. elata* flower,^{11–13} which is a time-consuming and expensive process. In addition, this preparation procedure was challenged by the extremely low content (0.025 %) in the rhizome as well as the ever-increasing shortage of *G. elata* flower due to over exploitation. To circumvent these problems associated with the extraction of gastrodin from *G. elata* flower, a chemical synthesis of gastrodin was developed (Scheme 1),¹⁴ in which 2,3,4,6-tetra-*O*-acetyl- α -D-glucopyranosyl bromide **3** was employed as a glycosyl donor. As shown in Scheme 1, this preparation of **3** involves the employment of bromine and red phosphorus in the presence of perchloric acid as catalyst, thereby generating a large volume of highly toxic and harmful bromine and phosphorus-containing waste pollutants that are detrimental to the environment and human health, and therefore raising additional safety concerns especially when handling on the industrial scale.



Scheme 1. Reported synthesis of gastrodin (**1**).

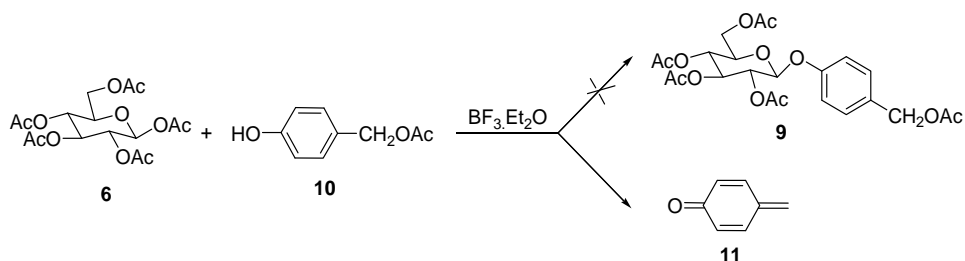
Although many new convenient and efficient alternatives for the synthesis of **3** in the absence of bromine and red phosphorus are available nowadays,¹⁵ the moisture and heat-labile **3** led to the subsequent glycosylation in poor yield under the aqueous conditions. Moreover, conversion of 4-formylphenyl 2,3,4,6-tetra-*O*-acetyl- β -D-glucopyranoside **4** to 4-hydroxyphenyl 2,3,4,6-tetra-*O*-acetyl- β -D-glucopyranoside **5** by either catalytic hydrogenation over Raney Ni at high pressure or chemical reduction with potassium (sodium) borohydride in methanol confers limited value for the large scale production of gastoind due to the use of relatively expensive catalysts and reagents.

Recently, a laboratory-scale preparation of gastrodin was realized *via* biotransformation.^{16–18} Unfortunately, preparation was seriously impaired by several drawbacks such as difficult strain development and cultivation, frequent strain variation, *i.e.*, large volumes of fermentation broth, a longer reaction time and extremely low yield, suggesting that it is still far removed from its commercial production *via* the biotransformation strategy.

In this context, the development of a chemical synthesis of gastrodin superior to the existing procedures is highly desired. Herein, a novel and efficient strategy for the chemical synthesis of gastrodin **1** using penta-*O*-acetyl- β -D-glucopyranose **6** and *p*-cresol **12** as a glycosyl donor and glycosyl acceptor, respectively, thereby avoiding many disadvantages inevitable in the previously reported procedures, is presented. The operational simplicity, cost-effectiveness and high overall yield of the procedure would make this new strategy suitable for the industrial production of gastrodin.

RESULTS AND DISCUSSION

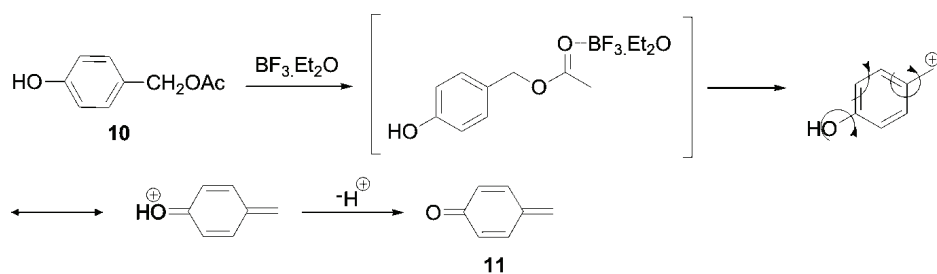
Initially, the synthesis of **1** according to Scheme 2 was attempted. Disappointedly, treatment of **6** with 4-hydroxybenzyl acetate **10**¹⁹ in the presence of $\text{BF}_3\cdot\text{Et}_2\text{O}$ as catalyst led to the undesired compound **11** as a pink precipitate instead of the desired compound **9**. The suggested mechanism underlying the formation of compound **11** is depicted in Scheme 3.



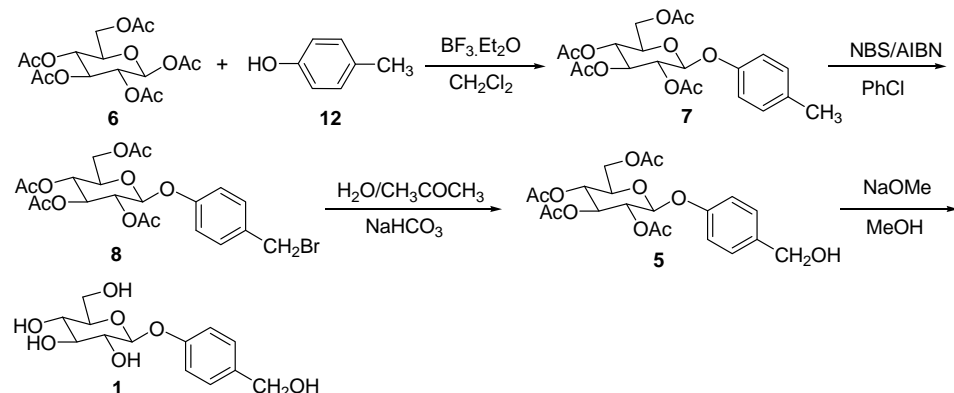
Scheme 2. Unsuccessful synthesis of gastrodin (**1**).

Frustrated with chemical synthesis of gastrodin **1** according to Scheme 2, another synthetic route was attempted, as shown in Scheme 4. As the first step, **6** was treated with **12** in the presence of $\text{BF}_3\cdot\text{Et}_2\text{O}$ as catalyst to generate 4-methylphenyl 2,3,4,6-tetra-*O*-acetyl- β -D-glucopyranoside **7** using a similar method as that described in the literature,²⁰ with some modifications, *i.e.*, the glycosylation was performed using $\text{BF}_3\cdot\text{Et}_2\text{O}$ alone as catalyst instead of the $\text{BF}_3\cdot\text{Et}_2\text{O}-\text{Et}_3\text{N}$ combination and the time for the glycosylation was much shorter than in the reference. Additionally, product **7** was purified by crystallization from ethanol in 76.3 % yield and confirmed to be the β anomer by the coupling constant ($J_{1,2} = 7.2$ Hz) calculated from the $^1\text{H-NMR}$ spectrum of **7** (Supplementary material to

this paper). Subsequently, radical bromination of **7** was accomplished through reaction with *N*-bromosuccinimide (NBS) at 67 °C in the presence of azodiisobutyronitrile (AIBN) or benzoyl peroxide (BPO, dibenzoyl peroxide) as initiator. At first, CCl_4 was selected as the reaction solvent for the radical bromination of **7**, but the reaction did not proceed at all irrespective of whether AIBN or BPO was used as the initiator. This indicates that the choice of the reaction solvent is of crucial importance for the successful synthesis of 4-(bromomethyl)phenyl 2,3,4,6-tetra-*O*-acetyl- β -D-glucopyranoside **8**.



Scheme 3. Plausible mechanism for the formation of **11**.



Scheme 4. Practical synthesis of gastrodin (**1**).

To this end, a solvent screening was conducted among solvents commonly used in the radical bromination reaction, including CCl_4 , *n*-hexane, cyclohexane, benzene, CHCl_3 and chlorobenzene, to determine the best solvent with respect to reaction yield. As a result, chlorobenzene was found to be the optimal one. Additionally, to test if the mole ratio of NBS to **7** and manner of NBS addition could affect the yield of **8**, a mole ratio titration was conducted and it was found that a molar ratio of NBS to **7** of 1.2:1 and the portion-wise addition of NBS gave the highest yield, presumably because it could significantly prevent the formation of the dibrominated side-product. Under these circumstances, **8** was obtained by reaction of **7** with NBS in 91% yield (the highest). Theoretically, the formation

of gastrodin **1** is achievable *via* direct hydrolysis of **8** under strong basic conditions, but separation of gastrodin **1** by extraction from aqueous mixture is difficult practice due to its strong hydrophilicity and insolubility in water-immiscible organic solvents. Consequently, a selective hydrolysis of **8** into **5** is advisable. Therefore, interaction of **8** with a mixture of acetone and saturated aqueous sodium bicarbonate solution at 50 °C gave rise to product **5**. Of special note is that the volume ratio of acetone to saturated aqueous sodium bicarbonate affects the reaction rate and yield. To determine the optimal ratio, a titration was performed and the results showed that a volume ratio of 4:1 of acetone to saturated aqueous sodium bicarbonate solution gave the best yield (93 %) after the usual aqueous work-up. Finally, global deprotection of **5** under Zemplen conditions (NaOMe/MeOH system) followed by recrystallization from methanol–chloroform (1:8, V/V) furnished gastrodin (**1**) as white crystals in 90 % yield.

EXPERIMENTAL

Materials and methods

Penta-*O*-acetyl- β -D-glucopyranose, *p*-cresol, $\text{BF}_3\text{-Et}_2\text{O}$, NBS and AIBN were obtained from Sigma–Aldrich. Sodium methoxide was obtained from the Qingdao Justness Reagent Co. (China). All solvents were of reagent grade and used without further purification unless otherwise stated and deionised water was used. CH_2Cl_2 was dried with CaH_2 under reflux and freshly distilled prior to use.

Instrumentation

All the synthesized compounds were confirmed by spectral methods, $^1\text{H-NMR}$ and $^{13}\text{C-NMR}$ spectroscopy and HRMS (ESI). The $^1\text{H-NMR}$ and $^{13}\text{C-NMR}$ spectra were acquired on a Bruker Avance III400 spectrometer, operating at 400 MHz for protons and 100 MHz for carbons. 2D NMR techniques (^1H – ^1H COSY, ^1H – ^{13}C HSQC) were used for full assignment of the spectra. Thin layer chromatography was performed on silica gel plates (GF254, Qingdao Haiyang Chemical Plant, China), and detection was effected by UV irradiation and subsequent charring with 10 % sulphuric acid in ethanol followed by heating. The melting points were determined with a digital melting point apparatus (WRS-1B) without correction. The optical rotations were measured with JASCO P1030 polarimeter.

Physical, analytic and spectral data are given in the Supplementary material to this paper.

Synthesis of 4-methylphenyl 2,3,4,6-tetra-O-acetyl- β -D-glucopyranoside (7). To a stirred solution of *p*-cresol (**12**, 27.0 g, 0.25 mol) and penta-*O*-acetyl- β -D-glucopyranose (**6**, 65.0 g, 0.16 mol) in 200 mL dry CH_2Cl_2 was added dropwise a solution of $\text{BF}_3\text{-Et}_2\text{O}$ (0.25 mol, 29.8 mL) in 30 mL dry CH_2Cl_2 at 0 °C within 1 h. The reaction mixture was then stirred for 2 h at room temperature, neutralized with saturated aqueous sodium bicarbonate (200 mL) and extracted with CH_2Cl_2 (2×100 mL). The combined organic layer was washed with saturated aqueous NaCl and dried over anhydrous sodium sulphate. Then, the filtrate was concentrated under reduced pressure to give yellowish solid crude product that was recrystallized from 95 % ethanol to afford the desired compound **7** as white crystals. Yield: 76.3 %.

Synthesis of 4-(bromomethyl)phenyl 2,3,4,6-tetra-O-acetyl- β -D-glucopyranoside (8). A suspension of 4-methylphenyl-2,3,4,6-tetra-*O*-acetyl- β -D-glucopyranoside (**7**) (43.8 g, 0.1 mol) in 300 mL chlorobenzene was heated to 67 °C to obtain a clear solution followed by the addition of AIBN (0.42 g, 0.0024 mol). To the obtained clear solution, a small portion of a

suspension containing NBS (21.4 g, 0.12 mol) in 100 mL of chlorobenzene was added. The initiation of the reaction was easily indicated by orange colour and a 2 °C temperature increase in the reaction mixture. Subsequently, the remaining NBS suspension in chlorobenzene was added portionwise within 1 h while maintaining the temperature at 64–69 °C. The reaction mixture was stirred for another 1 h at 67 °C before cooling to 40 °C. The succinimide formed in the reaction was removed by filtration and washed twice with chlorobenzene and the chlorobenzene washings were combined with the filtrate. The combined filtrate was evaporated to dryness under vacuum to give the crude glucopyranoside (**8**), which was recrystallised from absolute ethanol to furnish 52.5 g of compound **8** as white needle-like crystals. Yield: 91 %.

*Synthesis of 4-(hydroxymethyl)phenyl 2,3,4,6-tetra-O-acetyl- β -D-glucopyranoside (**5**).* To a stirred solution of 4-(bromomethyl)phenyl 2,3,4,6-tetra-O-acetyl- β -D-glucopyranoside (**8**) (22.70 g, 0.05 mol) in 200 mL acetone was added 50 mL of a saturated aqueous sodium bicarbonate solution, and then heated to 50 °C for 10 h. The reaction mixture was evaporated under vacuum to recover the acetone solvent and the remaining aqueous solution was extracted with CH₂Cl₂ (2×120 mL). The combined CH₂Cl₂ layers were washed with saturated aqueous NaCl (100 mL) and dried over anhydrous sodium sulphate and filtered. The filtrate was concentrated under reduced pressure to give a white solid crude product that on recrystallization from absolute ethanol afforded 21.12 g of the desired compound **5** as white crystals. Yield: 93 %.

*Synthesis of 4-(hydroxymethyl)phenyl β -D-glucopyranoside (**1**).* Sodium methoxide (200 μL, 1 M in MeOH) was added to a solution of **5** (9.92 g, 0.020 mol) in 100 mL dry methanol under a nitrogen atmosphere. The reaction mixture was stirred at room temperature for 5 h followed by neutralization with Amberlite IR 120(H⁺). Then the reaction mixture was filtered, and the resulting filtrate was evaporated to dryness under vacuum. Finally, recrystallization of the crude product from methanol–chloroform (1:8, V/V) yielded 5.21 g of the desired compound **1** as white crystals. Yield: 90 %

CONCLUSIONS

In summary, a novel efficient, and practical protocol for gastrodin synthesis in four sequential chemical steps was developed, in which penta-O-acetyl- β -D-glucopyranose was used as the glycosyl donor instead of 2,3,4,6-tetra-O-acetyl- α -D-glucopyranosyl bromide, in an overall yield of 58.1 %. Moreover, the presented protocol has the advantages over previous ones in terms of operational simplicity, commercially available and inexpensive reagents, easy separation and purification procedure dispensing with tedious and laborious chromatography, which render this protocol possibly suitable for the commercial production of gastrodin.

SUPPLEMENTARY MATERIAL

Physical, analytic and spectral data are available electronically from <http://www.shd.org.rs/JSCS/>, or from the corresponding author on request.

Acknowledgments. This work was supported by a grant from the Natural Science Foundation of Shandong Province (No. ZR2011BL003) and a grant from the Start-up Foundation of high talents in Qingdao Agricultural University, Qingdao, P. R. China (No. 630708).

ИЗВОД
УНАПРЕЂЕНА СИНТЕЗА ГАСТРОДИНА, БИОЛОШКИ АКТИВНЕ СУПСТАНЦЕ ИЗ
ТРАДИЦИОНАЛНЕ КИНЕСКЕ МЕДИЦИНЕ

YU-WEN LI¹ и CU-LI MA²

¹School of Chemistry and Pharmacy, Qingdao Agricultural University, Qingdao 266109, China и ²Affiliated Hospital, Qingdao Agricultural University, Qingdao 266109, China

Развијен је практичан поступак синтезе гастродина, употребом пента-*O*-ацетил- β -D-глукопиранозе и *p*-крезола као гликозил донора и акцептора, редом, у четири реакциона корака у укупном приносу од 58 %. Реакцијом између пента-*O*-ацетил- β -D-глукопиранозе и *p*-крезола у присуству $\text{BF}_3\text{-Et}_2\text{O}$ као катализатора добијен је (4-метилфенил)-2,3,4,6-тетра-*O*-ацетил- β -D-глукопиранозид у приносу од 76,3 %. Производ је бромован помоћу NBS и добијен је [4-(бромутил)фенил]-2,3,4,6-тетра-*O*-ацетил- β -D-глукопиранозид (принос 91 %) који је помоћу засићеног воденог раствора натријум-бикарбоната, реакцијом у ацетону, преведен у [4-(хидроксиметил)фенил]-2,3,4,6-тетра-*O*-ацетил- β -D-глукопиранозид (принос 93 %). Даљом реакцијом под Земпленовим условима добијен је гастродин (принос 90 %). У поређењу са раније описаним поступцима, нов протокол је једноставнији, омогућава лакше пречишћавање компоненти хроматографијом, висок укупан принос, употребу приступачних реагенаса, даје мање опасних отпадних компоненти и погодан је за индустријску производњу.

(Примљено 11. октобра 2013, ревидирано 23. марта, прихваћено 24. марта 2014)

REFERENCES

1. Q. Wang, G. Chen, S. Zeng, *Int. J. Pharm.* **341** (2007) 20
2. Q. Zhang, M. Yang, G. Y. Yu, *J. Chin. Integr. Med.* **6** (2008) 695 (in Chinese)
3. X. Xu, Y. Lu, X. Bie, *Planta Med.* **73** (2007) 650
4. X. H. Zeng, Y. Zhang, S. M. Zhang, X. X. Zheng, *Biol. Pharm. Bull.* **30** (2007) 80
5. C. L. Hsieh, S. Y. Chiang, K. S. Cheng, Y. H. Lin, N. Y. Tang, C. J. Lee, C. Z. Pon, C. T. Hsieh, *Am. J. Chin. Med.* **29** (2001) 331
6. W. Yong, T. R. Xing, S. Wang, L. Cheng, P. Hu, C. C. Li, H. L. Wang, M. Wang, J. T. Chen, D. Y. Ruan, *Planta Med.* **75** (2009) 1112
7. C. M. Shu, C. G. Chen, D. P. Zhang, H. P. Guo, H. Zou, J. Zong, Z. Y. Bian, X. Dong, J. Dai, Y. Zhang, Q. Z. Tang, *Mol. Cell. Biochem.* **359** (2012) 9
8. E. K. Ahn, H. J. Jeon, E. J. Lim, H. J. Jung, E. H. Park, *J. Ethnopharmacol.* **110** (2007) 476
9. P. Yang, Y. Han, L. Gui, J. Sun, Y. L. Chen, R. Song, J. Z. Guo, Y. N. Xie, D. Lu, L. Sun, *Biochem. Pharmacol.* **85** (2013) 1124
10. G. W. Shu, T. M. Yang, C. Y. Wang, H. W. Su, M. X. Xiang, *Toxicol. Appl. Pharmacol.* **269** (2013) 270
11. a) X. Wang, M. M. Zhou, *West China J. Pharm. Sci.* **18** (2003) 269 (in Chinese); b) X. C. Dai, X. Peng, S. F. Wu, W. S. Yang, Y. Miao, *J. Yunnan Nat. Univ. (Nat. Sci. Ed.)* **13** (2004) 83 (in Chinese)
12. Y. Yang, R. Tang, M. Y. Ding, *Chin. J. Anal. Lab.* **23** (2004) 1 (in Chinese)
13. Z. J. Guo, J. L. Su, K. Wang, X. J. You, *J. Chin. Med. Mater.* **25** (2002) 348 (in Chinese)
14. J. Zhou, Y. B. Yang, C. R. Yang, *Acta Chim. Sinica* **38** (1980) 162 (in Chinese)
15. Y. W. Li, Y. X. Li, W. Zhang, H. S. Guan, *Chin. J. Org. Chem.* **24** (2004) 438 (in Chinese)
16. H. L. Zhu, P. G. Dai, W. Zhang, E. F. Chen, W. X. Han, C. Chen, Y. L. Cui, *Biol. Pharm. Bull.* **33** (2010) 1680

17. L. L. Fan, Y. C. Dong, T. Y. Xu, H. F. Zhang, Q. H. Chen, *Appl. Biochem. Biotechnol.* **170** (2013) 138
18. H. L. Zhu, J. R. Song, J. X. Huang, J. Zhang, Z. Y. Ma, M. Y. Yang, *Acta Pharmacol. Sin.* **41** (2006) 1074 (in Chinese)
19. J. W. J. Bosco, B. R. Raju, K. Saika, *Synth. Commun.* **34** (2004) 2849
20. Y. S. Lee, E. S. Rho, Y. K. Min, B. T. Kim, K. H. Kim, *J. Carbohydr. Chem.* **20** (2001) 503.



SUPPLEMENTARY MATERIAL TO
Improved synthesis of gastrodin, a bioactive component of a traditional Chinese medicine

YU-WEN LI^{1*} and CUI-LI MA²

¹School of Chemistry and Pharmacy, Qingdao Agricultural University, Qingdao 266109, China and ²Affiliated Hospital, Qingdao Agricultural University, Qingdao 266109, China

J. Serb. Chem. Soc. 79 (10) (2014) 1205–1212

PHYSICAL, ANALYTIC AND SPECTRAL DATA

4-Methylphenyl 2,3,4,6-tetra-O-acetyl- β -D-glucopyranoside (7). Yield: 76.3 %; white crystals; m.p.: 117.0–117.8 °C; Anal. Calcd. for C₂₁H₂₆O₁₀: C, 57.53%; H, 5.98 %. Found: C, 57.32; H, 6.09 %; ¹H-NMR (400 MHz, CDCl₃, δ / ppm): 2.06, 2.09, 2.12, 2.18, 2.30 (5×3H, 5×s, 4×OCOCH₃, CH₃–Ar), 3.82–3.86 (1H, m, H-4), 4.16 (1H, dd, J = 12.4 Hz, 2.4 Hz, H-6b), 4.29 (1H, dd, J = 12.4 Hz, 5.2 Hz, H-6a), 5.03 (1H, d, J = 7.2 Hz, H-1), 5.17 (1H, t, J = 9.5 Hz, H-3), 5.24–5.32 (2H, m, H-2, H-5), 6.89 (2H, d, J = 8.4 Hz, Ar-H), 7.09 (2H, d, J = 8.4 Hz, Ar-H); ¹³C-NMR (100 MHz, CDCl₃, δ / ppm): 20.6, 20.7, 20.8 (4COCH₃, Ar–CH₃), 61.9 (C-6), 68.3 (C-3), 71.2 (C-5), 71.9 (C-4), 72.7 (C-2), 99.5 (C-1), 116.9, 130.0, 138.9, 154.8 (Ph), 169.3, 169.4, 170.3, 170.7 (4 COCH₃); HRMS (ESI) *m/z* Calcd. for C₂₁H₂₆O₁₀Na [M+Na]⁺: 461.1424. Found 461.1418; Specific rotation ([α]_D²³ / ° (c / g mL⁻¹: 1.05, CHCl₃)): -14.6.

4-(Bromomethyl)phenyl 2,3,4,6-tetra-O-acetyl- β -D-glucopyranoside (8). Yield: 91 %; white needle-like crystals; m.p.: 153–154 °C; Anal. Calcd for C₂₁H₂₅O₁₀Br: C, 48.76; H, 4.87; Br, 15.45 %. Found: C, 48.56, H, 4.61, Br, 15.29 %; ¹H-NMR (400 MHz, CDCl₃, δ / ppm): 2.05, 2.06, 2.08, 2.09 (4×3H, 4×s, 4×OCOCH₃), 3.85–3.89 (1H, m, H-4), 4.17 (1H, dd, J = 12.4 Hz, 2.4 Hz, H-6b), 4.29 (1H, dd, J = 12 Hz, 5.2 Hz, H-6a), 4.49 (2H, s, ArCH₂Br), 5.09 (1H, d, J = 7.2 Hz, H-1), 5.17 (1H, t, J = 9.2 Hz, H-3), 5.25–5.33 (2H, m, H-2, H-5), 6.96 (2H, dd, J = 6.8 Hz, 3.0 Hz, Ar-H), 7.33 (2H, dd, J = 6.8 Hz, 3.0 Hz, Ar-H); ¹³C-NMR (100 MHz, CDCl₃, δ / ppm): 20.7, 20.8 (4×COCH₃), 33.2 (ArCH₂Br), 61.9 (C-6), 68.2 (C-3), 71.1 (C-5), 72.1 (C-4), 72.6 (C-2), 98.8 (C-1), 117.1, 130.5, 132.8, 156.7 (C-Ar), 169.3, 169.4, 170.3, 170.6 (4 × COCH₃); HRMS

*Corresponding author. E-mail: ywli@qau.edu.cn

(ESI) *m/z* Calcd. for $C_{21}H_{25}O_{10}^{81}BrNa$ [M+Na]⁺: 541.0508. Found: 541.0514; Specific rotation ($[\alpha]_D^{23} / ^\circ$ (c / g mL⁻¹: 1.00, CHCl₃)): -13.4.

4-(Hydroxymethyl)phenyl 2,3,4,6-tetra-O-acetyl-β-D-glucopyranoside (5). Yield: 93 %; white crystals; m.p.: 108.9–109.7 °C; Anal. Calcd. for C₂₁H₂₆O₁₁: C, 55.50; H, 5.77 %. Found: C, 55.27, H, 5.49 %; ¹H-NMR (400 MHz, CDCl₃, δ / ppm): 2.04, 2.05, 2.06, 2.08 (4×3H, 4×s, 4×OCOCH₃), 3.84–3.88 (1H, *m*, H-5), 4.18 (1H, *dd*, *J* = 12.4 Hz, 4.2 Hz, H-6a), 4.29 (1H, *dd*, *J* = 12.4 Hz, 5.2 Hz, H-6b), 4.64 (2H, *s*, ArCH₂OH), 5.07 (1H, *d*, *J* = 7.2 Hz, H-1), 5.16 (1H, *t*, *J* = 9.6 Hz, H-4), 5.24–5.32 (2H, *m*, H-2, H-5), 6.98 (2H, *d*, *J* = 8.4 Hz, Ar-H), 7.27–7.31 (2H, *m*, Ar-H); ¹³C-NMR (100 MHz, CDCl₃, δ / ppm): 20.6, 20.7 (4 COCH₃), 61.9 (C-6), 64.7 (ArCH₂OH), 68.3 (C-4), 71.2 (C-2), 72.0 (C-3), 72.7 (C-5), 99.2 (C-1), 117.1, 128.5, 136.0, 156.4 (C-Ar), 169.3, 169.4, 170.3, 170.6 (4 COCH₃); HRMS (ESI) *m/z* Calcd._for C₂₁H₂₆O₁₁Na[M+Na]⁺: 447.1373. Found: 447.1378; Specific rotation ($[\alpha]_D^{23} / ^\circ$ (c / g mL⁻¹: 1.00, CHCl₃)): -12.4.

4-(Hydroxymethyl)phenyl β-D-glucopyranoside (1). Yield: 90 %; white crystals; m.p.: 154–155 °C (lit.¹ 153–155 °C); Anal. Calcd for C₁₃H₁₈O₇: C, 54.54; H, 6.34 %. Found: C, 54.37, H, 6.42 %; ¹H-NMR (400 MHz, CD₃OD, δ / ppm): 3.32–3.49 (4H, *m*, H-2, H-3, H-4, H-5), 3.72 (1H, *dd*, *J* = 12.4 Hz, 5.2 Hz, H-6a), 3.91 (1H, *dd*, *J* = 12.0 Hz, 1.6Hz, H-6b), 4.56 (2H, *s*, ArCH₂OH), 4.91 (1H, *d*, *J* = 7.6 Hz, H-1), 7.09 (2H, *d*, *J* = 8.8 Hz, Ar-H), 7.29 (2H, *d*, *J* = 8.8 Hz, Ar-H); ¹³C-NMR (100 MHz, CD₃OD, δ / ppm): 61.1 (C-6), 63.4 (ArCH₂OH), 69.9 (C-4), 73.5 (C-2), 76.6 (C-5), 76.7 (C-3), 100.9 (C-1), 116.2, 128.0, 135.2, 157.1 (C-Ar); HRMS (ESI) *m/z* Calcd. for C₁₃H₁₈O₇Na [M+Na]⁺: 309.0949. Found: 309.0945; Specific rotation ($[\alpha]_D^{23} / ^\circ$ (c / g mL⁻¹: 0.85, MeOH)): -52.2.

REFERENCE

1. L. L. Fan, Y. C. Dong, T. Y. Xu, H. F. Zhang, Q. H. Chen, *Appl. Biochem. Biotechnol.* **170** (2013) 138.



Chemical constituents and biological activities against *Tribolium castaneum* (Herbst) of the essential oil from *Citrus wilsonii* leaves

HAI PING CHEN^{1,2}, KAI YANG¹, CHUN XUE YOU¹, SHU SHAN DU^{1*}, QIAN CAI^{2**},
QING HE³, ZHU FENG GENG³ and ZHI WEI DENG³

¹State Key Laboratory of Earth Surface Processes and Resource Ecology, Beijing Normal University, Haidian District, Beijing 100875, China, ²College of Pharmacy, Liaoning University of Traditional Chinese Medicine, Dalian 116600, Liaoning, China and ³Analytical and Testing Center, Beijing Normal University, Beijing 100875, China

(Received 27 February, revised 4 April, accepted 7 April 2014)

Abstract: The essential oil obtained from *Citrus wilsonii* Tanaka leaves by hydrodistillation was investigated by GC and GC-MS. The main components of the essential oil were identified to be citronellol (16.94 %), neryl acetate (10.35 %), γ -terpinene (9.85 %), citronellal (9.36 %) and β -pinene (6.72 %). These four compounds, predicted with a bioactivity-test to be the active constituents, were isolated and identified. It was found that the essential oil of *C. wilsonii* leaves and the isolated compounds possessed fumigant and contact toxicity against *Tribolium castaneum* adults. The essential oil and γ -terpinene showed strong fumigant toxicity against *T. castaneum* (LC_{50} = 8.18 and 4.09 mg L⁻¹, respectively). The repellency of the crude oil and the active compounds was also determined. Citronellol, neryl acetate and β -pinene were strongly repellent (100, 86 and 92 %, respectively, at 78.63 nL cm⁻², after 2 h treatment) against *T. castaneum*. The essential oil and citronellol exhibited the same level of repellency compared with the positive control, *N,N*-diethyl-*meta*-toluamide (DEET, *N,N*-diethyl-3-methylbenzamide). The results indicate that the essential oil of *C. wilsonii* leaves and its active compounds had the potential to be developed as natural fumigants, insecticides and repellents for the control of *T. castaneum*.

Keywords: fumigant toxicity; contact toxicity; repellency; neryl acetate; γ -terpinene.

INTRODUCTION

The red flour beetle, *Tribolium castaneum* Herbst is one of the most widespread and destructive primary insect pests of stored cereals.¹ Control of stored product insects relies heavily on the use of synthetic insecticides and fumigants,

*,** Corresponding authors. E-mail: (*)dushushan@bnu.edu.cn; (**caiqianmail@sina.com
doi: 10.2298/JSC140227037C

which has led to several adverse effects, such as water and soil contamination, insect resistance and toxicity to non target species.² Especially, fumigants play a very important role in the elimination of insect pests in stored products because of their ability to kill a broad spectrum of pests and because of their easy penetration into the commodity while leaving minimal residues.³ Currently, phosphine and methyl bromide (MeBr) are the commonly used fumigants in store houses. Of the two fumigants, methyl bromide is an ozone-depletor and is being phased out as agreed through the Montreal Protocol.³ The other fumigant, phosphine, has some issues with insecticide resistance, requires air-tight conditions, and is associated with environmental and human safety concerns.^{4,5} Recent focus of attention among alternative fumigants has been directed toward biofumigants, which reflects the growing interest received by biopesticides or biorational pesticides.^{6,7} The use of essential oils or their constituents could effectively prevent and/or suppress insect pests especially in storage,⁶ and in some cases, have proven themselves to be more effective than traditionally used organophosphorus pesticides.^{7–9} During a screening program for new agrochemicals from local wild plants and Chinese medicinal herbs, the essential oil from *Citrus wilsonii* Tanaka leaves was found to possess fumigant/insecticidal repellent activity towards *T. castaneum*.

C. wilsonii is a good frost-resistant stock for citrus plants.¹⁰ Through a survey on the Anguo Medicinal Material Trading Market, *C. wilsonii* was discovered to be the main origin plant of Fructus Citri. Fructus Citri, one of the traditional Chinese medicines, is the dried mature fruits of *Citrus medica* L. or *C. wilsonii* that belongs to genus Citrus, family Rutaceae. *C. wilsonii* containing naringin and essential oil is used for regulating vital energy, relieving cough and resolving phlegm, and alleviating stomach pain, emesis and coughs.¹¹ A literature survey showed that there are no reports on fumigant/contact/repellency activity of the essential oil of *C. wilsonii* leaves against *T. castaneum*. Thus, it was decided to investigate the chemical constituents and fumigant/contact/repellency activity of the essential oil of *C. wilsonii* leaves against *T. castaneum* for the first time and to isolate any biologically active compounds from the essential oil.

EXPERIMENTAL

Insect

The *T. castaneum* was obtained from laboratory cultures maintained for the last 2 years in the dark in incubators at 29±1 °C and 70–80 % relative humidity. The insects were reared in glass containers (0.5 L) containing wheat flour at 12–13 % moisture content mixed with yeast (wheatfeed/yeast, 10:1, *m/m*). The adults used in all the experiments were about 7±2 days old.

Plant material and essential oil extraction

Leaves (3.0 kg) of *C. wilsonii* were collected in May 2013 from Suzhou City (31.97° N and 120.49° E), Jiangsu Province, China. The leaves were air-dried for one week and ground

to powder. The species was identified according to the voucher specimen (BNU-CMH-Dushushan-2013-05-25-007) deposited at the Herbarium (BNU) of College of Resources Science and Technology, Beijing Normal University, China. The ground powder of *Citrus wilsonii* Tanaka leaves was subjected to hydrodistillation using a modified Clevenger-type apparatus for 6 h and extracted with *n*-hexane. Anhydrous sodium sulfate was used to remove the water after extraction. The essential oil was stored in airtight container in a refrigerator at 4 °C.

Gas chromatography–mass spectrometry

GC–MS analysis was performed on a Thermo Finnigan Trace DSQ instrument equipped with a flame ionization detector and an HP-5MS (30 m×0.25 mm×0.25 µm) capillary column. The column temperature was programmed at 50 °C for 2 min, then increased at 2 °C min⁻¹ to the temperature of 150 °C and held for 2 min, and then increased at 10 °C min⁻¹ until the final temperature of 250 °C was reached, where it was held for 5 min. The injector temperature was maintained at 250 °C and the volume injected was 0.1 mL of 1 % solution (diluted in *n*-hexane). The carrier gas was helium at flow rate of 1.0 mL min⁻¹. The MS spectra were scanned from 50 to 550 *m/z*. Most constituents were identified by comparison of their retention indices with those reported in the literature. The retention indices were determined in relation to the retention times of a homologous series of *n*-alkanes (C₁₀–C₃₆) obtained under the same operating conditions. GC retention time and their mass spectra that are stored in NIST 05 and Wiley 275 libraries or from the literature were used to identify the essential oil components.¹²

Isolation and characterization of four constituent compounds

The crude essential oil (5 mL) was chromatographed on a silica gel (Qingdao Marine Chemical Plant, Shandong province, China) column (30 mm i.d., 500 mm length) by gradient elution with *n*-hexane first, then with *n*-hexane–ethyl acetate, and last with ethyl acetate to obtain 20 fractions. Based on contact toxicity, fraction 2, 7 and 14 were chosen for further fractionation. With PTLC, four purified compounds were obtained. The isolated compounds were elucidated by their NMR spectra. The NMR experiments were performed on a Bruker Avance DRX 500 instrument using CDCl₃ as the solvent with TMS as the internal standard.

Fumigant toxicity bioassay

The fumigant activity of the essential oil/pure compounds against *T. castaneum* adults was tested as described by Liu and Ho.¹ Serial dilutions of the essential oil/compounds (1.33–2.75 % for γ-terpinene, 1.98–10.00 % for the oil and β-pinene, five concentrations) were prepared in *n*-hexane. The 10-µL dilution was placed onto Whatman filter paper disks of 2.0 cm diameter. Each filter paper disk was then air-dried for 20 s and placed on the underside of the screw cap of a glass vial (25 mL). Ten insects were placed into each vial (5 replicates per dose) before the cap was screwed tightly and the lid was sealed with Parafilm. *n*-Hexane was used as the control. The mortality of insect was noted 24 h after treatment, and the LC₅₀ values were calculated using Probit analysis.¹³

Contact toxicity by topical application

The contact toxicity of the essential oil/pure compounds against *T. castaneum* adults was measured as described by Liu and Ho.¹ Aliquots of 0.5 µL of the essential oil and four isolated compounds at different concentrations (0.00, 2.96, 4.44, 6.67, 10.00 or 15.00 % of oils or compounds diluted with *n*-hexane) were applied topically to the dorsal thorax of the insects (10 insects per replicate, five replicates per dose). Insects treated with *n*-hexane alone were

used as controls. Both treated and control insects were then transferred to glass vials (10 insects per vial) with culture media and kept in incubators. The insect mortality was checked after 24 h, and the LD_{50} values were calculated using Probit analysis.¹³ The positive control, pyrethrins (pyrethrin 1: 24%; pyrethrin 2: 13%; cinnerin 1: 2%; cinnerin 2: 2%; jasmolin 1: 1%; jasmolin 2: 1%), were purchased from Dr Ehrenstorfer GmbH, Germany.

Repellent test

The repellent activity of the essential oil/pure compounds to *T. castaneum* adults was tested using the area preference method.¹⁴ The essential oil/compounds were diluted in *n*-hexane so that different final concentrations (78.63, 15.73, 3.15, 0.63 and 0.13 nL cm⁻²) will be achieved at the paper, and *n*-hexane was used as the control. A filter paper (9 cm in diameter) was cut in half. 500 µL of a treatment solution was placed on one half of the filter paper and allowed to dry for 30 s. The other half was treated with 500 µL of *n*-hexane. The treated side was then joined to the control side by tape and placed in glass Petri dishes (9 cm in diameter). Twenty insects were released in the center of each filter paper disk, and a cover was placed over the Petri dish. Five replicates were used. Counts of the insects present on each strip were made after 2 and 4 h. The percent repellency (*PR*) of each volatile oil/compound was then calculated using the equation:

$$PR(\%) = 100 \frac{(N_c - N_t)}{(N_c + N_t)} \quad (1)$$

where N_c is the number of insects present in the negative control half and N_t is the number of insects present in the treated half. Analysis of variance (One-Way ANOVA and GLM Univariate) and Tukey's test were conducted by using SPSS 20.0 for Windows 2007. Percentage mortality data were subjected to arcsine square-root transformation before analysis of variance. The commercial repellent *N,N*-diethyl-*meta*-toluamide (DEET, *N,N*-diethyl-3-methylbenzamide) was purchased from the National Center of Pesticide Standards (Shenyang, China) and used as a positive control.

RESULTS AND DISCUSSION

Chemical constituent of essential oil

The yield of *C. wilsonii* leaves essential oil was 0.55% (V/m) with a density 0.87 g mL⁻¹. GC-MS analysis of the essential oil of *C. wilsonii* leaves led to the identification and quantification of a total of 15 major components, accounting for 84.12% of the total components present (Table I). The main constituents of *C. wilsonii* leaves essential oil were citronellol (16.94%), neryl acetate (10.35%), γ -terpinene (9.85%), citronellal (9.36%) and β -pinene (6.72%).

There is only one report on the extraction of the essential oil from *C. wilsonii* leaves. γ -Terpinene (27.1%), *p*-cymene (10.3%), limonene (8.4%), nerol (7.5%), β -pinene (5.2%), nerol (4.8%), ocimene (4.4%) and citronellal (4.3%) were the main components of the essential oil of *C. wilsonii* leaves obtained from Georgian SSR.¹⁰ However, there are a few reports about the extraction of essential oil from other parts of *C. wilsonii*. For example, the essential oil of Xianggyuan (*C. wilsonii*) peel collected from the Jiangsu Province contained limonene (50.53%), *p*-ocimene (16.40%), γ -terpinene (8.75%), β -ocimene (5.03%),

β -pinene (3.35 %), α -pinene (2.66 %) and β -myrcene (2.30 %).¹⁵ The essential oil of *Fructus Aurantii Immaturus* of *C. wilsonii* collected from Shaanxi Province contained D-limonene (58.09 %), γ -terpinene (23.76 %), β -cubebene (2.83 %) and α -pinene (2.00 %). Furthermore, D-limonene (65.32 %), γ -terpinene (17.36 %), 1-methyl-5-methylene-8-(1-methylethyl)-1,6-cyclodecadiene (1.80 %) and α -terpineol (1.43 %) were the major compounds of the essential oil of the *Fructus Aurantii* of *C. wilsonii*.¹⁶

TABLE I. Chemical composition of the essential oil of *Citrus wilsonii* Tanaka leaves; *RI* – retention index as determined on a HP-5MS column using the homologous series of *n*-hydrocarbons

Compound	RI	Content, %
(+)- α -Pinene	931	1.41
β -Pinene	981	6.72
4-Cymene	1024	4.66
(S)-(–)-Limonene	1029	1.28
β -Phellandrene	1031	2.41
γ -Terpinene	1057	9.85
Linalool	1094	3.97
D-Citronellal	1152	9.36
Citronellol	1226	16.94
3-Methyl-3-(4-methyl-3-pentenyl)-2-oxiranecarboxaldehyde	1234	1.33
2,6-Dimethylocta-2,6-diene	1338	4.89
Neryl acetate	1362	10.35
(–)-Spathulenol	1577	4.04
Caryophyllene oxide	1584	3.06
Phytol	2119	3.85
Total		84.12

Structure confirmation of isolated compounds

On further isolation, four purified compounds were obtained that were analyzed by several NMR techniques including ^1H - and ^{13}C -NMR. Combining all the NMR spectra data, the four isolated compounds were finally recognized as citronellol (0.44 g),^{17–19} γ -terpinene (0.22 g),^{17,20} neryl acetate (0.23 g)¹⁷ and β -pinene (0.15 g).²¹

Fumigant toxicity

The essential oil of *C. wilsonii* leaves showed strong fumigant toxicity against *T. castaneum* adults with an LC_{50} value of 8.18 mg L^{–1} (Table II). The isolated compounds γ -terpinene and β -pinene also exhibited strong fumigant toxicity against *T. castaneum* adults with LC_{50} values of 4.09 and 15.22 mg L^{–1}, respectively (Table II).

The crude essential oil was almost five times less toxic to *T. castaneum* adults compared with MeBr ($LC_{50} = 1.75$ mg L^{–1}).²² However, as most commer-

cial fumigants (*e.g.*, phosphine and MeBr) are synthetic insecticides and highly toxic to humans and other non-target organisms, the fumigant activity of the essential oil of *C. wilsonii* leaves and γ -terpinene were quite promising. Compared with the commercial fumigant MeBr, γ -terpinene exhibited an almost two times lower fumigant toxicity against *T. castaneum* adults. Nevertheless, compared with other essential oils reported in the literature, the crude essential oil had a stronger level of fumigant toxicity towards *T. castaneum* adults than, for example, the essential oils of *Illicium difengpi* ($LC_{50} = 16.22 \text{ mg L}^{-1}$),²³ *I. pachyphyllum* ($LC_{50} = 15.08 \text{ mg L}^{-1}$),²⁴ *Zanthoxylum schinifolium* seeds ($LC_{50} = 11.77 \text{ mg L}^{-1}$),²⁵ *Perovskia abrotanoides* ($LC_{50} = 11.39 \mu\text{L L}^{-1}$),²⁶ *Citrus reticulata* ($LC_{50} = 19.47 \mu\text{L L}^{-1}$) and *Schinus terebinthifolius* ($LC_{50} = 20.50 \mu\text{L L}^{-1}$),²⁷ but a lower toxicity than the essential oil of *Carum carvi* ($LC_{50} = 2.53 \text{ mg L}^{-1}$).²⁸

TABLE II. Fumigant toxicity of the essential oil of *Citrus wilsonii* Tanaka leaves and its main components against *Tribolium castaneum* adults

Treatment	$LC_{50} / \text{mg L}^{-1}$ air ^a	Slope \pm SE	df	χ^2	P
<i>C. wilsonii</i>	8.18 (6.44–9.32)	5.44 \pm 1.07	23	11.71	0.975
Citronellol	>150.75	—	—	—	—
γ -Terpinene	4.09 (3.74–4.32)	10.24 \pm 1.64	23	5.13	1.000
Neryl acetate	>157.75	—	—	—	—
β -Pinene	15.22 (13.69–16.96)	4.04 \pm 0.44	23	20.93	0.585
MeBr ^b	1.75	—	—	—	—

^a95 % lower and upper measurement limits are shown in parentheses; ^bdata from Liu and Ho¹

The development of natural fumigants would help to decrease the negative impact of synthetic fumigants, such as residues, resistance and environmental pollution. In this respect, natural fumigants may be effective, biodegradable, and less harmful to the environment. In the present study, the crude essential oil, γ -terpinene and β -pinene showed strong fumigant toxicities against *T. castaneum*. Based on these findings, these or other essential oil may serve as viable alternatives to synthetic insecticides.

Contact toxicity

The essential oil of *C. wilsonii* leaves showed contact toxicity against *T. castaneum* adults with LD_{50} values of 48.49 μg per adult (Table III). Compared with the positive control pyrethrins the crude essential oil demonstrated 186 times lower toxicity against the red flour beetle because the pyrethrins have acute contact toxicity to *T. castaneum* with an LD_{50} value of 0.26 μg per adult. The isolated compounds citronellol, γ -terpinene, neryl acetate and β -pinene also exhibited contact toxicity against *T. castaneum* adults with LD_{50} values of 35.89, 35.59, 25.84 and 22.10 μg per adult, respectively (Table III). Among the four isolated compounds, β -pinene demonstrated a stronger contact toxicity against *T. castaneum* than the other three isolated compounds.

TABLE III. Contact toxicity of essential oil of *Citrus wilsonii* Tanaka leaves and its main components against *Tribolium castaneum* adults

Treatment	$LD_{50}^a / \mu\text{g adult}^{-1}$	Slope $\pm SE$	df	χ^2	P
<i>C. wilsonii</i>	48.49 (44.19–54.03)	5.39 \pm 0.67	23	21.30	0.563
Citronellol	35.89 (32.50–39.93)	4.45 \pm 0.47	23	12.12	0.969
γ -Terpinene	35.59 (32.57–39.07)	5.33 \pm 0.56	23	16.12	0.850
Neryl acetate	25.84 (23.49–28.33)	4.75 \pm 0.49	23	15.13	0.890
β -Pinene	22.10 (16.10–27.05)	2.55 \pm 0.42	23	20.24	0.627
Pyrethrins	0.26 (0.22–0.30)	3.34 \pm 0.32	23	13.11	0.950

^a95 % lower and upper measurement limits are shown in parentheses

Repellent activity

The results of the repellency assays for the essential oil and isolated compounds against *T. castaneum* adults are presented in Figs. 1 and 2. The essential oil from *C. wilsonii* leaves at a dose of 78.63 nL cm⁻² showed 98 and 96 % repellency against *T. castaneum* adults 2 and 4 h after exposure, respectively. At the lowest concentration (0.13 nL cm⁻²), the essential oil still showed strong repellency (78 and 72 %) against *T. castaneum* at 2 and 4 h after exposure, respectively (Figs. 1 and 2). Among the four constituents of the crude essential oil, citronellol produced strong repellency (100 % at 78.63 nL cm⁻², after both 2 and

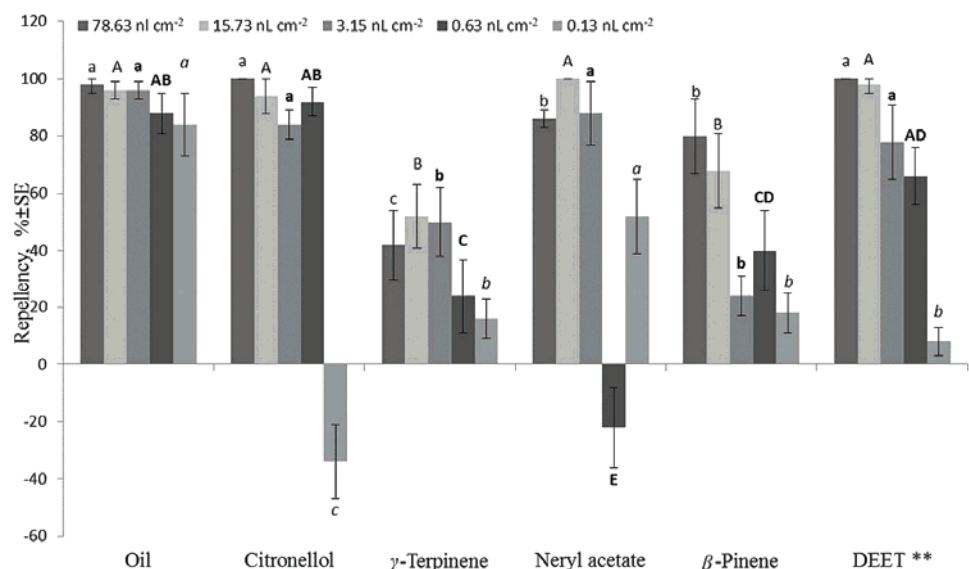


Fig. 1. Percentage repellency (PR) of the essential oil from *Citrus wilsonii* Tanaka leaves and its constituents against *Tribolium castaneum* at 2 h after exposure; means in the same column followed by the same letters do not differ significantly ($P > 0.05$) in ANOVA and Tukey's tests. The PR values were subjected to an arcsine square-root transformation before the ANOVA and Tukey's tests; ** – positive control.

4 h treatment). Citronellol at dose of 0.63 nL cm⁻² still showed strong repellency (92 and 94 %, respectively) against *T. castaneum* at 2 and 4 h after exposure (Figs. 1 and 2). Neryl acetate and β -pinene also showed obvious repellency (>68 %) at dose of 78.63 and 15.73 nL cm⁻² after 4 h treatment. However, compared with the other three constituents, γ -terpinene produced less repellency (42 and 26 %, respectively, at 78.63 nL cm⁻² after 2 and 4 h treatment).

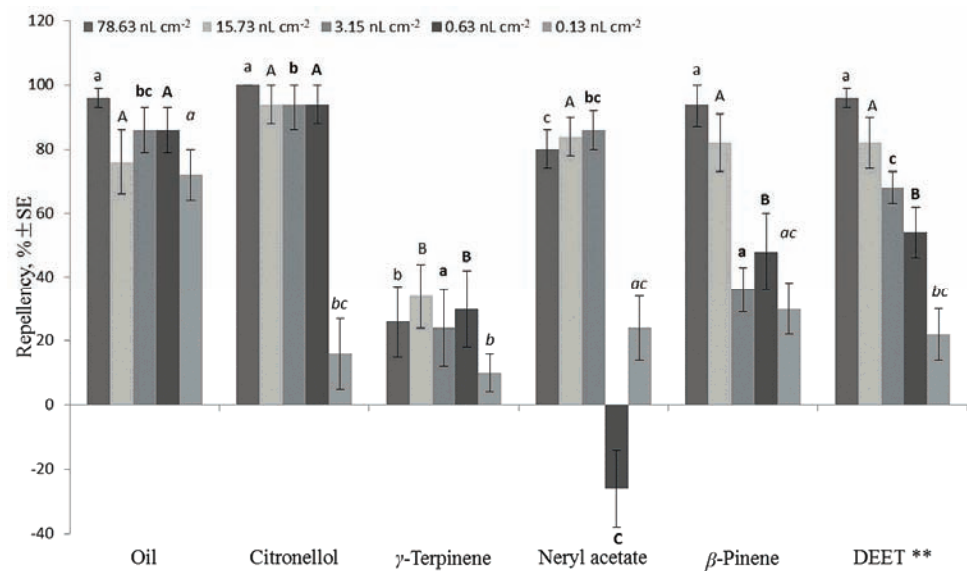


Fig. 2. Percentage repellency (*PR*) of the essential oil from *Citrus wilsonii* Tanaka leaves and its constituents against *Tribolium castaneum* at 4 h after exposure; means in the same column followed by the same letters do not differ significantly ($P > 0.05$) in ANOVA and Tukey's tests. The *PR* values were subjected to an arcsine square-root transformation before the ANOVA and Tukey's tests; ** – positive control.

Many essential oils and their constituents have been evaluated for repellency against insects.²⁹ For example, Zhang *et al.* reported that geraniol and citronellol exhibited stronger repellency against the red flour beetle than DEET, whereas limonene and citronella showed the same level of repellency against the red flour beetle as DEET.¹⁴ At 0.03 mg cm⁻², origanum oil, linalool and *p*-cymene showed 98, 83 and 85 % repellency (after 2 h treatment) against *T. castaneum* adults, respectively.³⁰ However, in this paper, we report the repellency of the essential oil of *C. wilsonii* leaves for the first time. The essential oil and citronellol exhibited the same level of repellency against *T. castaneum* adults as DEET, the positive control.

To the best of our knowledge, this is the first report regarding the fumigant/insecticidal/repellent action of the essential oil of *C. wilsonii* leaves against *T. castaneum*. The results suggest that the essential oil and the four compounds

show potential for development as natural fumigants, insecticides and repellents for stored product protection. However, for the practical application of the essential oil and the four compounds as novel fumigants/insecticides/repellents, further studies on the safety of the essential oil and the four compounds toward humans and on the development of formulations are necessary to improve the efficacy and stability, and to reduce cost.

Acknowledgments. This project was supported by the State Key Laboratory of Earth Surface Processes and Resource Ecology and National Natural Science Foundation of China (No. 81374069). The authors thank Dr. Q. R. Liu from the College of Life Sciences, Beijing Normal University, Beijing 100875, for the identification of the investigated medicinal herb.

ИЗВОД

ХЕМИЈСКИ САСТАВ И БИОЛОШКА АКТИВНОСТ ЕТАРСКОГ УЉА ЛИСТОВА *Citrus wilsonii* СПРАМ БРАШНЕНОГ МОЉЦА *Tribolium castaneum* (HERBST)

HAI PING CHEN^{1,2}, KAI YANG¹, CHUN XUE YOU¹, SHU SHAN DU¹, QIAN CAI², QING HE³, ZHU FENG GENG³
и ZHI WEI DENG³

¹State Key Laboratory of Earth Surface Processes and Resource Ecology, Beijing Normal University, Haidian District, Beijing, China, ²College of Pharmacy, Liaoning University of Traditional Chinese Medicine, Dalian, Liaoning, China и ³Analytical and Testing Center, Beijing Normal University, Beijing 100875, China

Етарско уље листова *Citrus wilsonii* Tanaka добијено је дестилацијом воденом паром и анализирано методама GC и GC-MS. Главни састојци уља су идентификовани као цитронелол (16,94 %), нерил-ацетат (10,35 %), γ-терпинен (9,85 %), цитронеал (9,36 %) и β-пинен (6,72 %). Четири састојка су била активна, што је утврђено тестом биоактивности: цитронелол, нерил-ацетат, γ-терпинен и β-пинен. Утврђено је да етарско уље листова *C. wilsonii* и изолована једињења имају фумигантну и контактну токсичност спрам одрасле форме *Tribolium castaneum*. Етарско уље и γ-терпинен су испољили јаку фумигантну токсичност спрам *T. castaneum* (LC_{50} 8,18 и 4,09 mg L⁻¹, редом). Репелентност сировог уља и активних једињења је, такође, одређивана. Цитронелол, нерил-ацетат и β-пинен су били јако репелентни спрам *T. castaneum* (100, 86 и 92 %, редом, при 78,63 nL cm⁻², после 2 h третмана). Етарско уље и цитронелол су испољили исту репелентност као и позитивна контрола, DEET. Резултати указују да етарско уље листова *C. wilsonii*, као и његова активна једињења, имају потенцијал да се развију као природни фумиганти, инсектициди и репеленти за контролу *T. castaneum*.

(Примљено 27 фебруара, ревидирано 4. априла, прихваћено 7. априла 2014)

REFERENCES

1. Z. L. Liu, S. H. Ho, *J. Stored Prod. Res.* **35** (1999) 317
2. M. B. Isman, *ACS Symp.* **887** (2004) 41
3. C. H. Bell, *Crop Prot.* **19** (2000) 563
4. M. Q. Chaudhry, *Pestic. Sci.* **49** (1997) 213
5. J. L. Zettler, F. H. Arthur, *Crop Prot.* **19** (2000) 577
6. M. B. Isman, *Annu. Rev. Entomol.* **51** (2006) 45
7. S. Rajendran, V. Srianjini, *J. Stored Prod. Res.* **44** (2008) 126
8. S. S. Chu, Q. R. Liu, Z. L. Liu, *Biochem. Syst. Ecol.* **38** (2010) 489

9. R. Fang, C. H. Jiang, X. Y. Wang, H. M. Zhang, Z. L. Liu, L. Zhou, S. S. Du, Z. W. Deng, *Molecules* **15** (2010) 9391
10. N. A. Kekelidze, M. I. Dzhanikashvili, *Chem. Nat. Compd.* **18** (1983) 753
11. State Pharmacopoeia Committee, *Chinese Pharmacopoeia (Part I)*, Chemical Industry Press, Beijing, 2005, p. 224
12. R. P. Adams, *Identification of essential oil components by gas chromatography/ quadrupole mass spectroscopy*, Allured, Carol Stream, IL, 2001
13. M. Sakuma, *Appl. Entomol. Zool.* **33** (1998) 339
14. J. S. Zhang, N. N. Zhao, Q. Z. Liu, Z. L. Liu, S. S. Du, L. G. Zhou, Z. W. Deng, *J. Agric. Food Chem.* **59** (2011) 9910
15. L. Y. Niu, M. Yu, F. G. Liu, D. J. Li, C. Q. Liu, *Food Ferment. Ind.* **39** (2013) 186 (in Chinese)
16. H. Yang, P. J. Yang, *J. Food Sci. Biotechnol.* **29** (2010) 219 (in Chinese)
17. F. Bohlmann, R. Zeisberg, E. Klein, *Org. Magn. Reson.* **7** (1975) 426
18. V. P. Talzi, *Russ. J. Appl. Chem.* **7** (2006) 107
19. K. E. O'Brien, D. K. Wicht, *Green Chem. Lett.* **1** (2008) 149
20. M. Ishifune, H. Yamashita, Y. Kera, N. Yamashita, K. Hirata, H. Murase, S. Kashimura, *Electrochim. Acta* **48** (2003) 2405
21. A. Y. Badiah-Hadj-Ahmed, B. Y. Meklati, H. Waton, Q. T. Pham, *Magn. Reson. Chem.* **30** (1992) 807
22. Z. L. Liu, S. S. Chu, G. H. Jiang, *J. Agric. Food Chem.* **57** (2009) 10130
23. S. Liu, Y. Z. He, Y. Zhao, Q. J. Qin, Y. Y. Zheng, *Chin. Agric. J. Sci. Bull.* **23** (2007) 427 (in Chinese)
24. S. Y. Paik, K. H. Koh, S. M. Beak, S. H. Paek, J. A. Kim, *Biol. Pharm. Bull.* **28** (2005) 802
25. C. F. Wang , K. Yang , H. M. Zhang , J. Cao , R. Fang , Z. L. Liu, S. S. Du, Y. Y. Wang, Z. W. Deng, L. G. Zhou, *Molecules* **16** (2011) 3077
26. X. G. Yang, *J. Agric. Food Chem.* **56** (2008) 1689
27. L. R. Jia, Z. F. Zhao, S. R. Lei, Z. Tan, *Food Machin.* **24** (2008) 105 (in Chinese)
28. S. R. Wu, J. Q. Kan, B. Liu, Z. D. Chen, *Flav. Fragr. Cosmetics* **12** (2007) 1 (in Chinese)
29. L. S. Nerio, J. Olivero-Verbel, E. Stashenko, *Bioresour. Technol.* **101** (2010) 372
30. S. I. Kim, J. S. Yoon, J. W. Jung, K. B. Hong, Y. J. Ahn, H. W. Kwon, *J. Asia Pacific Entomol.* **13** (2010) 369.



Influence of yeast and nutrients on the quality of apricot brandy

IVAN UROŠEVIĆ¹, NINOSLAV NIKIĆEVIĆ¹, LJUBIŠA STANKOVIĆ¹, BOBAN ANĐELKOVIĆ², TIJANA UROŠEVIĆ¹, GORDANA KRSTIĆ² and VELE TEŠEVIĆ^{2*}

¹Faculty of Agriculture, University of Belgrade, Nemanjina 6, 11080 Zemun, Serbia and

²Faculty of Chemistry, University of Belgrade, Studentski trg 16, 11000 Belgrade, Serbia

(Received 25 January, revised 13 March, accepted 14 March 2014)

Abstract: Five yeast strains *Saccharomyces cerevisiae* and *S. bayanus* (SB, Top Floral, Top 15, Aroma White and Red Fruit) and two nutrients, diammonium phosphate and Nutriferm Arom, were examined for their influence on young apricot brandies, with a special emphasis on the chemical, volatile and sensory characteristics. Analyses of the major and minor volatiles and sensory analysis of the apricot brandies showed important differences between the samples. The total sensory scores of the apricot brandies ranged between 16.88 for the control sample to 18.35 for the sample produced with the SB yeast strain and diammonium phosphate as nutrient. All the samples of apricot brandies fulfilled EU requirements as regards their content of methanol and other components, such as acetaldehyde, ethyl acetate, and higher alcohols.

Keywords: apricot brandy; yeast strain; nutrients; volatile compounds.

INTRODUCTION

Fruit brandies are a large group of alcoholic beverages the consummation of which is increasing from year to year, especially on the Balkan region. During the last ten years in Serbia, many small distilleries started to work and produce many different types of fruits brandies, such as plum, apricot, Williams pear, quince and apple. In most cases, the producers make fruit brandies in the traditional way without using selected yeast strains, enzymes or other agents. As the culture for the consummation of good quality brandy grew, many producers decided to improve the quality of their fruit brandy.

Apricots (*Prunus armeniaca* L.) are appreciated by consumers all over the world, and are presently cultivated in all Mediterranean countries, in Central and South Asia, South Africa and in North and South America.¹ The main varieties of apricots cultivated in Serbia are Hungarian best, Kecskemét and Ceglédi bibor.

*Corresponding author. E-mail: vtesevic@chem.bg.ac.rs
doi: 10.2298/JSC140125024U

Selected yeast strains are used in fruit brandy technology to increase the speed of the fermentation process, to kill wild microflora and obtain a clean fermentation. When using a selected yeast strain, it is important to obtain good fermenting condition for yeast growth (temperature, oxygen and pH) and sufficient nutrients to improve the characteristics of the compounds newly formed during fermentation.² Depending of the biological predisposition, the conditions and the nutrients available during yeast growth, many minor compounds are formed that impart specific organoleptic characteristics to the final product.^{3,4} Aroma is one of the main characteristics that determine an organoleptic quality and style of a brandy. This is the result of the contribution of hundreds of volatile compounds, including higher alcohols, esters, acids, aldehydes, ketones, terpenes, norisoprenoids and volatile phenols that are derived from volatile chemical compounds arising from the fruit, and the fermentation and distillation processes.⁵ During alcoholic fermentation, many volatile components are formed and modified by the yeast, and the yeast strain has a great influence on the profile and production levels of these compounds.⁶

Flavor compounds have a range of common chemical group characteristics. The main apricot flavor compounds are esters, some terpenes, alcohols, aldehydes and lactones. In apricot fruit, over 100 flavor compounds were detected.⁷

The first significant studies on apricot flavor were performed by Tang and Jennings utilizing direct extraction, vacuum steam distillation and charcoal adsorption to isolate the volatiles.^{8,9} Several studies on the relative importance of some volatile compounds to the typical aroma of apricot were completed. Studies on odor threshold demonstrated that the major contributors to the aroma of blended apricot included β -ionone, linalool, γ -decalactone, β -cyclocitral, phenylacetaldehyde and γ -octalactone.¹⁰ β -Ionone and linalool may be responsible for the floral character and the lactones for the fruity, peach and coconut background aroma.^{10,11} Some authors suggested that, in particular, hexanal, (E)-2-hexenal, α -terpineol, myrcene, limonene and geraniol should also be considered as key odorants of apricot.¹² Benzaldehyde gives a very strong almond aroma and is also a typical compound found in apricots.⁷

After alcohol fermentation, the fermented fruit pomace must be distilled once or several times, depending on the type of the distillation units and the required final product. Copper distillation units are traditionally used for the distillation of fruit pomace. During distillation, the fermented fruit pomace is heated to boiling and the formed steam containing alcohol, water and volatile compounds is introduced into the condenser where condensation occurs and at the end of the distillation units, condensate is obtained. When simple traditional distillation units (alembic type) are used, first condensate must undergo a second distillation – a redistillation. During the distillation process, the concentrations of alcohol, water and volatile compounds change. From the beginning of the distil-

lation to the end, the concentrations of alcohol and high volatile compounds (aldehydes and esters) slowly decrease and the concentrations of water and low volatile compounds (higher alcohols, acids) increase.¹³

The separation of a certain fraction of the condensate can be made to improve the final condensate and give a product having the characteristics required by the producer. For this reason, it is very important that during fermentation, the yeast produce satisfactory amounts of the volatile compounds that have a positive influence on the final product.⁶

The aim of this study was to identify the relationship between the chemical composition, volatile profile and sensory characteristics of freshly distilled apricot brandy, and the influence of commercial yeast strains on the quality of apricot distillates.

MATERIAL AND METHODS

Yeast strains and apricot

The experiments were performed to obtain apricot distillate using five different strains of selected yeasts and nutrients. For this purpose, the fruits were picked at the stage of full ripeness during July 2012. Hungarian cultivar "Kecskemét apricots" from an apricot plantation in the village Miokovci in central Serbia were used. The fruit was manually selected and transported to the laboratory on the day of collection.

On the day of fruit collection, the pits from the apricots were removed and apricot was pulped. The mashed apricot pomace had the following characteristics: total soluble solids 17 °Bx*, pH 3.3 and titratable acidity 2.21 g L⁻¹.

Alcoholic fermentation

Eleven plastic tanks of 25 L were filled with 20 kg of pulped apricot. Ten of the plastic tanks were inoculated with one of five *S. cerevisiae* and *S. bayanus* commercial wine strain yeast, in combination with one of two types of nutrients. The eleventh tank was the control tank without yeast or nutrients. The dried commercial yeast strains were rehydrated in water at 35 °C for at least 20 min. The nutrients were dissolved in water (1:5, V/V). Quantity of yeast added to the fruit during the experiments was 0.2 g kg⁻¹. The same amount of nutrients was added. The combination in tanks was that each yeast strain was in two tanks with different nutrients (Table I).

The fermentations were performed at 15–18 °C for 10 days (until the sugar concentration was reduced to below 4 °Bx). At the end of the fermentation, the yeast cells were allowed to sediment naturally for 2 days more. The alcohol content at the end of the fermentation was 7–8 vol. %

Distillation

When the alcoholic fermentations were finished, the fermented fruit mashes were immediately distilled in small copper units by double distillation. The distillation units had a capacity of 25 L. During the first distillation, no fractions were collected. After the first distillation, the obtained distillate contained between 25 and 27 vol. % alcohol. The redistillation was performed using a small copper unit of 5-L capacity. During the redistillation, fractions were collected: the first fraction (head) was 1.5 % by volume, the second fraction

* 1 Bx = 1 g of sucrose in 100 g of solution.

(heart), which contained on average 61 vol. % of alcohol, and a third fraction (tail).¹³ All the second fraction distillates were gradually reduced with distilled water to 43 vol. % alcohol.

TABLE I. Nutrients and yeast used in the experiments

Sample	Yeast	Commercial name	Nutrients	Origin
SB1	<i>S. cerevisiae</i> ex r.f. bayanus	SB	Diammonium phosphate	EssecoSrl, Italy
TF1	<i>S. bayanus</i>	Top Floral	Diammonium phosphate	EssecoSrl, Italy
TOP1	<i>S. cerevisiae</i> ex ph.r. bayanus	Top 15	Diammonium phosphate	EssecoSrl, Italy
AW1	<i>S. cerevisiae</i>	Aroma white	Diammonium phosphate	EssecoSrl, Italy
RF1	<i>S. cerevisiae</i>	Red Fruit	Diammonium phosphate	EssecoSrl, Italy
SB2	<i>S. cerevisiae</i> ex r.f. bayanus	SB	Nutriferm Arom	EssecoSrl, Italy
TF2	<i>S. bayanus</i>	Top Floral	Nutriferm Arom	EssecoSrl, Italy
TOP2	<i>S. cerevisiae</i> ex ph.r. bayanus	Top 15	Nutriferm Arom	EssecoSrl, Italy
AW2	<i>S. cerevisiae</i>	Aroma white	Nutriferm Arom	EssecoSrl, Italy
RF2	<i>S. cerevisiae</i>	Red Fruit	Nutriferm Arom	EssecoSrl, Italy
CONT	<i>S. cerevisiae</i>	Control	—	Wild

All experiments were performed in triplicate, and the ethanol content was determined after the first distillation and redistillation. The major and minor volatile compounds were determined only in samples obtained after redistillation.

Analytical methods

Total soluble solids, sugar content, pH, titratable acidity and ethanol. The total soluble solid and the sugar contents of the apricot fruits were determined using a hand refractometer (Carl Zeiss Jena Model 711849, Germany) with an attached thermometer. The pH was measured by a 320 pH meter (Mettler Toledo). The titratable acidity was determined by titration with sodium hydroxide to pH 8.1 using phenolphthalein as an indicator. Ethanol was determined after distillation using an Alcoholmeter Guy–Lussac Classe II calibrated at 20 °C.

GC analysis of the major volatile compounds. The major volatile components were analyzed on the basis of the European Community Reference Methods for the Analysis of Spirits using gas chromatography (GC) with a flame-ionization detector (FID).¹⁴ The main components, including methanol, acetaldehyde, 1-propanol, ethyl acetate, 2-methyl-1-propanol, 1-butanol, amyl alcohols and 1-hexanol, were identified by comparing their retention times with those of authentic compounds. For quantitative evaluation, the internal standard method was applied, with a known amount of 4-methyl-1-pentanol as an internal standard (IS). Thus, an ethanol solution containing 5 g L⁻¹ 4-methyl-1-pentanol was added to 10 mL of each sample. The concentration of each volatile was determined with respect to the internal standard from the relative response factors (RRF), which were obtained during

calibration under the same chromatographic conditions as those of the sample analysis.¹⁵ The GC analysis was performed with an HP 5890 gas chromatograph equipped with a flame ionization detector (FID) and a split/splitless injector. A capillary column (30 m×0.25 mm i.d., 0.25 µm film thickness) coated with HP-5 (5 % biphenyl and 95 % dimethylpolysiloxane) was used. The column oven temperature was programmed from 50 °C to 285 °C at a rate of 4.3 °C min⁻¹, and the injection port and detector temperatures were maintained at 250 °C. Hydrogen was used as the carrier gas at a flow rate of 1.6 mL min⁻¹ and the split ratio was 60:1. The sample volume was 1 µL.

Extraction and concentration of minor volatile constituents. Fifty milliliters of distillate was mixed with 100 mL of ultrapure water, 20 mL 1 mg mL⁻¹ internal standard (methyl 10-undecenoate) added and then extracted with 40 mL of dichloromethane. NaCl (10 g) was added, and the mixture was stirred magnetically during 30 min. Layers were separated in a separator funnel, and the organic layer was dried (2 h) over anhydrous sodium sulfate. The extract was concentrated to 1.0 mL under nitrogen and directly analyzed on GC/MS.

GC/MS analysis of minor volatile compounds. Gas chromatographic analysis was performed using the same gas chromatograph and the same conditions as were employed for the analysis of the major volatile compounds, except the oven temperature was held at 50 °C for 6 min before heating to 285 °C, the detector temperature was 280 °C and the injection mode was splitless. GC/MS analysis was performed using an Agilent 6890 gas chromatograph coupled with Agilent 5973 Network mass selective detector (MSD) operated in the positive ion electron impact (EI) mode. The separation was achieved on an Agilent 19091S-433 HP-5MS fused silica capillary column, 30 m×0.25 mm i.d., 0.25 µm film thickness. The GC oven temperature was programmed from 60 to 285 °C at a rate of 4.3 °C min⁻¹. Helium was used as the carrier gas, the inlet pressure was 25 kPa, and the velocity was 1 mL min⁻¹ at 210 °C. The injector temperature was 250 °C and the injection mode was splitless. The MS scan conditions were source temperature, 200 °C; interface temperature, 250 °C; energy of electron beam was 70 eV and the mass scan range was 40–350 amu (atomic mass units). The identification of the components was based on retention indices and comparison with reference spectra (Wiley and NIST databases). The percentages (relative) of the identified compounds were computed from the GC peak areas.

Quantitative descriptive analysis

An expert panel composed of three expert testers (all males) performed the quantitative descriptive analysis. The panelists were recruited according to their years of experience as expert tasters for fruit brandy. The evaluation was conducted anonymously using the modified Buxbaum method, which is the worldwide-accepted method for sensory evaluation of strong alcoholic drinks.^{16,17} The maximum numbers of points was 20. After tasting, the results of all testers for each sample were summarized and the mean value was calculated.

RESULTS AND DISCUSSION

Volatile compounds in apricot brandy

The heart fraction results of gas chromatography analysis of major volatile compounds are given in Table II. These results show the concentrations of acetaldehyde, ethyl acetate, methanol and six higher alcohols. The concentrations of these compounds and their ratios have a large influence on the final impression of the taste and smell of a sample. The results of the experiments showed signi-

fificant differences between the samples. The results of the GC/MS analysis of the minor volatile compounds in the heart fraction are presented in Table S-I of the Supplementary material to this paper.

TABLE II. Chemical composition in apricot brandies (mg L⁻¹, mean±SD, unless otherwise indicated)

Sample	AW1	AW2	RF1	RF2	TF1	TF2	SB1	SB2	TOP1	TOP2	CONT.
Acetaldehyde	80 ±1.2	41 ±0.7	39 ±0.6	49 ±0.9	39 ±0.7	46 ±0.9	47 ±0.8	51 ±1.0	59 ±1.1	52 ±1.1	62 ±1.2
Ethyl acetate	343 ±5.3	161 ±3.1	174 ±3.4	338 ±6.3	287 ±5.3	236 ±4.3	297 ±4.6	489 ±7.2	303 ±3.5	329 ±4.1	367 ±4.3
Methanol	1928 ±10.2	1048 ±11.3	1462 ±12.1	1562 ±11.2	2485 ±16.2	2254 ±16.1	2146 ±15.2	1921 ±13.2	2014 ±11.3	1460 ±16.2	1441 ±10.9
1-Propanol	1404 ±9.2	1406 ±10.1	1359 ±11.3	1380 ±13.2	1161 ±12.4	1208 ±14.1	1535 ±12.8	1466 ±13.2	1758 ±14.2	1548 ±13.4	1112 ±10.9
2-Methyl-1-propanol	253 ±3.4	267 ±3.2	209 ±2.9	223 ±2.6	296 ±3.1	274 ±3.0	203 ±3.2	213 ±1.9	227 ±2.1	199 ±2.1	247 ±2.3
1-Butanol	16 ±0.9	16 ±0.9	15 ±0.5	18 ±0.8	18 ±0.7	14 ±0.5	17 ±0.8	16 ±0.6	19 ±1.0	17 ±0.9	16 ±0.8
Amyl alcohols	527 ±5.3	585 ±5.7	509 ±6.3	562 ±6.4	487 ±7.5	517 ±8.1	501 ±5.8	538 ±5.6	585 ±5.7	526 ±4.9	553 ±4.7
1-Hexanol	12 ±0.2	13 ±0.2	15 ±0.3	14 ±0.4	15 ±0.1	17 ±0.3	13 ±0.2	12 ±0.3	16 ±0.4	15 ±0.3	17 ±0.3
Ethanol, vol. %	43.1 ±1.1	43.2 ±1.2	43.0 ±1.2	42.8 ±1.4	43.3 ±1.3	43.1 ±1.7	42.9 ±1.4	43.1 ±1.5	43.0 ±1.2	43.2 ±1.1	43.1 ±1.0

Alcohols

Alcohols are the most significant and dominate group of volatile compounds in fruit brandies and they have important influences on the sensory characteristics and quality of the products. Primary, they are formed by yeast from amino acids *via* the Ehrlich metabolic pathway.⁴ The second way of their formation is by yeast through the reduction of the corresponding aldehydes.¹⁸ The odor threshold of alcohols is considerably higher than that of the corresponding aldehydes, so alcohols are normally less important to the flavor profiles.⁷

The contents of alcohols in the tested samples varied significantly, as evidenced by the results obtained for major compounds. The highest content of 1-propanol, which has a pungent and alcoholic odor, was found in the sample TOP1 (1758 mg L⁻¹) and the smallest content contained sample CONT (1112 mg L⁻¹). The quantity of 1-butanol ranged from 19 mg L⁻¹ in sample TOP1 to 14 mg L⁻¹ in sample TF2. The highest amounts of 2-methyl-1-propanol, with a sweet musty odor,¹⁹ were found in samples TF1 and TF2 (296 mg L⁻¹ and 274 mg L⁻¹, respectively) and the smallest content was found in sample TOP 2 (199 mg L⁻¹). The content of amyl alcohols, with a mild and characteristic alcoholic odor,²⁰

ranged from 585 mg L⁻¹ in samples AW2 and TOP1 to 487 mg L⁻¹ in sample TF1. The largest amount (17 mg L⁻¹) of 1-hexanol, with herbal and fruity odor, was present in samples TF2 and CONT and the yeast SB in sample SB2 produced lowest amount of this alcohol (12 mg L⁻¹). Concentration of methanol varied from 1048 mg L⁻¹ in the AW2 brandy to 2485 mg L⁻¹ in TF1 brandy. This study showed that all five tested yeast varieties produce a small quantity of methanol irrespective of the nutrient.

Esters

Esters are mainly produced during alcohol fermentation by yeast in the reaction between alcohols and acids.²¹ Typically they have a “fruity” and “floral” descriptor, and contribute to fruity, sweet, apple, pineapple and floral odor in brandies.²² Ethyl acetate is the most common and typical ester in fruit brandy.²⁰ In small concentrations, they have floral notes but at high concentration, they can be very repulsive with the odor of solvent. The largest concentrations of ethyl acetate were found in sample SB2 (489 mg L⁻¹) and in CONT (367 mg L⁻¹) and the smallest amounts were present in sample AW1 (161 mg L⁻¹) and sample RF1 (174 mg L⁻¹). The presence of ethyl acetate makes a significant contribution to the volatile profile and taste impression of fruit brandies.¹⁵ Ethyl octanoate, which has a cooked fruit-like aroma,²² was detected in high concentrations in sample CONT, TF2 and TOP1 and smallest concentration in sample TF1 and AW1. Sample RF2 and TF1 contained higher concentrations of ethyl palmitate (ethyl hexadecanoate) (1.33 and 1.27 mg L⁻¹). Ethyl lactate (ethyl (S)-2-hydroxypropanoate) with a creamy and coconut profile²² was found in high concentrations in the samples CONT, TOP1 and TF2 (2.87–3.04 mg L⁻¹).

Acids

Volatile acids in brandy arise through the fermentation conditions, the nutrients levels and the yeast used.³ Among the identified acids, relatively high amounts of decanoic acid, dodecanoic acid, hexadecanoic and octanoic acid were present. Acetic acid, a product of the oxidation of acetaldehyde and ethanol,²³ was found in highest concentration in sample TF1 (0.59 mg L⁻¹) and the smallest concentration was found in sample RF1 (0.03 mg L⁻¹). A significant difference in the concentrations of decanoic acid, which imparts a fatty odor,²⁰ was found in sample TOP2 with 5.8 mg L⁻¹ and sample AW1 with 1.9 mg L⁻¹. The highest content of octanoic acid was found in sample TOP2 (3.2 mg L⁻¹).

Aldehydes and ketones

Aldehydes play an important role in providing the flavor characteristics of a wide range of food. The unsaturated aliphatic aldehydes tend to produce stronger aromas. Moreover, ketones are compounds rich in flavor.⁷ In alcoholic beverages, aldehydes and ketones arise by yeast promoted decarboxylation of pyru-

vate during alcoholic fermentation.²⁴ In this study, the employed yeast strains produced average amounts of acetaldehyde and benzaldehyde. Acetaldehyde is commonly present in many alcoholic beverages and in small concentrations has a fresh "fruity" odor.¹³ The highest content of this compound was found in sample AW1 (80 mg L^{-1}) while the other samples were characterized by a fairly uniform level of this compound ($39\text{--}62 \text{ mg L}^{-1}$). Yeast SB in sample SB1 and yeast Aroma white in sample AW2 produced the highest level of benzaldehyde (0.15 and 0.14 mg L^{-1} , respectively). This compound has an almond-like odor.²⁰

Terpenes and C₁₃-norisoprenoids

Terpenes and C₁₃-norisoprenoids have a very pleasant aroma and a very low olfactory threshold but are rich in flavor.⁷ This means that they are readily perceived, even at low concentrations.²² Due to this, they have a large influence on the organoleptic impression of brandy. In this study, many of these compounds were found, such as citronellol, eugenol, geraniol, limonen-10-ol, linalool, α -terpineol, β -pinene and γ -decalactone. According to Issanchou *et al.*, β -octalactone in apricot gives a fruity taste.²⁵ The concentrations of linalool, which is perceived as sweet, floral, petitgrain-like, were in the range between 3.79 mg L^{-1} in sample TOP2 and 5.77 mg L^{-1} in sample SB2. The highest content of geraniol was detected in sample TF1 in a quantity of 2.28 mg L^{-1} . α -Terpineol has a pleasant odor similar to that of mint²¹ and the highest concentration was found in sample TF1 (4.15 mg L^{-1}), while the lowest concentration was found in sample CONT. γ -Decalactone, which has an intensive peach flavor, was detected in uniform concentrations that ranged from 2.33 mg L^{-1} in sample AW1 to 2.93 mg L^{-1} in sample SB2. In general, terpenes and C₁₃-norisoprenoids are released from their non-odorous precursors (in the form of glycosides) in wine making from grapes. Their content in brandies are reported to be connected to the activity of β -glycosidase in the yeast strain.²¹ A large variation of these compounds among the tested samples probably indicated that the β -glycosidase activity varied significantly across the tested yeast strains.

Quantitative descriptive analysis of young apricot brandies

A professional tasting commission of three members made the tasting of all the obtained samples and the points they assigned are given in Table III. The attributes used by the tasting commission to define and classify the samples were taste, smell, color, clarity and distinction. The maximum score in the evaluation was 20 points.¹⁷ The best tasting results is a consequence of good balances of the quantities of aromatic compounds.

The Aroma white strain in combination with simple nutrients, sample AW1, and complex nutrients Nutriferm Arom, sample AW2, gave intermediate results in both cases. Sample AW1 on taste was clean with bitterness and small astrin-

gency and obtained 17.10 points and the eighth place. Sample AW2 was devoid of taste with astringency and bitterness and some unclean smell, which could be the result of a high content of benzaldehyde and pentanol. The tasting commission gave it 17.06 points and ninth place. In this case, it could be concluded that the type of nutrient did not have a large influence on the final products of fermentation with Aroma white strain.

TABLE III. Sensory assessment of the apricot brandies

Sample	Member of tasting commission			Average grade	Range
	1	2	3		
AW1	17.10	17.00	17.20	17.10	VIII
AW2	17.20	17.00	17.00	17.06	IX
RF1	17.25	17.30	17.30	17.28	VI
RF2	17.70	17.95	18.00	17.88	V
TF1	16.90	16.75	17.00	16.90	X
TF2	17.90	17.95	17.90	17.91	IV
SB1	18.40	18.35	18.30	18.35	I
SB2	17.95	18.05	18.05	18.02	II
TOP1	17.25	17.20	17.20	17.21	VII
TOP2	17.85	18.00	18.00	17.95	III
CONT	17.00	16.80	16.90	16.88	XI

Red fruit strain with diammonium phosphate, sample RF1, gave an average quality sample and took sixth place with 17.28 points. The sample had a clear note with some astringency. Better results were obtained with the complex nutrients Nutriferm Arom, sample RF2, even though the concentrations of ethyl acetate and amyl alcohols were the highest compared with the concentrations in the other samples, and the sample occupied fifth place with 17.88 points. The sample was with a clean typical smell and soft taste that could be a result of the high content of ethyl palmitate.

The yeast strain Top floral gave a low quality distillate using diammonium phosphate, sample TF1, which obtained 16.90 points in the tasting test (tenth place). On taste, the sample was without an intensive typical apricot smell, with herbal notes, which can be the results of high quantities of 2-methyl-1-propanol and geraniol. Using Nutriferm Arom, sample TF2 gave a middle quality distillate assessed with 17.91 (fourth place). On taste, this sample had a good balance between acidity and softness with less smell.

The gas chromatography analysis showed that Yeast strain SB with the simple nutrient diammonium phosphate, sample SB1, gave the lowest quantity of some compounds, such as esters and higher alcohols, in the distillate. On taste, this sample was clean, typical, with a slight impression of a sharp odor that was the consequence of a higher amount of benzaldehyde. The same yeast strain with complex nutrients Nutriferm Arom, sample SB2, gave a high amount of the vola-

tile compound, especially of ethyl lactate, ethyl butanoate, 1-butanol, isoamylalcohol (3-methyl-1-butanol), citronellol and linalool. In terms of sensor, this sample had a soft taste, good and rich typical smell, and the impression was that this was a very complex sample. The good balance of the volatile compounds ensured that these two samples were rated with the highest grades, first and second place, in the tasting test.

The yeast strain Top 15 with simple nutrients, sample TOP1, gave an intermediate result with the highest quantities of amyl alcohol and 1-propanol. This sample had some medicinal odor and a not good balance in taste. This distillate was on seventh place with 17.21 points. On the contrary, strain Top 15 with complex nutrients, sample TOP2, gave a high quality distillate with 17.95 points and was on third place. With high content of linalool, this sample had a very complex odor with floral notes and good balance.

Sample CONT was among the worst with higher concentration of ethyl acetate, 1-butanol, 1-hexanol and amyl alcohols. The sample had a hard taste with untypical notes on smell. The presence of wild microflora, which contained wild yeast, bacteria and fungi, resulted in this impression.

CONCLUSIONS

This paper presents an investigation of the influence of the yeast and nutrients on the total quality of apricot brandy. All chemical parameters for the quality of the obtained experimental apricot brandies complied with the standard of quality as prescribed by the regulations for alcoholic drinks quality.

The sensory qualities of the assessed apricot brandies indicated that the quality depended on the combination of yeast and nutrients. Nutriferm Arom, as complex nutrient, gave in all combinations better results than diammonium phosphate, a simple nutrient. The exception was the yeast strain SB that with simple nutrients gave the lowest amounts of some compounds, such as esters and higher alcohols, in the distillate and with better sensory results than the other sample. The best results were obtained with yeast strain SB with both nutrients and yeast strain Top 15 only with complex nutrients, which gave a high content of linalool. The control sample with no nutrients and selected yeast gave a distillate that was evaluated as having the worst quality with higher concentration of ethyl acetate, 1-butanol, 1-hexanol and amyl alcohols. This means that using selected yeast and nutrients in the production of apricot brandy gave better results than production without using selected yeast and nutrients.

SUPPLEMENTARY MATERIAL

Concentrations of the minor volatile compounds in the apricot brandies are available electronically from <http://www.shd.org.rs/JSCS/>, or from the corresponding author on request.

Acknowledgement. The authors acknowledge their gratitude to the Ministry of Education, Science and Technological Development of Republic of Serbia for financial support (Project No. 172053).

И З В О Д
УТИЦАЈ КВАСАЦА И ХРАНИВА НА КВАЛИТЕТ РАКИЈЕ КАЈСИЈЕВАЧЕ

ИВАН УРОШЕВИЋ¹, НИНОСЛАВ НИКИЋЕВИЋ¹, ЉУБИША СТАНКОВИЋ¹, БОБАН АНЂЕЛКОВИЋ²,
ТИЈАНА УРОШЕВИЋ¹, ГОРДАНА КРСТИЋ² и ВЕЛЕ ТЕШЕВИЋ²

¹Пољопривредни факултет у Београду, Немањина 6, 11080 Земун и ²Хемијски
факултет, Универзитет у Београду, Студентски трг 16, 11000 Београд

Пет сојева квасаца *Saccharomyces cerevisiae* и *S. bayanus* (SB, Top Floral, Top 15, Aroma White и Red Fruit) и два хранива, диамонијум-фосфат и *Nutriferm Arom*, испитивани су кроз њихов утицај на свежу ракију кајсијевачу, са посебним освртом на хемијске, испарљиве и сензорске карактеристике. Анализе главних и мање заступљених испарљивих компонената и сензорска анализа ракије кајсијеваче показују значајне разлике између узорака. Резултати сензорског оцењивања су рангирани између 16,88 за контролни узорак и 18,35 за узорак произведен са SB сојем квасаца и диамонијум-фосфатом као хранивом. Сви узорци ракије кајсијеваче испуњавају захтеве ЕУ у погледу садржаја метанола и других једињења као што су ацеталдехид, етил-ацетат и виши алкохоли.

(Примљено 25. јануара, ревидирано 13. марта, прихваћено 14. марта 2014)

REFERENCES

1. V. Greger, P. Schieberle, *J. Agric. Food Chem.* **55** (2007) 5221
2. N. I. Nikićević, *J. Agric. Sci.* **50** (2005) 183
3. N. Nikićević, R. Paunović, *The technology of spirit drinks*, University of Belgrade, Faculty of Agriculture, Belgrade, 2013, pp. 204–210 (in Serbian)
4. A. Querol, G. H. Fleet, *The Yeast Handbook – Yeasts in Food and Beverages*, Springer, Berlin, 2006, pp. 22–34
5. P. Satora, T. Tuszyński, *Food Microbiol.* **27** (2010) 418
6. A. M. Molina, V. Guadalupe, C. Varela, J. H. Swiegers, I. S. Pretorius, E. Agosin, *Food Chem.* **117** (2009) 189
7. Y. H. Hui, F. Chen, L. M. L. Nollet, *Handbook of Fruit and Vegetable Flavors*, Wiley, Hoboken, NJ, 2010, p. 534
8. W. G. Jennings, C. S. Tang, *J. Agric. Food Chem.* **15** (1967) 24
9. C.-S. Tang, W. G. Jennings, *J. Agric. Food Chem.* **16** (1968) 252
10. G. R Takeoka, R. E. Guichard, P. Schlich, S. Issanchou, *J. Food Sci.* **55** (1990) 735
11. E. Gomez, C. A. Ledbetter, *J. Sci. Food Agric.* **74** (1997) 541
12. N. Nikićević, V. Tešević, *Production of high quality fruit brandy*, University of Belgrade, Faculty of Agriculture, Belgrade, 2010, pp. 101–110
13. EEC Council Regulation No. 110/2008 of 15 January 2008, *Laying down general rules on the definition, description and presentation of spirit drinks*, Off. J. Eur. Union **L 39/16** (2008)

14. M. L. Silva, F. X. Malcata, G. De Revel, *J. Food Compos. Anal.* **9** (1996) 72
15. V. Tešević, N. Nikićević, A. Jovanović, D. Djoković, Lj. Vujišić, I. Vučković, *Food Technol. Biotechnol.* **43** (2005) 367
16. N. Nikićević, *J. Agric. Sci.* **50** (2005) 89
17. S. Patel, T. Shibamoto, *J. Food Compos. Anal.* **16** (2003) 469
18. G. Semb, *Percept. Psychophys.* **4** (1968) 335
19. N. Nikićević, V. Tešević, *Spirits analytics and practice*, Poljoknjiga, Belgrade, 2009, p. 20, 82 (in Serbian)
20. Y. Zhao, J. Li, B. Zhang, Y. Yu, C. Shen, P. Song, *J. Inst. Brew.* **118** (2012) 315
21. A. G. Panosyan, G. V. Mamikonyan, M. Torosyan, E. S. Gabrielyan, S. A. Mkhitaryan, M. R. Tirakyan, A. Ovanesyan, *J. Anal. Chem.* **56** (2001) 945
22. J. C. Bhardwaj, V. K. Joshi, *Nat. Prod. Rad.* **8** (2009) 452
23. T. Cabaroglu, M. Yilmaztekin, *J. Inst. Brew.* **117** (2011) 98
24. S. Issanchou, P. Schlich, E. Guichard, *Sci. Aliments.* **9** (1989) 351.



SUPPLEMENTARY MATERIAL TO
Influence of yeast and nutrients on the quality of apricot brandy

IVAN UROŠEVIĆ¹, NINOSLAV NIKIĆEVIĆ¹, LJUBIŠA STANKOVIĆ¹, BOBAN ANĐELKOVIĆ², TIJANA UROŠEVIĆ¹, GORDANA KRSTIĆ² and VELE TEŠEVIĆ^{2*}

¹Faculty of Agriculture, University of Belgrade, Nemanjina 6, 11080 Zemun, Serbia and

²Faculty of Chemistry, University of Belgrade, Studentski trg 16, 11000 Belgrade, Serbia

J. Serb. Chem. Soc. 79 (10) (2014) 1223–1234

TABLE S-I. Concentrations of the minor volatile compounds in the apricot brandies (mg L⁻¹)

Compound	AW1	AW2	RF1	RF2	TF1	TF2	SB1	SB2	TOP1	TOP2	CONT
Esters											
Benzyl acetate			2.37		2.59	2.55			2.55	2.02	2.63
Butyl acetate							8.21				
Ethyl 2-hydroxy- -3-methyl-butyrate	4.86	4.31	5.40	4.97	4.77	5.80	7.36	3.58	5.80	6.51	4.58
Ethyl 2-hydroxy- -hexanoate				1.59				3.24			
Ethyl benzoate	13.07	22.55	20.52	13.25	20.70	11.16	16.31	18.64	11.16	12.63	17.50
Ethyl butanoate	42.71	29.99	12.44	40.61	17.11	37.56	13.14	48.13	37.56	25.55	35.55
Ethyl (E)-cinnamate	24.16	36.77	35.22	32.06	29.20	38.36	26.26	38.74	38.36	41.09	33.81
Ethyl (Z)-cinnamate	9.70	11.50	10.50	10.18	7.47	10.19	11.19	5.85	10.19	8.07	6.97
Ethyl dodecanoate	2.69			3.80				6.75		6.75	4.76
Ethyl lactate	1670.7	1849.2	1851.1	1756.6	2059.4	2871.4	1700.0	1960.1	2871.4	1973.1	3041.1
Ethyl linolenate	29.93	42.69	48.10	1535.0	1812.1		52.65	66.75			80.18
Ethyl linoleate	7.35	38.29	9.90	31.31	49.31	34.52			34.52	29.23	64.30
Ethyl octanoate	39.88	56.34	82.40	51.59	27.33	90.69	49.76	82.17	90.69	49.50	1198.9
Ethyl oleate	262.4	604.6	419.4	564.1	799.2	783.3	539.7	613.0	783.3	464.3	537.0
Ethyl palmitate	379.9	403.5	46.4	1330.6	1272.5	1137.6	492.3	644.2	1137.6	32.9	711.8
Ethyl salicylate											13.0
Ethyl tetradecanoate	13.6	43.4	70.6	73.5	110.6	124.4			124.4	51.9	63.7
2-Phenylethyl acetate			43.9	16.4		43.9	39.4		39.4	16.4	21.3
Isoamyl acetate	69.4	299.7	212.9	355.7	156.3	387.0	254.7	552.2	387.0	320.1	634.7

*Corresponding author. E-mail: vtesevic@chem.bg.ac.rs

TABLE S-I. Continued

Compound	AW1	AW2	RF1	RF2	TF1	TF2	SB1	SB2	TOP1	TOP2	CONT
Esters											
Isoamyl lactate	28.1	50.9	0.0921	0.0831	0.3613	0.1110	0.1316	0.0370	0.1110	0.0864	0.0660
Methyl salicylate	0.2734				343.8			49.8			233.8
Alcohols											
1-Butanol	2806.7	2721.1	1246.6	1997.8	2265.4	1928.1	2607.9	3003.9	1928.1	2683.5	3.3729
2,6,6-Trimethyl- -1-cyclohexen-1- -ethanol	67.3	55.1	75.0	67.3	64.4	80.0	69.8	46.5	80.0	62.2	83.9
3-(Z)-Hexenol	68.0	110.4	90.6	115.3	190.5	119.0	146.8	144.2	119.0	171.4	88.0
3-(Z)-Octenol	59.4			105.1	71.3	93.9	80.7	93.4	24.6	80.7	83.9
3-(Z)-Nonenol				39.9	63.8	58.6	50.7		50.7	48.8	46.3
3-Methyl-2-butano- nol	57.5			30.9		37.8	48.9	28.6	52.6	48.9	53.9
3-Methyl-2- -buten-1-ol	41.9	51.2	36.4	53.3	47.7	52.6			52.6	55.9	59.9
3-Methylpen- tanol	45.5	51.9	41.6	49.9	42.6	45.8			45.8	69.1	85.4
4-(Z)-Decenol		63.7	53.6	70.8	90.7	79.2	58.3	62.8	79.2	80.3	63.3
4-Methyl pen- tanol	31.6	28.5	18.9			19.7			19.7	33.3	33.0
5-(Z)-Octenol					17.98						20.4
Benzyl alcohol	41.3	134.0	70.5			160.6		65.0	160.6	78.5	69.7
1-Decanol			46.6			39.6			39.6		29.6
2-Phenylethanol	5882.7	5474.4	4191.2	4340.5	95.0	4635.8	2980.6	4073.9	4635.8	2661.8	4911.8
1-Hexanol	2968.6	3100.1	2497.3	3043.2	2672.9	2621.9	2879.5	2742.2	2621.9	3556.4	3575.6
1-Heptanol				65.7		55.7			55.7		93.6
Isoamyl alcohol	210371	230716	138205	179959	157104	176370	192592	223657	176370	203089	253261
Isobutyl alcohol	44033	46752	15046	22482	35099	33460	36641	41785	33460	29637	52620
1-Nonanol	89.2	102.2	39.7	165.2	151.1	46.8	132.5	133.7	46.8	50.8	134.3
1-Octanol	170.2	120.1	160.0		165.3	151.7	131.0	153.5	151.7	196.2	241.6
1-Pentanol	272.1	307.9	210.0	249.5	246.3	221.1	284.1	276.0	221.1	301.9	350.6
1-Propanol	56543	58690	13480	24164	25300	27607	69457	71575	27607	43822	56553
Acids											
2-Methylbutano- nic acid			41.9	78.56	2113.7	19.1	1308.8		19.1	377.8	
Decanoic acid	1918.6	3535.1	5469	4584.3	5570.1	5041.8	4699.8	3943.5	5041.8	5809.8	3315.9
Dodecanoic acid	1547.9	2162.5	2527.5	2093.4	3074.8	2599.2	2199.1	2210.6	2599.2	2072.6	2625.6
2-Furanoic acid	52.0	66.3	84.5	95.2	102.1	120.5	51.6		120.5	137	61.8
Hexadecanoic acid	1222.7	935.0	1348.1	1747.7	2000.7	1513.9	907.2	848.6	1513.9	1340.7	1203.4
Octanoic acid	187.9	862.7	1887	2483.8	2807.9	1690	2628.2	1084.5	1690	3270.7	313.1
Acetic acid	40.2	43.9	30.4	214.2	590.6	44.2	395	80	44.2	37	110.6

TABLE S-I. Continued

Compound	AW1	AW2	RF1	RF2	TF1	TF2	SB1	SB2	TOP1	TOP2	CONT	
Aldehydes and ketones												
Benzaldehyde	56.3	142.5	67.9	123.5	98.8	135.2	156.7	51.8	135.2	84.4	113.7	
Furfural	818.3	441.3	687.4	663.1	1964.9	1312.2	873.6	756.3	1312.2	944.1	583.1	
3-Nonen-2-one	278.6	288.5	329.2	392.5	345	313.4	316.8	455.5	313.4	290.8	312.1	
Terpenes and C13-norisoprenoids												
Citronellol		333	352.3	386.2	298.3	285.4	197.4	358.2	285.4	342.2	88.6	
Dihydro- β -ionol	118	123.7	162	107.2	89	100.9	52.3	88.3	100.9	61	127.1	
Dihydro- β -ionone	219.6	139.7	132.1	189.6	178	129.7	149.4	216.1	129.7	127.4	171.6	
Eugenol	59.4	133.4	166.2	136.5	194.5	170.2	109.9	155.7	170.2	123	134.1	
Geraniol	1002.2	1004.3	1104	1933.7	2281.4	1046.2	1856.4	1248.2	1046.2	1463.9	980.9	
Limonen-10-ol	45.9	46.8	51.8	51.6	59.9	72.1			72.1	36.2	46.9	
(3 <i>R</i> ,6 <i>R</i>)-2,2,6-tri-methyl-6-vinyl-tetrahydro-2 <i>H</i> -pyran-3-ol				40.9		46.3	45.2			45.2	39.2	48.4
Linalool	4765.6	4427.5	4622.5	5325	4962.8	4393.7	5003.5	5769.3	4393.7	3798	4512.7	
Linalool oxide (epoxide)	148.3	128	27.7							27.6	30.9	
(3 <i>R</i> ,6 <i>S</i>)-2,2,6-tri-methyl-6-vinyl-tetrahydro-2 <i>H</i> -pyran-3-ol				159	198.2	308.8	211.4	193.9		211.4	182.4	148.3
Menthen-9-ol	93.9	88.4			93.2		126.1	69.3	169.7	126.1	80.4	122.3
Nerol	344	311.2	331.4	56.2	347.3	326.6	334.6	389.1	326.6	272.3	337.1	
α -Ionol	58.2		76.7	84.9	135.2	97.6	97.1	42.9	97.6	64.7	66.2	
α -Terpineol	2179.1	2281.9	2641	3077.8	4147.5	2744.4	2774.5	2751.5	2744.4	2439.8	2166	
β -Cyclocitral	86.3	102.9	155.2	133.1	43.4	111.7	123.8	92.2	111.7	155.1	102.2	
β -Pinene	93.7	120.1	120.7	134.1	164.1	150.3	86.2	118.1	150.3	89.9	125	
γ -Decalactone	2330.7	2349.4	2561.6	2606.9	2646.5	2691.6	2623.3	2935.9	2691.6	2803.3	2366.6	



Correlations between the *in vitro* antiproliferative activity, structure and thermal stability of some macrocyclic dinuclear Cu(II) complexes

SLADANA B. TANASKOVIĆ^{1#}, MIRJANA ANTONIJEVIĆ-NIKOLIĆ^{2#},
BERTA BARTA HOLLÓ^{3#}, BRANKA DRAŽIĆ^{1**}, TATJANA STANOJKOVIĆ⁴,
KATALIN MÉSZÁROS SZÉCSÉNYI^{3#} and GORDANA VUČKOVIC^{5#}

¹Faculty of Pharmacy, University of Belgrade, Vojvode Stepe 450, 11000 Belgrade, Serbia,

²Higher Technological School of Professional Studies 15000, Šabac, Serbia, ³Faculty of Sciences, University of Novi Sad, Trg Dositeja Obradovića 3, 21000 Novi Sad, Serbia,

⁴Institute for Oncology and Radiology of Serbia, Pasterova 14, 11000 Belgrade, Serbia and

⁵Faculty of Chemistry, University of Belgrade, Studentski trg 16, 11158 Belgrade, Serbia

(Received 4 April, revised 15 April, accepted 15 April 2014)

Abstract: Seven macrocyclic dinuclear Cu(II) complexes with tpmc = N,N',N'',N''' -tetrakis(2-pyridylmethyl)-1,4,8,11-tetraazacyclotetradecane of coordination formulae $[Cu_2tpmc](ClO_4)_4$ (**1**), $[Cu_2(X)tpmc](ClO_4)_3 \cdot nH_2O$, X = F⁻, n = 0 (**2**), X = Cl⁻, n = 1 (**3**), X = Br⁻, n = 0 (**4**), X = I⁻, n = 1 (**5**), X = NO₂⁻, n = 0 (**6**), $[Cu_2(NCS)_2tpmc](ClO_4)_2$ (**7**) were evaluated for their cytotoxic activity against human cervix adenocarcinoma (HeLa), human melanoma (Fem-x) and human colon carcinoma (LS174) cell lines. The results were compared with the corresponding data for the *cis*-diamminedichloroplatinum(II) (CDDP) as referent cytostatic, as well as with the free ligands and the solvent dimethyl sulfoxide (DMSO) as controls. The complexes showed considerable antiproliferative effect, although significantly less than CDDP. The thermal decomposition pattern of the complexes was determined by simultaneous TG/DSC measurements. The thermal stability of the compounds **2–7** followed the trend of their antiproliferative activity against the HeLa cell line, as well as their corresponding stability constants. The highest thermal stability and cytotoxicity belonged to complex $[Cu_2tpmc](ClO_4)_4$, with no anionic co-ligand. Complex $[Cu_2(NO_2)tpmc](ClO_4)_3$ exhibited a selective cytotoxicity against LS174 cells, at the level of the most active $[Cu_2tpmc](ClO_4)_4$.

Keywords: copper(II)complexes; octaazamacrocycles; antiproliferative activity; thermal analysis.

* Corresponding author. E-mail: bdrazic@pharmacy.bg.ac.rs

Serbian Chemical Society member.

doi: 10.2298/JSC140404044T

INTRODUCTION

The coordination chemistry of macrocyclic ligands has attracted much attention.¹ Macroyclic ligands coordinated with metal ions give stable complexes of different structures, and different catalytic, redox, *etc.* characteristics. They are applied as antitumor,² antiviral (including HIV activity),^{3,4} antibacterial, antifungal or antimarial agents.^{5–10} The clinical success of cisplatin in the treatment of several human malignant tumors motivated major research efforts toward the discovery of alternative metal complexes with potential anticancer activity^{11,12} but with fewer side effects. Copper is a physiologically important metal that plays a significant role in endogenous oxidative DNA damage associated with aging and cancer.¹³ For the past several decades, great effort has been devoted to binding studies of copper complexes with DNA.^{14–16} In particular, many studies were focused on binuclear copper complexes due to their presence in metalloproteinase as well as their affinity for DNA.^{17–22}

The ligand *N,N',N'',N'''*-tetrakis(2-pyridylmethyl)-1,4,8,11-tetraazacyclotetradecane (tpmc) has four pendant arms that could participate in coordination with metal ions.²³ Depending on the metal centre, the structure and the number of co-ligand(s), it forms mono-, bi- or tetra-nuclear complexes. Metal centers linked to tpmc are either *exo* or *endo*, or may be bridged with additional ligands or bound in the *trans* position (one for each metal ion). Numerous complexes containing various co-ligands have been previously described.^{24–29}

The aim of this study was to investigate the potential antiproliferative activity of seven macrocyclic binuclear Cu(II) complexes with or without co-ligands with the formulas: $[\text{Cu}_2\text{tpmc}](\text{ClO}_4)_4$ (**1**), $[\text{Cu}_2(\text{X})\text{tpmc}](\text{ClO}_4)_3 \cdot n\text{H}_2\text{O}$, $\text{X} = \text{F}^-$, $n = 0$ (**2**), $\text{X} = \text{Cl}^-$, $n = 1$ (**3**), $\text{X} = \text{Br}^-$, $n = 0$ (**4**), $\text{X} = \text{I}^-$, $n = 1$ (**5**), $\text{X} = \text{NO}_2^-$, $n = 0$ (**6**), $[\text{Cu}_2(\text{NCS})_2\text{tpmc}](\text{ClO}_4)_2$ (**7**), which were earlier described.³⁰

Thermal stability may be crucial in assessing the applicability of new compounds. Due to this, the thermal behavior of the ligand and the complexes are discussed in details in this article.

EXPERIMENTAL

Chemicals and materials

Macrocyclic ligand (tpmc),³¹ $\text{Cu}(\text{ClO}_4)_2 \cdot 6\text{H}_2\text{O}$,³² complex **1** ($[\text{Cu}_2\text{tpmc}](\text{ClO}_4)_4$)^{30a} and complexes **2–7** ($[\text{Cu}_2(\text{X})\text{tpmc}](\text{ClO}_4)_3 \cdot n\text{H}_2\text{O}$, $\text{X} = \text{F}^-$, $n = 0$ (**2**), $\text{X} = \text{Cl}^-$, $n = 1$ (**3**), $\text{X} = \text{Br}^-$, $n = 0$ (**4**), $\text{X} = \text{I}^-$, $n = 1$ (**5**), $\text{X} = \text{NO}_2^-$, $n = 0$ (**6**), $[\text{Cu}_2(\text{NCS})_2\text{tpmc}](\text{ClO}_4)_2$ (**7**))^{30b} were obtained and purified according to literature procedures*. All other chemicals were of p.a. grade and were used as supplied, except for recording electronic spectra, when acetonitrile (MeCN) for HPLC was used.

*Warning: perchlorate salts of metal complexes with organic ligands are potentially explosive and should be stored and handled with great caution!

Antiproliferative assay

Human cervix adenocarcinoma (HeLa), human melanoma (Fem-x) and human colon carcinoma (LS174) cell lines were obtained from the American Type Culture Collection (Manassas, VA, USA). All cancer cell lines were maintained in the recommended RPMI-1640 medium supplemented with 10 % heat-inactivated (56 °C) fetal bovine serum, L-glutamine (3 mM), streptomycin (100 mg mL⁻¹), penicillin (100 IU mL⁻¹), 25 mM HEPES and adjusted to pH 7.2 with bicarbonate solution. Cells were grown in a humidified atmosphere of 95 % air and 5 % CO₂ at 37 °C. Stock solutions (10 mM) of the compounds, made in DMSO, were dissolved in the corresponding medium to the required working concentrations. Neoplastic HeLa cells (2000 cells per well), Fem-x cells (5000 cells per well) and LS174 cells (7000 cells per well) were seeded into 96-well microtiter plates, and 24 h later, after cell adherence, five different, double diluted concentrations of the investigated compounds were added to the wells. The final concentrations applied to the target cells were: 200, 100, 50, 25 and 12.5 µM, except to the control wells, where only nutrient medium was added. The cultures were incubated for 72 h. The effect of compounds on cancer cell survival was determined by the MTT test according to Mosmann,³³ with modification by Ohno and Abe,³⁴ 72 h upon addition of the compounds, as was described earlier. Briefly, 20 µL of MTT solution (5 mg mL⁻¹ PBS) were added to each well. The samples were incubated for a further 4 h at 37 °C in a 5 % CO₂ humidified air atmosphere. Then, 100 µL of 10 % SDS were added to extract the insoluble product formazan, resulting from the conversion of the MTT dye by viable cells. The number of viable cells in each well was proportional to the intensity of the absorbance of light, which was then read in an ELISA plate reader at 570 nm. Absorbance (*A*) at 570 nm was measured 24 h later. To obtain cell survival (%), the *A* of a sample with cells grown in the presence of various concentrations of the investigated extracts was divided by the control optical density (the *A* of control cells, grown only in nutrient medium), and multiplied by 100. Absorbance, of the blank, *A_s*, was subtracted from the absorbance of the treated cells, *A_t*, of the corresponding sample with target cells. Concentration *IC*₅₀ was defined as the concentration of an agent inhibiting cell survival by 50 %, compared with a vehicle-treated control. All experiments were performed in triplicate. The cell survival (*S*) was calculated by the equation:

$$S (\%) = 100 \frac{(A_t - A_s)}{(A_c - A_s)}$$

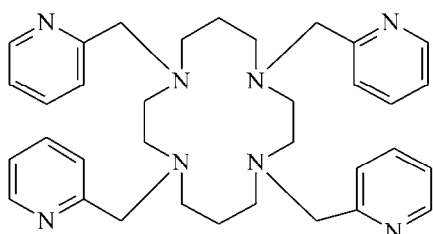
where *A_c* is the absorbance of the control.

Thermal analysis

Thermogravimetric (TG) measurements were performed on a simultaneous TGA/DSC thermal analyzer Q600 SDT (TA Instruments) using open alumina sample pans and the corresponding empty reference pan in a dynamic nitrogen atmosphere (flow rate: 100 cm³ min⁻¹). Sample mass: ≈1 mg; heating rate: 20 °C min⁻¹ and temperature range: up to 500 °C. For the evolved gas analysis (TGA/DTA-MS), an SDT 2960 Simultaneous TGA/DTA (TA Instruments Inc.) thermal analyzer and a Thermostar GSD 200 (Balzers Instruments) quadrupole mass spectrometer were coupled. Measurements data: open platinum crucible, *m* ≈ 2 mg, heating rate: 10 °C min⁻¹, heated capillary connection (*t* = 200 °C, methyl deactivated fused silica capillary tube, $\phi = 0.15$ mm).

RESULTS AND DISCUSSION

Binuclear Cu(II) complexes **1–7** were prepared and purified according to described procedures.³⁰ All the tested Cu(II) complexes are binuclear wherein the macrocycle is *exo*-bonded to the metal ions. The structure of the tpmc ligand is presented in Scheme 1 while the structures of selected complexes are presented in Scheme 2a–c. As can be seen, each Cu(II) is coordinated to two nitrogen atoms of the cyclam ring and to two nitrogens from the two 2-pyridylmethyl groups of the macrocyclic ligand. For complexes **1** and **7** (Scheme 2a and c), the chair conformation was found.³⁰ In **7**, an NCS[–] ligand is bonded in the *trans* position to each copper(II) ion (Scheme 2c). In complexes **2–6**, only one monovalent anion is coordinated to the binuclear complex cations. Due to the coordinated co-ligand anions, the complex cations have different charges: 4+ in **1**, 3+ in complexes **2–6** and 2+ in **7**. For complexes with F[–] (**2**) and Cl[–] (**3**) co-ligands, X-ray analysis confirmed the bridged coordination of the fluoride and chloride with Cu(II) that is *exo*-coordinated with respect to the cyclam ring in the boat conformation (Scheme 2b).^{30b} For the complexes containing Br[–], I[–] and NO₂[–], the same coordination mode is proposed based on their analytic data, and physical and chemical properties.^{30b}

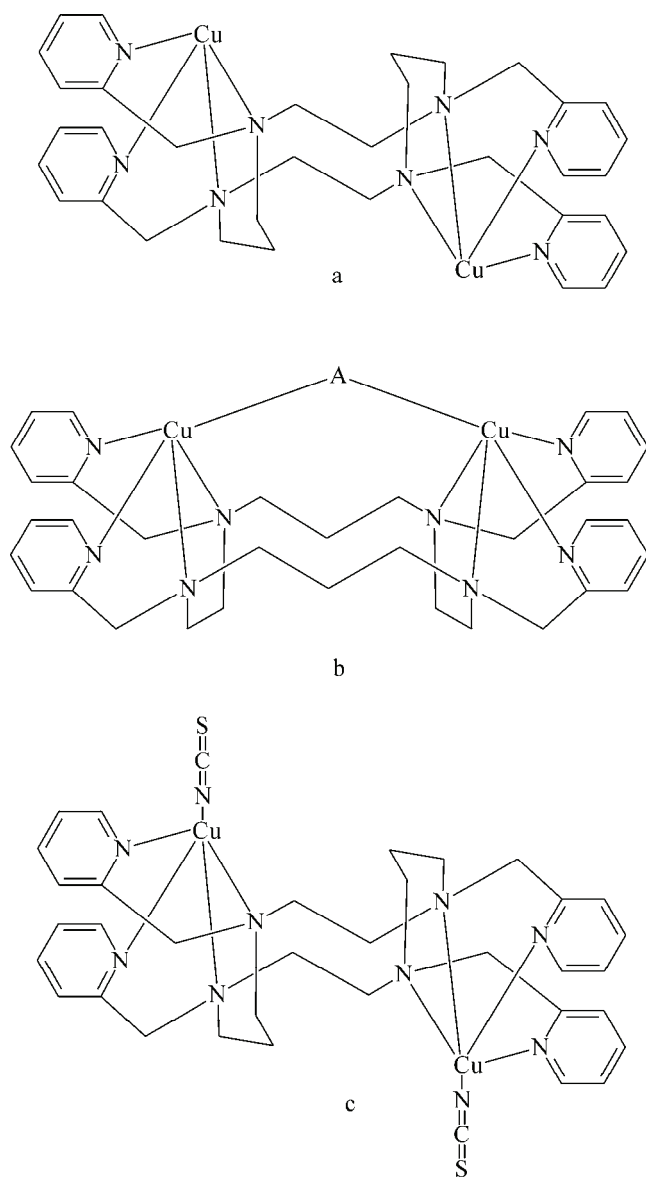


Scheme 1. Ligand *N,N',N'',N'''*-tetrakis(2-pyridylmethyl)-1,4,8,11-tetraazacyclotetradecane (tpmc).

The *in vitro* antiproliferative activity of the compounds **1–7**, tpmc, Cu(ClO₄)₂·6H₂O, co-ligands **2a–7a** and DMSO was tested against HeLa, Fem-x and LS174 cell lines and with *cis*-diamminedichloroplatinum(II) (CDDP) as the referent cytostatic by the MTT colorimetric assay method. The IC₅₀ values of the complexes were in the range 17.7–133.4 μM for the Cu(II) complexes against all the tested cell lines, while they were in the range 2.1–7.8 μM for CDDP. The tpmc ligand, Cu(ClO₄)₂·6H₂O and the free co-ligands showed significantly lower activity (IC₅₀ > 200 μM).

The order of sensitivity of various cell lines to antiproliferative action of the complexes was cervix adenocarcinoma HeLa > colon carcinoma LS174 > melanoma Fem-x. In contrast, ligands used in doses from 0–200 μM were ineffective (IC₅₀ > 200 μM) against the same cell lines. Only **2a** showed a moderate antiproliferative activity against all the tested lines, while **3a**, **4a** and **7a** exhibited very weak activity against HeLa cells. Generally, complexes **1–7** showed marked

effects compared to those of the ligands. Complex **1** showed remarkable cytotoxicity towards all three cell lines (Table I). The cytotoxic curves from the MTT assay showing the survival of HeLa, Fem-x and LS174 cells grown for 72 h in the presence of increasing concentrations of complexes **1** and **2** are depicted in Fig. 1a and b, respectively.



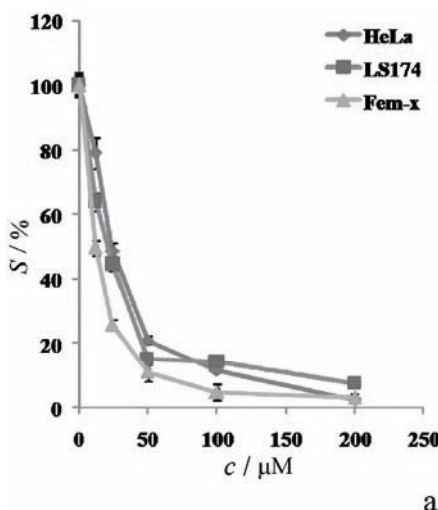
Scheme 2. Structure of the complex cation in the Cu(II) complexes: **1** (a), **2–6**, X = F⁻, Cl⁻, Br⁻, I⁻ or NO₂⁻ (b) and **7** (c).

TABLE I. Results of the MTT (IC_{50} / μM) analysis for Cu(II) tpmc complexes (**1–7**), $\text{Cu}(\text{ClO}_4)_3 \cdot 6\text{H}_2\text{O}$, free ligand (tpmc), compounds **2a–7a** and CDDP; tpmc = *N,N',N'',N'''*-tetrakis(2-pyridylmethyl)-1,4,8,11-tetraazacyclotetradecane; CDDP = *cis*-diammine-dichloroplatinum(II)

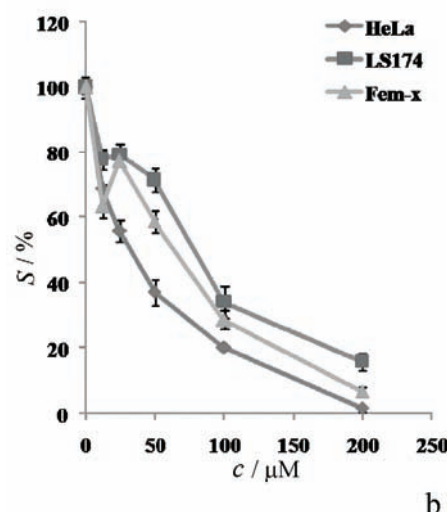
Compound	HeLa	Fem-X	LS174
$[\text{Cu}_2\text{tpmc}](\text{ClO}_4)_4$ (1)	19.0±0.3	17.7±2.3	22.0±0.5
$[\text{Cu}_2(\text{F})\text{tpmc}](\text{ClO}_4)_3$ (2)	35.9±3.0	66.8±2.4	79.2±0.4
$[\text{Cu}_2(\text{Cl})\text{tpmc}](\text{ClO}_4)_3 \cdot \text{H}_2\text{O}$ (3)	46.9±0.4	104.5±2.4	86.0±1.6
$[\text{Cu}_2(\text{Br})\text{tpmc}](\text{ClO}_4)_3$ (4)	48.3±2.9	72.9±3.9	75.5±1.4
$[\text{Cu}_2(\text{I})\text{tpmc}](\text{ClO}_4)_3$ (5)	45.0±3.4	79.0±1.9	57.9±0.2
$[\text{Cu}_2(\text{NO}_2)\text{tpmc}](\text{ClO}_4)_3$ (6)	51.4±4.1	133.4±4.0	22.1±0.2
$[\text{Cu}_2(\text{NCS})_2\text{tpmc}](\text{ClO}_4)_2$ (7)	61.0±0.9	103.5±0.6	51.8±0.1
$\text{Cu}(\text{ClO}_4)_2 \cdot 6\text{H}_2\text{O}$, tpmc	>200	>200	>200
NaF (2a)	91.5±1.0	76.5±4.1	148.3±6.1
NaCl (3a)	186.2±3.8	>200	>200
KBr (4a)	186.9±1.3	>200	>200
KI (5a) NaNO ₂ (6a)	>200	>200	>200
KSCN (7a)	108.5±4.0	>200	>200
CDDP	2.1±0.2	3.2±0.4	7.8±0.3

Complex **2** had the highest activity against the HeLa cell line. Complexes **3–6** showed decreasing activity in the series $\text{I}^- > \text{Cl}^- > \text{Br}^- > \text{NO}_2^-$. The order of the cytotoxicity of the complexes in the case of the HeLa cell line could be related to the corresponding stability constants.^{30b} The lowest stability constants exhibited **5** (with I^- , $\log K = 2.76$) and **2** (with F^- , $\log K = 3.03$), in agreement with the Pearson Theory.^{35,36} Copper(II), as a transition acid, forms stable complexes with transition bases, in the present case with Br^- , Cl^- and NO_2^- ($\log K = 3.77$, 4.80, 4.20, respectively). When comparing the IC_{50} values for the HeLa cell line, it is clear that the least stable complexes had the highest activity, *i.e.*, the complexes with the hardest (F^-) and softest (I^-) bases acting as co-ligands. The cytotoxic effects of the complexes towards Fem-x and LS174 (IC_{50} 55–135 μM) were significantly lower than towards the HeLa cell line. An increasing order of cytotoxicity was observed with increasing ionic radii going from Cl^- to I^- in the case of LS174 cell line. However, complex **6** with an NO_2^- co-ligand showed a significantly higher activity against LS174 compared to the other complexes in all other cell lines. While complex **1** exhibited a rather high cytotoxicity against all three cell lines (IC_{50} 18–22 μM), complex **6** had a selective cytotoxicity towards the LS174 cell line, comparable with that of **1**.

The cytotoxic effect of the complexes partly originates from their amphiphilic nature, which bestows on them the capacity to penetrate easily the cell membrane. However, the mechanism of the cytotoxicity of the complexes in the different cell lines is obviously different and might involve changes in the energy or hypoxic status³⁷ in the microenvironment of cancer cell and other factors.



a



b

Fig. 1. Representative graph showing survival of HeLa, LS174 and Fem-x cells grown for 72 h in the presence of increasing concentrations of complexes: a) **1** and b) **2**.

Thermal methods have a special place in the characterization of samples with biological activity.^{38–41} Namely, some of these compounds may be the active ingredients of newly developed drugs. Therefore, much attention has been paid to the thermal properties of these compounds.

The thermal decomposition of all the complexes was continuous. As complex **3** is a crystal hydrate, the first change in the TG curve resulted from loss of the crystal water. The water evaporation occurred at a steady rate up to the onset of complex decomposition at 264 °C. The amount of water lost was more than that calculated based on the stoichiometric composition (exp.: ≈3 %, calcd.: 1.73 %).

According to the stepwise isothermal (SWI) curve, this mass loss involves at least three steps referring to the different characters of the interactions of water or to solvent residue (MeCN) within the crystal of **3**. Except for **1**, the TG curves show a small mass loss up to the decomposition temperature in all complexes. The mass loss in these compounds may be related to strongly bonded water (< 2 %) or the consequence of residual solvent. When the samples were kept in a desiccator, the hygroscopic water could be partially eliminated. However, in **2**, **3** and **5** some mass loss (< 2 %) was detected even after drying over anhydrous CaCl_2 . By coupled TG–MS measurements, no traces of MeCN were found and the mass loss belonged exclusively to water evaporation. It is important to note that SWI curves show that on isothermal heating at around 120 °C, all the compounds lost moisture completely.

The thermal stability of the compounds increased in order of **7** < **6** ≈ **5** < **4** < **3** ≈ **2** < **1** from 203 °C in **7** to 282 °C onset in **1**. The decomposition is presented in Figs. 2 and 3 by the corresponding DTG curves. For all the complexes, the decomposition was accompanied by a highly exothermic effect, which was expected and is primarily due to the presence of the perchlorate ion. As the course of the DSC curves agreed with the course of the corresponding DTG curves, only the DTG curves are presented. In compounds with halide ligands, the rate of decomposition decreases with decreasing electronegativity of the halide. The exothermic effect of the reactions decreased in the same order. The decomposition of complexes **2** and **3** (with F^- and Cl^- co-ligands) is seemingly a one-step process. Starting from the bromide complex, fragmentation of the ligand

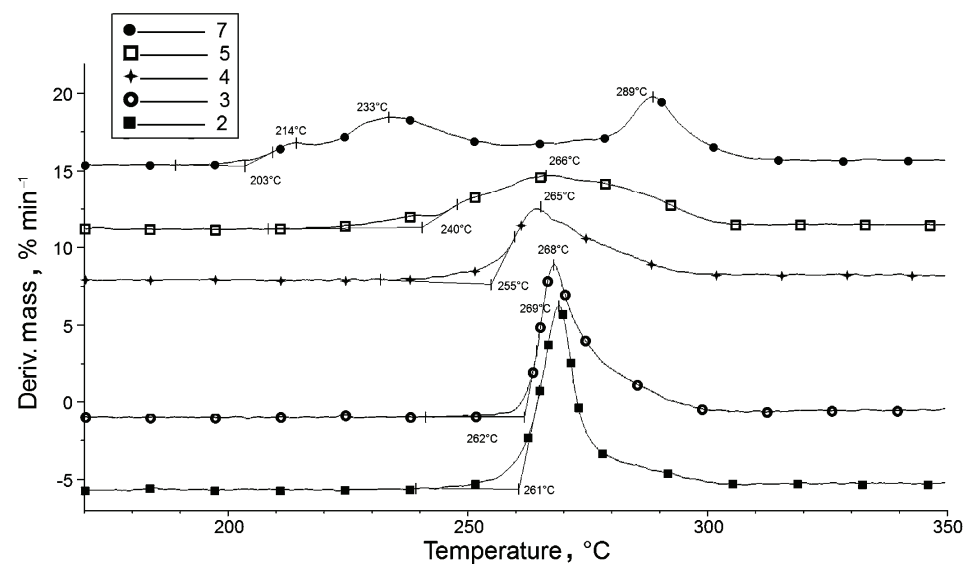


Fig. 2. DTG curves of compounds **2**–**5** and **7**.

is observable. In the complex with the two NCS⁻ (**7**), the decomposition steps are clearly separated (see Fig. 2).

In Fig. 3, the DTG curves of compound without a co-ligand (**1**) and with a coordinated oxoanion (NO₂⁻, **6**) are presented together with the corresponding curves of the most and the least stable (pseudo)halido complexes (**2** and **7**). As can be seen in Fig. 2, the thermal stability of **1** is by far the highest. The enthalpy of its decomposition is about the same as that for **2**. The thermal stability and the decomposition pattern of **6** with nitrito ligand are similar to the corresponding ones in **5**. These facts refer to the role of the coordinated anion in decreasing thermal stability of the complexes. Moreover, the thermal stability can be related to the stability constants of the compounds and is in accordance with the Pearson Hard and Soft Acids and Bases (HSAB) principle.^{35,36}

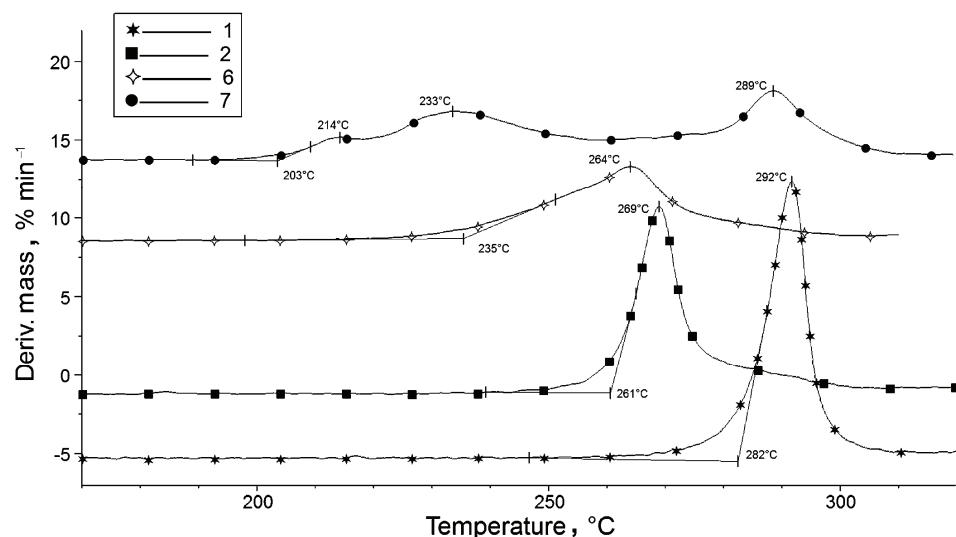


Fig. 3. Comparison of the DTG curves for compounds **1** and **6** with those for compounds **2** and **7**.

The thermal stability of the compounds and the corresponding *IC*₅₀ values against HeLa cell line are presented in Fig. 4. As can be seen, the course of the curves is very similar and with decreasing thermal stability, the antiproliferative activity of the complexes decreases. When comparing the cytotoxic activity of the compounds against HeLa cells, it seems as if the dissociation of the molecule plays an important role in cytotoxicity. Namely, by dissociation of the co-ligand of the compounds **2–7**, complex **1** with the highest cytotoxicity is formed. The easier is the dissociation, the higher is the activity of the compound. In addition, on dissociation a conversion from the boat to the chair conformation is expected. As the thermal stability of the compounds depends on the least stable bond in the

molecule, it could be assumed that the thermal decomposition in complexes **2–7** starts with the loss of the co-ligand/s*. It could be expected, therefore, that with decreasing thermal stability, the cytotoxicity would increase. However, experimental data confirmed just the opposite, *i.e.*, with decreasing thermal stability, the cytotoxicity also decreased. This seemingly contradictory observation could be explained by changes in the rigidity^{30b} of the complex molecules and/or to reduced possibility of H-bond formation by the coordination of the co-ligands. Therefore, the conformation of the molecule may significantly affect the interactions of the complexes with HeLa cells.

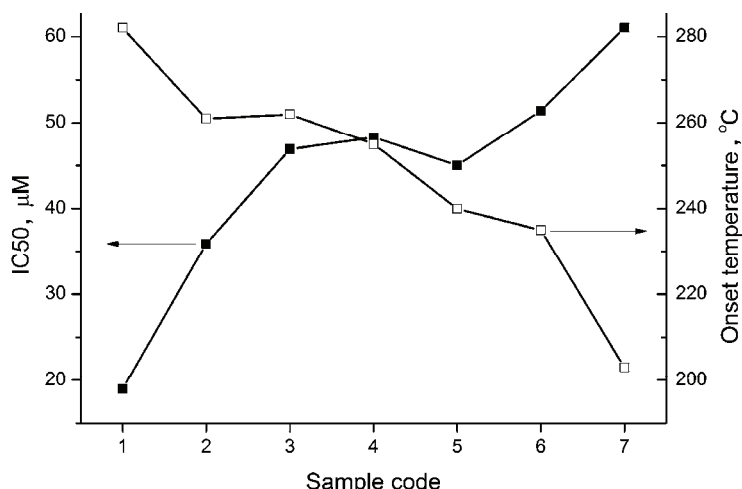


Fig. 4. Comparison of the thermal stability and the antiproliferative activity of compounds **1–7**.

The activity of the compounds against the human melanoma (Fem-x) and human colon carcinoma (LS174) cell lines indicate different reaction routes and compound **6** with nitrito co-ligand showed a high selectivity toward LS174 cells.

CONCLUSIONS

The significantly higher thermal stability of **1** and its significantly higher cytotoxicity could be related to both the electronic and steric factors. Additional coordination of the co-ligands decreases the charge on the complex cation. The charge distribution in the molecule depends on the co-ligand, and may have a role in decreasing antiproliferative activity. In addition, the bridging of the two metal centers by one co-ligand modifies the geometry of the entire molecule, and the chair conformation of **1** is converted to the boat conformation in the other complexes, except in **7** in which the two NCS[–] ligands are bonded in the *trans* configuration. The decrease in the thermal stability and stability constants of

*Unfortunately, due to the presence of perchlorates, the rate of the decomposition was too high, so the detection of the fragments belonging to the co-ligands was not possible.

compounds **2–7** is in accordance with the HSAB principle. However, the cytotoxicity of the compounds against the HeLa cell line with decreasing thermal stability also decreased, inferring the importance of the steric factors in the interaction of the complexes with the target cells. With the other two cell lines, the antiproliferative activities of the complexes were lower than that observed for **1**, except for **6** with a coordinated nitrite ion that exhibits a selective cytotoxicity against LS174 cell line that is comparable with the cytotoxicity observed for **1**.

Acknowledgements. We gratefully acknowledge the Ministry of Education, Science and Technological Development of the Republic of Serbia (Project Nos. 172014 and 175011) for the financial support. Dr. I. M. Szilágyi (Budapest University of Technology, Department of Inorganic and Analytical Chemistry) is acknowledged for the TG/DTA–MS measurements.

ИЗВОД
КОРЕЛАЦИЈА ИЗМЕЂУ *IN VITRO* АНТИПРОЛИФЕРАТИВНЕ АКТИВНОСТИ,
СТРУКТУРЕ И ТЕРМИЧКЕ СТАБИЛНОСТИ НЕКИХ МАКРОЦИКЛИЧНИХ
ДИНУКЛЕАРНИХ Cu(II) КОМПЛЕКСА

СЛАЂАНА Б. ТАНАСКОВИЋ¹, МИРЈАНА АНТОНИЈЕВИЋ-НИКОЛИЋ², ВЕРТА ВАРТА ХОЛЛО³, БРАНКА
ДРАЖИЋ¹, ТАТЈАНА СТАНОКОВИЋ⁴, КАТАЛИН МЕШАРОС СЗЕСЕНЬИ и ГОРДАНА ВУЧКОВИЋ⁵

¹Фармацеутички факултет, Универзитет у Београду, Војводе Степе 450, 11000 Београд, ²Висока
школа струковних студија, Хајдук Вељкова 10, 15000 Шабац, ³Природно-математички факултет,
Универзитет у Новом Саду, Трг Доситеја Обрадовића 3, 21000 Нови Сад, ⁴Институт за онкологију и
радиологију Србије, Пасцирова 14, 11000 Београд, ⁵Хемијски факултет, Универзитет у Београду,
Студентски трг 16, 11158 Београд

За седам макроцикличних динуклеарних Cu(II) комплекса са *N,N',N'',N'''*-тетра-
кис(2-пиридилметил)-1,4,8,11-тетраазациклотетрадеканом (tpmc) формуле [Cu₂tpmc]
(ClO₄)₄ (**1**), [Cu₂(X)tpmc](ClO₄)₃·nH₂O, X= F⁻, n = 0 (**2**), X = Cl⁻, n = 1 (**3**), X = Br⁻, n = 0 (**4**),
X= I⁻, n = 1 (**5**), X = NO₂⁻, n = 0 (**6**), [Cu₂(NCS)₂tpmc](ClO₄)₂ (**7**) испитивана је њихова
цитотоксичност на хуманим малигним ћелијским линијама: цервикалног аденокарци-
нома (HeLa), меланома (Fem-x) и хуманог карцинома дебелог превра (LS174). Резултати
су упоређени са одговарајућим подацима за *cis*-диамминдицхлоридоплатину (II) (CDDP)
као референтним цитостатиком (слободни лиганди и растворач DMSO су били кон-
тролни). Комплекси су показали значајно антипролиферативно дејство, иако знатно
мање него CDDP. Термичка разградња комплекса је одређена TG/DSC мерењем. Тер-
мичка стабилност једињења **2–7** прати тренд њихове антипролиферативне активности
према HeLa ћелијској линији, као и њихове одговарајуће константе стабилности. Нај-
већу термичку стабилност и цитотоксичност има комплекс **1** без анионског колиганда.

(Примљено 4. априла, ревидирано 15. априла, прихваћено 15. априла 2014)

REFERENCES

1. P. A. Vigato, S. Tamburini, *Coord. Chem. Rev.* **248** (2004) 1717
2. W. Sibert, A. H. Cory, J. G. Cory, *J. Chem. Soc. Chem. Commun.* (2002) 154
3. S. J. Paisey, P. J. Sadler, *J. Chem. Soc. Chem. Commun.* (2004) 306
4. X. Liang, J. A. Parkinson, M. Weishaupl, R. O. Gould, S. J. Paisey, H. Park, T. M. Hunter, C. A. Blidauer, S. Parsons, P. J. Sadler, *J. Am. Chem. Soc.* **124** (2002) 9105
5. Z. Iakovidou, A. Papageorgiou, M. A. Demertzis, E. Mioglou, D. Mourelatos, A. Kotsis, P. N. Yadav, D. Kovala-Demertzzi, *Anti-Cancer Drugs* **12** (2002) 65

6. J. Patole, S. Dutta, S. Pathye, E. Sinn, *Inorg. Chim. Acta* **318** (2001) 207
7. R. I. Maurer, P. J. Blower, J. R. Dilworth, C. A. Reynolds, Y. Zheng, G. E. D. Mullen, *J. Med. Chem.* **45** (2002) 1420
8. A. R. Cowly, J. R. Dilworth, P. S. Donnelly, E. Labisbal, A. Sousa, *J. Am. Chem. Soc.* **124** (2002) 5270
9. M. B. Ferrari, F. Bisceglie, G. Pelosi, M. Sassi, P. Tarasconi, M. Cornia, S. Capacchi, R. Albertini, S. Pinelli, *J. Inorg. Biochem.* **90** (2002) 113
10. E. M. Jouad, X. D. Thanh, G. Bouet, S. Bonneau, M. A. Khan, *Anticancer Res.* **22** (2002) 1713
11. M. A. Jakupc, M. Galanski, V. B. Arion, C. G. Hartinger, B. K. Keppler, *Dalton Trans.* **14** (2008) 183
12. S. Francisco, M. Fernanda, I. C. Santos, P. António, S. R. António, R. José, S. Isabel, *J. Inorg. Biochem.* **104** (2010) 52
13. B. N. Ames, M. K. Shigenaga, T. M. Hagen, *Proc. Natl. Acad. Sci. USA* **90** (1993) 7915
14. Q. Cheng, H. Zhou, Z. Pan, J. Chen, *Transition Met. Chem.* **37** (2012) 407
15. D. R. McMillin, K. M. McNett, *Chem. Rev.* **98** (1998) 1201
16. P. R. Reddy, A. Shilpa, *Indian J. Chem., A* **49** (2010) 1003
17. Q. Q. Zhang, F. Zhang, W. G. Wang, X. L. Wang, *J. Inorg. Biochem.* **100** (2006) 1344
18. A. M. Thomas, G. Neelakanta, S. Mahadevan, M. Nethaji, A. R. Chakravarty, *Eur. J. Inorg. Chem.* (2002) 2720
19. J. Z. Wu, H. Li, J. G. Zhang, J. H. Xu, *Inorg. Chem. Comm.* **5** (2002) 71
20. A.M. Thomas, M. Nethaji, A. R. Chakravarty, *J. Inorg. Biochem.* **98** (2004) 1087
21. J. Z. Wu, L. Yuan, J. F. Wu, *J. Inorg. Biochem.* **99** (2005) 2211
22. W.-J. Zhang, F. Wang, Y.-T. Li, Z.-Y. Wu, *Transition Met. Chem.* **38** (2013) 69
23. S.-G. Kang, S.-J. Kim, *Bull. Korean Chem. Soc.* **24** (2003) 269 and references cited therein
24. G. Vučković, D. Opsenica, S. P. Sovilj, D. Poleti, *J. Coord. Chem.* **47** (1999) 331
25. G. Vučković, D. Opsenica, S. P. Sovilj, D. Poleti, M. Avramov-Ivić, *J. Coord. Chem.* **42** (1997) 241
26. S. P. Sovilj, G. Vučković, K. B. Babić-Samardžija, N. Matsumoto, V. M. Jovanović, J. Mrožinski, *Synth. React. Inorg. Met.-Org. Chem.* **29** (1999) 785
27. G. Vučković, V. Stanić, S. P. Sovilj, M. Antonijević-Nikolić, J. Mrožinski, *J. Serb. Chem. Soc.* **70** (2005) 1121
28. G. Vučković, M. Antonijević, D. Poleti, *J. Serb. Chem. Soc.* **67** (2002) 677
29. S. B. Tanasković, G. Vučković, M. Antonijević-Nikolić, T. Stanojković, G. Gojgić-Cvijović, *J. Mol. Struct.* **1029** (2012) 1
30. a) E. Asato, H. Toftlund, S. Kida, M. Mikuriya, K. S. Murray, *Inorg. Chim. Acta* **165** (1989) 207; b) G. Vučković, E. Asato, N. Matsumoto, S. Kida, *Inorg. Chim. Acta* **171** (1990) 45
31. S. Chandrasekhar, W. L. Waltz, L. Prasad, J. W. Quail, *Can. J. Chem.* **75** (1997) 1363
32. R. Portillo, L. Albertola, *An. Soc. Esp. Fis. Quim.* **28** (1930) 1117
33. T. Mosmann, *J. Immunol. Methods* **65** (1983) 55
34. M. Ohno, T. Abe, *J. Immunol. Methods* **145** (1991) 199
35. R. G. Pearson, *J. Chem. Educ.* **64** (1987) 561
36. B. Holló, Z. D. Tomić, P. Pogány, A. Kovács, V. M. Leovac, K. Mészáros Szécsényi, *Polyhedron* **28** (2009) 3881
37. D. C. Ware, B. D. Palmer, W. R. Wilson, W. A. Denny, *J. Med. Chem.* **36** (1993) 1839
38. D. Tita, T. Jurca, A. Fulias, E. Marian, B. Tita, *J. Therm. Anal. Calorim.* **112** (2013) 407

39. R. Cássia da Silva, F. S. Semaan, Cs. Novák, E. T. G. Cavalheiro, *J. Therm. Anal. Calorim.* **111** (2013) 1933
40. M. L. Dianu, A. Kriza, A. M. Musuc, *J. Therm. Anal. Calorim.* **112** (2013) 585
41. L. Findoráková, K. Győryová, D. Hudecová, D. Mudroňová, J. Kovářová, K. Homzová, F. A. N. El-Dien, *J. Therm. Anal. Calorim.* **111** (2013) 1771.



Sorption of different phenol derivatives on a functionalized macroporous nanocomposite of poly(glycidyl methacrylate-*co*-ethylene glycol dimethacrylate) and acid modified bentonite

SANJA R. MARINOVIC^{1*}, ALEKSANDRA D. MILUTINOVIC-NIKOLIC^{1#},
ALEKSANDRA B. NASTASOVIC², MARIJA J. ZUNIĆ¹, ZORICA M. VUKOVIĆ¹,
DUŠAN G. ANTONOVIC³ and DUŠAN M. JOVANOVIĆ¹

¹University of Belgrade - Institute of Chemistry, Technology and Metallurgy, Center for Catalysis and Chemical Engineering, Njegoševa 12, Belgrade, Serbia, ²University of Belgrade - Institute of Chemistry, Technology and Metallurgy, Department of Chemistry, Njegoševa 12, Belgrade and ³University of Belgrade, Faculty of Technology and Metallurgy, Kardeljeva 4, Belgrade, Republic of Serbia

(Received 6 February, revised 11 April, accepted 14 April 2014)

Abstract: Macroporous nanocomposite of poly(glycidyl methacrylate-*co*-ethylene glycol dimethacrylate) and acid modified bentonite was prepared by radical suspension copolymerization. Nanocomposite was functionalized with diethylenetriamine (DETA), by ring-opening reaction of the pendant epoxy groups. Functionalization was performed in order to enable phenol derivatives sorption. This new, not sufficiently investigated material, with developed porous structure was denoted CP-S_A-DETA. In this study, the influence of temperature on 4-nitrophenol (4NP) sorption on CP-S_A-DETA was investigated. The chemisorption was estimated as dominant process since activation energy of sorption of 4NP of 54.8 kJ mol⁻¹ was obtained. After determining the optimal sorption conditions for 4NP, the sorption of 2-nitrophenol (2NP) and 2-chloro-4-nitrophenol (2Cl4NP) on CP-S_A-DETA was investigated with respect to pH, initial concentration and contact time. The 2NP sorption was seldom tested, while according to our knowledge, the 2Cl4NP sorption was not investigated. The isotherm data were best fitted with Langmuir model, while the sorption dynamics obeyed the pseudo-second-order kinetic model for all derivatives.

Keywords: functionalized nanocomposite; wastewater sorbent; 4-nitrophenol; 2-nitrophenol; 2-chloro-4-nitrophenol.

* Corresponding author. E-mail: sanja@nanosys.ihtm.bg.ac.rs
Serbian Chemical Society member.
doi: 10.2298/JSC140206043M

INTRODUCTION

Phenol and its derivatives are harmful to organisms even at low concentrations,^{1,2} which qualifies them as priority pollutants. Many have been classified as hazardous pollutants because of their potential harm to human health.^{3,4} The US Environmental Protection Agency (EPA) limited the quantity of phenols in wastewater to 1 mg dm⁻³.^{1,2,5} The removal of phenolic compounds from wastewater before discharge into water bodies is a necessity in order to reduce their side effects on the environment and human health.^{6,7}

Phenolic compounds are widely found in the wastewaters from pesticide, pharmaceutical, petroleum, petrochemical and other industries.^{2,8}

The available concentration data regarding industrial wastewaters are generally expressed as the total concentration of phenols and they depend on the plant potentiality and operating conditions. The total concentrations of phenols in the wastewaters of some chemical industries were as follows: phenolic resin production, ≈400 mg dm⁻³; refineries, < 50 mg dm⁻³; naphthalenic acid production, 12 mg dm⁻³ and shale dry distillation, ≈200 mg dm⁻³.^{9,10}

Conventional processes that are used for the removal of phenol and its derivatives from wastewaters are biodegradation,^{11,12} liquid membrane processes,^{13–15} electrochemical oxidation,¹⁶ photocatalytic degradation¹⁷ and adsorption.^{18–20}

Adsorption is being employed extensively for the removal of phenol and its derivatives from aqueous solutions.^{18–20} Activated carbons as adsorbents for the removal of phenolic compounds are the most widely used method for water treatment.²¹ However, the use of effective commercial activated carbons based on relatively expensive starting materials, such as wood and coal, lead to limitation in their application in the pollution sector.⁵ Other adsorbents used for the removal of phenols from wastewaters are: zeolites,² bentonites,^{3,22} organo-modified bentonites,²³ synthetic resins,²⁴ and different polymeric materials.^{25–27} In the past few decades, polymeric adsorbents have been used as an alternative to activated carbon in terms of high surface area and improved mechanical rigidity. Macroporous poly(glycidyl methacrylate-*co*-ethylene glycol dimethacrylate)s have been used for the removal of organic pollutants,^{28–30} due to their chemical resistance, regenerability and reuse in adsorption processes.

In the present study, a functionalized nanocomposite obtained by incorporation of acid-modified bentonite into a poly(glycidyl methacrylate-*co*-ethylene glycol dimethacrylate) matrix was investigated as a sorbent for phenol derivatives. The incorporation of the acid modified bentonite into the copolymer matrix led to an increase of porosity, total pore volume and, particularly, the specific surface area.³¹ Further amino functionalization of the nanocomposite with diethylenetriamine (DETA) enabled the sorption of phenol derivatives.²⁹ The obtained composite CP-S_A-DETA was used for an investigation of 4-nitrophenol (4NP), 2-nitrophenol (2NP) and 2-chloro-4-nitro phenol (2Cl4NP) sorption

from aqueous solutions. The starting concentrations of the phenol derivatives in the presented experiments were in range of 0.05 to 0.30 mmol dm⁻³ (7.0 to 41.7 mg dm⁻³), which is comparable to reported industrial wastewater concentrations of phenols.^{9,10} The influence of temperature, pH, sorption time and initial sorbent concentration on the sorption efficiency of CP-S_A-DETA were studied in order to evaluate this material as a wastewater sorbent.

EXPERIMENTAL

Materials

Bentonite clay was obtained from the coal and bentonite mine "Bogovina", Serbia. It was crushed, ground and sieved through a 74-μm sieve and acid modified.²⁹ The chemical and the textural properties of the acid-modified bentonite were reported previously.^{32,33} All the chemicals used for the synthesis of the composite were analytical grade products and used as received. Glycidyl methacrylate, GMA, and ethylene glycol dimethacrylate, EGDMA, were obtained from Fluka and Merck, respectively. Poly(*N*-vinyl pyrrolidone), PVP, (BASF with $\bar{M}_w = 1 \times 10^6$ g mol⁻¹) was used as the stabilizer in the suspension copolymerization and 2,2'-azobisisobutyronitrile, AIBN (Merck), was used as the reaction initiator. Cyclohexanol (Merck) and 1-tetradecanol (Merck) were used as an inert component in the polymerization. For the sorption experiments, 4-nitrophenol (4NP, Ciba, solubility in water 16 g dm⁻³ at 25 °C), 2-nitrophenol (2NP, Alfa Aesar, solubility in water 2 g dm⁻³ at 25 °C) and 2-chloro-4-nitrophenol (2Cl4NP, Alfa Aesar, solubility in water – slightly soluble) were used as received.

Synthesis and functionalization of nanocomposite

Macroporous nanocomposite of poly(glycidyl methacrylate-*co*-ethylene glycol dimethacrylate) and acid modified bentonite was prepared by the radical suspension copolymerization of GMA and EGDMA in the presence of the acid-modified bentonite (S_A) and an inert component. The synthesis procedure was previously reported.^{29,31}

The obtained sample was denoted as CP-S_A. TEM analysis confirmed the CP-S_A was a nanocomposite.³⁴ The functionalization was realized as follows. A mixture of 3.6 g of CP-S_A and 15.7 g of diethylenetriamine (DETA) and 100 cm³ of toluene was left at room temperature for 24 h, and then heated at 80 °C for 6 h. The modified sample was filtered, washed with ethanol, dried and labeled as CP-S_A-DETA.³⁵

Sorption experiments

Batch-type sorption experiments were conducted in aqueous suspensions in a temperature-controlled shaker water bath (Memmert WNE 14 and SV 1422). Aliquots were withdrawn from the shaker at regular time intervals and the suspension was centrifuged at 17000 rpm for 6 min (Hettich EBA-21) in order to separate the sorbent from the dispersion. The absorbance of the supernatant solution was measured. The spectra were obtained using a Thermo Electron Nicolet Evolution 500 UV-Vis instrument. Since the UV-Vis spectra of all phenol derivatives vary with pH, the pH of the supernatant solution was adjusted to pH 11 before every UV-Vis measurement. The calibration curves at λ_{max} of 227, 417 and 399 nm for 4NP, 2NP and 2Cl4NP, respectively, were obtained with coefficients of determination $R^2 > 0.9999$. A pH value of 11 was chosen to keep the phenol derivatives in their ionic state.³⁶

Sorption of phenol derivatives by CP-S_A-DETA was investigated with respect to temperature, pH, initial concentration and contact time. The mass of sorbent and solution volume were kept constant ($m_{\text{sorb}} = 25$ mg, $v = 50.0$ cm³) in all experiments.

The effect of temperature was studied at 25, 40, 50 and 60 °C. For these experiments, the solute concentration was kept constant at 2×10^{-4} mol dm⁻³ and pH was unadjusted (pH 5.1).²⁹

The amount of sorbed derivative at time t , q_t / mmol g⁻¹, was calculated from the following mass balance relationship:

$$q_t = \frac{(c_0 - c_t)v}{m_{\text{sorb}}} \quad (1)$$

where: c_0 and c_t in mol dm⁻³ are the initial and the solution concentrations after sorption time t , respectively.

The pH of the solution was monitored using a Jenway 3320 pH meter.

RESULTS AND DISCUSSION

The characterization of functionalized macroporous nanocomposite was previously reported.²⁹ Textural properties determined by mercury intrusion porosimetry were as follows: specific surface area ($S_{\text{Hg}} = 90 \text{ m}^2 \text{ g}^{-1}$), total pore volume per mass of sample (the specific pore volume, $V_p = 1.09 \text{ cm}^3 \text{ g}^{-1}$), porosity ($P = 64 \%$), and the pore diameter that corresponds to half of the pore volume ($d_{V/2} = 62 \text{ nm}$). Amino group content was estimated to be 2.7 mmol g⁻¹.²⁹

The sorption of 4NP on CP-S_A-DETA was previously investigated with respect to contact time, pH and initial concentration.²⁹ These experiments were complemented with new experiments where the effect of temperature on sorption efficiency was investigated. The effect of temperature was studied at 25, 40, 50 and 60 °C and the results are presented in Fig. 1.

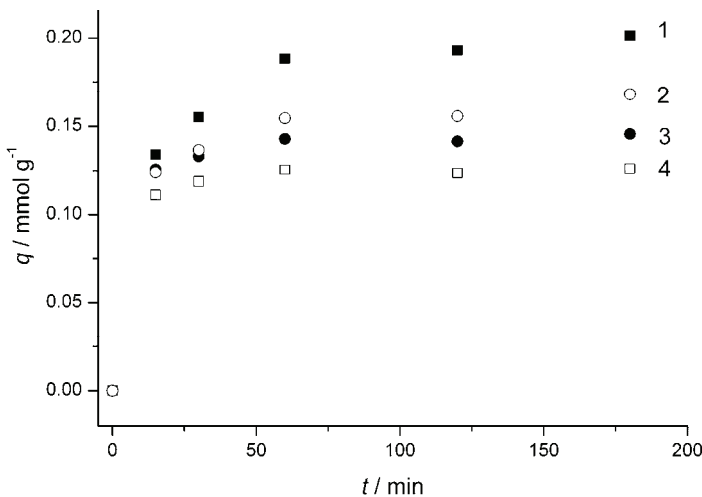


Fig. 1. The effect of temperature on the sorption of 4NP on CP-S_A-DETA: 1) 25, 2) 40, 3) 50 and 4) 60 °C ($c_0 = 2 \times 10^{-4}$ mol dm⁻³, pH 5.1).

The sorption efficiency decreased with increasing temperature. The decrease in the sorption efficiency indicates an exothermic process. This effect may be

ascribed to the increasing trend of desorption of 4NP from the interface into the solution at elevated temperatures.⁴

Kinetic analysis of temperature effect for 4NP sorption was performed using the data given in Fig. 1. The pseudo-first-order and the pseudo-second-order kinetic models were tested.³⁷ The integrated rate laws for pseudo-first-order and pseudo-second-order reactions in linear form are presented by Eqs. (2) and (3), respectively:

$$\log(q_e - q_t) = \log q_e - k_1 t / 2.303 \quad (2)$$

$$t/q_t = 1/k_2 q_e^2 + t/q_e \quad (3)$$

where q_t is the amount of sorbed sorbate (mmol g^{-1}) at any time t , q_e is the amount of sorbed sorbate at equilibrium (mmol g^{-1}), k_1 is the pseudo-first-order rate constant (min^{-1}), k_2 is the pseudo-second-order rate constant ($\text{g mmol}^{-1} \text{ min}^{-1}$).

The kinetic results were also analyzed using the intraparticle diffusion model³⁸ in order to determine the rate-controlling step of the sorption process. The rate of intraparticle diffusion can be calculated according to the equation:

$$q_t = C_{id} + k_{id} t^{0.5} \quad (4)$$

where k_{id} ($\text{mmol g}^{-1} \text{ min}^{-0.5}$) is the intraparticle diffusion rate constant and C_{id} is the intercept, which is proportional to the boundary layer thickness.

Parameters for pseudo-first-order, pseudo-second-order kinetics model as well as intraparticle diffusion kinetic model are presented in Table I.

TABLE I. Kinetic parameters for sorption of 4NP on CP-S_A-DETA at different temperatures

Parameter	Temperature, °C			
	25	40	50	60
$q_e^{\exp} / \text{mmol g}^{-1}$	0.201	0.169	0.146	0.126
Pseudo-first-order				
$q_e^{\text{calc}} / \text{mmol g}^{-1}$	0.324	0.254	0.169	0.130
$k_1 \times 10^2 / \text{min}^{-1}$	2.00	1.19	1.49	1.66
R^2	0.866	0.770	0.554	0.303
Pseudo-second-order				
$q_e^{\text{calc}} / \text{mmol g}^{-1}$	0.210	0.172	0.147	0.126
$k_2 / \text{g mmol}^{-1} \text{ min}^{-1}$	0.51	0.77	3.04	7.96
R^2	0.999	0.998	0.999	0.999
Intraparticle diffusion				
$k_{id} \times 10^2 / \text{mmol g}^{-1} \text{ min}^{-0.5}$	1.41	0.79	0.45	0.36
$C_{id} / \text{mmol g}^{-1}$	0.079	0.093	0.108	0.098
R^2	0.999	0.999	0.999	0.982

The coefficients of determination (R^2) for the pseudo-second-order kinetics model are closer to unity in comparison to the corresponding R^2 for the pseudo-first-order kinetics. Furthermore, the experimentally obtained values for the equilibrium amount (q_e^{\exp}) were almost identical to the values calculated (q_e^{calc})

using the pseudo-second-order kinetics model. Therefore, it could be stated that the adsorption of 4NP on CP-S_A-DETA obeyed pseudo-second-order kinetics model, which is in accordance with finding of other authors for 4NP for similar systems.^{25,39,40}

The obtained $R^2 \geq 0.982$ for the intraparticle diffusion model for all investigated temperatures showed that this model was applicable for the investigated system. The linear plot of q_t vs. $t^{0.5}$ did not pass through the origin, indicating that both intraparticle diffusion and external mass transfer were rate-controlling steps.^{41,42}

The Arrhenius Equation was used to evaluate the activation energy of sorption:

$$\ln k_2 = \ln A - E_a/RT \quad (5)$$

where E_a is activation energy of sorption (kJ mol^{-1}), A is the Arrhenius factor, R is the universal gas constant ($R = 8.314 \text{ J K}^{-1} \text{ mol}^{-1}$), T is thermodynamic temperature (K) and k_2 is the equilibrium rate constant of the pseudo-second-order reaction ($\text{g mmol}^{-1} \text{ min}^{-1}$) given in Table I.

The magnitude of E_a indicates the dominant type of sorption, *i.e.*, either physisorption (E_a in range of 5–40 kJ mol^{-1}) or chemisorption (E_a in range of 40–800 kJ mol^{-1}).⁴³ E_a was found to be 54.8 kJ mol^{-1} , indicating that chemisorption was the dominant sorption process.

In order to evaluate the synthesized sorbent as sorbent of various phenol derivatives, sorption experiments were performed using 2NP and 2Cl4NP in addition to 4NP. Considering that the investigation of the influence of temperature on 4NP sorption showed that the best sorption was achieved at 25 °C, the experiments with 2NP and 2Cl4NP were performed at this temperature.

The effect of initial pH on the sorption of 2NP and 2Cl4NP was determined within the pH range of 2–11 and the results are presented in Fig. 2, together with the pH behavior of CP-S_A-DETA that was previously reported.²⁹ The diagram shows initial pH of suspension of CP-S_A-DETA in 0.01 M NaCl (pH_i) vs. pH after 24 h of shaking (pH_f). A plateau in the pH value between 4 and 9 was observed and the pH at the point of zero charge, pHPZC , was estimated to be 7.8.

It was observed that sorption of both derivatives significantly depended on the initial pH value. Sorption capacity was very low in extremely acidic and alkaline environments. The maximal sorption of 2NP of 35.3 % was determined at pH 7.2 and 79.7 % for 2Cl4NP at pH 3.9. The sorption efficiency for both derivatives at unadjusted pH 5.8 for 2NP and pH 4.8 for 2Cl4NP were close to the maximal values. Further experiments were performed at the unadjusted pH values. Additional pH adjustment would increase the purification costs and would be ecologically unjustified.

The effect of contact time on the amount of sorbed 2NP and 2Cl4NP on CP–SA–DETA was investigated in the range of initial concentrations (0.5×10^{-4} – 2×10^{-4} mol dm $^{-3}$, Fig. 3a and b). Due to significant removal of 2Cl4NP on CP–SA–DETA, experiments were also conducted at the higher initial concentration of 3×10^{-4} mol dm $^{-3}$.

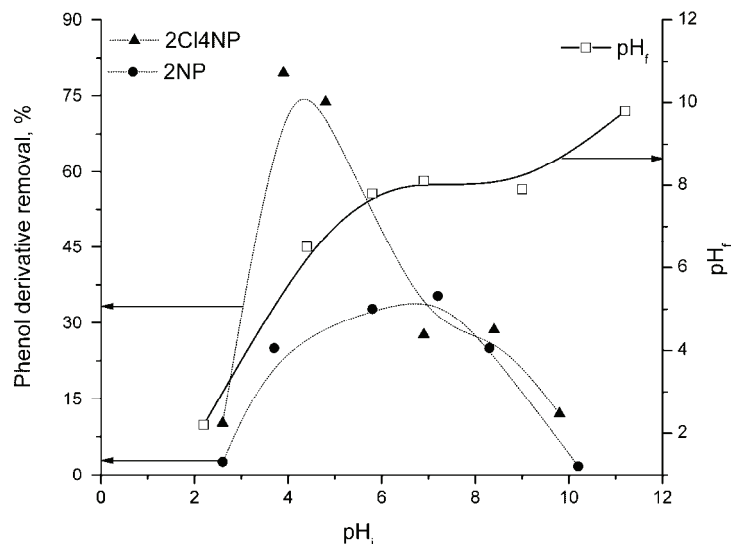


Fig. 2. The pH behavior of CP–SA–DETA in the sorption 2NP and 2Cl4NP and the pH_i vs. pH_f diagram.

The rate of removal of both phenol derivatives was initially high. The initial rapid phase may be due to increased number of vacant surface sites available during the initial stage. Therefore, there was an increased concentration gradient between sorbate in the solution and sorbate on the sorbent.^{44,45} Subsequently, the remaining vacant surface sites were difficult to occupy due to repulsive forces between already sorbed phenol derivative molecules and these molecules in solution.⁴⁶

For initial concentrations of sorbate, for both phenols, the equilibrium was reached after 60 min. The time when half of total sorption capacity was reached ($t_{1/2}$) was in the range 8–14 min and 13–24 min for all initial concentration of 2NP and 2Cl4NP, respectively.

Pseudo-first-order and pseudo-second-order kinetic models were applied (Table II) in order to predict the adsorption kinetics.

The coefficients of determination R^2 for pseudo-first order kinetic were low showing that this model was not applicable for the investigated sorption systems. On the other hand, a linear correlation was obtained for pseudo-second-order

kinetics with $R^2 > 0.990$ and the q_e^{calc} calculated from the pseudo-second order kinetic model were in good agreement with q_e^{exp} .

In order to illustrate different sorption efficiencies of CP-S_A-DETA toward 4NP, 2NP and 2Cl4NP, the results of sorption experiments realized under the same experimental conditions ($c_0 = 2 \times 10^{-4}$ mol dm⁻³, for 3 h at 25 °C and unadjusted pH) are presented in Fig. 4.

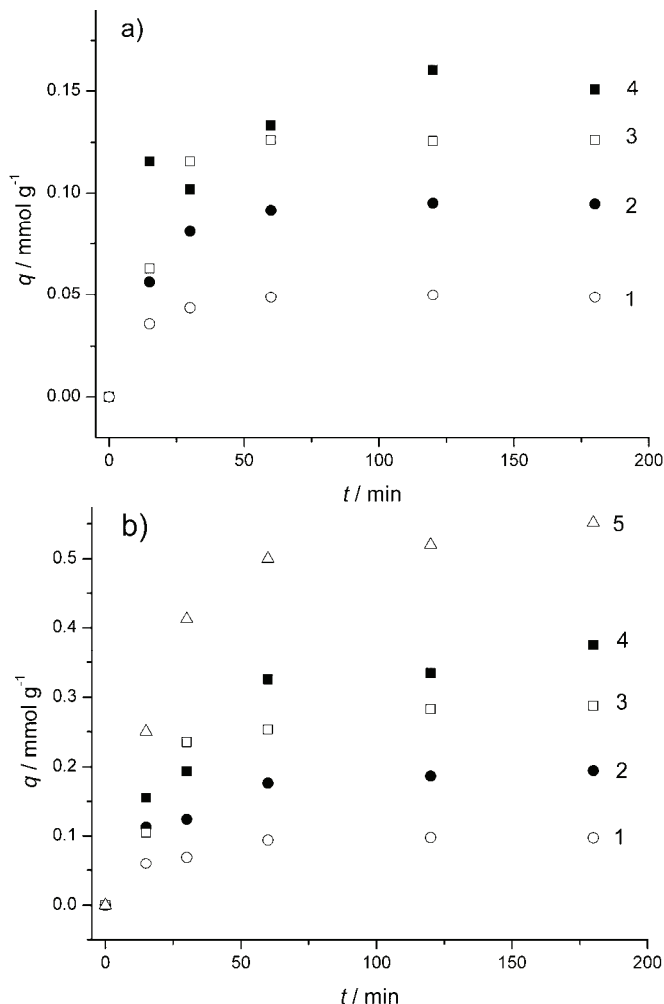


Fig. 3. The effect of contact time on the sorption of a) 2NP and b) 2Cl4NP on CP-S_A-DETA at different initial concentrations: 1) 0.5×10^{-4} , 2) 1×10^{-4} , 3) 1.5×10^{-4} , 4) 2×10^{-4} and 5) 3×10^{-4} mol dm⁻³.

The affinity of CP-S_A-DETA toward phenol derivatives was found to increase in the following order 2NP < 4NP < 2Cl4NP. This could be ascribed to

chemical structure of these phenol derivatives and the hydrogen bonds that they could form with the sorbent. Intramolecular hydrogen bonds are present in 2NP making it less soluble in water than 4NP. Due to the intramolecular hydrogen bonds and steric hindrance in 2NP, this derivative is less capable of making hydrogen bonds with the amino groups in the functionalized composite CP-SA-DETA. Both 2NP and 4NP are hydrophobic while the amino-functionalized composite is hydrophilic. The adsorption capacity of different phenols, in general, is related to their solubility in water²⁰ and to the hydrophobic character of their substituents. Therefore, it could be expected that 2NP being less soluble in water than 4NP would be more efficiently sorbed on CP-SA-DETA, but due to intramolecular hydrogen bonds and steric hindrance, this is not the case.

TABLE II. Pseudo-first-order-kinetics and pseudo-second-order-kinetics for the sorption of 2NP and 2Cl4NP on CP-SA-DETA at 25 °C

Parameter	2NP				2Cl4NP			
$c_0 \times 10^4 / \text{mol dm}^{-3}$	0.5	1.0	1.5	2.0	0.5	1.0	1.5	2.0
$q_{\text{exp}} / \text{mmol g}^{-1}$	0.050	0.122	0.126	0.161	0.098	0.195	0.288	0.376
Pseudo-first-order								
$k_1 \times 10^2 / \text{min}^{-1}$	1.02	4.20	2.47	1.28	2.02	1.66	3.15	2.39
$q_{\text{e}}^{\text{calc}} / \text{mmol g}^{-1}$	0.295	0.317	0.223	0.123	0.577	0.541	0.510	0.388
R^2	0.931	0.946	0.921	0.560	0.856	0.800	0.954	0.933
Pseudo-second-order								
$k_2 / \text{g mmol}^{-1} \text{ min}^{-1}$	0.540	0.818	1.366	4.666	0.102	0.079	0.324	0.302
$q_{\text{e}}^{\text{calc}} / \text{mmol g}^{-1}$	0.164	0.134	0.117	0.050	0.601	0.433	0.305	0.212
R^2	0.995	0.997	0.999	0.999	0.997	0.990	0.999	0.997

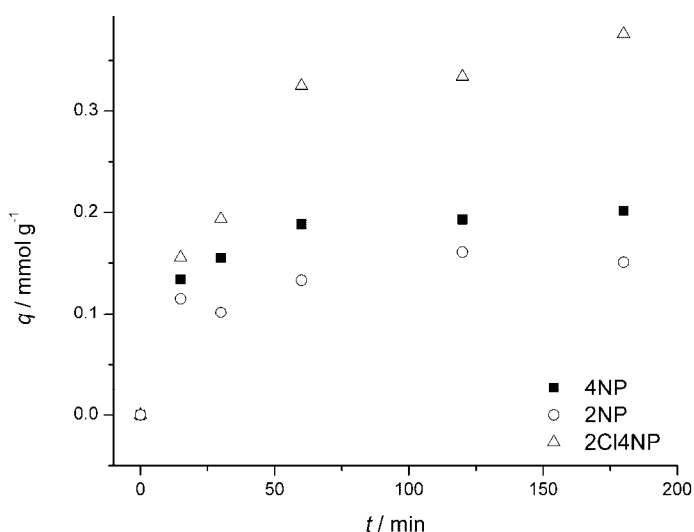


Fig. 4. The effect of contact time on the sorption of different phenol derivatives by CP-SA-DETA ($c_0 = 2 \times 10^{-4} \text{ mol dm}^{-3}$, at 25 °C).

2Cl4NP has the lowest solubility in water. The chlorine atom is electron withdrawing and stabilizes the negative charge at the *ortho* position through the inductive withdrawing effect. However, it also has a weak resonance donating effect. The negative inductive effect of chlorine prevails over the positive resonance effect in this case. In addition, the NO₂ group has a negative resonance and a negative inductive effect.

The pK_a values of the phenol derivatives are 7.16, 7.23 and 5.42 for 2NP, 4NP and 2Cl4NP, respectively.¹ Therefore, 2Cl4NP is the strongest acid and it can easier release a proton than 2NP and 4NP. All three derivatives are in their molecular form in the presented sorption experiments ($pK_a < pH_{unadjusted}$).

The amino groups on CP–S_A–DETA are in the protonated form when $pK_a < pH$. The pK_a of diethylenetriamine is 10.45.⁴⁷ It could be assumed that diethylenetriamine in CP–S_A–DETA was in the protonated form during the sorption experiments and thus, the sorbent surface was positively charged.⁴⁸ Since phenols act as proton acceptor hydrogen bonds, this creation is a favorable process in this system.

Boyd⁴⁹ studied the sorption of undissociated phenol and its derivatives on a soil sample at pH 5.7 to evaluate the effect of the presence of other functional groups in the phenol molecule. With decreasing water solubility of the phenol derivatives with the following functional groups: –CH₃, –OCH₃, –NO₂, or –Cl, the sorption increased. Moreover, the sorption of the substituted phenols, with the exception of 2NP, was generally greater than that predicted for hydrophobic sorption, most likely due to hydrogen bond formation. Probably, a similar explanation could be applied to the experimental data obtained in the present study.

The isotherm data were fitted with the Freundlich and Langmuir models, and a better correlation was found with the Langmuir model, with the coefficients of determination for all the studied phenol derivatives > 0.99 . Maximal sorption capacities (q_{max}) were calculated using Langmuir model. The obtained values of q_{max} of CP–S_A–DETA toward phenol derivatives increased in the following order $q_{max}(2NP) = 0.342 \text{ mmol g}^{-1} < q_{max}(4NP) = 0.581 \text{ mmol g}^{-1} < q_{max}(2Cl4NP) = 0.704 \text{ mmol g}^{-1}$. The $q_{max}(4NP)$ was previously reported.²⁹

Among phenol and phenol derivatives, the sorption of phenol^{2,3} and 4NP^{6,23,50–52} were the most investigated. The sorption of 2NP was seldom tested,^{23,53} while, to the best of our knowledge, the sorption of 2Cl4NP has not been investigated. The literature data on $q_{max}(4NP)$ varied from 2.26 mmol g⁻¹ at 25 °C for activated carbon fibers,⁶ down to 0.33 mmol g⁻¹ on commercial Amberlite XAD-4 resin.⁵² With $q_{max}(4NP) = 0.581 \text{ mmol g}^{-1}$, CP–S_A–DETA could be regarded as an acceptable sorbent for 4NP. The more expressed affinity of CP–S_A–DETA for the 2Cl4NP evaluates CP–S_A–DETA as a promising sorbent for phenolic wastewater.

CONCLUSION

A macroporous nanocomposite of poly(glycidyl methacrylate-*co*-ethylene glycol dimethacrylate) and acid modified bentonite was prepared by the radical suspension copolymerization of their mixture and then functionalized with diethylenetriamine.

The obtained functionalized nanocomposite CP-S_A-DETA, was investigated as wastewater sorbent for the removal of phenol derivatives. Sorption of 4NP was exothermic, having $E_a = 54.8 \text{ kJ mol}^{-1}$ that indicates chemisorption. Kinetics of sorption of all phenol derivatives (2NP, 4NP and 2Cl4NP) was well described by the pseudo-second-order kinetic model. The isotherm data were best fitted with Langmuir model for all derivatives. It was found that the affinity of CP-S_A-DETA toward phenol derivatives increases in the following order 2NP < 4NP < 2Cl4NP. Such behavior could be ascribed to the chemical structure of these phenol derivatives and the hydrogen bonds that they could form with the sorbent.

Acknowledgements. This work was supported by the Ministry of Education, Science and Technological Development of the Republic of Serbia (Project Nos. III 45001 and III 43009).

И З В О Д

СОРПЦИЈА ДЕРИВАТА ФЕНОЛА НА ФУНКЦИОНАЛИЗОВАНОМ МАКРОПОРОЗНОМ НАНОКОМПОЗИТУ ПОЛИ(ГЛИЦИДИЛ-МЕТАКРИЛАТ-КО-ЕТИЛЕН-ГЛИКОЛ- -ДИМЕТАКРИЛАТ) И КИСЕЛО-МОДИФИКОВАНОГ БЕНТОНИТА

САЊА Р. МАРИНОВИЋ¹, АЛЕКСАНДРА Д. МИЛУТИНОВИЋ-НИКОЛИЋ¹, АЛЕКСАНДРА Б. НАСТАСОВИЋ²,
МАРИЈА Ј. ЖУНИЋ¹, ЗОРИЦА М. ВУКОВИЋ¹, ДУШАН Г. АНТОНОВИЋ³ и ДУШАН М. ЈОВАНОВИЋ¹

¹Универзитет у Београду – Институт за хемију, технолођију и мешалуртију, Центар за катализу и хемијско инжењерство, Његошева 12, Београд, ²Универзитет у Београду – Институт за хемију, технолођију и мешалуртију, Центар за хемију, Његошева 12, Београд и ³Универзитет у Београду – Технолошко-мешаларски факултет, Карнејевса 4, Београд

Макропорозни нанокомпозит добијен је радикалном суспензионом кополимеризацијом полиглицидил-метакрилат-ко-етилен-гликол-диметакрилата) и кисело-модификовани бентонита. Како би се омогућила сорпција деривата фенола добијени нанокомпозит је функционализован диетилен триамином (DETA), реакцијом отварања прстена епоксидне групе. Овај нови, недовољно испитани материјал, развијене порозне структуре, је означен са CP-S_A-DETA. У овом раду је испитан утицај температуре на сорпцију 4-нитрофенола (4NP) на CP-S_A-DETA. Добијена вредност енергије активације од 54,8 kJ mol⁻¹ указује на хемисорпцију као доминантан процес. По одређивању оптималних услова сорпције за 4NP, испитана је сорпција 2-нитрофенола (2NP) и 2-хлор-4-нитрофенола (2Cl4NP) на CP-S_A-DETA. Проучаван је утицај pH, почетне концентрације и времена контакта на сорпцију. 2NP је у малој мери испитиван као сорбат, док, по нашим сазнањима, 2Cl4NP није испитиван. Потврђено је да је CP-S_A-DETA добар сорбент за сва три деривата фенола, а поготову за 2Cl4NP. Утврђено је да Лангмирова изотерма најбоље описује сорпцију у испитаним системима, а да сорпциона динамика прати кинетику псевдо-другог реда за све дерivate.

(Примљено 6 фебруара, ревидирано 11. априла, прихваћено 14. априла 2014)

REFERENCES

1. N. Calace, E. Nardi, B. M. Petronio, M. Pietroletti, *Environ. Pollut.* **118** (2002) 315
2. R. I. Yousef, B. El-Eswed, A. H. Al-Muhtaseb, *Chem. Eng. J.* **171** (2011) 1143
3. F. A. Banat, B. Al-Bashir, S. Al-Asheh, O. Hayajneh, *Environ. Pollut.* **107** (2000) 391
4. M. Kilic, E. Apaydin-Varol, A. E. Putun, *J. Hazard. Mater.* **189** (2011) 397
5. Z. Ioannou, J. Simitzis, *J. Hazard. Mater.* **171** (2009) 954
6. Q. S. Liu, T. Zheng, P. Wang, J. P. Jiang, N. Li, *Chem. Eng. J.* **157** (2010) 348
7. O. A. Ekpete, M. Horsfall Jr., T. Tarawou, *Int. J. Biol. Chem. Sci.* **5** (2011) 1143
8. S. Suresh, V. C. Srivastava, I. M. Mishra, *Chem. Ind. Chem. Eng. Q.* **19** (2013) 195
9. J. Chen, W. H. Rulkens, H. Bruning, *Water Sci. Technol.* **35** (1997) 231
10. M. C. Tomei, S. Rossetti, M. C. Annesini, *Chemosphere* **63** (2006) 1801
11. S. A. Boyd, D. R. Shelton, D. Berry, J. M. Tiedje, *Appl. Environ. Microbiol.* **46** (1983) 50
12. G. Gonzalez, G. Herrera, M. T. Garcia, M. Peña, *Bioresource Technol.* **80** (2001) 137
13. S. H. Lin, C. L. Pan, H. G. Leu, *J. Hazard. Mater.* **65** (1999) 289
14. Y. Park, A. H. P. Skelland, L. J. Forney, J. H. Kim, *Water Res.* **40** (2006) 1763
15. J. Luana, A. Plaisier, *J. Membrane Sci.* **229** (2004) 235
16. Y. Yavuz, A. S. Kopalal, *J. Hazard. Mater.* **136** (2006) 296
17. S. H. Lin, C. H. Chiou, C. K. Chang, R. S. Juang, *J. Environ. Manage.* **92** (2011) 3098
18. S. H. Lin, R. S. Juang, *J. Environ. Manage.* **90** (2009) 1336
19. J. M. Chern, Y. W. Chien, *Water Res.* **37** (2003) 2347
20. C. Moreno-Castilla, J. Rivera-Utrilla, M. V. Lopez-Ramon, F. Carrasco-Marín, *Carbon* **33** (1995) 845
21. B. H. Hameed, A. A. Rahman, *J. Hazard. Mater.* **160** (2008) 576
22. S. Al-Asheh, F. Banat, L. Abu-Aitah, *Sep. Purif. Technol.* **33** (2003) 1
23. H. Koyuncua, N. Yıldız, U. Salginc, F. Koroglu, A. Calımlı, *J. Hazard. Mater.* **185** (2011) 1332
24. K. Abburi, *J. Hazard. Mater.* **105** (2003) 143
25. B. Pan, W. Du, W. Zhang, X. Zhang, Q. Zhang, B. Pan, L. Lv, Q. Zhang, J. Chen, *Environ. Sci. Technol.* **41** (2007) 5057
26. A. Li, Q. Zhang, G. Zhang, J. Chen, Z. Fei, F. Liu, *Chemosphere* **47** (2002) 981
27. R. Ardelean, C. M. Davidescu, A. Popa, *Chem. Bull. "Politehnica" Univ. Timisoara, Romania* **55** (2010) 132
28. Z. Sandić, A. Nastasović, N. Jović-Jovičić, A. Milutinović-Nikolić, D. Jovanović, *J. Appl. Polym. Sci.* **121** (2011) 234
29. S. Marinović, A. Milutinović-Nikolić, M. Žunić, Z. Vuković, D. Maksin, A. Nastasović, D. Jovanović, *Russ. J. Phys. Chem. A* **85** (2011) 2386
30. V. V. Podlesnyuk, J. Hradil, R. M. Marutovskii, N. A. Klimenko, L. E. Fridman, *React. Funct. Polym.* **33** (1997) 275
31. S. Marinović, Z. Vuković, A. Nastasović, A. Milutinović-Nikolić, D. Jovanović, *Mater. Chem. Phys.* **128** (2011) 291
32. Z. Vuković, A. Milutinović-Nikolić, Lj. Rozić, A. Rosić, Z. Nedić, D. Jovanović, *Clay Clay Miner.* **54** (2006) 697
33. Z. Vuković, A. Milutinović-Nikolić, J. Krstić, A. Abu-Rabi, T. Novaković, D. Jovanović, *Mater. Sci. Forum* **494** (2005) 339
34. M. Žunić, A. Milutinović-Nikolić, A. Nastasović, Z. Vuković, D. Lončarević, I. Vuković, K. Loos, G. ten Brinke, D. Jovanović, *Polym. Bull.* **70** (2013) 1805
35. Lj. Malović, A. Nastasović, Z. Sandić, J. Marković, D. Đorđević, Z. Vuković, *J. Mater. Sci.* **42** (2007) 3326

36. L. Zhu, B. Chen, S. Tao, C. T. Chiou, *Environ. Sci. Technol.* **37** (2003) 4001
37. P. K. Malik, *Dyes Pigments* **56** (2003) 239
38. W. J. Weber Jr., J. C. Morris, *J. Sanit. Eng. Div. Am. Soc. Civ. Eng.* **89** (1963) 31
39. W. Guan, J. Pan, X. Wang, W. Hu, L. Xu, X. Zou, C. Li, *J. Sep. Sci.* **34** (2011) 1244
40. Q. Zhou, H. P. He, J. X. Zhu, W. Shen, R. L. Frost, P. Yuan, *J. Hazard. Mater.* **154** (2008) 1025
41. S. J Allen, L. J. Whitten, M. Murray, O. Duggan, *J. Chem. Technol. Biot.* **68** (1997) 442
42. M. Dogan, M. Alkan, *Chemosphere* **50** (2003) 517
43. M. Dogan, H. Abak, M. Alkan, *J. Hazard. Mater.* **164** (2009) 172
44. V. Singh, A. K. Sharma, D. N. Tripathi, R. Sanghi, *J. Hazard. Mater.* **161** (2009) 955
45. D. Kavitha, C. Namasivayam, *Bioresource Technol.* **98** (2007) 14
46. V. O. Arief, K. Trilestari, J. Sunarso, N. Indraswati, S. Ismadji, *Clean-Soil Air Water* **36** (2008) 937
47. J. A. Riddick, W. B. Bunger, T. K. Sakano, *Techniques of Chemistry, Vol. II, Organic Solvents*, 4th ed., Wiley, New York, 1985, p. 420
48. D. Maksin, A. Nastasović, A. Milutinović-Nikolić, Lj. Surucić, Z. Sandić, R. Hercigonja, A. Onjia, *J. Hazard. Mater.* **209–210** (2012) 99
49. S. A. Boyd, *Soil Sci.* **134** (1982) 337
50. S. Dutta, J. K. Basu, R. N. Ghar, *Sep. Purif. Technol.* **21** (2001) 227
51. F. Ahmada, W. M. A. W. Daud, M. A. Ahmad, R. Radzi, *Chem. Eng. J.* **178** (2011) 461
52. J. Huang, C. Yan, K. Huang, *J. Colloid Interface Sci.* **332** (2009) 60
53. S. J. Allen, B. Koumanova, Z. Kircheva, S. Nenkova, *Ind. Eng. Chem. Res.* **44** (2005) 2281.



Spectrophotometric and conductometric study of the complexation of *N*-salicylidene-2-aminophenol with Cu²⁺ in methanol + 1,4-dioxane binary solutions

RASHMIDIPTA BISWAS, DHIRAJ BRAHMAN and BISWAJIT SINHA*

Department of Chemistry, University of North Bengal, Darjeeling-734013, India

(Received 29 January, revised 26 March, accepted 1 April 2014)

Abstract: The complexation reaction between *N*-salicylidene-2-aminophenol, abbreviated as SAP, with the Cu²⁺ was studied in binary mixtures of methanol and 1,4-dioxane using conductometric and spectrophotometric methods at different temperatures. The stability constants (K_f) for the 1:1 complex, Cu²⁺–SAP, were calculated from computer fitting of the absorbance and molar conductance data against various mole ratios ($c_M:c_L$ or $c_L:c_M$) in different binary solvent mixtures. A non-linear behaviour was observed for the variation of log K_f for the complex against the solvent composition. Various thermodynamic parameters (ΔH , ΔS and ΔG) for the formation of the Cu²⁺–SAP complex were determined from the temperature dependence of the stability constants (K_f). The overall results showed that the complexation reaction is entropy driven and is affected by the nature and composition of the mixed solvents.

Keywords: *N*-salicylidene-2-aminophenol; Cu²⁺; stability constants; binary mixtures; methanol; 1,4-dioxane.

INTRODUCTION

The coordination chemistry of nitrogen–oxygen donor ligands is an interesting area of research. A great deal of attention in this area has been focused on the complexes formed by transition metal ions with Schiff bases because of the presence of both nitrogen and oxygen donor atoms in the backbones of these ligands.^{1,2} Schiff base ligands can also accommodate different metal centres in various coordination modes, thereby allowing the successful synthesis of homo and hetero metallic complexes with different stereochemistries.³ Schiff base complexes have undergone a phenomenal growth during the recent years because of the versatility offered by these complexes in the fields of industries, catalysis, biological systems, etc.^{4–8} Metal complexes of Schiff bases derived from sali-

*Corresponding author. E-mail: biswachem@gmail.com
doi: 10.2298/JSC140129034S

cylaldehyde and various amines have been widely investigated.^{9–13} Among the first row transition metals, copper plays a pivotal role in cell physiology as a catalytic cofactor in the redox chemistry of mitochondrial respiration, iron absorption, free radical scavenging, and elastin cross-linking.¹⁴ Cu(II) complexes show distorted octahedral and tetrahedral symmetries due to their d⁹ configuration (Jahn–Teller effect). The distortion is usually seen as an axial elongation consistent with the lability and geometric flexibility of the complex. Therefore, Cu(II) complexes may have square planar or square pyramidal geometries with weakly associated ligands in the axial position, but some Cu(II) complexes possess trigonal bipyramidal geometry. The Schiff base *N*-salicylidene-2-amino-phenol (SAP) behaves as a tridentate ligand with ONO donor sites. In the complexes Cu²⁺–SAP, three of the four coordination sites of metal ion remain occupied by nitrogen atom of the azomethine group, two oxygen atoms of the hydroxyl ions and the fourth site was reported to be occupied by a solvent or water molecule.¹⁵ The complexes of copper with Schiff bases have wide applications in the food and dye industries, analytical chemistry, catalysis, have fungicidal, agro-chemical, anti-inflammatory antiradical and biological activities.¹⁶ The fundamental role of copper and the recognition of its complexes as important bioactive compounds *in vitro* and *in vivo* aroused an ever-increasing interest in these compounds as potential therapeutic drugs for various diseases. Hence studies on the thermodynamics of complex formation of Cu²⁺ with different Schiff bases in different solvent media are worthy of thorough studies and are demanded.^{17–20}

Among the various organic solvents, methanol (MeOH) is one of the simplest amphiphile-like molecules.²¹ Alcohols in non-polar solvents associate by means of hydrogen bonds into series of *n*-mers. In solvents such as 1,4-dioxane (DO) that can form hydrogen bonds with MeOH, the self-association of alcohols may be reduced or perturbed in favour of hydrogen-bonded structures when mixed together, leading to intermolecular association between MeOH and DO molecules.²² A literature survey revealed that no reports on the thermodynamics of complex formation between the ligand SAP and transition metal ions in binary solvent mixtures exist. Hence, in this study, the complexation behaviour of SAP with Cu²⁺ in different MeOH–DO mixed solvents was investigated in order to understand the thermodynamics of complex formation between SAP and Cu²⁺ in the mixed solvents studied.

EXPERIMENTAL

Materials

Analytical grade of 2-aminophenol (s), salicyaldehyde (l), copper(II) nitrate trihydrate, Cu(NO₃)₂·3H₂O (s) were procured from Thomas Backer, India and used as received. Spectroscopic grade methanol (MeOH) and 1,4-dioxane (DO) (both of purity > 99 %, S. D. Fine Chemicals, India) were used without further purification. The Schiff base ligand *N*-salicylidene-2-aminophenol (SAP) was prepared according to a literature procedure and its purity

was checked by spectroscopic and other analytical methods.²³ The various binary solvent mixtures were prepared by mass and necessary adjustments were realised to achieve exact mass fractions ($w_1 = 0.40, 0.60, 0.80$ and 1.00) of MeOH in the binary solvent mixtures at 298.15 K under atmospheric pressure. Utmost care was taken during the mixing process to avoid evaporation losses and moisture uptake. The mass measurements were achieved on a digital electronic analytical balance (Mettler, AG 285, Switzerland) with a precision of $\pm 0.01\text{ mg}$. The relative error in the solvent composition was about 1 %. The physical properties of these solvent–solvent mixtures are available in the literature.²⁴

Preparation of the ligand

To a magnetically stirred methanolic solution of 2-aminophenol (10 mmol) in a round bottom flask was added drop wise salicylaldehyde (10 mmol). The reaction mixture was then refluxed for 2 h. After cooling, the orange red Schiff base was collected by filtration and purified by repeated recrystallisation from MeOH. The purified ligand was dried in a desiccator over anhydrous CaCl₂ under vacuum for several days. The orange crystalline compound was obtained in a yield of 85–90 %.

The melting point of the ligand was determined by the open capillary method. Elemental micro-analyses were realised with the aid of a Perkin–Elmer (Model 240C) analyser. The FT-IR spectrum of the ligand SAP in the range (400–4000) cm⁻¹ was recorded on a Perkin–Elmer FT-IR spectrophotometer (RX-1). The ¹H-NMR spectrum was taken with a Spectrospin-Brucker AC 300 MHz spectrometer using DMSO-*d*₆ as the solvent and TMS as an internal reference. The mass spectra was recorded at 70 eV on a GC-MS-QP 100 Ex 5988 mass spectrometer

N-Salicylidene-2-aminophenol (SAP). Yield: 85–90 %; orange crystalline compound; m.p.: 187–188 °C; Anal. Calcd. for C₁₃H₁₁NO₂: C, 73.22; H, 5.20; N, 6.45 %. Found: C, 73.01; H, 5.18; N, 6.45 %; FTIR (KBr, cm⁻¹): 3429.86 (3430¹⁵), 1630.95 (1631¹⁵), 1412.84 (1413¹⁵), 1273.92 (1274¹⁵); ¹H-NMR (300 MHz, DMSO-*d*₆, δ / ppm): 13.74 (2H, *s*, OH), 8.95 (1H, *s*, CH=N), 6.84–7.62 (8H, *m*, ArH); MS (*m/z* (relative abundance %)): 214 (100), 215 (16).

The structure of the Schiff base, SAP, is depicted in Fig. 1.

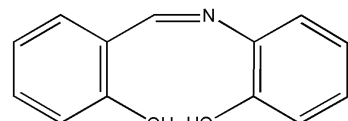


Fig. 1. Structure of *N*-salicylidene-2-aminophenol (SAP).

UV/Vis spectrophotometric titration

The absorbance spectra were recorded using a Jasco V-530 spectrophotometer equipped with a thermostated bath. During the complexation studies, the temperature of the quartz cell was maintained at $298.15 \pm 0.1\text{ K}$. In the spectrophotometric titration, the addition of metal ion solution ($1.3 \times 10^{-3}\text{ mol dm}^{-3}$) to 2 mL of a solution of ligand ($5.0 \times 10^{-5}\text{ mol dm}^{-3}$) was realised using a 10 μL pre-calibrated micropipette. The absorbance (*A*) of the solution was measured after each addition of metal ion solution to the ligand solution. The addition of metal ion solution was continued until the desired metal to ligand mole ratio (*c*_M:*c*_L) of 3:1 was achieved.

Conductometric titration

The conductance measurements were performed with a Systronics-308 conductivity bridge (with a precision $\pm 0.1\text{ %}$) and a dip-type immersion conductivity cell (type CD-10) at a

frequency of 1 KHz. The measurements were made in a water bath maintained at ± 0.01 K of the desired temperatures. The cell was calibrated with a standard KCl solution as described earlier,²⁷ and the cell constant was 1.18 cm^{-1} . During conductometric titration, a solution of copper nitrate ($5.0 \times 10^{-4}\text{ mol dm}^{-3}$, 15 mL) was placed in the conductivity cell and the conductance of the solution was measured. A solution of the ligand ($2.5 \times 10^{-2}\text{ mol dm}^{-3}$) was added stepwise to the conductivity cell using a pre-calibrated micropipette (50 μL) and the conductance of the solution was measured after each addition. The addition of the ligand solution was continued until the total concentration of the ligand was approximately three times greater than that of the metal ion concentration ($c_L:c_M = 3:1$).

RESULTS AND DISCUSSION

UV/Vis spectrophotometric titration

The UV/Vis spectra of the ligand SAP and its Cu^{2+} complex in pure MeOH and in the binary mixtures of MeOH with DO are shown in Fig. 2. This figure shows that the absorption spectrum of the solution of the ligand (initially $5.0 \times 10^{-5}\text{ mol dm}^{-3}$) suffered from marked changes when a solution of Cu^{2+} cations ($1.3 \times 10^{-3}\text{ mol dm}^{-3}$) was added in a stepwise fashion to the ligand solution until

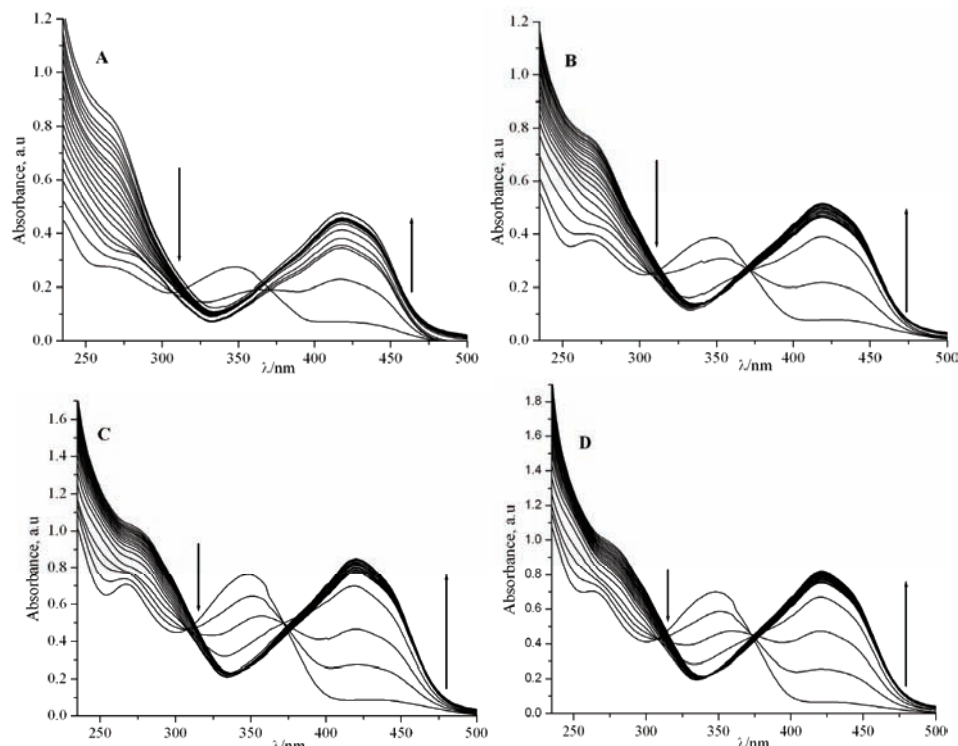


Fig. 2. UV/Vis spectra of the ligand SAP ($5.0 \times 10^{-5}\text{ mol dm}^{-3}$) in the presence of increasing concentration of Cu^{2+} in different solvent mixtures of MeOH and DO at 298.15 K. MeOH mass fractions (w_1) A, $w_1 = 1.00$; B, $w_1 = 0.80$; C, $w_1 = 0.60$; D, $w_1 = 0.40$.

the mole ratio ($c_M:c_L$) = 3:1 was achieved. Thereafter, further addition of metal solution affected no noticeable changes in the spectra. The UV/Vis spectra of the ligand showed two characteristic bands at around 270 and 348 nm. These bands originated from the azomethine chromophore and the phenol moiety, respectively. During spectrophotometric titration, complex formation was indicated by a decrease in the intensity of 348 nm peak and a concomitant development of a peak at around 418 nm. The complex formation was further manifested by a strong spectral shift of about 70 nm towards longer wavelength, in comparison to the free ligand. These changes in UV/Vis spectra were due to the coordination of Cu²⁺ through the imine nitrogen atom with an additive effect from the deprotonation of phenolate groups upon chelation, thereby resulting in the formation of six and five-membered ring systems between the metal atom and ligand in the complex.¹⁷ Thus, analysis of the spectrophotometric data was performed with absorbance values at $\lambda = 418$ nm, as shown in Fig. 3. It was evident from Fig. 3 that when the ligand SAP reacted with Cu²⁺ in MeOH and its binary mixtures with DO, it formed a 1:1 complex. The mass balance for metal-ligand (ML) complex can be given by the following relation:²⁵

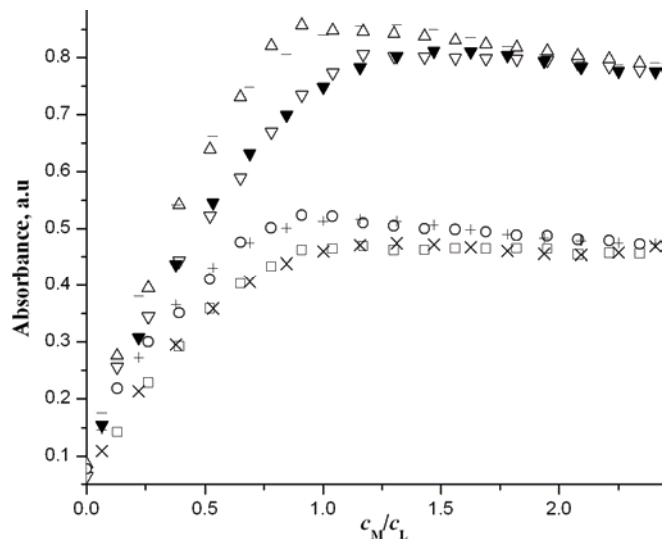


Fig. 3. Mole ratio plot ($c_M:c_L$) for the complexation reaction of the ligand SAP with Cu²⁺ against different mass fractions (w_1) of MeOH in the solvent mixtures at 298.15 K. Symbols for the experimental data: \square , $w_1 = 1.00$; \circ , $w_1 = 0.80$; Δ , $w_1 = 0.60$; ∇ , $w_1 = 0.40$. Symbols for the calculated data (program generated): \times , $w_1 = 1.00$; $+$, $w_1 = 0.80$; $-$, $w_1 = 0.60$; \blacktriangledown , $w_1 = 0.40$.



Therefore, the formation constant (K_f) is given by:

$$K_f \approx \frac{[ML]}{[M][L]} \quad (2)$$

where [M], [L] and [ML] are the concentrations of free metal ion, free ligand and formed complex, respectively. The mass balance for Eq. (1) can be solved provided the following relations for the concentrations of total metal ion and ligand remain valid in equilibrium:

$$c_M = [M] + [ML] \quad (3)$$

$$c_L = [L] + [ML] \quad (4)$$

When [M] and [L] obtained from Eqs. (3) and (4), respectively, are substituted into Eq. (2), K_f is obtained as:

$$K_f = \frac{[ML]}{(c_M - [ML])(c_L - [ML])} \quad (5)$$

If only the complex absorbs at a particular wavelength, total absorbance (A) is given by:

$$A = \varepsilon l [ML] \quad (6)$$

or

$$A = \varepsilon [ML] \quad (7)$$

where ε is molar absorptivity coefficient of the complex and at the path length $l = 1$ cm.

When $c_M \gg [ML]$, Eq. (5) could be rearranged as:

$$K_f = \frac{[ML]}{c_M(c_L - [ML])} = \frac{A / \varepsilon}{c_M(c_L - A / \varepsilon)} \quad (8)$$

Rearranging the above relation, one obtains:²⁶

$$\frac{c_M c_L}{A} = \frac{c_M}{\varepsilon} + \frac{1}{\varepsilon K_f} \quad (9)$$

Thus a linear regression of $c_M c_L / A$ against c_M gives the molar absorptivity (ε) from the slope and K_f from the intercept. Using these ε and K_f values obtained from Eq. (9) as initial guess values, the absorbance ($A_{cal,i}$) of each solutions were iteratively calculated and then the final ε and K_f values were obtained from Eq. (10) using the Newton–Raphson method with the aid of a C-program. Eq. (10) was obtained after some rearrangement of Eq. (5).

$$(A / \varepsilon)^2 - \{(c_M + c_L) + 1 / K_f\} + c_M c_L = 0 \quad (10)$$

The standard errors (σ) in the absorbances were calculated from the following relation:

$$\sigma = \left[\sum_{i=1}^n \{A_{\text{exp},i} - A_{\text{cal},i}\}^2 / n \right]^{1/2} \quad (11)$$

where n stands for number of solutions. The standard errors (σ) were 0.159, 0.188, 0.117 and 0.119 in solvent mixtures with $w_1 = 0.40, 0.60, 0.80$ and 1.00, respectively.

Conductometric titration

It is known that the equilibrium for 1:1 complexation is represented by Eq. (1) and the formation constant (K_f) is given by:

$$K_f = \frac{[\text{ML}]}{[\text{M}][\text{L}]} \frac{f_{\text{ML}}}{f_{\text{M}} f_{\text{L}}} \quad (12)$$

where the f terms stand for the activity coefficients of the species indicated in the subscripts. Under the dilute concentration range used, the activity coefficient of the uncharged ligand (f_L) could be assumed to be unity.^{28,29} Furthermore, according to Debye-Hückel limiting law $f_M \approx f_{\text{ML}}$, and hence the activity coefficients in Eq. (12) cancel each other.³⁰ The fraction of the total metal ion concentration (α) remaining free at equilibrium could be expressed by the relation:

$$\alpha = \frac{\Lambda_m - \Lambda_{\text{ML}}}{\Lambda_{\text{MA}} - \Lambda_{\text{ML}}} \quad (13)$$

where Λ_m , Λ_{MA} and Λ_{ML} stand for the total molar conductance, and the molar conductance of the electrolyte and the complex, respectively. Λ_{ML} was calculated by a least square linear regression of the data points after the curve (Λ_m vs. c_L/c_M) changes its slope at $c_L:c_M$ ratios (Fig. 4). The next α values were calculated from Eq. (13) for each solution and an initial K_f value for each solution was also calculated using [M] and [L] values. Eq. (12) could also be rearranged as:³¹

$$K_f [\text{ML}]^2 - \{1 + (c_M + c_L) K_f\} [\text{ML}] + K_f c_M c_L = 0 \quad (14)$$

The final K_f values and $[\text{ML}]$ were then calculated iteratively using the Newton-Raphson method and successive approximation with the aid of a C-program.²⁰

Stability of the complex

The nature of the solvent can strongly influence the stoichiometry of the complex and complexation of transition metal ions in solution. The stability of transition metal complexes with a polydentate ligand depends on several factors such as the number and type of the donor sites present, the number and size of the chelate rings formed on complexation, etc.³² In addition, the stability also

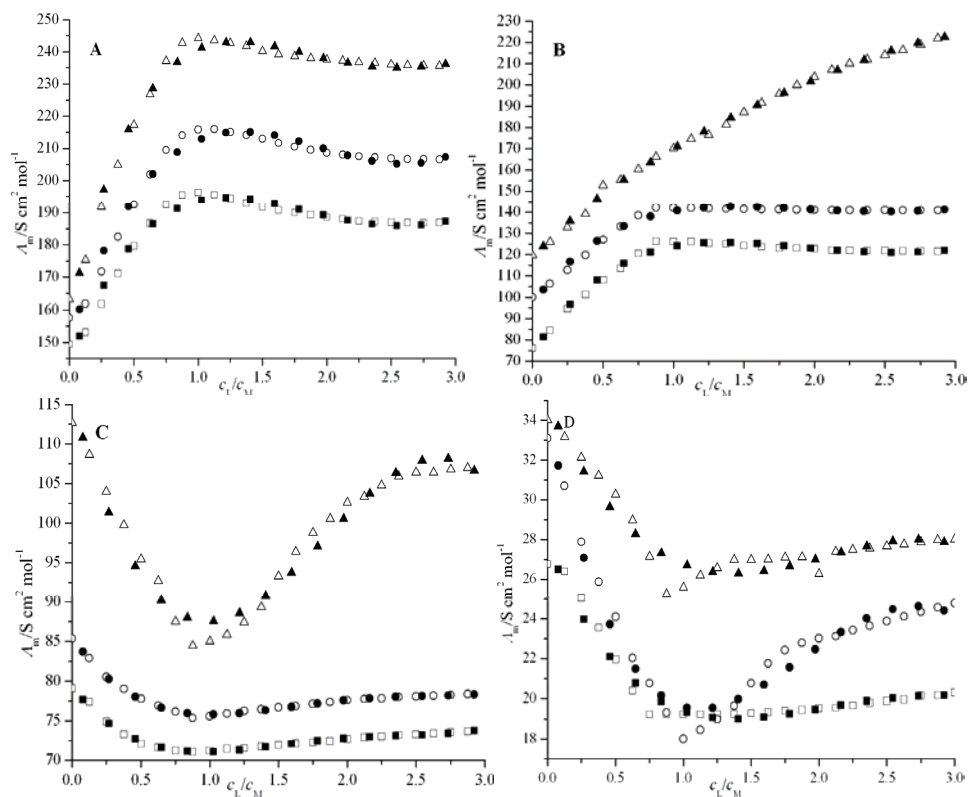


Fig. 4. Molar conductance (A_m) vs. mole ratio plot ($c_L:c_M$) for the Cu^{2+} -SAP complex in different solvent mixtures with different mass fractions (w_1) of MeOH at different temperatures: A, $w_1 = 1.00$; B, $w_1 = 0.80$; C, $w_1 = 0.60$; D, $w_1 = 0.40$. Symbols for the experimental data: \square , $T = 298.15\text{ K}$; \circ , $T = 308.15\text{ K}$; Δ , $T = 318.15\text{ K}$ and symbols for the calculated data (program generated): \blacksquare , $T = 298.15\text{ K}$; \bullet , $T = 308.15\text{ K}$; \blacktriangle , $T = 318.15\text{ K}$.

depends on the donor strength and the dielectric constants of solvent–solvent mixtures.³³ The molar conductance (A_m) vs. mole ratio ($c_L:c_M$) plots are depicted in Fig. 4. Although the ligand solution has negligible conductance, its addition to the metal ion solution when dissolved in pure MeOH and the MeOH–DO mixture with $w_1 = 0.80$ caused a continuous increase in the molar conductance (A_m) up to the mole ratio ($c_L:c_M$) = 1, except for the solvent mixtures with higher amounts of DO, in which the molar conductance (A_m) rather decreased initially on addition of the ligand solution. Such trends in the molar conductance vs. mole ratio ($c_L:c_M$) plots for MeOH rich solvent mixtures is because the complex Cu^{2+} -SAP is more mobile than the free solvated Cu^{2+} and the release of some high-mobility protons and NO_3^- into the solution but for DO rich solvent mixtures, the reversed trend is probably because of the lower dielectric constants and greater solvation of the resulting complex in such solvent mixtures.^{34,35} The slope of molar con-

ductivity (A_m) vs. c_L/c_M plots for all solvent mixtures showed significant changes in slopes when the mole ratio ($c_L:c_M$) was about 1; thus indicating the formation of a relatively stable 1:1 complex (ML) between Cu²⁺ with SAP. From Fig. 4, it is also evident that the curvature of the molar conductivity plots of the Cu²⁺-SAP complex increased as the temperature increased; this is due to the formation of a comparatively stronger complex at higher temperatures. Therefore, the complexation process between SAP and Cu²⁺ is endothermic. This is also evident from Table I, where it could be seen that the log K_f values for the complex Cu²⁺-SAP in pure MeOH and in the binary solvent mixtures increased with temperature. However, slightly higher values of log K_f for solvent mixtures with $w_1 = 0.80$, 0.60 and 0.40 than that of $w_1 = 1.00$. This is probably due to the enhanced stability of the complex at higher contents of DO and its low dielectric constant.

TABLE I. Values log K_f of Cu²⁺-SAP complex obtained from conductometric titration in MeOH-DO binary mixtures at different temperatures; standard errors are given in parentheses

w_1	T / K		
	298.15	308.15	318.15
1.00	4.69 (± 0.11)	4.78 (± 0.13)	4.91 (± 0.10)
0.80	4.79 (± 0.10)	4.94 (± 0.14)	5.49 (± 0.15)
0.60	4.49 (± 0.12)	5.06 (± 0.12)	5.09 (± 0.12)
0.40	4.57 (± 0.16)	4.66 (± 0.17)	4.72 (± 0.12)

MeOH has a higher Gutmann donor number ($DN = 19.0$) than that of DO ($DN = 14.8$).³⁶ However, a comparison of the stability constants given in Table I and II revealed that Cu²⁺ was strongly solvated and hardly complexed by the ligand in solvent mixtures with higher content of MeOH and the stability constants increased with increasing the concentration of DO in binary solvents.²⁰ This fact is in accordance with the reverse order of their solvating ability as represented by their Gutmann donor numbers. It is known that the solvating ability of a solvent plays an important role in complexation reactions. Moreover the stability and selectivity of the formed complexes are affected by a number of molecular factors, such as the number and character of the donor atoms in the Schiff base, the polarisability and charge density of the metal ion, the nature of the sub-

TABLE II. Values of log K_f for Cu²⁺-SAP complex obtained from spectrophotometric titration in different binary mixtures of MeOH and DO at 298.15 K; standard errors are given in parentheses

w_1	log K_f
1.00	4.82 (± 0.12)
0.80	5.19 (± 0.10)
0.60	4.95 (± 0.13)
0.40	4.70 (± 0.10)

stituents and the character of the co-anion with the cationic species.^{37,38} In the Cu²⁺-SAP complex, the ligand binds the Cu²⁺ through its three binding sites (O, N, O) and the fourth coordination site is most probably occupied by solvent molecules, *i.e.*, MeOH or DO or H₂O molecules.^{15,17} The variation of the log K_f of Cu²⁺-SAP complex as a function of solvent composition (w_1) is shown in Fig. 5 and it showed that the change in the stability constants for Cu²⁺-SAP complex vs. the solvent composition (w_1) was not linear. This evidence reflects that changes might be occurring in the structure of the solvent mixtures²² and these changes probably alter the solvation of the metal ion, the Schiff base and even the resulting complex as well as the preferential solvation of these species in the mixed solvents. Such changes caused changes in the interactions of the solvents with the solutes.³⁹ It is well known that preferential solvation of ions in mixed solvent systems depends on two factors: the relative donor-acceptor abilities of the component molecules towards the ion and the interactions between solvent molecules themselves. The solvating properties of the components in mixed solvents can even be significantly modified by solvent-solvent interactions when the energy of the latter is comparable with the energy difference of solvent-ion interactions for both components.⁴⁰

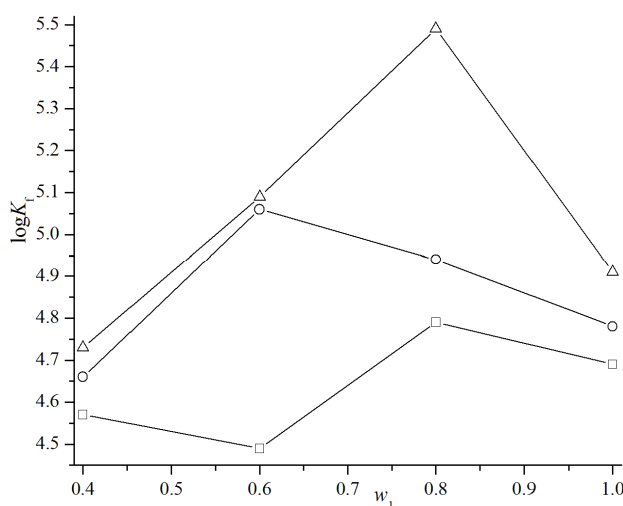


Fig. 5. Variation of the stability constant (log K_f) for the Cu²⁺-SAP complex against different mass fractions (w_1) of MeOH in the binary solvent mixtures at different temperatures:
 □, 298.15 K; ○, 308.15 K; Δ, 318.15 K.

Nevertheless, the stability constants given in Tables I and II have nearly same order although the formation constants evaluated by two methods (spectro-photometric and conductometric) were not same but close in magnitude. This is because the experimental data were analysed by two different approaches in the

two methods to obtain the stability constants (K_f) and they have their own intrinsic error limit.

Thermodynamic parameters

In order to gain a better understanding of the thermodynamics of the complexation reaction between Cu²⁺ and SAP, it is useful to determine the contribution of enthalpy and entropy of the reaction. The thermodynamic parameters were calculated from the temperature dependence of the complexation constants (Van't Hoff plot shown in Fig. 6):

$$2.303 \log K_f = -\frac{\Delta H}{RT} + \frac{\Delta S}{R} \quad (15)$$

For all the solvent mixtures, plots of $\log K_f$ vs. $1/T$ were almost linear and the ΔS and ΔH values were determined in the usual way from the slope and the intercept of the plots, respectively. The various calculated thermodynamic parameters are listed in Table III. The ΔH values associated with the complexation reaction were positive for all the solvent mixtures and the values decreased for the mixed solvents with decreasing the mass fraction of MeOH in the binary solvent mixtures of MeOH with DO. The ΔS values were all always positive and generally decreased with increasing temperature. Moreover, the ΔG values for the present complexation reaction were negative for all the solvents indicating that the reaction was spontaneous and entropy factors were observed to be the dominating factor in making the ΔG values negative. Thus, it is evident that the complexation reactions were spontaneous and entropy-driven in all solvent systems. These trends

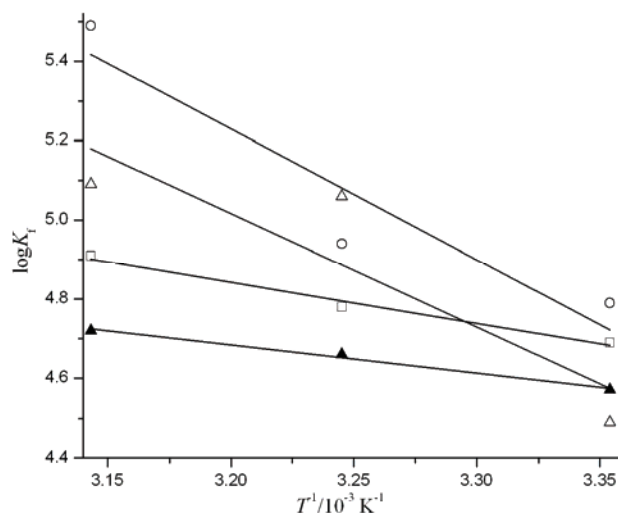


Fig. 6. Van't Hoff Plot for the Cu²⁺-SAP complex in different solvent mixtures with MeOH mass fractions: $\square, w_1 = 1.00$; $\circ, w_1 = 0.80$ (\circ), $w_1 = 0.60$ (Δ) and $w_1 = 0.40$ (\blacktriangle).

TABLE III. Thermodynamic parameters (ΔH , ΔS and ΔG) for the formation of the Cu^{2+} -SAP complex in different binary mixtures of MeOH and DO; standard errors are given in parentheses

w_1	$\Delta G / \text{kJ mol}^{-1}$			ΔH	ΔS
	298.15 K	308.15 K	318.15 K	kJ mol^{-1}	$\text{J mol}^{-1} \text{K}^{-1}$
1.00	-26.73(± 0.12)	-28.29(± 0.12)	-29.86(± 0.16)	19.93(± 0.13)	156.51(± 0.19)
0.80	-26.95(± 0.21)	-29.98(± 0.12)	-33.00(± 0.21)	63.15(± 0.23)	302.23(± 0.13)
0.60	-26.11(± 0.13)	-28.83(± 0.13)	-31.55(± 0.15)	55.00(± 0.21)	272.04(± 0.21)
0.40	-26.11(± 0.12)	-27.44(± 0.14)	-28.78(± 0.12)	13.65(± 0.14)	133.35(± 0.15)

are the thermodynamic parameters for the complexation reaction is an overall result of several factors, such as solvation/desolvation of the species involved in the complexation reaction and variation in flexibility of Schiff base during the complexation process as well as the degree of ion-solvent, ligand-solvent, complex-solvent and solvent-solvent interactions.^{41,42} Again electrostatic forces of attraction between two ions of opposite charge depends on the dielectric constants* (ε_r) of the solvents. For the solvents used in this study, ε_r of the solvents decreased as the amount of DO in the solvent mixture increased; thus, addition of DO resulted in a greater attractive force that in effect reduces the dissociation of $\text{Cu}(\text{NO}_3)_2$ in the solutions and thus the values of $\log K_f$ decreased as the amount of DO increased the solvent mixtures.⁴³ However, a non-linear relation between $\log K_f$ and $1/\varepsilon_r$ was found, as shown in Fig 7. Such non-linearity may partly be attributed to preferential solvation of the ionic reactants by one component, in

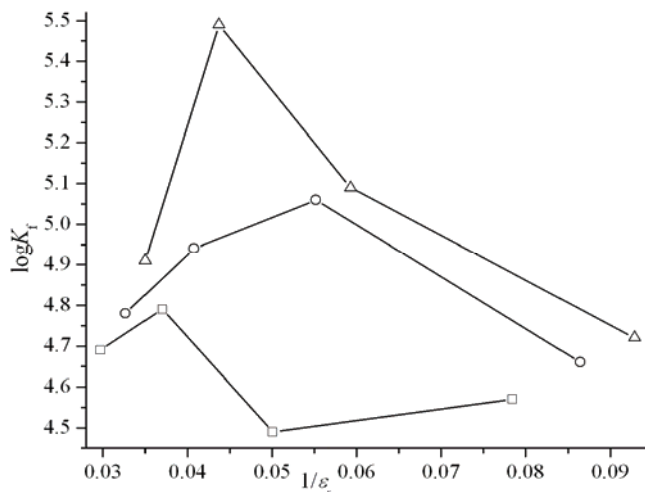


Fig. 7. Plots of the stability constant ($\log K_f$) for the Cu^{2+} -SAP complex against $1/\varepsilon_r$ (ε_r is dielectric constant of the solvent mixtures) at different temperatures; \square , 298.15 K; \circ , 308.15 K; Δ , 318.15 K.

*Relative permittivity.

general the more polar component, of the solvent mixture and partly to other solvent properties, such as viscosity, cohesion, hydrogen bonding tendencies and solvolysis propensities, etc.⁴⁴

CONCLUSIONS

The stability constants for the complexation of copper(II) ion with *N*-Salicylidene-2-aminophenol (SAP) were determined conductometrically and spectrophotometrically at different temperatures. Thermodynamic parameters of complexation were determined from the temperature dependence of the formation constant. The stoichiometry of the Cu²⁺-SAP complex in pure MeOH and all MeOH-DO binary mixtures was found to be 1:1. The negative values of ΔG showed the ability of the ligand SAP to form stable complex with Cu²⁺ and the complexation process proceed spontaneously.

Acknowledgements. The authors are grateful to the Departmental Special Assistance Scheme under the University Grants Commission, India (DRS-SAP-III, No. F540/12/DRS/2013) for financial support. One of the authors (D. B) is also thankful to UGC, India for granting him a UGC BSR Research Fellowship in Science (Ref. No. 4-1/2008 (BSR)).

ИЗВОД

СПЕКТРОФОТОМЕТРИЈСКО И КОНДУКТОМЕТРИЈСКО ИСПИТИВАЊЕ
КОМПЛЕКСИРАЊА *N*-САЛИЦИЛИДЕН-2-АМИНОФЕНОЛА СА Cu²⁺ У БИНАРНИМ
РАСТВОРИМА МЕТАНОЛ + 1,4-ДИОКСАН

RASHMIDIPTA BISWAS, DHIRAJ BRAHMAN и BISWAJIT SINHA

Department of Chemistry, University of North Bengal, Darjeeling-734013, India

Реакција комплексирања између *N*-салицилиден-2-аминофенола, скраћено SAP, са Cu²⁺ је испитивана у бинарним мешавинама метанола и 1,4-диоксана применом кондуктометријске и спектрофотометријске методе на различитим температурама. Константе стабилности (K_f) за 1:1 комплекс, Cu²⁺-SAP, су израчунате на основу компјутерског фитовања апсорбације и моларне проводљивости у функцији различитих молских односа ($c_M:c_L$ или $c_L:c_M$) у различитим бинарним мешавинама раствараца. Нелинерано понашање је опажено у зависности log K_f за комплекс од састава раствараца. Равните термодинамички параметри (ΔH , ΔS и ΔG) за формирање Cu²⁺-SAP комплекса су одређени на основу температурске зависности константе стабилности (K_f). Сви резултати показују да је реакција комплексирања вођена ентропијом и да на њу утиче природа и састав помешаних раствараца.

(Примљено 29. јануара, ревидирано 26. марта, прихваћено 1. априла 2014)

REFERENCES

1. Z. L. You, H. L. Zhu, W. S. Liu, Z. *Anorg. Allg. Chem.* **630** (2004) 1617
2. A. Gölcü, M. Tümer, H. Demirelli, R. A. Wheatley, *Inorg. Chim. Acta* **358** (2005) 1785
3. C. R. Choudhury, S. K. Dey, N. Mondal, S. Mittra, S. O. G. Mahalli, K. M. A. Malik, *J. Chem. Crystallogr.* **31** (2002) 57
4. T. Katsuki, *Coord. Chem. Rev.* **140** (1995) 189
5. S. Di Bella, *Chem. Soc. Rev.* **30** (2001) 335

6. D. A. Cogan, G. C. Liu, K. J. Kim, B. J. Backes, J. A. Ellman, *J. Am. Chem. Soc.* **120** (1998) 8011
7. S. N. Pandeya, D. Sriram, G. Nath, E. DeClercq, *Eur. J. Pharm. Sci.* **9** (1999) 25
8. E. S. Raper, *Coord. Chem. Rev.* **153** (1996) 199
9. S. Yamada, H. Kuma, K. Yamanouchi, *Inorg. Chim. Acta* **10** (1974) 151
10. G. C. Percy, H. S. Stenton, *Spectrochim. Acta A* **32** (1976) 1615
11. B. A. Kushekar, D. D. Khanolkar, *Indian J. Chem. A* **22** (1983) 881
12. V. V. Dixit, B. H. Mehta, *Natl. Acad. Sci. Lett.* **9** (1986) 179
13. A. A. Abd El-Gaber, A. M. A. Hassaan, M. El-Shabasy, A. M. El-Roudi, *Synth. React. Inorg. Met-Org. Chem.* **21** (1991) 1265
14. J. R. Turnlund, W. R. Keyes, H. L. Anderson, L. L. Acord, *Am. J. Clin. Nutr.* **49** (1989) 870
15. A. A. Aziz, A. N. M. Salem, M. A. Sayed, M. M. Aboaly, *J. Mol. Struct.* **1010** (2012) 130
16. J. M. Gemi, C. Biles, J. B. Keiser, S. M. Poppe, S. M. Swaney, W. G. Tarapley, D. L. Romeso, Y. Yage, *J. Med. Chem.* **43** (2004) 1034
17. E. A. Enyedy, E. Zsigo, N. V. Nagy, C. R. Kowol, A. Roller, B. K. Keppler, T. Kiss, *Eur. J. Inorg. Chem.* **25** (2012) 4036
18. A. Shokrollahi, M. Ghaedi, H. Ghaedi, *J. Chin. Chem. Soc.* **54** (2007) 933
19. A. Shokrollahi, M. Ghaedi, M. Montazerozohori, A. H. Kainfar, H. Ghaedi, N. Khanjari, S. Noshadi, S. Joybar, *E-J. Chem.* **8** (2011) 495
20. R. Biswas, D. Brahman, B. Sinha, *J. Serb. Chem. Soc.* **79** (2014) 565
21. S. Dixit, W. C. K. Poon, J. Crain, *J. Phys. Condens. Matter* **12** (2000) L323
22. Y. K. Syrkin, M. E. Dyatkina, *Structure of Molecules and the Chemical Bond*, Dover, New York, 1964, p. 127
23. A. G. J. Ligtenbarg, R. Hage, A. Meetsma, B. L. Feringa, *J. Chem. Soc., Perkin Trans. 2* (1999) 807
24. D. Brahman, B. Sinha, *J. Chem. Eng. Data* **56** (2011) 3073
25. M. Joshaghani, M. B. Ghavidel, F. Ahmadi, *Spectrochim. Acta, A* **70** (2008) 1073
26. H. A. Benesi, J. H. Hildebrand, *J. Am. Chem. Soc.* **71** (1949) 2703
27. B. K. Sarkar, M. N. Roy, B. Sinha, *Indian J. Chem. A* **48** (2009) 63
28. A. J. Sharma, A. I. Popov, *J. Chem. Thermodyn.* **11** (1979) 1145
29. K. M. Tawarah, S. A. Mizyed, *J. Solution. Chem.* **18** (1989) 387
30. P. Debye, H. Hückel, *Phys. Z.* **24** (1928) 305
31. V. S. Ijeri, A. K. Srivastava, *Eur. J. Inorg. Chem.* (2001) 943
32. V. Gutmann, *The Donor-Acceptor Approach to Molecular Interactions*, Plenum Press, New York, 1978, p. 26
33. A. I. Popov, J. M. Lehn, in: *Coordination Chemistry of Macrocyclic Compounds*, G. A. Melson, Ed., Plenum Press, New York, 1985
34. B. O. Strasser, A. I. Popov, *J. Am. Chem. Soc.* **107** (1985) 7921
35. M. R. Ganjali, A. Rohollahi, A. Monghim, M. Shamsipur, *Pol. J. Chem.* **70** (1996) 1172
36. Z. Pourghobadi, F. Sayyed-Majidi, M. Daghighi-Asli, F. Parsa, A. Monghim, M. R. Ganjali, H. Aghabozorg, M. Shamsipur, *Pol. J. Chem.* **74** (2000) 837
37. R. M. Izatt, J. S. Bradshaw, S. A. Nielsen, J. D. Lamb, J. J. Christensen, D. Sen, *Chem. Rev.* **85** (1985) 271
38. R. M. Izatt, K. Pawlak, J. S. Bradshaw, R. L. Bruening, *Chem. Rev.* **91** (1991) 1721
39. G. H. Rounaghi, R. S. Khoshnood, M. H. A. Zavar, *J. Incl. Phenom. Macrocycl. Chem.* **54** (2006) 247

40. J. Zymanśka-Cybulska, E. Kamieńska-Piotrowich, *J. Solution. Chem.* **35** (2006) 1631
41. G. Khayatian, S. Shariati, M. Shamsipur, *J. Incl. Phenom. Macrocycl. Chem.* **45** (2003) 117
42. M. Shamsipur, M. Saeidi, *J. Solution. Chem.* **29** (2000) 1187
43. G. E. Papanastasiou, I. I. Zlogas, *J. Chem. Eng. Data* **37** (1992) 167
44. E. S. Amis, *Solvent Effects on Reaction Rates and Mechanisms*, Academic Press, New York, 1996, p. 8.



Application of gas chromatography analysis to quality control of residual organic solvents in clopidogrel bisulfate

ALEKSANDAR D. PAVLOVIĆ¹, LJUBIŠA M. IGNJATOVIĆ^{1*}, SAŠA Z. POPOV¹,
ALEKSANDAR R. MLADENOVIĆ² and IGOR N. STANKOVIĆ³

¹University of Belgrade, Faculty of Physical Chemistry, Studentski trg 12–16, Belgrade, Serbia,

²University of Belgrade, Faculty of Technology and Metallurgy, Karnegijeva 4, Belgrade, Serbia and ³University of Novi Sad, Faculty of Sciences, Trg Dositeja Obradovića 3, Novi Sad, Serbia

(Received 20 November 2013, revised 4 February, accepted 23 February 2014)

Abstract: A direct-injection, split-mode capillary gas chromatographic procedure with flame ionization detection was developed for the analysis of eight solvents used in the synthesis and purification of the anti-thrombotic drug clopidogrel bisulfate. The solvents analyzed were methanol, acetone, dichloromethane (DCM), 2-butanol, cyclohexane, toluene, acetic acid and *N,N*-dimethylformamide (DMF). In addition, because of dehydration of 2-butanol during the drying process, significant amounts of 2-butanol dehydration products (1-butene, *cis*- and *trans*-isomers of 2-butene, 2,2'-oxybis[butane] and 1-(1-methylpropoxy)butane) may be detected in clopidogrel bisulfate samples. The content of each of these volatile products can be evaluated using the same gas-chromatographic method, with quantification based on the response factor established for the chromatographic peak of 2-butanol. Based on a large number of result sets, retrospectively, from many different batches analyzed, conclusions were made about process variations and reliability and a lack of consistency was identified in the quality of the active substance from a particular producer source. Multivariate analysis was used as the statistical technique to classify the samples. From the analyzed set of 11 solvents, 6 of them were preselected based upon their occurrence in the samples and both Principal Component Analysis (PCA) and Hierarchical Cluster Analysis (HCA) were performed.

Keywords: volatile impurities; validation; chemometrics; multivariate analysis; GC.

* Corresponding author. E-mail: ljignjatovic@ffh.bg.ac.rs

Serbian Chemical Society member.

doi: 10.2298/JSC131120013P

INTRODUCTION

Clopidogrel bisulfate (structural formula is shown in Fig. 1) is a potent anti-thrombotic drug used for the prevention of vascular thrombosis in patients with coronary artery disease, peripheral vascular disease, and cerebrovascular disease.^{1–4}

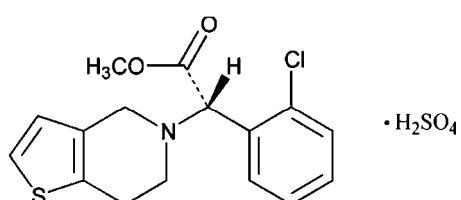


Fig.1. The structural formula of clopidogrel bisulfate, methyl (2*S*)-2-(2-chlorophenyl)-2-(6,7-dihydro-4*H*-thieno[3,2-*c*]pyridin-5-yl)-acetate hydrogen sulfate.

Clopidogrel is a dihydro thieno pyridine derivative pro-drug which is inactive *in vitro* and is only active after intravenous or oral administration.⁵ *In vivo* studies have demonstrated that for its activation, clopidogrel has to undergo CYP2C19 metabolism to obtain an intermediate metabolite.⁶ This intermediate metabolite is hydrolyzed and produces the active form.⁷

Regardless of the efficiency drying techniques, it is impossible to remove completely organic solvents routinely used in the synthesis and purification of active pharmaceutical ingredients. The solvents remaining in pharmaceutical products are designated as “residual solvents” or “volatile organic impurities”.⁸ The residual organic solvents have no therapeutic function, can be toxic and may also accelerate the degradation of the active substance and thereby threaten the stability of the drug. Moreover, they are not desirable in the final product because of their odor or taste, which could be unpleasant for patients. Testing of drug substances, excipients, and drug products for residual solvents should be performed when production or purification processes are known to result in the presence of such residual solvents. Compendial methods of testing for the content of residual solvent are described in USP-NF general chapter.⁹ However, as it is only necessary to test for residual solvents that are used or produced in the manufacture or purification of drug substances, the use of other alternative methods is encouraged.^{10,11} Gas chromatography (GC) was the natural method of choice for residual solvent analysis. It is a relatively old analytical technique, well documented in the literature, but still irreplaceable in this issue.^{12–18} Modern capillary-column GC can separate a large number of volatile components, permitting identification through retention characteristics and detection at ppm levels using a broad range of detectors.¹⁹ However, flame ionization detection (FID) is by far the most preferred because of its universality, low detection limits, robustness, ease of operation, and general accessibility and reliability.^{20,21} Residual solvent determination using direct-injection sample preparation is the oldest technique, and it was preferred because of its simplicity, reliability and ease of operation.^{22–}

²⁵ The drug substance is dissolved in or extracted with a high-boiling-point solvent, such as water, dimethyl sulfoxide (DMSO), dimethylformamide (DMF), dimethylacetamide (DMA) and benzyl alcohol, and then directly injected. Using high-boiling-point solvent has the advantage that the diluent solvent peak elutes later, thus not interfering with the earlier eluting analyte peaks. The aim of this study was to set up a method for the determination of residual solvents in clopidogrel bisulfate that uses the simplest GC instrumentation that is available to almost every laboratory.

Chemometric methods were used for the classification and comparison of several different samples of clopidogrel bisulfate according to the profiles of the residual solvents obtained by using this GC method of analysis. The application of chemometry to monitoring data enables these data to be compared with data for older samples in order to obtain a complete overview of the quality and reliance of a particular clopidogrel bisulfate source. The applications of chemometric pattern recognition techniques (principal component analysis – PCA and hierarchical cluster analysis – HCA) were used to reduce the complexity of the large data sets and to achieve a better interpretation and understanding of the quality of the samples.^{26–28}

Taking the above-mentioned consideration into account, the aim of this study was to develop and validate a simple analytical method that allows the determination of residual solvents in clopidogrel bisulfate and to obtain a complete overview of the quality and reliance of a particular source of clopidogrel bisulfate.

EXPERIMENTAL

Chemicals and reagents

Analytical grade solvents were obtained from the following suppliers: 2-butanol, cyclohexane, DMA and acetic acid were purchased from Merck (Darmstadt, Germany); methanol, acetone, DMF were purchased from Sigma–Aldrich (Steinheim, Germany), and DCM from J. T. Baker (Deventer, The Netherlands). The samples of clopidogrel bisulfate, under investigation were kindly provided by Hemofarm (Vršac, Serbia). All the solvents and reagents were commercial products, suitable for GC analysis and more than 99 % pure, were used without further purification. Nitrogen, hydrogen and hydrocarbon-free synthetic air were of 6.0 purity purchased from Messer Tehnogas (Belgrade, Serbia).

Equipment

All experiments were performed on an Agilent Technologies 6850 series gas chromatograph (Santa Clara, CA, USA), which was equipped with a standard oven for temperature ramping, split/splitless injection ports, 6850 series automatic liquid sampler and flame ionization detector (FID). An analytical balance CPA 225D from Sartorius, (Göttingen, Germany) was used for weight measurements. Variable micropipettes (20–200 µL and 10–100 µL from Carl Roth (Karlsruhe, Germany) and 0.5–10 µL from Biohit (Helsinki, Finland) were used.

Chromatography conditions

Chromatographic separation was performed using a low to medium polarity, megabore capillary column DB-624, Agilent Technologies, with a stationary phase composition: 6 % cyanopropylphenyl/94 % dimethylpolysiloxane, with an internal diameter of 0.53 mm, film thickness of 3.0 µm and length of 30.0 m. The initial oven temperature of 40 °C was maintained for 10 min, then raised at a rate of 6 °C min⁻¹ to 130 °C and maintained for 5 min, increased at a rate of 35 °C min⁻¹ to reach a final temperature of 260 °C and maintained for 16 min.

The temperature of the injection port was maintained at 220 °C. The samples were injected by the direct injection method in the split mode at a split ratio of 1:5, a split flow rate of 20.2 cm³ min⁻¹, and a total flow rate of 26.7 cm³ min⁻¹. The injection volume was 1 µL, injected in GC injection port automatically by the Agilent 6890 series auto sampler. Nitrogen was used as the carrier gas at a constant flow rate of 4.0 cm³ min⁻¹ with the pressure maintained at 19.3 kPa. The average velocity of the gas through the column was 30 cm s⁻¹ at 45 °C. The FID temperature was 250 °C, and the FID flow rate was 30 cm³ min⁻¹ for hydrogen, 400 cm³ min⁻¹ for air. Nitrogen was used as the makeup gas at a constant flow rate of 25 cm³ min⁻¹. Chromatographic data were collected and processed by the ChemStation chromatography data management system (rev. B.02.01. Agilent Technologies). The data were stored in data organizing and storage module ChemStore C/S (rev. B03.03, Agilent Technologies).

Preparation of the standard and test solutions

A common standard stock solution in DMA containing all the known residual solvents of clopidogrel bisulfate (*i.e.*, methanol, acetone, DCM, 2-butanol, cyclohexane, toluene, acetic acid and DMF) was prepared in such a way that after dilution it had a final concentration of 500 µg g⁻¹ for methanol, 500 µg g⁻¹ for acetone, 600 µg g⁻¹ for DCM, 5000 µg g⁻¹ for 2-butanol 2000 µg g⁻¹ for cyclohexane, 890 µg g⁻¹ for toluene, 2600 µg g⁻¹ for acetic acid and 880 µg g⁻¹ for DMF each with respect to 20 mg cm⁻³ of the respective test concentration. About 13 µL of methanol, 13 µL of acetone, 9 µL of DCM, 124 µL of 2-butanol, 51.3 µL of cyclohexane, 21 µL of toluene, 50 µL of acetic acid and 19 µL of DMF were transferred by suitable autopipettes into a 10-mL volumetric flask partially filled with DMA and diluted to volume with the same solvent. The calibration standard solution was prepared by diluting 100 µL of the standard stock solution to 10.0 mL with DMA. The test solution was prepared as follows: accurately weighed 200 mg sample of clopidogrel bisulfate was dissolved with DMA in a 10-mL volumetric flask.

Quantification

The concentration c_i of *i*-th residual solvents in µg per g of the drug substance sample (µg g⁻¹) was calculated by using the external standards method. The employed equation was:

$$c_i = \frac{10^4 r_{t,i} v_i \rho_i}{r_{s,i} m_t} \quad (1)$$

where $r_{t,i}$ is the area response of solvent *i* in an injected sample solution, $r_{s,i}$ is the average area response of solvent *i* in six injected standard solutions, ρ_i and v_i are the density and volume, respectively, of solvent *i* in the standard solution, and m_t is measured mass in mg of the clopidogrel bisulfate sample. The densities of methanol, acetone, DCM, 2-butanol, cyclohexane, toluene, acetic acid and DMF used in the calculation were 0.79, 0.78, 1.32, 0.81, 0.78, 0.87, 1.05 and 0.95 g cm⁻³, respectively. All degradation products of 2-butanol (*cis*-

-2-butene, *trans*-2-butene, 2,2'-oxydibutane and 1-(1-methylpropoxy)butane) were quantified using the same response as that of the 2-butanol peak.

Data analysis

PCA and HCA were realized using Statgraphics Plus 5.1 software. All data were mean centered and scaled to the unit standard deviation prior to any multivariate analysis.

RESULTS AND DISCUSSION

Method development

The boiling points for 1-butene, -6.5 °C, *cis*-2-butene, 0.9 °C, and *trans*-2-butene, 3.7 °C, are lower than room temperature and for this reason, short retention times were obtained for these substances. As the oven had no cryogenic cooling option to cool the column to under room temperature, it was not possible to achieve the higher resolution that would be obtained at lower temperatures. Therefore, an isocratic part of the temperature ramp at 40 °C was chosen to ensure robustness of the method, regardless of the ambient temperature, and satisfactory separation of the low boiling solvents was attained. After this isothermal part, two temperature ramps of 6 and 35 °C min⁻¹ were used to speed up the chromatographic analysis for the late-eluting peaks and for fast elution of DMA. DMA was selected as the sample diluent as it has a high boiling point of 165 °C that does not interfere with the more volatile analytes. Clopidogrel bisulfate is freely soluble in DMA allowing 1 g of substance to be dissolved in less than 10 cm⁻³ of this solvent.

There was no noticeable degradation of the matrix components in the injection port or on the column, which would generate products that could interfere with the components of interest. Accordingly, direct-injection sample preparation was selected as an entry-level in terms of the necessary instrumentation.

Method validation

Using a well-designed experiment and statistically relevant analysis, method validation was performed and accomplished in accordance with relevant guidelines.^{29,30} The method validation was realized by evaluating the specificity, limit of detection (*LOD*) and limit of quantification (*LOQ*), linearity, accuracy, precision and robustness. The range of the method was determined by in-house specification limits given in Table S-I of the Supplementary material to this paper.

System suitability test. System suitability test was developed for the routine application of the method based on the results obtained in several representative performances of the method. Prior to each analysis, the chromatographic system must satisfy requirements (resolution and repeatability) of the suitability test. System suitability was determined from six replicate injections of the standard solution. The peak-to-peak resolution between each peak measured on a reference solution must be above 1.0 and the relative standard deviation (*RSD*) must be less than 15.0 % for the peak area for each solvent. All the system suitability

criteria during validation of the study and batch analysis study were within the acceptance limits.

Specificity. Clopidogrel bisulfate samples were spiked with all the solvents individually and each sample was chromatographed to examine interference, if any, of the residual solvents peak on each other. The selectivity was confirmed by injecting a blank solution of DMA, the standard solution (Fig. S-1 of the Supplementary material), the test solution, and the test solution spiked with residual solvents at the level of the specifications (Fig. S-2 of the Supplementary material). The relative retention times for methanol, acetone, DCM, 2-butanol, cyclohexane, toluene, acetic acid and DMF were found to be 0.14, 0.22, 0.26, 0.47, 0.52, 0.86, 0.93 and 1.00, respectively. The resolution between each two adjacent chromatographic peaks in test solution was found to be less than 1.0, as given in Table I.

TABLE I. Some of the achieved chromatographic parameters

Peak origin	Retention time, min	RRT	USP tailing	Resolution
1-Butene	2.526	0.055	1.030	—
<i>trans</i> -2-Butene	2.661	0.062	1.085	2.2
<i>cis</i> -2-Butene	2.794	0.069	1.035	1.9
Methanol	2.931	0.071	1.055	1.7
Acetone	4.448	0.158	1.095	10
DCM	5.282	0.202	1.003	6.2
2-Butanol	9.463	0.426	1.086	18
Cyclohexane	10.503	0.482	1.010	3.2
Toluene	17.263	0.844	1.014	26
2,2'-Oxydibutane	17.855	0.876	1.098	3.1
1-(1-Methylpropoxy)butane	18.080	0.888	1.069	1.1
Acetic acid	18.658	0.919	1.313	2.5
DMF	20.180	1.000	1.459	6.8

Limits of detection and quantification. For predicting the limit of detection (*LOD*) and limit of quantification (*LOQ*) values of each residual solvent, a standard solution was prepared with all residual solvents at the level of about 30 µg g⁻¹ with respect to 20 mg cm⁻³ of the test concentration. This standard solution was injected into the chromatographic system and the *LOD* and *LOQ* values were predicted from the signal to noise (*S/N*) ratio data. The *LOD* and *LOQ* correspond to the concentration with signal of 3 and 10 times the noise level, respectively. Solutions containing all the residual solvents at the predicted *LOQ* concentration levels were prepared and analyzed six times to evaluate the precision of the method at this concentration level, detailed in Table II.

Linearity. The linearity of the method was confirmed by injecting solutions at twelve standard concentration levels, corresponding approximately to 0.5–150 % of the specification level for each of the residual solvents. The concentrations

studied were within the ranges 2.5–750 µg g⁻¹ for methanol and acetone, 3–900 µg g⁻¹ for DCM, 25–7500 µg g⁻¹ for 2-butanol, 10–3000 µg g⁻¹ for cyclohexane, 4.5–1300 µg g⁻¹ for toluene, 13–3900 µg g⁻¹ for acetic acid and 4.4–1300 µg g⁻¹ for DMF. The linearity was evaluated by linear regression analysis, which was calculated by least-square regression analysis. The area and concentration were treated by least square linear regression analysis plot (area count in terms of intensity, pA s, on the y-axis vs. concentration, µg g⁻¹, on the x-axis). The statistical parameters, slope, intercept, residual standard deviation and correlation coefficient values, were calculated and are given in Table III. The standard mixture showed good linearity for all residual solvents in the tested ranges. The area response obeyed the equation $y = ax + b$, where the intercept b was zero within 95 % confidence limits and the square correlation coefficient (R^2) was always greater than 0.9997 (Table III).

TABLE II. *LOQ* and *LOD* values and the precision at the *LOQ* values

Compound	<i>LOD</i> / µg g ⁻¹	<i>LOQ</i> / µg g ⁻¹	Precision at <i>LOQ</i> , <i>RSD</i> / % (n=6)
Methanol	5	22	3.0
Acetone	7	25	5.6
DCM	21	65	6.2
2-Butanol	23	75	4.8
Cyclohexane	14	45	2.3
Toluene	6	22	2.2
Acetic acid	10	40	7.2
DMF	12	35	5.7

TABLE III. Linearity data for standard mixtures: $y = ax + b$, where x is the concentration of residual solvent (µg g⁻¹), y is peak area count (pA s), *RRSD* is the residual relative standard deviation ($S\Delta y/y$, n=2)

Compound	<i>R</i> ²	Regression equation	Slope pA s µg ⁻¹ g	Intercept pA s	<i>RRSD</i> / %
Methanol	0.999956	$y = 1548x + 438$	1548±7	438±1991	0.99
Acetone	0.999984	$y = 3885x + 355$	3885±11	355±2998	0.59
DCM	0.999747	$y = 145x + 353$	145±2	353±535	2.37
2-Butanol	0.999970	$y = 300x + 1420$	300±1	1420±3192	0.82
Cyclohexane	0.999705	$y = 999x + 4824$	999±12	4824±13289	2.56
Toluene	0.999988	$y = 901x + 918$	901±2	918±1079	0.52
Acetic acid	0.999982	$y = 263x + 1721$	263±1	1721±2115	0.63
DMF	0.999980	$y = 932x - 308$	932±3	-308±1433	0.67

Precision. The system precision was evaluated with replicate injections of the standard and spiked sample solutions. The percent relative standard deviation (*RSD*) was found to be 2.04 % for methanol, 2.27 % for acetone, 2.63 % for DCM, 1.72 % for 2-butanol, 3.31 % for cyclohexane, 2.10 % for toluene, 1.34 % for acetic acid and 8.73 % for DMF. The repeatabilities were the intra-day vari-

ation (method precision) and the inter-day variation (ruggedness). The repeatability of the method was studied by analyzing six sample solutions, separately, by addition of solvents at known concentration levels (100 % of specification limits). The *RSD* was found to be 0.98 % for 1-butene, 0.90 % for 2-butene, 2.28 % for methanol, 1.33 % for acetone, 0.89 % for 2-butanol, 0.93 % for cyclohexane, 0.90 % for toluene, 4.89 % for acetic acid, 6.82 % for DMF and 1.99 % for the butyl ethers. The degree of reproducibility, known as ruggedness, was obtained by the analysis of the same sample concentration (which is used for method precision determination) under a variety of conditions using different column series, with a different analyst on different days using new standards and calibration. The overall *RSD* from such a measurement series of twelve runs was found to be 3.85 % for 1-butene, 2.49 % for 2-butene, 2.04 % for methanol, 7.49 % for acetone, 1.87 % for DCM, 1.05 % for 2-butanol, 1.70 % for cyclohexane, 1.12 % for toluene, 8.08 % for acetic acid, 6.99 % for DMF and 1.66 % for the butyl ethers.

Accuracy. The accuracy of the method was evaluated by recovery experiment using the standard addition technique. The recoveries were determined by spiking the respective residual solvents at five different levels ranging from the *LOQ* values to 150 % of the specification level into clopidogrel bisulfate drug substance. The samples were prepared as per the methodology, and analyzed in triplicate and percentage recoveries were calculated. The average recovery values are summarized in Table IV.

Robustness. For the determination of the robustness of the method, a number of method parameters, such as flow rate, initial column temperature, FID temperature and split ratio, were varied within a realistic range, and the quantitative influences of the variables were determined. The method was challenged by varying the following parameters within the limits: flow rate of carrier gas $\pm 10\%$, initial temperature of the column oven $40 \pm 5^\circ\text{C}$, split ratio $(5 \pm 1):1$ and FID temperature $240 \pm 10^\circ\text{C}$. For each set of variations, six replicate injections of the standard solution were performed. The system suitability results met the acceptance criteria at each of the deliberately varied conditions. The *RSD* of the solvent obtained at conditions deliberately varied from those of the developed methodology did not vary much. In all the varied conditions, the chromatographic resolution between any of the two components was not less than 1.0. Hence, the test method is robust for all the varied chromatography conditions.

Result of the analysis for multiple batches of clopidogrel bisulfate

The validated method was used for the analysis of 18 clopidogrel bisulfate samples originating from a single production source (Table S-II of the Supplementary material). From the eight solvents used in the process of synthesis and purification of clopidogrel bisulfate, it was found that the following organic sol-

TABLE IV. Accuracy of the method expressed as the percent recovery (*R*) at different levels, for: I – methanol, II – acetone, III – DCM, IV – 2-butanol, V – cyclohexane, VI – toluene, VII – acetic acid and VIII – DMF

Parameter	I	II	III	IV	V	VI	VII	VIII
Level <i>LOQ</i>	106.2	102.9	105.3	103.5	103.6	105.6	105.3	98.3
	105.3	107.7	110.2	105.2	98.9	102.2	99.8	103.8
	104.2	101.6	101.4	101.3	98.9	103.7	108.4	107.0
Average	105.2	104.1	105.6	103.3	100.5	103.8	104.5	103.0
<i>RSD</i> / %	0.95	3.10	4.17	1.89	2.71	1.63	8.88	4.27
	99.5	100.3	103.7	100.4	97.8	99.7	97.5	97.5
	101.8	101.1	105.3	102.3	98.3	100.9	93.9	105.7
Level 25 %	100.6	100.4	104.1	98.8	97.9	98.3	100.3	99.6
	100.6	100.6	104.4	100.5	98.0	99.6	97.2	100.9
	1.16	0.42	0.82	1.77	0.26	1.31	3.30	4.22
Level 50 %	104.6	103.0	106.8	100.3	99.7	100.1	97.5	102.7
	101.2	97.9	98.7	97.3	99.0	97.0	97.0	99.0
	103.6	101.9	102.4	99.0	98.7	99.3	98.1	102.5
Average	103.1	100.9	102.6	98.9	99.1	98.8	97.5	101.4
<i>RSD</i> / %	1.68	2.62	3.99	1.53	0.52	1.65	0.55	2.03
	102.1	100.7	100.8	101.6	100.2	101.2	99.4	104.9
	99.8	100.1	99.9	100.1	100.2	100.2	96.7	104.3
Level 100 %	97.1	96.7	95.9	97.1	96.3	96.8	98.4	95.6
	99.7	99.2	98.9	99.6	98.9	99.4	98.2	101.6
	2.53	2.22	2.65	2.32	2.32	2.28	1.39	5.09
Level 150 %	100.8	101.7	101.7	101.0	101.5	101.2	101.2	101.5
	99.7	100.2	100.4	100.7	101.1	100.9	101.2	98.5
	98.6	98.6	98.1	99.1	99.8	99.1	100.4	98.3
Average	99.7	100.2	100.0	100.3	100.8	100.4	100.9	99.4
<i>RSD</i> / %	1.14	1.54	1.83	1.02	0.86	1.16	0.44	1.77

vents were frequently present in the samples: 2-butanol, cyclohexane and acetic acid. Due to intramolecular and intermolecular dehydration of 2-butanol, significant amounts of products derived from 2-butanol, 1-butene, *cis*-2-butene, *trans*-2-butene, 2,2'-oxydibutane and 1-(1-methylpropoxy)butane, could be found in the samples. Intramolecular dehydration of 2-butanol results in a mixture containing: 1-butene, *cis*-2-butene and *trans*-2-butene, predominantly the last two in a 50:50 ratio. Intermolecular dehydration of two 2-butanol molecules results in a mixture containing 50:50 ratio of 2,2'-oxybis[butane] and 1-(1-methylpropoxy)-butane. Although *cis*-2-butene and *trans*-2-butene were chromatographically separated from each other, for regulation reasons, they shall be reported as 2-butene by the sum of their contents. A similar approach was used in the case of 2-butan-2-yloxybutane and 1-(1-methylpropoxy) butane, where the total amount was designated as dibutyl ethers. Validation tests of the accuracy showed that 2-butanol products were not formed during GC analysis but were already present

in the clopidogrel samples. The presence of these is likely to be caused by the course of the drying process in clopidogrel bisulfate production.

Substantial contents of acetic acid and 2-butanol (further products derived from 2-butanol, likewise) were found. However, in all the samples they were within the regulatory tolerance limits and without much impact on the quality and stability of final drug product. It should also be taken into account that the contents of residual solvents in the final product were lower than those in the active substance, because only 75 mg of clopidogrel bisulfate is present in 350 mg of total tablet mass.

Multivariate analysis and pattern recognition

Generally, there are two main causes of variation in the quality of products or processes: random causes and patterns that could be recognized. As no deeper insights into the production and purification process of active pharmaceutical ingredients are available, continuous quality control of purchased materials is the only option remaining. Using this approach, based on the result sets of multiple batches of clopidogrel bisulfate (Table S-II), some conclusions may be drawn on the reliability of the sources for providing high-quality material. Multivariate analysis is a commonly used statistical technique to classify samples. From the analyzed set of 11 solvents, 6 of them were preselected based upon their occurrence in the samples and both PCA and HCA were performed. PCA is a method that projects multi-dimension space to a lower dimensional space, reducing the number of variables and enabling graphical interpretation of the results. It could be assumed that a correlation exists between the amount of 2-butanol and its products, or between the amount of 2-butanol and the presence and quantity of the other used solvents. Thus, the implementation of PCA is justified, and in the present case, two principal components were extracted (PC1 and PC2), since these two components had eigenvalues greater than or equal to 1.0. The first principal component had the equation:

$$\text{PC1} = 0.5481 \times [\text{2-Butanol}] - 0.5234 \times [\text{1-Butene}] - 0.5621 \times [\text{2-Butene}] + \\ + 0.1726 \times [\text{Cyclohexane}] + 0.2467 \times [\text{Acetic acid}] + 0.1376 \times [\text{Butyl ethers}] \quad (2)$$

The second principal component had the equation:

$$\text{PC2} = -0.6281 \times [\text{Cyclohexane}] - 0.4282 \times [\text{Acetic Acid}] + \\ 0.1430 \times [\text{2-Butanol}] - 0.1329 \times [\text{1-Butene}] - 0.2558 \times [\text{2-Butene}] - \\ - 0.5644 \times [\text{Butyl ethers}] \quad (3)$$

In Eqs. (2) and (3), the values of the solvent concentrations were standardized by subtracting their means and dividing by their standard deviations. Thus, the PCs are dimensionless quantities. The PCA results showed that the first component accounted for about 41.5 %, and second component for 27.1 % of total variance in the data set. These two components together explained 68.6 %

of total variance accounting for most of the variability in the original data. Since the eigenvalues were greater than 1.0 (2.48 for PC1 and 1.62 for PC2), the discussion is focused only on these two components. PC1 had a relatively high positive weight for 2-butanol, and almost the same high negative weights for 1-butene and 2-butene (the weights are the coefficients from Eq. (2)). PC2 had relatively high weights for cyclohexane, acetic acid and butyl ethers (the weights are the coefficients from Eq. (3)). A weight close to 0 indicates little contribution of the variable to the component. Vectors pointing in the same direction are positively correlated and those pointing in the opposite direction are negatively correlated (Fig. 2). Based on these findings, it was concluded that PC1 could be denoted as being the part dependent on 2-butanol and its main products. On the other hand, PC2, which has high weights for cyclohexane, acetic acid and butyl ethers, can be designated as being the component dependent on the other relevant solvents.

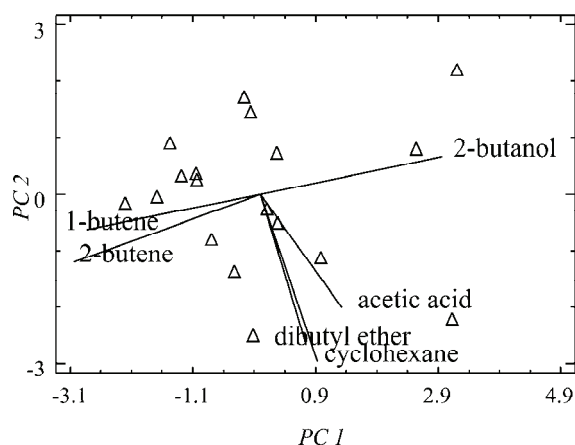


Fig. 2. A bi-plot which involves superimposition of the scores and the loadings plot, with solvents (variables) and samples represented on the same diagram with two selected principal components PC1 and PC2 that are standardized (dimensionless quantities).

The dendrogram analysis (Fig. 3) showed the result of the clustering the 18 batches using the furthest neighbor method and the squared Euclidean distance indicated 6 different classes exist within the data. Strictly speaking, there is only one true class of samples within 12 batches of the population. In this class, the samples were very closely clustered, and were well separated from the other samples. The remaining 6 samples are not similar to any other sample in the all data set. The highest degree of similarity in these 6 samples was observed between two samples that form the same cluster, the similarity was lower than that expressed in the separate 12-member cluster. Generally, it could be assumed that six of the samples are unusual, but that does not help in locating the cause. The

observed dissimilarities were linked with the appearance of cyclohexane, acetic acid or 2-butanol at unusually high levels, in various mutual combinations. In the case of acetic acid, there is a strong variation of its contents from batch to batch (over all, and within the most populated cluster), which is likely to be a problem in controlling the process by which it is removed. Therefore, the manufacturer used the option to set the specifications of 5000 µg g⁻¹, the highest permissible limit for this USP class of residual solvent. Contrary to this, the total content of 2-butanol and its dehydration products are relatively consistent (average of 2800 µg g⁻¹ with RSD of 14.1 %), indicating a good control of the process (Fig. S-III of the Supplementary material). The content of residual solvents could be changed with time due to a further dehydration of 2-butanol and evaporation of all the solvent present, which is dependent on the aging time, packaging and storing conditions, as well as by some of the significant factors.

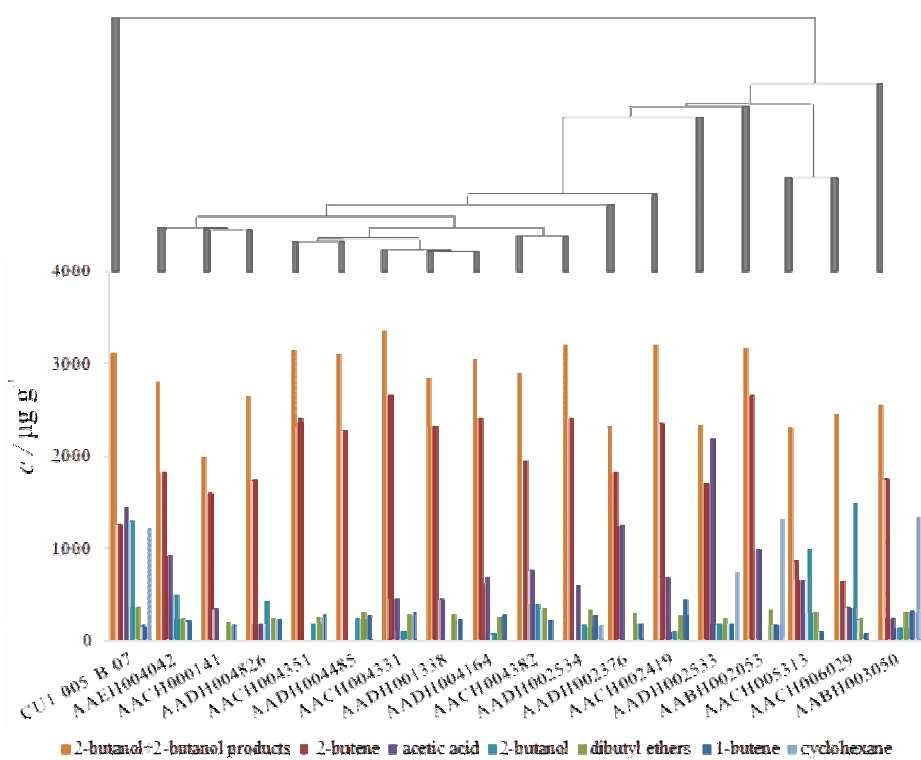


Fig. 3. Graph of variation of content from batch to batch of the most frequent and most abundant organic solvents: 2-butene, acetic acid, 2-butanol, dibutyl ethers, 1-butene and cyclohexane. In the first column, the total amount of 2-butanol and its dehydration products is presented. In the upper part of the image, a dendrogram obtained by the means of HCA is suitably placed. A horizontal line connecting two groups shows that the groups were combined at the distance shown on the vertical axis.

The general conclusion could be that the observed variations in the content of the detected residual solvents between the different batches are probably due to an on-going process of optimization attempts (in 6 of the 18 batches). However, the remaining 12 batches constitute one cluster with similar characteristics and a negligible variation within the group. Other five solvents used in the process, methanol, acetone, DCM, toluene and DMF are present at low levels or completely absent, which are well below the required regulatory limits. In this case, it is possible to narrow the limits of their presence in the specification of the clopidogrel bisulfate samples. Generally speaking, the fact that the manufacturer remained within acceptable limits for all residual solvents in all 18 batches is encouraging, but the observed variations indicate the need for permanent control of material from this source.

CONCLUSIONS

In this work, a GC method for the evaluation of residual solvents in clopidogrel bisulfate samples is presented and validated. Methanol and acetone have a linear response from 2.5 to 750 $\mu\text{g g}^{-1}$ (with respect to a drug concentration of 20 mg cm^{-3}), DCM from 3 to 900 $\mu\text{g g}^{-1}$, 2-butanol from 25 to 7500 $\mu\text{g g}^{-1}$, cyclohexane from 10 to 3000 $\mu\text{g g}^{-1}$, toluene from 4.5 to 1300 $\mu\text{g g}^{-1}$, acetic acid from 13 to 3900 $\mu\text{g g}^{-1}$ and DMA from 4.4 to 1300 $\mu\text{g g}^{-1}$. Calibration line intercepts were zero within the 95 % confidence limit and the square correlation coefficients (R^2) were at least 0.9997. Average recovery values ranged from 97.2 to 105.6 %. Relative standard deviations for precision were not more than 8.08 %. The quantification limits (in $\mu\text{g g}^{-1}$) were as follows: methanol, 22; acetone, 25; DCM, 65; 2-butanol, 75; cyclohexane, 45; toluene, 22; acetic acid, 40; DMA, 35.

The proposed analytical method coupled with the chemometrics data analysis technique was used as a powerful tool for quality control purposes to differentiate the content of residual solvents among samples of clopidogrel bisulfate. The application of chemometry to monitoring data enables a complete overview of the quality and reliability of a particular clopidogrel bisulfate source to be obtained.

SUPPLEMENTARY MATERIAL

Tables S-I and S-II, and Figs. S-1–S-3 are available electronically from <http://www.shd.org.rs/JSCS/>, or from the corresponding author on request.

И З В О Д

ПРИМЕНА ГАСНО-ХРОМАТОГРАФСКЕ АНАЛИЗЕ ЗА ОДРЕЂИВАЊЕ САДРЖАЈА
ЗАОСТАЛИХ ОРГАНСКИХ РАСТВАРАЧА У КОНТРОЛИ КВАЛИТЕТА
КЛОПИДОГРЕЛ-БИСУЛФАТА

АЛЕКСАНДАР Д. ПАВЛОВИЋ¹, ЉУБИША М. ИГЊАТОВИЋ¹, САША З. ПОПОВ¹,
АЛЕКСАНДАР Р. МЛАДЕНОВИЋ² И ИГОР Н. СТАНКОВИЋ³

¹Универзитет у Београду, Факултет за физичку хемију, Студентски трг 12–16, Београд,

²Универзитет у Београду, Технолошко-мештаришки факултет, Карнејијева 4, Београд и

³Универзитет у Новом Саду, Природно-математички факултет, Три Доситеја Обрадовића 3, Нови Сад

Развијена је капиларна гасно-хроматографска метода, у *split* моду, уз директно инјекција и пламено-јонизацијону детекцију, за анализу растворача који су коришћени у синтези и пречишћавању антитромботске активне фармацеутске супстанце, кло-пидогрел-бисулфата. У процесу производње коришћено је осам растворача: метанол, ацетон, дихлорметан, 2-бутанол, циклохексан, толуен, сирћетна киселина и диметилформамид. Додатно, као резултат дехидратације 2-бутанола током процеса сушења, у испитиваним узорцима кло-пидогрел-бисулфата, у значајним количинама се могу наћи дехидратациони производи: 1-бутен, *cis* и *trans* изомери 2-бутена, 2-ди-sec-бутил-етар и sec-бутил-*n*-бутил-етар. Садржај сваког од ових испарљивих производа може се проценити коришћењем исте гаснохроматографске методе, уз квантификацију засновану на фактору одговора успостављеном за хроматографски пик 2-бутанола. За сваки од ових растворача метода је валидирана на селективност, линеарност, тачност, прецизност, робусност, лимит квантификације и лимит детекције. На основу комплексне групе резултата анализа, ретроспективно, за већи број различитих производних серија, закључено је о степену одступања у процесу производње и његовој поузданости, и препознат је недостатак доследности у квалитету активне супстанце која води порекло од једног од комерцијалних производа. Мултиваријантна анализа је коришћена као статистичка техника у међусобном разврставању узорака. Од анализираног скупа од 11 растворача, 6 растворача је било унапред одобрено на основу њихове редовне појаве у узорцима. Изведене су мултиварјантне статистичке технике: анализа главних компоненти (PCA) и хијерархијска кластер анализа (HCA).

(Примљено 20. новембра 2013, ревидирано 4. фебруара, прихваћено 23. фебруара 2014)

REFERENCES

1. J. M. Herbert, D. Frehel, E. Vallee, G. Kieffer, D. Gouy, Y. Berger, J. Necciari, G. Defreyn, J. P. Maffrand, *Cardiovasc. Drug Rev.* **11** (1993) 180
2. B. Jarvis, K. Simpson, *Drugs* **60** (2000) 347
3. S. Yusuf, F. Zhao, S. R. Mehta, S. Chrolavicius, G. Tognoni, K. K. Fox, *N. Engl. J. Med.* **345** (2001) 494
4. P. J. Sharis, C. P. Cannon, J. Loscalzo, *Ann. Intern. Med.* **129** (1998) 394
5. Q. Liu, D. S. Dang, Y. F. Chen, M. Yan, G. B. Shi, Q. C. Zhao, *Genet. Test. Mol. Biomarkers* **16** (2012) 1293
6. P. Savi, J. M. Herbert, A. M. Pflieger, F. Dol, D. Delebasse, J. Combalbert, G. Defreyn, J. P. Maffrand, *Biochem. Pharmacol.* **44** (1992) 527
7. M. Cattaneo, *Eur. Heart J.* **27** (2006) 1010
8. K. Grodowska, A. Parczewski, *Acta Pol. Pharm. Drug Res.* **67** (2010) 3

9. *The United States Pharmacopeia–National Formulary*, US Pharmacopeial Convention, Rockville, MD, 2013, p. 5707
10. ICH Q3C(R5), *Guidance on Impurities: Residual Solvents*, European Medicines Agency, London, 2011
11. C. Witschi, E. Doelker, *Eur. J. Pharm. Biopharm.* **43** (1997) 215
12. K. Grodowska, A. Parczewski, *Acta Pol. Pharm. Drug Res.* **67** (2010) 13
13. C. B. Hymer, *Pharm. Res.* **20** (2003) 337
14. I. D. Smith, D. G. Waters, *Analyst* **116** (1991) 1327
15. B. Iosefzon-Kuyavskaya, *Accred. Qual. Assur.* **4** (1999) 240
16. M. V. Russo, *Chromatographia* **39** (1994) 645
17. L. Zhong, H. Yieng-Hau, P. M. Gregory, *Pharm. Biomed. Anal.* **28** (2002) 637
18. J. Drozd, J. Novak, *J. Chromatogr., A* **165** (1979) 141
19. D. G. Westmorland, G. R. Rhodes, *Pure Appl. Chem.* **61** (1989) 1148
20. I. G. McWilliam, *Chromatographia* **17** (1983) 241
21. I. G. McWilliam, R. A. Dewar, *Nature* **181** (1958) 760
22. C. F. Poole, S. A. Schuette, *J. High. Res. Chromatogr.* **6** (1983) 526
23. C. C. Camarasu, M. Meqe-Szuts, G. B. Varga, *J. Pharm. Biomed.* **18** (1998) 623
24. T. P. Wampler, W. A. Bowe, E. J. Levy, *J. Chromatogr. Sci.* **23** (1985) 64
25. S. Legrand, J. Dugay, K. Vial, *J. Chromatogr., A* **999** (2003) 195
26. K. R. Beebe, R. J. Pell, M. B. Seasholtz, *Chemometrics: A Practical Guide*, Wiley, Mississauga, 1998, p. 56
27. R. G. Brereton, *Applied Chemometrics for Scientists*, Wiley, Chichester, 2007, p. 145
28. J. N. Miller, J. C. Miller, *Statistics and Chemometrics for Analytical Chemistry*, Pearson Education, Edinburgh, 2005, p. 221
29. ICH Q2A, *Text on Validation of Analytical Procedures: Definitions and terminology*, 1994
30. ICH Q2B, *Validation of Analytical Procedures: Methodology*, 1996.



SUPPLEMENTARY MATERIAL TO
Application of gas chromatography analysis to quality control of residual organic solvents in clopidogrel bisulfate

ALEKSANDAR D. PAVLOVIĆ¹, LJUBIŠA M. IGNJATOVIC^{1*}, SAŠA Z. POPOV¹,
ALEKSANDAR R. MLADENOVIĆ² and IGOR N. STANKOVIĆ³

¹University of Belgrade, Faculty of Physical Chemistry, Studentski trg 12–16, Belgrade, Serbia,

²University of Belgrade, Faculty of Technology and Metallurgy, Kardeljeva 4,

Belgrade, Serbia and ³University of Novi Sad, Faculty of Sciences,

Trg Dositeja Obradovića 3, Novi Sad, Serbia

J. Serb. Chem. Soc. 79 (10) (2014) 1279–1293

TABLE S-I. USP class,¹ USP¹ and in-house specification limits

Solvent name	USP class	USP specifications, µg g ⁻¹	In house specifications, µg g ⁻¹
Cyclohexane	2	3880	2000
DMF	2	880	880
Methanol	2	3000	500
DCM	2	600	600
Toluene	2	890	890
Acetic acid	3	5000	2600
Acetone	3	5000	500
2-Butanol	3	5000	5000
1-Butene	4	No data	450
2-Butene	4	No data	3500
Dibutyl ethers	4	No data	700

TABLE S-II. Results of the analysis of 18 batches of clopidogrel bisulfate

Compound	CU1 005 B 07	AAEH0 04042	AACH0 02419	AABH0 02053	AABH0 03050	AACH0 00141	AADH0 02533	AACH0 04351	AACH0 04331
Cyclohex- ane	1228	<LOD	<LOD	1315	1349	<LOD	735	<LOD	<LOD
DMF	<LOD	<LOD	<LOD	<LOD	45	<LOQ	<LOD	<LOD	<LOD
Methanol	<LOD	<LOD	<LOD	<LOD	26	<LOD	<LOQ	<LOD	<LOD
DCM	43	<LOD							
Toluene	<LOQ	<LOQ	<LOD						
Acetic acid	1449	924	694	996	238	353	2186	<LOD	462

*Corresponding author. E-mail: ljgnjatovic@ffh.bg.ac.rs

TABLE S-II. Continued

Compound	CU1 005 B 07	AAEH0 04042	AACH0 02419	AABH0 02053	AABH0 03050	AACH0 00141	AADH0 02533	AACH0 04351	AACH0 04331
Acetone	<LOQ	<LOQ	<LOD	<LOD	<LOD	<LOD	<LOD	683	<LOD
2-Butanol	1306	506	107	<LOQ	156	<LOQ	188	188	104
1-Butene	174	220	450	176	325	180	193	282	311
2-Butene	1261	1832	2369	2653	1763	1600	1706	2418	2659
Dibutyl ethers	372	251	277	335	306	210	247	258	289
	AACH004 382	AACH0 05313	AACH0 06029	AADH0 01338	AADH0 02376	AADH0 02533	AADH0 04826	AADH0 04485	AADH0 04164
Cyclohex- ane	<LOD	<LOD	<LOD	<LOD	<LOQ	173	<LOD	<LOQ	<LOD
DMF	<LOD	<LOD	<LOD	<LOD	<LOD	<LOD	<LOD	<LOD	<LOD
Methanol	<LOD	<LOD	28	<LOD	<LOD	<LOQ	32	41	<LOD
DCM	<LOD	<LOD	<LOD	<LOD	<LOQ	<LOQ	<LOD	<LOD	<LOD
Toluene	<LOD	<LOD	<LOQ	<LOD	<LOD	<LOD	<LOQ	<LOQ	<LOD
Acetic acid	766	666	372	456	1257	610	195	<LOD	683
Acetone	<LOD	<LOD	<LOD	<LOD	<LOD	<LOD	<LOD	47	<LOD
2-Butanol	387	998	1486	<LOQ	<LOQ	180	433	248	88
1-Butene	215	116	87	236	197	266	227	272	282
2-Butene	1946	880	641	2323	1826	2420	1750	2281	2418
Dibutyl ethers	349	317	251	284	298	337	239	306	258

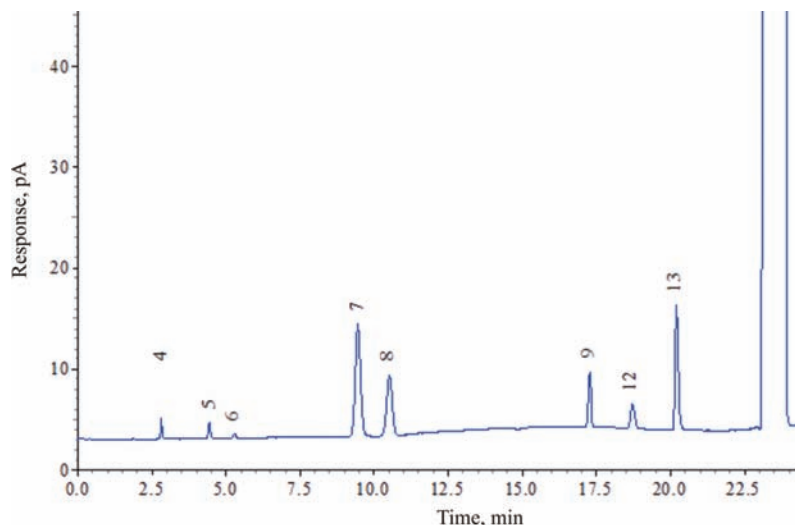


Fig. S-1. Chromatogram of the standard solution. Peaks marked with numbers belong to the following solvents: 4) methanol, 5) acetone, 6) DCM, 7) 2-butanol, 8) cyclohexane, 9) toluene, 12) acetic acid and 13) DMF.

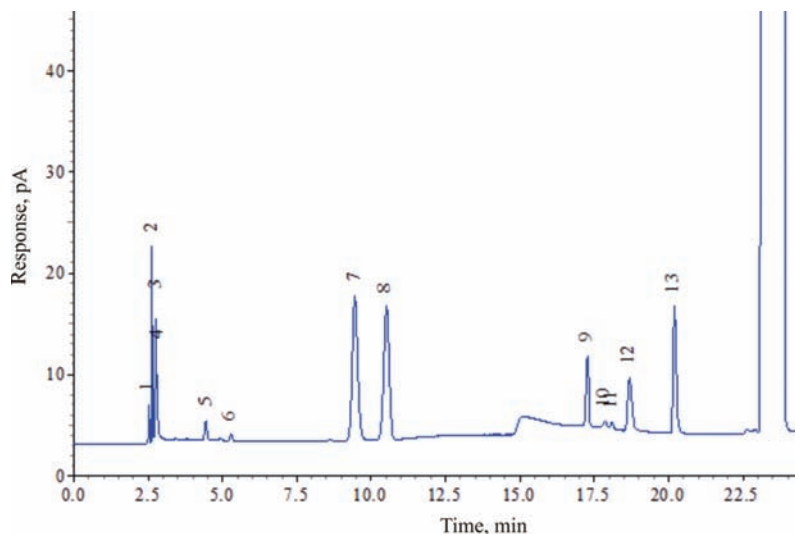


Fig. S-2. Chromatogram of the test solution spiked with residual solvents at the level of specifications. Peaks marked with numbers belong to the following solvents: 1) 1-butene, 2) *trans*-2-butene, 3) *cis*-2-butene, 4) methanol, 5) acetone, 6) DCM, 7) 2-butanol, 8) cyclohexane, 9) toluene, 10) 2,2'-oxybis[butane], 11) 1-(1-methylpropoxy)butane, 12) acetic acid and 13) DMF.

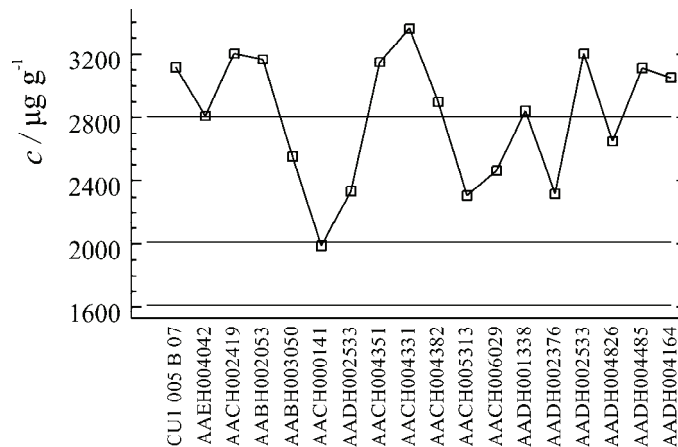


Fig. S-3. The means of the sum of 2-butanol and its dehydration products ($2806.0 \mu\text{g g}^{-1}$) for the 18 different batches and lower control limits ($LCL = 1612.0 \mu\text{g g}^{-1}$). Lower warning limit, at $2010 \mu\text{g g}^{-1}$, is represented as two standard errors.

REFERENCES

1. *The United States Pharmacopeia–National Formulary*, US Pharmacopeial Convention, Rockville, MD, 2013, p. 5707



The effect of the size and shape of alumina nanofillers on the mechanical behavior of PMMA matrix composites

SOMAYA AHMED BEN HASAN¹, MARIJA M. DIMITRIJEVIĆ¹, ALEKSANDAR KOJOVIĆ¹, DUŠICA B. STOJANOVIĆ¹, KOSOVKA OBRADOVIĆ-ĐURIĆIĆ², RADMILA M. JANČIĆ HEINEMANN^{1*} and RADOSLAV ALEKSIĆ¹

¹University of Belgrade, Faculty of Technology and Metallurgy, Karnegijeva 4, Belgrade, Serbia and ²University of Belgrade, Faculty of Stomatology, Dr Subotića 8, Belgrade, Serbia

(Received 21 January, revised 31 March, accepted 2 April 2014)

Abstract: Composites with the addition of alumina nanofillers show improvement in mechanical properties. Poly(methyl methacrylate), PMMA, was used as a matrix and two different types of nanofillers having extremely different shapes were added into the matrix to form the composites. The reinforcements were based on alumina nanoparticles having either a spherical shape or whiskers with a length to diameter ratio of 100. The influence of the size and shape of the alumina fillers and the loading on the mechanical properties of the prepared composite were studied using nanoindentation measurements and dynamic mechanical analysis. It was observed that both alumina whiskers and spherical alumina nanoparticles added in the PMMA matrix improved the mechanical properties of the composites, but the improvement was significantly higher with reinforcement by alumina whiskers. The concentration of the reinforcing spherical alumina nanoparticles and alumina whiskers in the PMMA matrix varied up to 5 wt. %. The best performance was obtained by the addition of 3 wt. % of alumina whiskers in the PMMA matrix in terms of the mechanical properties of the obtained composite.

Keywords: polymer composite; particle shape; nanoindentation; dynamic mechanical analysis.

INTRODUCTION

Poly(methyl methacrylate) (PMMA) has been used in a wide range of fields and applications, such as for rear-lights and instrument clusters of vehicles, and appliances and lenses for glasses. PMMA in the form of sheets affords panels for building windows, skylights, signs, displays, sanitary ware, LCD screens, furniture and many other applications where transparency is an important factor.¹ PMMA is prepared by an addition reaction that requires the presence of an ini-

*Corresponding author. E-mail: radica@tmf.bg.ac.rs
doi: 10.2298/JSC140121035B

tiator, such as benzoyl peroxide that is decomposed by either heating or the addition of a chemical activator such as dimethyl-*p*-toluidine that can serve in an autopolymerization reaction.^{2,3} PMMA polymer based materials are used as bone cement. The pure resin does not have sufficient strength and is reinforced using oxide particles or other fillers in order to obtain the material that could be used under load bearing conditions.^{4,5} Another use of PMMA based resins is in dentistry for different applications, such as denture basis, orthodontic appliances, and provisional restorations.⁶

The addition of fillers in the form of alumina nanoparticles having different shapes and sizes into a polymer that serves as a matrix improves the mechanical behavior of the obtained composite material. The main problems encountered with addition of nanoparticles are mixing and uniform distribution of the nanoparticles in the matrix material because nanoparticles tend to agglomerate.^{7–11} There are several techniques of enabling a good dispersion of nanoparticles and these include: direct mixing of polymer and nanoparticles, *in situ* polymerization in the presence of nanoparticles, and simultaneous *in situ* polymerization and nanoparticles formation.¹² The main candidate materials for addition as nanofillers into a polymer matrix are fine nanoparticles of oxides, such as silica,¹³ titania,¹⁴ zirconia¹⁵ and alumina.¹⁶ The addition of oxide nanoparticles into a polymer matrix for preparation of bulk composites and films was the topic of a large number of research publications.¹⁷ Ultrasonication was reported to be an effective method to obtain a homogeneous dispersion of nanofillers in the monomer.¹⁸

The shape of the fillers also influenced an improvement of the mechanical properties of composites.^{17–21} It is well known that shape is very important when describing the flow properties of powder particles.^{22–24} As much as the particle shape is important in flow characteristics of fillers, it is also of importance in interactions with a composite matrix that determine the performance of composite materials on the macro scale.

The focus of the present research was a study of the influence of the shape and quantity of the alumina nanofillers in a PMMA polymer matrix on the mechanical properties of the obtained composite material. Composites based on a PMMA matrix with the addition of alumina nanofillers of different shapes, *i.e.*, spherical alumina nanoparticles and alumina whiskers, were prepared. The mechanical behavior of the obtained composites was studied using the dynamic mechanical analysis (DMA) and nanoindentation techniques. The shape of the fillers and their distribution in the composite were studied by scanning electron microscopy. The dimensions of the reinforcements were measured using image analysis techniques.

EXPERIMENTAL

The spherical aluminum oxide nanoparticles were declared to have a diameter of less than 50 nm and were obtained from Aldrich. The alumina whiskers were also commercially

available from Aldrich, and they were characterized by diameters of 2–4 nm and lengths of 200–400 nm. This enabled the use of very different alumina fillers with the spherical alumina nanoparticles having a length to diameter ratio of 1, while this ratio was approximately 100 for the alumina whiskers.

Mecaprex KM, PRESI (Grenoble, France) is a two-component autopolymerizing acrylic resin. The first component consists of KM powder (PMMA powder containing dibenzoyl peroxide (DBPO) initiator) and the second contains KM liquid monomer (methyl methacrylate monomer (MMA) with *N,N*-dimethyl-*p*-toluidine activator). Spherical alumina nanoparticles or alumina whiskers were added to the KM liquid. The mixture was sonicated for 60 min and KM powder was dispersed in the mixture. The mixing was realized by hand during 2 min and the mixture was poured into a form having dimensions suitable for dynamic mechanical analysis (DMA) and nanoindentation testing. The form was covered with a glass cover to ensure that the surface of the specimen remained smooth. A PMMA/MMA mass ratio of 0.75 was used as this ratio minimizes shrinkage, as suggested by the manufacturer (PRESI) and as previously reported in the literature.¹⁸ The monomer was polymerized at 25 °C. The instruction for use given by the producer says that the polymerization is complete in 20 min at a temperature between 20 and 23 °C. However, the obtained composites were then additionally exposed to a temperature of 37 °C for 30 days in order to obtain a stable composition of the polymer matrix before the samples were mechanically tested.²⁵ The compositions of the PMMA/alumina whiskers and PMMA/alumina spherical nanoparticles composites prepared for analysis in this study are summarized in Table I. The samples prepared using the spherical alumina nanoparticles as fillers are denoted as P1, P3 and P5 for contents of 1, 3 and 5 wt. % of the filler, respectively. The samples using alumina whiskers as fillers were denoted as W1, W3 and W5 for contents of 1, 3 and 5 wt. % alumina whiskers, respectively.

TABLE I. The compositions of composite specimens prepared using the PMMA as the matrix and alumina spherical nano particles and alumina whiskers as fillers

Sample description	Sample	Quantity particles/whiskers, g	MMA+initiator mass, g	PMMA Mass g
PMMA without filler	PMMA	—	2.290	1.710
PMMA with 1 wt. % spherical alumina nanoparticles	P1	0.045	2.540	1.910
PMMA with 3 wt. % spherical alumina nanoparticles	P3	0.135	2.540	1.870
PMMA with 5 wt. % spherical alumina nanoparticles	P5	0.225	2.440	1.830
PMMA with 1 wt. % alumina whisker	W1	0.045	2.540	1.910
PMMA with 3 wt. % alumina whisker	W3	0.135	2.540	1.870
PMMA with 5 wt. % alumina whisker	W5	0.225	2.440	1.830

The mechanical behaviors of neat polymer and PMMA/alumina fillers nanocomposites were studied by DMA – cantilever bending and force control nanoindentation. Scanning electron microscopy was used to study the morphology of the spherical alumina nanoparticles and

alumina whiskers prior to incorporation into the polymer and to study the distribution of the spherical alumina nanoparticles and alumina whiskers in the matrix after polymerization.

Methods of characterization

DMA analyzes. Dynamic mechanical analysis was used to examine the performance of the PMMA matrix composite reinforced using alumina spherical nanoparticles or alumina whiskers and to measure the influence of the shape of the alumina fillers on the behavior of the resulting materials. The data obtained from this analysis included the storage modulus (E'), tangent delta ($\tan \delta$) and the glass transition temperature (T_g). The storage modulus reveals the ability of the composite to store elastic energy associated with recoverable elastic deformation. Together with $\tan \delta$, the storage modulus describes the behavior of the composite under stress in a defined temperature range. DMA was performed on a DMA Q800 (TA Instruments) under a nitrogen atmosphere in the single cantilever mode. Storage modulus and loss factor ($\tan \delta$) were calculated for rectangular specimens of size 35 mm×13 mm×3 mm at a frequency $\omega = 1$ Hz. Temperature range was changed from room temperature to 160 °C at a heating rate of 3 °C min⁻¹.

Nanoindentation. The nanoindentation test was performed using a Hysitron TI 950 TriboIndenter equipped with *in situ* SPM imaging (Hysitron, MN). The Berkovich indenter has an average radius of curvature of about 100 nm. The tests were performed in the force-controlled feedback mode. The indentation maximum load was set at 4 mN for each tested sample. The loading and unloading times as well as the hold time at the peak force were set to 25 s each. For each loading/hold/unloading cycle, the applied load value was plotted with respect to the corresponding position of the indenter. The resulting load/displacement curves provide data specific to the mechanical nature of the material under examination. All the results were obtained by the Oliver and Pharr method²⁴ and using an assumed sample Poisson ratio of 0.36 for the calculation of the reduced elastic modulus. Established models were used to calculate the quantitative indentation hardness (H) and reduced elastic modulus values (E) for such data.

The specimens were polished using alumina paste having abrasive grains of up to 0.02 µm until a flat surface was obtained. The specimens were about 1 mm thick, having dimensions 3 mm×3 mm×2 mm and were placed on the specimen holder in the nanoindenter. Loads of 4 mN were used for the tests. In order to obtain reliable results, 9 indentations were made for each type of sample on random locations.

Analysis of the morphology of the specimens. The morphologies of the alumina nanofillers were examined using a field emission scanning electron microscope (FESEM), MIRA3 TESCAN, operated at 20 kV. The morphology of the PMMA polymer matrix and composites reinforced by the nanofillers were examined using a scanning electron microscope (SEM), Jeol JSM 5800, operated at 20 kV.

RESULTS AND DISCUSSION

Very fine spherical alumina nanoparticles and alumina whiskers tend to agglomerate and they were delivered in their agglomerated form from the producer. The field emission scanning electron microscopy (FESEM) micrographs of the agglomerated spherical alumina nanoparticles and alumina whiskers prior to sonication are shown in Fig. 1. The mean diameter of the spherical alumina nanoparticle agglomerates as received from producer was 87 µm and that for the

alumina whiskers was of $1.1\text{ }\mu\text{m}$. These values were obtained using image analysis tools applied to the images shown in Fig. 1.

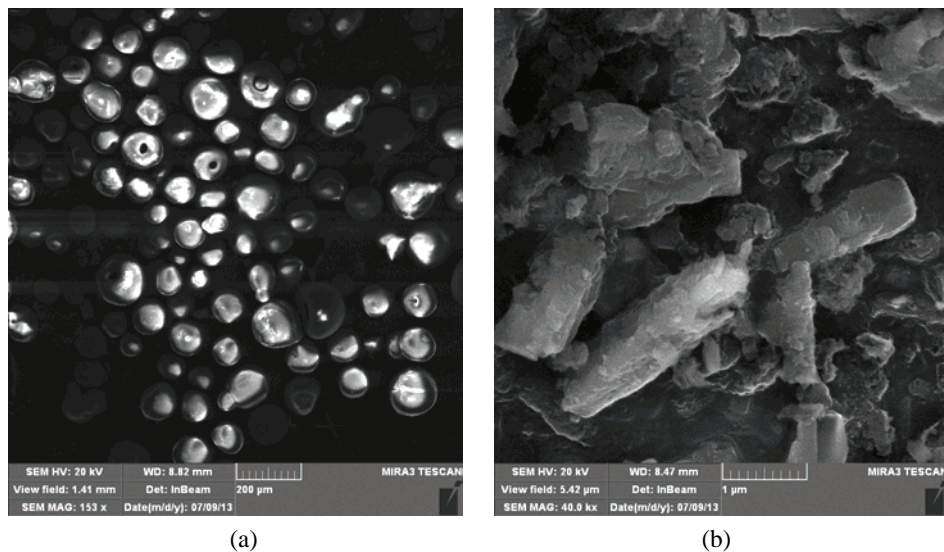


Fig. 1. The FESEM micrographs of agglomerated alumina nanoparticles and whiskers as received from the producer prior to sonication, a) particles agglomerates having a mean diameter of $87\text{ }\mu\text{m}$ b) whiskers having a mean diameter of $1.1\text{ }\mu\text{m}$.

The morphology of the samples having 3 wt. % of spherical alumina nanoparticles and 3 wt. % of alumina whiskers and of the polymer without reinforcement were examined using a scanning electron microscope (SEM), Jeol JSM 5800, operated at 20 kV, Fig. 2. In Fig. 2b, the micrograph of the sample having 3 wt. % of alumina whiskers is given and in Fig. 2c, the micrograph of the composite having 3 wt. % of the spherical alumina nanoparticles is presented. These images were used to measure the diameters of the alumina spherical nanoparticles agglomerates still visible in the micrograph. The results of measurements presented in Fig. 2c show that the mean diameter of the spherical alumina nanoparticle agglomerates decreased to $0.47\text{ }\mu\text{m}$ in the composite containing 3 wt. % spherical alumina nanoparticles. The main length of the agglomerates of the alumina whiskers visible in the composite was reduced to $0.27\text{ }\mu\text{m}$. The appreciable reduction in the sizes of the visible agglomerates of the spherical alumina nanoparticle, as well as the reduction in the sizes of the visible agglomerates of the alumina whiskers, indicate that the agglomerates dimensions were reduced and that the spherical alumina nanoparticles and the alumina whiskers that were not agglomerated were well distributed in the polymer, bringing improvements in the mechanical properties.

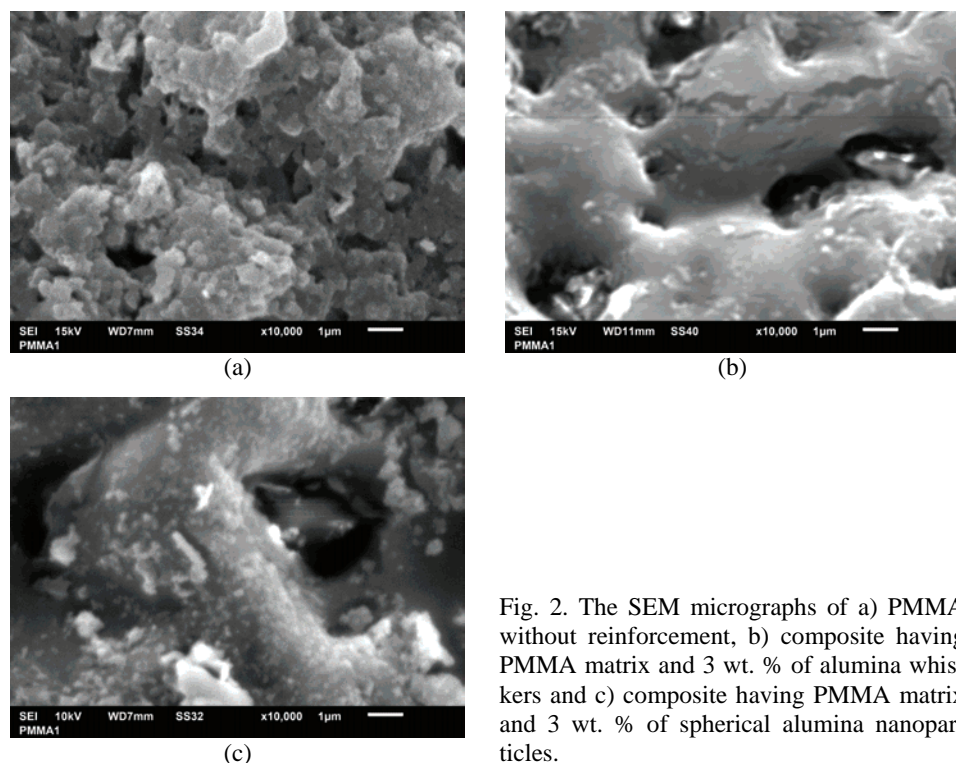


Fig. 2. The SEM micrographs of a) PMMA without reinforcement, b) composite having PMMA matrix and 3 wt. % of alumina whiskers and c) composite having PMMA matrix and 3 wt. % of spherical alumina nanoparticles.

DMA was used to compare the behavior of the pure PMMA to the behavior of the composites with additions of alumina fillers. It was observed that incorporation of both spherical alumina nanoparticles and alumina whiskers resulted in an increase in the values of the storage modulus for the composites in the measured range of temperatures, Fig. 3.

The glass transition temperature T_g can be determined from the DMA results as the maximum of the curve showing the dependence of $\tan \delta$ vs. temperature. The changes of T_g in dependence on the type and quantity of additives are shown in Fig. 4. Composites having 3 wt. % of added alumina whiskers showed an increase in the T_g value of 3 °C, which was the maximum increase observed in specimens prepared within the scope of this research. For samples containing spherical alumina nanoparticles, the largest increase in the T_g value was also observed for the composite with 3 wt. %, but this increase was less significant. This proves that both the spherical alumina nanoparticles and the alumina whiskers were in good contact with the matrix.

The storage moduli for composites having a PMMA matrix and spherical alumina nanoparticles or alumina whiskers as reinforcements are compared to the values for the unreinforced PMMA in Fig. 5. The composite containing 3 wt. % of

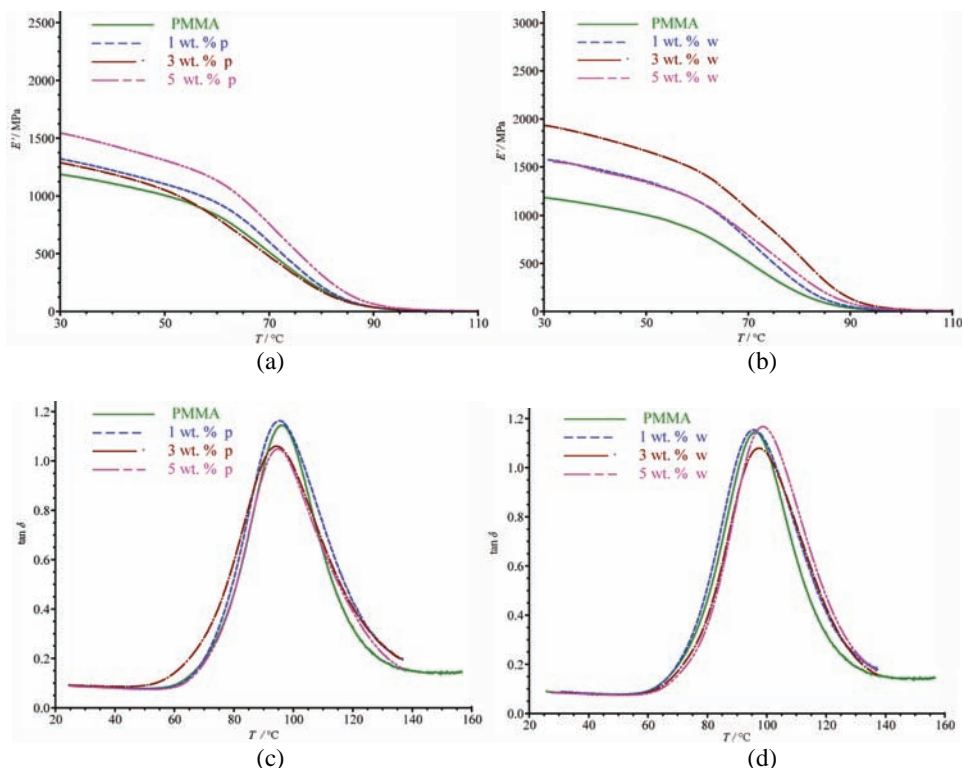


Fig. 3. Changes in the storage modulus (a and b) and $\tan \delta$ (c and d) for the PMMA matrix composites reinforced with spherical alumina nanoparticles (a and c) and alumina whiskers (b and d).

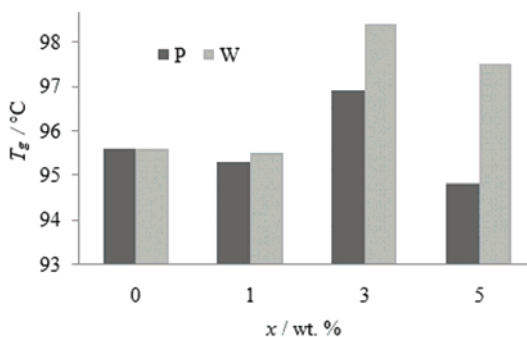


Fig. 4. Changes in T_g of the PMMA matrix composite materials having spherical alumina nanoparticles or alumina whiskers as additives.

spherical alumina nanoparticles showed the largest increase in the value of the storage modulus (23 %) among the composites prepared with spherical alumina nanoparticles. All the composites having the alumina whiskers as reinforcements showed increases in storage modulus compared to that of pure PMMA. The addition of 3 wt. % alumina whiskers resulted in an increase of 63 %. The addi-

tion of 5 wt. % of alumina whiskers did not improve the storage modulus value more than the addition of 3 wt. % of alumina whiskers and this could be explained by the difficulty in mixing and breakage of the agglomerates when the concentration of alumina whiskers was larger than 3 wt. %. The values of $\tan \delta$ presented in Fig. 6 are in accordance with observations made for the storage modulus.

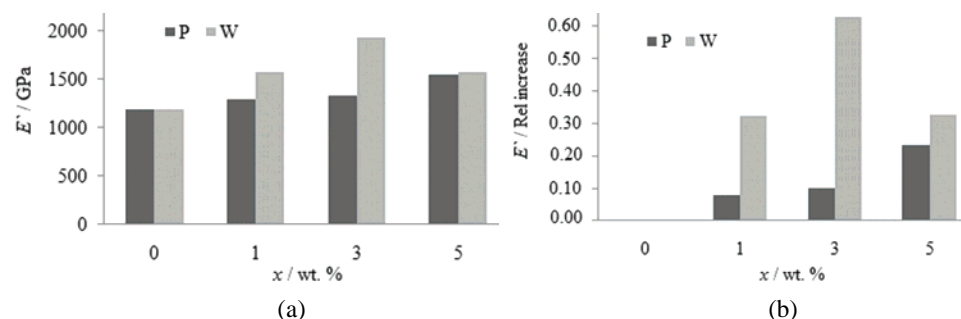


Fig. 5. a) The dependence of E' for the PMMA matrix composite materials having spherical alumina nanoparticles or alumina whiskers as additives; b) relative increase in E' of the composites compared to the PMMA polymer matrix.

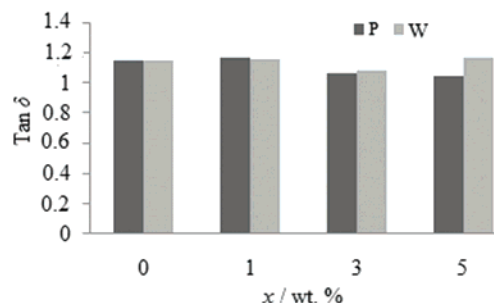


Fig. 6. Dependence of $\tan \delta$ on the quantity and morphology of the reinforcement by spherical alumina nanoparticles or alumina whiskers as additives in PMMA matrix composite materials.

DMA gave the characteristics of the composite at the macro-level and such properties describe the behavior of the entire specimen under load at different temperatures. The nanoindentation test enabled the properties of the composite to be studied at the nano- and micro-level. From nanoindentation results, it is possible to determine whether the properties have uniform values throughout the specimen and to discuss possible inhomogeneities of the distribution of the reinforcement in the composite.

The obtained results gave insight into the influence of the shape and amount of the alumina fillers added on the obtained mechanical properties of PMMA matrix composite. Data showing the changes of the modulus of elasticity of the PMMA matrix/alumina spherical nanoparticles and PMMA matrix/alumina whisker composites in dependence on the type and amount of alumina fillers added

are given in Fig. 5. It could be seen that both the alumina spherical nanoparticles and alumina whiskers made the composites stiffer compared to the PMMA polymer, even if only 1 wt. % of spherical alumina nanoparticles was added. Addition of spherical alumina nanoparticles into the composition did not dramatically change the values of mechanical properties, modulus and hardness, of the obtained composite. The addition of 3 wt. % spherical alumina nanoparticles resulted in a composite material having properties that had higher values of the modulus of elasticity and hardness as measured using the nanoindentation method. The addition of 5 wt. % of spherical alumina nanoparticles did not improve additionally the mechanical properties of the PMMA matrix composite. The improvement of mechanical properties obtained using 1 wt. % of alumina whiskers gave better properties than the PMMA matrix composite containing the same quantity of spherical alumina nanoparticles. The addition of 3 wt. % of whiskers gave maximum stiffness improvement of the PMMA matrix composite material and the obtained composite had the maximum value of the modulus of elasticity that was improved by 56 % compared to the polymer without reinforcement. The addition of 5 wt. % of alumina whiskers did not further improve the values of mechanical properties measured using the nanoindentation method. From the data presented, the addition of 3 wt. % of alumina whiskers gave the material having the best modulus of elasticity. This is a considerable reinforcement for a small addition of alumina whiskers.

The results of hardness measurement exhibited the same trend as those for the modulus of elasticity for PMMA matrix/spherical alumina nanoparticle composites. The addition of 1 wt. % of spherical alumina nanoparticles gave a slight deterioration in the hardness of the material. The PMMA matrix composite with 3 wt. % of spherical alumina nanoparticles gave the best performance concerning the hardness of the PMMA/spherical alumina nanoparticle composites. The addition of 5 wt. % of alumina whiskers did not improve additionally the hardness of the PMMA matrix composite. The addition of 3 wt. % of alumina whiskers gave an increase in hardness of the material that was 40 % improvement compared to the PMMA polymer without the addition of the fillers.

A comparison of the nanoindentation curves for the PMMA polymer without the addition of reinforcement and for composites having 3 wt. % of spherical alumina nanoparticles and 3 wt. % alumina whiskers is given in Fig. 7.

Comparison of DMA and nanoindentation results

Both the nanoindentation measurements of the modulus of elasticity and hardness and the DMA measurement of the storage modulus prove that the composite having 3 wt. % of alumina whiskers had the best mechanical properties among the studied composites. The nanoindentation (Figs. 8 and 9) and DMA (Fig. 5) results are in accordance proving that the addition of spherical alumina

nano particles was less efficient compared to the addition of alumina whiskers with a very high value of the length to diameter ratio.

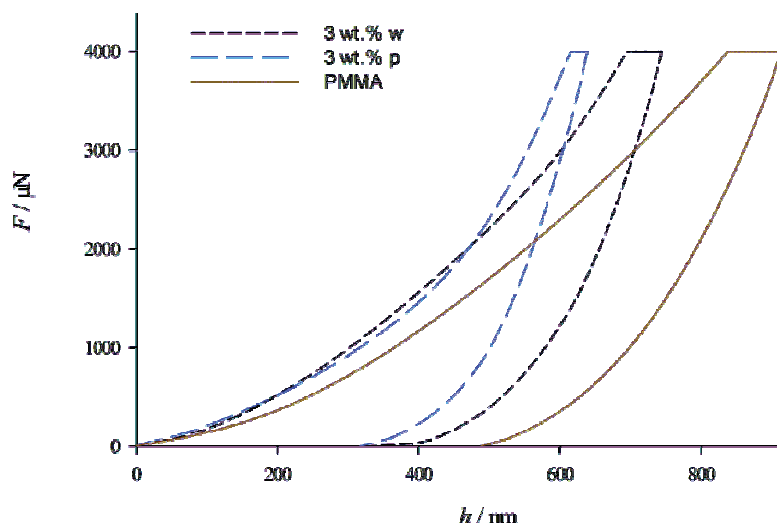


Fig. 7. Nanoindentation curves showing the dependence of the force on displacement for the PMMA polymer and the composite having 3 wt. % of spherical alumina nanoparticles or alumina whiskers.

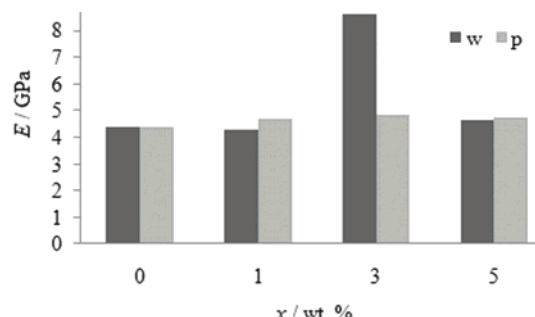


Fig. 8. Dependence of the modulus of elasticity measured during nanoindentation tests for PMMA matrix composite materials containing spherical alumina nanoparticles or alumina whiskers as additives.

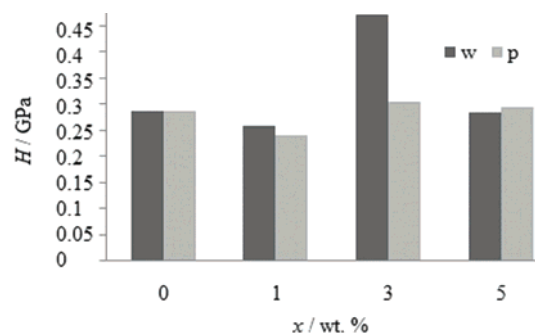


Fig. 9. A summary of the results from the nanoindentation testing of PMMA matrix composite materials containing spherical alumina nanoparticles or alumina whiskers.

When comparing the results obtained on reinforcing a PMMA matrix of a composite with spherical alumina nanoparticles to those obtained on reinforcing the same PMMA polymer with functionalized spherical particles, it could be observed that better values of the mechanical properties, *i.e.*, modulus of elasticity and hardness, were obtained using the functionalized silica particles than the values found in the present study.¹³ The preparation of the samples in this study was performed according to the instructions obtained from the producer and the specimens were left at a temperature of 37 °C for 30 days. In the previous study, the specimens were heated at 60 °C after the preparation and later up to 110 °C in order to eliminate stress and residual monomer. It is possible that these conditions that included heat treatment of the specimen to eliminate completely the monomer from the composition whereas in the present case when only a temperature of 37 °C was applied for 30 days, complete monomer conversion was not attained. This could be the reason that the small amount of residual monomer was present that served as a plasticizer in the composite.¹³ The content of residual monomer and allergic or cytotoxic effects of dentures based on acrylic resins may be related to powder to liquid ratio, storage time, temperature, polymerization method and this will be the subject of a future study. In this paper, the basic research was focused on the influence of size, shape and loading of nanoparticles on the mechanical properties of acrylic polymers.

As has been shown, alumina nanofillers have the possibility to improve the values of mechanical properties of the polymer when added in very small amounts. Similar improvements in the values of the mechanical properties could be obtained using very high loadings of functionalized alumina microparticles. In order to obtain the improvement of the mechanical properties in the same range as those obtained with the addition of 3 wt. % of alumina whiskers, 30 % of functionalized microparticles had to be added to the polymer matrix.²⁶

CONCLUSIONS

The PMMA matrix composites were prepared in the presence of spherical alumina nanoparticles and alumina whiskers as reinforcements. Ultrasonication was used to mix the components and to deagglomerate the spherical alumina nanoparticles and alumina whiskers prior to the polymerization of the matrix material. The DMA and nanoindentation techniques were used to characterize the mechanical behavior of the obtained composites. The DMA results showed that the spherical alumina nanoparticles were able to increase the storage modulus of the composite by up to 30 % compared to that of PMMA, while the alumina whiskers led to an improvement in the storage modulus value of 62 %. The T_g of the composite increased by up to 1.2 °C in the presence of spherical alumina nanoparticles and by 3 °C in the presence of alumina whiskers. Among the composites studied containing 1, 3 and 5 wt. % of either added spherical alumina

nanoindentation results for the same set of composite materials containing alumina fillers of different shape in the PMMA matrix, the best results for the modulus of elasticity and hardness were obtained for the specimen reinforced with 3 wt. % of alumina whiskers in the PMMA matrix.

Concerning the influence of the morphology of the reinforcement, better results were obtained using the alumina whisker reinforcement, for which the length to diameter was much more important than for the alumina nanoparticles that were declared as spherical. The increase in all properties, *i.e.*, storage modulus, T_g , measured using the DMA, and modulus of elasticity and hardness measured using the nanoindentation technique, were better in the presence of alumina whiskers than in the presence of spherical alumina nanoparticles. The use of an ultrasonic bath for the homogenization of the composite was satisfactory for the production of the specimens and this was proved by the increase in the mechanical properties measured using the presented techniques.

Acknowledgement. This research has been financially supported by the Ministry of Education, Science and Technological Development of the Republic of Serbia as a part of the project TR34011.

И З В О Д
УТИЦАЈ ВЕЛИЧИНЕ И ОБЛИКА АЛУМИНИЈУМ-ОКСИДНИХ НАНОПУНИЛА НА
МЕХАНИЧКО ПОНАШАЊЕ КОМПОЗИТА СА МАТРИЦОМ ОД
ПОЛИ(МЕТИЛ-МЕТАКРИЛАТА)

SOMAYA AHMED BEN HASAN¹, МАРИЈА М. ДИМИТРИЈЕВИЋ¹, АЛЕКСАНДАР КОЛОВИЋ¹,
ДУШИЦА Б. СТОЈАНОВИЋ¹, КОСОВКА ОБРАДОВИЋ-ЂУРИЧИЋ², РАДМИЛА ЈАНЧИЋ ХАЈНEMAN¹
и РАДОСЛАВ АЛЕКСИЋ¹

¹Универзитет у Београду, Технолошко-мештапурски факултет, Карнеијева 4, Београд и
²Универзитет у Београду, Стоматолошки факултет, Др Суботића 8, Београд

Композити са додатком нанопунила показују побољшање механичких својстава у односу на полимерну матрицу. За израду композита, коришћен је полиметилметакрилат, PMMA, као полимерна матрица у комбинацији са два нанопунила, потпуно различитих облика. Полимерна матрица је ојачана коришћењем две врсте нанопунила на бази алуминијум-оксида: наночестица сферног облика и игличастих вискерса, који имају однос дужине према пречнику од 100. Утицај величине честица, њихов облик и удео, на механичка својства композита проучавани су помоћу наноиндентационих мерења и динамичко-механичке анализе. Примећено је да и сферне наночестице и вискери побољшавају механичка својства композита, али веће побољшање је постигнуто додатком вискера. Концентрација обе врсте нанопунила, сферних наночестица и вискера је варирана у опсегу до 5 мас. %. Најбоља механичка својства композита су добијена додатком 3 мас. % вискера у полимерну ПММА матрицу.

(Примљено 21. јануара, ревидирано 31. марта, прихваћено 2. априла 2014)

REFERENCES

1. E. N. Peters, *Plastics: Thermoplastics, Thermosets, and Elastomers*, in *Handbook of Materials Selection*, M. Kutz, Ed., John Wiley & Sons, Inc., New York, 2002
2. P. K. Vallittu, V. Miettinen, P. Alakuijala, *Dent. Mater.* **11** (1995) 338
3. A. A. Del Bel Cury, R. N. Rached, S. M. Ganzarolli, *J. Oral Rehabil.* **28** (2001) 433
4. S. Shinzato, T. Nakamura, T. Kokubo, Y. Kitamura, *J. Biomed. Mater. Res.* **59** (2002) 225
5. J.M. Yang, C.S. Lu, Y.G. Hsu, C.H. Shih, *J. Biomed. Mater. Res.* **38** (1997) 143
6. J. A. Bartoloni, D. F. Murchison, D. T. Wofford, N. Sarkar, *J. Oral Rehabil.* **27** (2000) 488
7. F. Pervin, Y. Zhou, V. Rangari, S. Jeelani, *Mater. Sci. Eng., A* **405** (2005) 246
8. T. Adachi, M. Osaki, W. Araki, S. Kwon, *Acta Mater.* **56** (2008) 2101
9. H. Al-Turaif, *Prog. Org. Coat.* **38** (2000) 43
10. A. Omrani, L. Simon, A. Rostami, *Chem. Phys.* **114** (2009) 145
11. B. Ahmadi, M. Kassiriha, K. Khodabakhshi, E. Mafi, *Prog. Org. Coat.* **60** (2007) 99
12. P. M. Ajayan, P. V. Braun, L. S. Schadler, *Nanocomposite Science and Technology*, Wiley–VCH, Weinheim, Germany, 2004, p. 77
13. D. Stojanovic, A. Orlovic, S. Markovic, V. Radmilovic, P. Uskokovic, R. Aleksic, *J. Mater. Sci.* **44** (2009) 6223
14. T. E. Motaung, A. S. Luyt, F. Bondioli, M. Messori, M. L. Saladino, A. Spinella, G. Nasillo, E. Caponetti, *Polym. Degrad. Stabil.* **97** (2012) 1325
15. H. Wang, P. Xu, W. Zhong, L. Shen, Q. Du, *Polym. Degrad. Stabil.* **87** (2005) 319
16. A. Omrani, L. C. Simon, A. A. Rostami, *Mater. Chemi. Phys.* **114** (2009) 145
17. A. Allahverdi, M. Ehsani, H. Janpour, S. Ahmadi, *Progr. Org. Coat.* **75** (2012) 543
18. M. Hussain, A. Nakahira, K. Niihara, *Mater. Lett.* **26** (1996) 185
19. B. Wetzel, P. Rosso, F. Haupert, K. Friedrich, *Eng. Fract. Mech.* **73** (2006) 2375
20. A. Chatterjee, M. S. Islam, *Mater. Sci. Eng., A* **487** (2008) 574
21. T. Mahrholz, J. Stängle, M. Sinapius, *Compos., A* **40** (2009) 235
22. M. S. Goyat, S. Ray, P. K. Ghosh, *Compos., A* **42** (2011) 1421
23. X. Fu, D. Huck, L. Makein, B. Armstrong, U. Willen, T. Freeman, *Particuology* **10** (2012) 203
24. J. Mellmann, T. Hoffmann, C. Fürll, *Powd. Tech.* **249** (2013) 269
25. W. C. Oliver, G. M. Pharr, *J. Mater. Res.* **7** (1992) 1564.
26. S. Omar Alshari, H. Bin Md Akil, N. Abbas Abd El-Aziz, Z. Arifin Bin Ahmad, *Mater. Design* **54** (2014) 430.



Modification of natural clinoptilolite for nitrate removal from aqueous media

JELENA B. PAVLOVIĆ^{1*}, JELENA K. MILENKOVIĆ¹ and NEVENKA Z. RAJIĆ²

¹Innovation Centre of the Faculty of Technology and Metallurgy, University of Belgrade,
Karnegijeva 4, 11000 Belgrade, Serbia and ²Faculty of Technology and Metallurgy,
University of Belgrade, Karnegijeva 4, 11000 Belgrade, Serbia

(Received 16 January, revised 7 April, accepted 9 April 2014)

Abstract: Natural zeolitic tuff from the Zlatokop mine (Vranjska Banja deposit, Serbia) was investigated as the starting material to obtain a low cost adsorbent for the removal of nitrate from aqueous media. The tuff rich in zeolite, clinoptilolite, was modified with several oxides, iron(III), manganese(IV) and magnesium, by simple procedures in order to make the clinoptilolite surface accessible for binding nitrate ions. The obtained oxide-modified zeolite samples were characterized by scanning electron microscopy and energy dispersive X-ray analysis (SEM/EDS), powder X-ray diffraction (PXRD), infrared spectroscopy (FTIR) and by measurement of their specific surface area. The effects of the adsorbent dosage (0.5, 1.0, 1.5 and 2.0 g), temperature (25, 35 and 45 °C) and initial nitrate concentration (c_0 , 100, 200 and 300 mg dm⁻³) on the binding efficiency were also studied. For all adsorbents, the efficiency increased with temperature. The type of the oxide affected the adsorption mechanism. The Fe(III) oxide-modified zeolite exhibited the best binding ability. For this adsorbent, the adsorption kinetics were studied and it was found that they were best represented by the pseudo-second-order model.

Keywords: natural zeolite; clinoptilolite; oxide-modified zeolite; nitrate; adsorption.

INTRODUCTION

Many pollutants in water represent a serious problem for humans and the environment. Nitrates attract special attention because they readily leach from soil, have good solubility in water and accordingly, they are globally the most widespread contaminant.^{1,2} Nitrate contamination of water is mainly caused by the excessive use of fertilizers, the increase in agricultural activities and by human and animal wastes. A high nitrate level in potable water is responsible for methemoglobinemia, commonly called the “blue baby syndrome”. Moreover, nit-

*Corresponding author. E-mail: jelena.pavlovic@tmf.bg.ac.rs
doi: 10.2298/SC140116038P

rates promote algal growth and eutrophication of water bodies and interact with organics forming carcinogenic nitrosamines.³

Various methods and technologies, such as adsorption, ion-exchange, biological denitrification, reverse osmosis and chemical reduction, have been tested and developed for nitrate removal.⁴ Due to the fact that the majority are expensive, of low efficiency and/or have a problem with the management of the by-products, many investigations have been directed towards natural, environmental friendly, low cost materials which could be applied as filters in water purifications.

Owing to their adsorbent, ion exchange and catalytic properties, zeolites have attracted great attention. In particular, natural zeolites have been recognized as highly effective materials for the removal of different water contaminants.^{5–8} Clinoptilolite, as the most abundant natural zeolite, could therefore be regarded as a cost-minimizing choice of adsorbent for developing countries such as Serbia. In Serbia, about 70 % of drinking water comes from groundwater sources and many of the springs suffer from high nitrate levels. Therefore, it is necessary to find a cost effective, efficient and easy to perform method for the removal of nitrates.

In this study, natural zeolite – clinoptilolite from the Zlatokop deposit in Serbia was examined as an adsorbent for nitrate removal from aqueous media. Since the aluminosilicate lattice of the zeolite is negatively charged, the zeolite has no adsorptive ability towards anionic nitrate ions and it has to be modified. Some of the reported modifications include coating of zeolite surface with surfactants⁹ and low cost chitosan¹⁰ or impregnation with different metal precursors.¹¹

Taking into account that iron(III) and manganese(IV) oxide-modified clinoptilolite were reported as efficient adsorbents for different anionic species^{12–14} and an MgO–biochar nanocomposite for the removal of phosphate and nitrate ions,¹⁵ the modification of the natural clinoptilolite by oxides of iron(III), manganese(IV) and magnesium were investigated in order to obtain adsorbents for nitrates. Furthermore, the influence of different parameters on the adsorbent efficiency (adsorbent dosage, temperature and the initial nitrate concentration) were studied.

EXPERIMENTAL

Materials

In this study, a natural zeolite (Z) which contains about 73 % clinoptilolite phase, 14.6 % feldspar plagioclase and 12.8 % quartz¹⁶ was used as the starting material. Before modification, the zeolite samples (grain size 0.063–0.1 mm) were washed several times with distilled water to remove impurities and then dried at 60 °C.

Preparation of the manganese/magnesium-modified zeolite (MnZ and MgZ)

The employed procedure was similar to that described by Camacho *et al.*¹² Z (10 g) was suspended in a glass beaker containing 10 cm³ of 2.5 M MnCl₂ or MgCl₂ and 1.0 cm³ of 1 M NaOH. The suspension was heated to dryness at 150 °C for 5 h and then the product was calcined at 500 °C for 1 h. Finally, the calcined products (MnZ and MgZ) were washed several times with distilled water and dried to a constant mass at 105 °C.

Preparation of the iron-modified zeolite (FeZ)

The modification was performed in a similar manner to that described by Stanic *et al.*¹⁷ Z (10 g) was mixed with 50 cm³ of 0.1 M FeCl₃ in an acetate buffer at pH 3.6, for 1 h at room temperature. Then 45 cm³ of 4 % NaOH were added, the suspension was stirred for 1 h and finally mixed with 25 cm³ of a 4 % NaCl solution. The suspension was then stirred for another hour at 50 °C. After filtering, the Fe-containing sample (FeZ) was heated to dryness, calcined and washed as described above.

Characterization

Powder X-ray diffraction (PXRD) patterns of Z and of the modified zeolite samples were recorded at room temperature on a APD2000 Ital Structure diffractometer with CuK_α radiation ($\lambda=0.15418\text{ nm}$) in the 2θ range 5–50° with a step 0.04° s⁻¹. The thermal behavior of the samples obtained before the calcination step was examined by thermal analysis using a SDT Q600 simultaneous TGA–DTA instrument (TA Instruments). The samples were heated from room temperature to 800 °C at a heating rate of 10 °C min⁻¹ under synthetic air.

The morphology and elemental composition of the samples were examined by energy dispersive X-ray spectroscopy (EDS) using a scanning electron microscope (SEM, Jeol, JSM-6610LV). For EDS, the samples were carefully prepared by embedding grains in an epoxy film, polishing the crystallites, cutting them with a fine-grid diamond cutter and coating them with carbon. In this manner, an intersection view of the crystallite grains was obtained that enabled detailed EDS analysis of the major mineral phases.

All samples were characterized by Fourier transform infrared spectroscopy (FTIR) using KBr pellets. The FTIR spectra were obtained on a Digilab-FTS 80 interferometer in the 400–4000 cm⁻¹ range. The specific surface area was measured by the N₂-BET method (Micromeritics ASAP 2020).

Nitrate adsorption experiments

The adsorption experiments were realized by the batch method. The adsorption capacity of nitrates on MZ (M –Fe, Mn or Mg) samples was investigated as a function of the adsorbent dosage, temperature and the initial concentration of the nitrate solution. All nitrate solutions were prepared by dissolving KNO₃ in deionized water. The influence of different parameters on the removal efficiency was investigated as follows. The effect of adsorbent dosage was investigated at 25 °C by shaking different amounts of MZ (0.5, 1.0, 1.5 and 2.0 g) with 50.0 cm³ of nitrate solution ($c_0 = 100\text{ mg dm}^{-3}$) for 24 h. The effect of temperature was studied with 1.0 g of MZ and 50.0 cm³ of nitrate solution ($c_0 = 100\text{ mg dm}^{-3}$) at 25, 35 and 45 °C during 24 h. The influence of the initial nitrate concentration was studied at three different concentrations, 100, 200 and 300 mg dm⁻³. 1.0 g of MZ was shaken with 50.0 cm³ of the appropriate nitrate solution at 45 °C for 24 h.

Kinetic studies

For kinetic experiments, 1.0 g of each adsorbent was shaken in a thermostated water bath (Memmert, WBE 22) with 50.0 cm³ of an aqueous solution of nitrate ($c_0 = 300 \text{ mg dm}^{-3}$) at 45 °C, for contact times of 30, 240, 360, 600 and 1440 min.

In all the experiments, the suspensions were separated using 0.45 µm filter and the filtrate was analyzed. The amount of nitrate in the solutions was determined (Hach DR/2800) with NitraVer 5 reagents by the Cadmium Reduction Method (Hach method 8039) using a UV–Vis spectrophotometer. The amount of the adsorbed nitrate after time t , q_t , was calculated using the following formula:

$$q_t = \frac{c_0 - c_t}{m} V \quad (1)$$

where c_0 and c_t are concentrations of nitrate ions in the aqueous solution (mg dm⁻³) before and after contact with the adsorbent, respectively, V is the volume of the solution in dm³ and m is mass of the adsorbent in g.

RESULTS AND DISCUSSION

Physical and chemical properties of natural and the modified zeolites

The results of SEM analysis are given in Fig. 1. The shape and color contrast evident in Fig. 1a indicate that the zeolite sample consisted of different mineral phases, which were analyzed by EDS (Table I). It is evident that one of the phases is the most abundant and this was clinoptilolite with a Si/Al molar ratio of about 4.7.

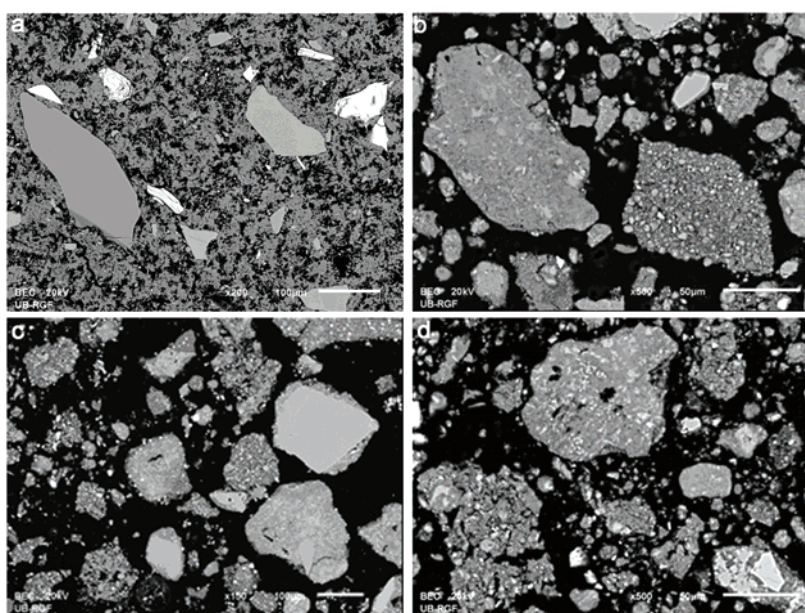


Fig. 1. SEM microphotographs of: a) natural zeolite and the modified products, b) MgZ, c) MnZ and d) FeZ.

TABLE I. Elemental composition (mass %) of zeolite (Z) and the metal-modified zeolite samples

Element	Sample			
	Z	MgZ	MnZ	FeZ
Na	0.43	0.45	0.41	0.56
Mg	0.72	5.45	0.54	0.90
Al	6.39	6.16	6.07	6.65
Si	32.07	32.47	33.07	32.39
K	1.37	1.46	0.96	1.55
Ca	2.44	2.27	2.07	2.17
Fe	1.94	0.67	0.21	7.25
Mn	—	—	4.87	—

Figure 1b-d show that modification resulted in the appearance of white spots, mainly on the clinoptilolite phase, in all three modified products. EDS analysis indicated that the spots belong to different oxide phases. Furthermore, the results of EDS clearly showed that the modification did not proceed *via* an ion-exchange process. Namely, the content of exchangeable cations in clinoptilolite phase remained almost constant. Moreover, since the modification occurred in an alkaline medium, it seems likely that some complex hydroxo species were adsorbed at the clinoptilolite surface that then during the calcination were converted to the respective oxides. This was confirmed by PXRD and TG analyses.

The PXRD patterns of the MZ products (Fig. 2) showed that the crystallinity of the clinoptilolite lattice remained generally preserved during the modification. In addition, some new diffraction peaks appeared in the patterns of all samples, indicating the presence of novel crystalline phases. A new diffraction peak in the PXRD pattern of MnZ at $2\theta = 32^\circ$ corresponded to Mn_3O_4 .¹⁸ In the pattern of FeZ, a new diffraction peak occurred at $2\theta = 36^\circ$, suggesting the presence of Fe_2O_3 ,¹⁹ whereas the diffraction peak at $2\theta = 42^\circ$ in the pattern of MgZ indicates the presence of MgO .²⁰

The results confirmed that the modification yielded products that contained different oxide phases. This was supported by the TG/DTG analyses. The analyses were performed on the metal-modified samples before their calcination in order to examine possible transformations of hydrous metal species into oxides at elevated temperatures.

The results of thermal analyses are presented in Table II and Fig. 3. The DTG curves (Fig. 3) of the samples displayed novel maxima and the corresponding mass losses differed from those for the parent Z sample. The changes were most conspicuous in the thermogram of the Mg-modified sample. In contrast to the TG curve of Z, which showed a rather continuous weight loss during heating, the weight loss of Mg-modified zeolite proceeded in several steps. Three strong maxima centered at 172, 238 and 441 °C could be assigned not only to the

water loss from the zeolite lattice (the first maximum), but also to transformation of the hydrous magnesium species to magnesium oxide, which was formed under 400 °C. Namely, the maximum centered at 441 °C was reported to correspond to the formation of MgO from Mg hydroxide.²⁰

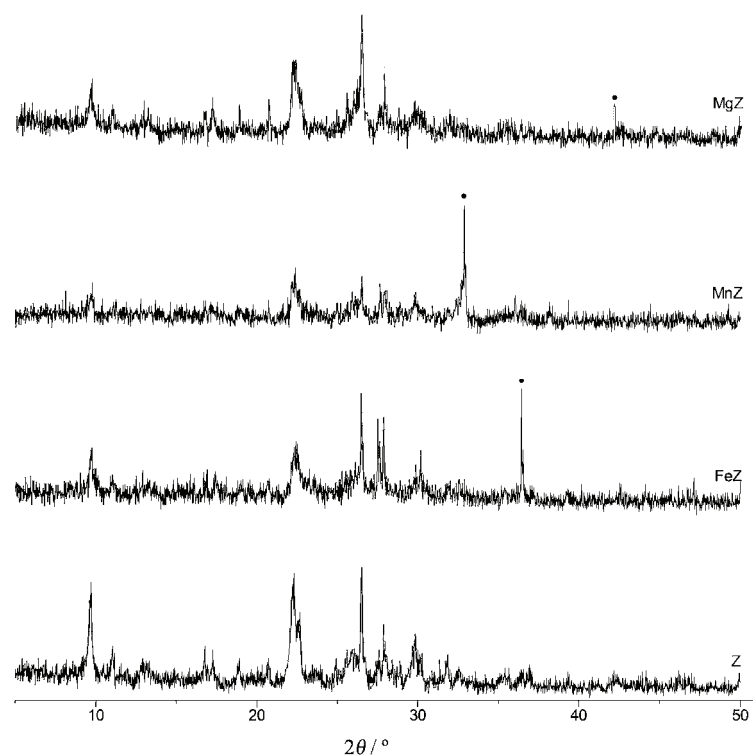


Fig. 2. Powder X-ray diffraction patterns of the zeolite samples.

TABLE II. Thermogravimetric results for the zeolite samples before calcination: natural zeolite (Z), Mg-modified zeolite (Mg-MZ), Mn-modified zeolite (Mn-MZ) and Fe-modified zeolite (Fe-MZ)

Parameter	Sample			
	Z	Mg-MZ	Mn-MZ	Fe-MZ
Total weight loss, %	14	21	17	12
Weight loss up to 300 °C, %	12	11	7	10

For the Mn- and Fe-modified samples, the differences were more pronounced below 300 °C. The maxima displayed below 140 °C most probably corresponded to the release of lattice water, whereas the further weight loss and the corresponding DGA events could be attributed to the dehydration of hydroxo species and formation of the corresponding oxides.

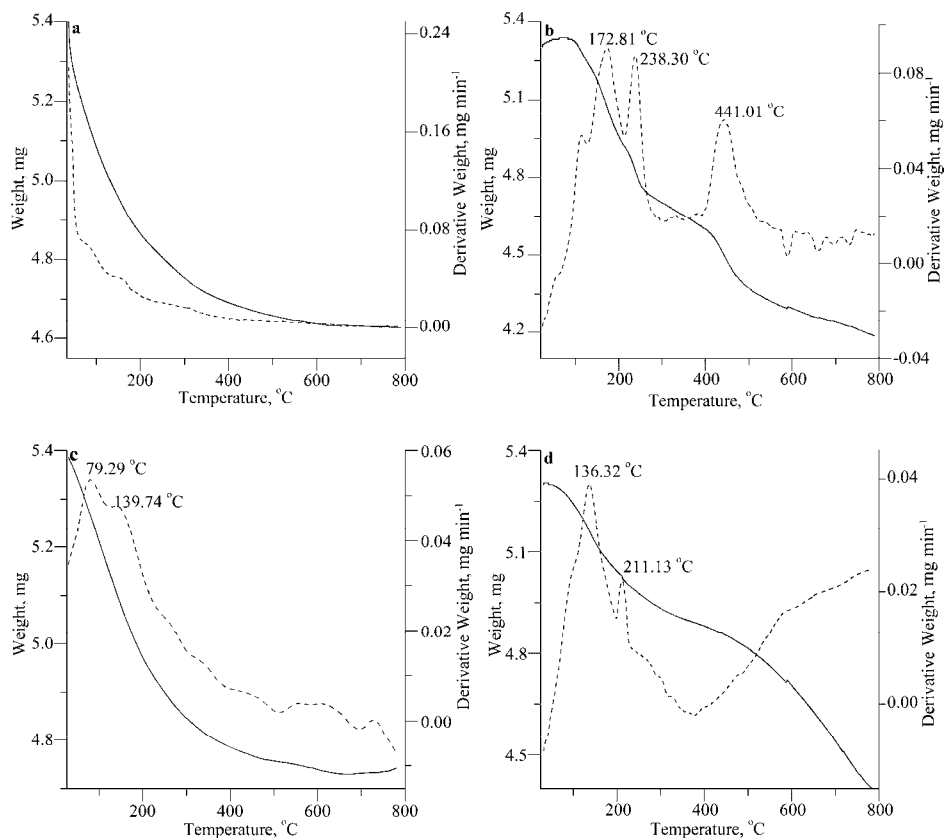


Fig. 3. TG/DTG curves of: a) Z and the zeolite samples modified by b) Mg, c) Fe and d) Mn; solid line: TG, dashed line: DTG.

In order to determine the specific surface area of the products, BET measurements were performed (Table III). The specific area for natural zeolite and modified samples differed mutually. The decrease in the specific area was most pronounced for MnZ, for which BET method gave a value of $17.5 \text{ m}^2 \text{ g}^{-1}$. A similar phenomenon was previously reported for the modification of Mn-containing clinoptilolite.¹² The modification also led to a decrease of the specific surface area in MgZ and FeZ. Generally, the decrease should be attributed to the formation of oxide particles at the surface of the zeolites, which causes a partial blockage of the pore system of clinoptilolite.

TABLE III. Specific surface areas for the natural zeolite and the oxide-modified products: natural zeolite (Z), MgO-modified zeolite (MgZ), Mn_3O_4 -modified zeolite (MnZ) and Fe_2O_3 -modified zeolite (FeZ)

Sample	Z	MgZ	MnZ	FeZ
Specific surface area, $\text{m}^2 \text{ g}^{-1}$	30.9	24.4	17.5	28.1

In order to check whether the modification procedure led to a change in the clinoptilolite surface and made it accessible towards nitrate ions, the samples (natural zeolite and modified ones) were treated with a nitrate solution for 24 h. The FTIR spectra of the products obtained after the treatment are shown in Fig. 4. In all spectra, a broad band at 3430 cm^{-1} and 1634 cm^{-1} , attributed to the vibrations of water molecules, and a broad vibration centered at 1069 cm^{-1} , corresponding to the zeolite lattice, are evident.²¹ However, a vibration band at about 1380 cm^{-1} corresponding to the asymmetric stretching vibrations that are characteristic for the nitrate ion^{22,23} could only be seen in the spectra of the modified samples. This indicates that the formation of MgO , Fe_2O_3 and Mn_3O_4 at the surface of clinoptilolite makes it available towards negatively charged nitrate ions.

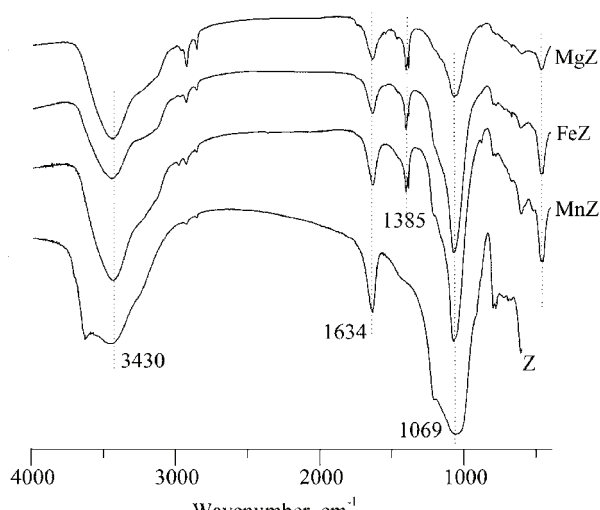


Fig. 4. FTIR spectra of Z and MZ samples after nitrate loading.

Effect of adsorbent dosage on the removal of nitrate by the different adsorbents

The removal of nitrate as a function of adsorbent dosage is shown in Fig. 5. Generally, increasing the adsorbent dosage increased the percent removal of nitrate, which could be attributed to the increase in adsorbent surface area of the adsorbents. For all samples, the percentage nitrate removal initially increased sharply with increasing adsorbent mass up to 1.0 g, above which the removal efficiency increased negligibly (*i.e.*, a two times increase in the mass of adsorbent at higher adsorbent masses increased the percentage of nitrate removal by only 10 %). Thus, a ration of 1.0 g of adsorbent per 50 cm^3 of liquid phase was chosen as the optimal for use in the further study.

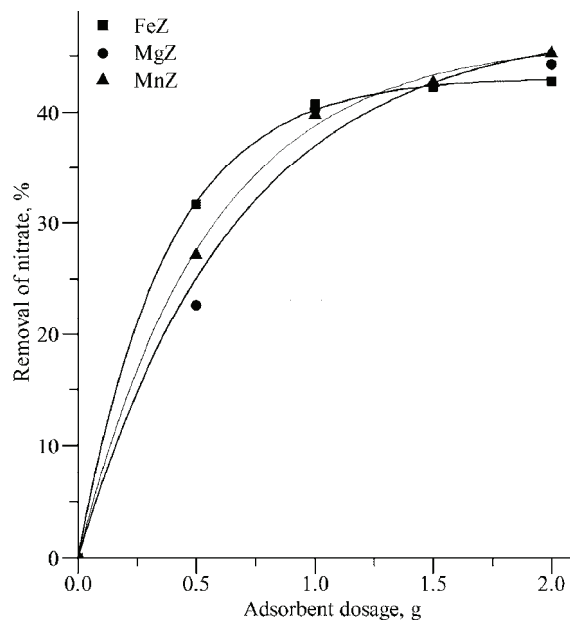


Fig. 5. Effect of the adsorbent dosage on nitrate removal by the different zeolite samples.

Effect of temperature on nitrate adsorption

The adsorption efficiency as a function of temperature was investigated at 25, 35 and 45 °C and the results are shown in Fig. 6. It is evident that concentration of the adsorbed nitrate (q_t) on adsorbent increases with increasing temperature for each MZ sample. Since the q_t values were highest at 45 °C, effect of initial concentration on nitrate removal efficiency was investigated at 45 °C.

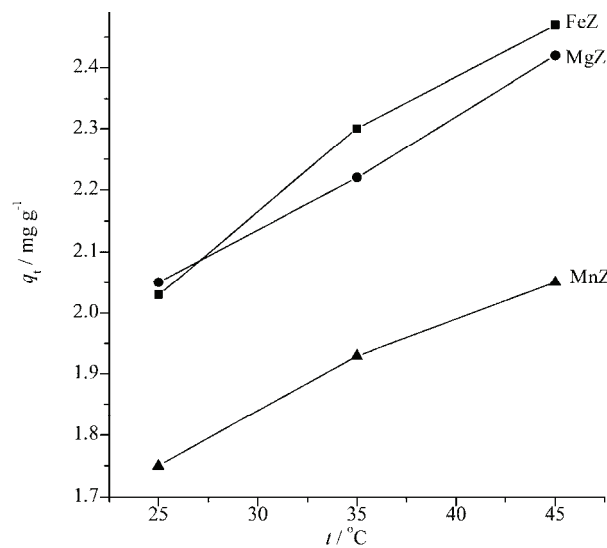


Fig. 6. Concentration of nitrate on different zeolite samples at different temperatures.

Effect of the initial concentration of nitrate on its removal efficiency

The results of the adsorption of nitrate by MZs at different initial concentration are presented in Fig. 7 as the amounts (q_t) of the nitrate adsorbed on MZ after a 24-h contact with nitrate solutions ($c_0 = 100, 200$ or $300 \text{ mg KNO}_3 \text{ dm}^{-3}$) at 45°C . The sharpest increase in removal efficiency with initial concentration was observed with FeZ. The nitrate concentration on FeZ increased from 2.5 ($c_0 = 100 = \text{mg dm}^{-3}$) to 5.6 mg g^{-1} ($c_0 = 300 \text{ mg dm}^{-3}$). The results indicate that nitrate removal efficiency depends on type of oxides present on the clinoptilolite surface.

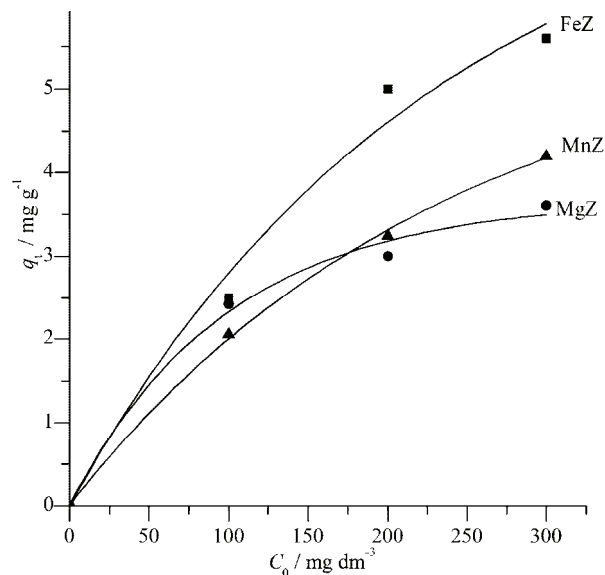


Fig. 7. Concentration of nitrate ions ($q_t / \text{mg g}^{-1}$) on different zeolite samples as a function of the initial nitrate concentration.

Adsorption kinetics

The study of nitrate adsorption on different adsorbents with time was performed at 45°C for a solution with $c_0 = 300 \text{ mg KNO}_3 \text{ dm}^{-3}$. The results are shown in Fig. 8, from which it could be seen that the adsorption for MgZ and MnZ occurred in two steps. In the first step in the initial stage, the nitrate adsorption increased rather sharply (up to 400 min), which was followed by a second step in which the uptake of nitrate was rather gradual. The second step for FeZ proceeded in a different manner, indicating that the type of the oxide affects the adsorption mechanism. FeZ, as the most perspective adsorbent, was used in the further experiments for studying the kinetics of the process.

Two reaction-based kinetic models were applied in order to describe nitrate adsorption by FeZ. The first model is given by the Lagergren first-order rate equation:²⁴

$$\frac{dq_t}{dt} = k_1(q_e - q_t) \quad (2)$$

where q_e (mg g^{-1}) is the adsorption capacity at equilibrium and k_1 (min^{-1}) is the rate constant of a first-order adsorption. In order to distinguish the kinetics equations based on the concentrations of solution from the adsorption capacities of solids, the Lagergren first-order rate equation is often called the pseudo-first-order rate equation.²⁵ Integrating the expression (2) between the limits $t = 0$ to $t = t$ and $q = 0$ to $q = q_e$, one obtains:

$$\log(q_e - q_t) = \log q_e - \frac{k_1}{2.303}t \quad (3)$$

A plot of $\log(q_e - q_t)$ vs. t should yield a straight line if the experimental data conform to this kinetic model.

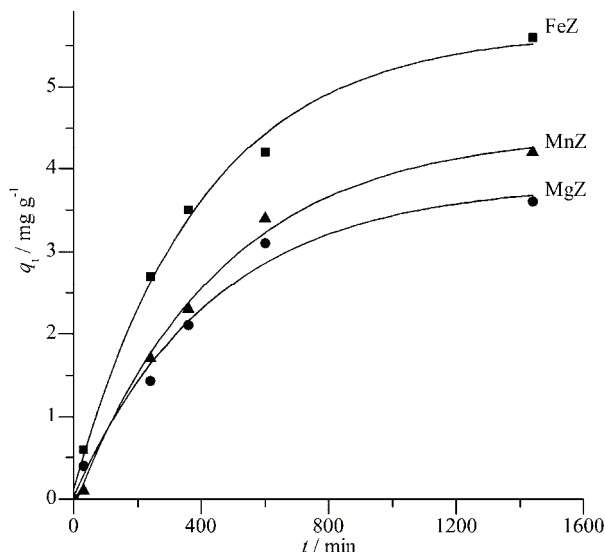


Fig. 8. Kinetics for the adsorption of nitrate ions on different zeolite samples.

The second reaction-based model that was applied in this study is described by the pseudo-second-order rate equation,²⁵ which is given as follows:

$$\frac{dq_t}{dt} = k_2(q_e - q_t)^2 \quad (4)$$

where k_2 ($\text{g mg}^{-1} \text{ min}^{-1}$) is the rate constant of the pseudo-second-order adsorption. Integration between the same limits as above yields the following expression:

$$\frac{t}{q_t} = \frac{1}{k_2 q_e^2} + \frac{1}{q_e} t \quad (5)$$

The plot of t/q_t vs. t will give a straight line if the experimental data conform to this kinetic model, and the values of q_e and k_2 are obtained, respectively, from the slope and intercept of such a plot (Fig. 9).

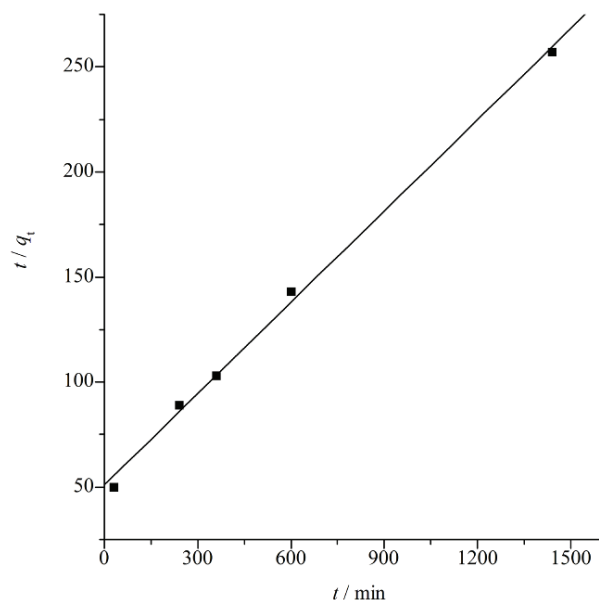


Fig. 9. Pseudo-second-order kinetic model for the adsorption of nitrate ions onto FeZ.

Application of the two models on the experimental data for the adsorption of nitrate on FeZ showed that the Lagergren first-order model gave rather poor agreement, the square of the linear regression correlation coefficient being lower than 0.90. Only the pseudo-second-order kinetic model gave satisfactory fits and the resulting parameters are listed in Table IV.

TABLE IV. Pseudo-second-order kinetic model parameters for Fe_2O_3 -modified zeolite (FeZ) samples

$q_e / \text{mg g}^{-1}$	$k_2 / \text{g mg}^{-1} \text{h}^{-1}$	R^2
6.9061	0.0246	0.9973

CONCLUSIONS

The obtained results showed that the natural zeolite tuff from the Zlatokop deposit could be modified according to the described procedure into an adsorbent for nitrate ions present in aqueous solutions. The procedure is simple consisting of two steps: 1) a treatment of the natural zeolite in an alkaline solution of Mg, Mn(II) or Fe(III) and 2) calcination of the metal-enriched samples at 500 °C. The procedure yielded MgO -, Mn_3O_4 - and Fe_2O_3 -containing zeolite adsorbents. For all the obtained adsorbents, the removal efficiency increased with temperature, and the concentration of nitrate on the adsorbents increased with increasing ini-

tial nitrate concentration. For all adsorbents, 1 part of the solid in 50 parts of the liquid was found to be the optimal solid/liquid ratio. The best removal efficiency at 45 °C was exhibited by the Fe₂O₃-containing zeolite adsorbent, for which the adsorption kinetics was also studied. The results showed that the Fe₂O₃-containing zeolite removed nitrate ions in accord with a pseudo second order equation (with the rate constant of 0.0246 g mg⁻¹ h⁻¹). From all the presented results, it could be concluded that the Serbian natural zeolite can be considered as a promising natural material for employment as a filter in a drinking water installation.

Acknowledgments. This work was supported by the Ministry of Education, Science and Technological Development of the Republic of Serbia (Project No. 172018).

ИЗВОД

МОДИФИКАЦИЈА ПРИРОДНОГ КЛИНОПТИЛОЛИТА ЗА УКЛАЊАЊЕ НИТРАТА ИЗ ВОДЕНИХ РАСТВОРА

ЈЕЛЕНА Б. ПАВЛОВИЋ¹, ЈЕЛЕНА К. МИЛЕНКОВИЋ¹ и НЕВЕНКА З. РАЈИЋ²

¹Иновационои центар Технолошко-мешалуршкој факултету, Универзитет у Београду, Карнеијева 4,
11000 Београд и ²Технолошко-мешалуршки факултет, Универзитет у Београду,
Карнеијева 4, 11000 Београд

Зеолитни туф из лежишта Златокоп (налазиште Врањска Бања) испитиван је са циљем добијања јефтиног адсорбента за уклањање нитрата из водених растворова. Како би се површина зеолита-клиноптилолита учинила прихватљивом за везивање нитрата, она је модификована: Fe(III)-, Mn(IV)- и Mg-оксидом. Карактеризација добијених адсорбената извршена је скенирајућом електронском микроскопијом са дисперзионом спектротекничком, рендгенском дифракцијом праха и инфрацрвеном спектроскопијом као и мерењем специфичне површине. Такође, испитиван је утицај различитих параметара на ефикасност везивања нитрата за адсорбенте: масе адсорбента (0,5; 1,0; 1,5 и 2,0), температуре (25, 35 и 45 °C) и почетне концентрације нитрата у раствору (100, 200 и 300 mg dm⁻³). Код свих адсорбената ефикасност везивања расте са температуром. Гвожђемодификован зеолит показује најбољу ефикасност а кинетика везивања нитрата за овај адсорбент следи кинетику псевдо-другог реда.

(Примљено 16 јануара, ревидирано 7. априла, прихваћено 9. априла 2014)

REFERENCES

1. T. S. Thomson, *Bull. Environ. Cont. Toxicol.* **66** (2001) 64
2. X. Jia, D. Larson, D. Slack, J. Walworth, *Eng. Geol.* **77** (2005) 273
3. M. Islam, R. Patel, *Desalination* **256** (2010) 120
4. A. Bhatnagar, M. Sillanpaa, *Chem. Eng. J.* **168** (2011) 493
5. H. Faghihian, R. S. Bowman, *Water Res.* **39** (2005) 1099
6. S. Jevtić, S. Grujić, J. Hrenović, N. Rajić, *Micropor. Mesopor. Mat.* **159** (2012) 30
7. N. Rajić, Dj. Stojaković, S. Jevtić, N. Zabukovec-Logar, J. Kovac, V. Kaucić, *J. Hazard. Mater.* **172** (2009) 1450
8. N. Rajić, Dj. Stojaković, M. Jovanović, N. Zabukovec-Logar, M. Mazaj, V. Kaucić, *Appl. Surf. Sci.* **257** (2010) 1524
9. J. Schick, P. Caullet, J. Paillaud, J. Patarin, C. Mangold-Callarec, *Micropor. Mesopor. Mat.* **132** (2010) 395

10. M. Arora, N. K. Eddy, K. A. Mumford, Y. Baba, J. M. Perera, G. W. Stevens, *Cold Reg. Sci. Technol.* **62** (2010) 92
11. F. Deganello, L. F. Liotta, A. Macaluso, A. M. Venezia, G. Deganello, *Appl. Catal., B* **24** (2000) 265
12. L. M. Camacho, R. R. Parra, S. Deng, *J. Hazard. Mater.* **189** (2011) 286
13. Z. Li, J.-S. Jean, W.-T. Jiang, P.-H. Chang, C.-J. Chen, L. Liao, *J. Hazard. Mater.* **187** (2011) 318
14. E. Bilgin Simsek, E. Ozdemir, U. Beker, *Water Air Soil Poll.* **224** (2013) 1614
15. M. Zhang, B. Gao, Y. Yao, Y. Xue, M. Inyang, *Chem. Eng. J.* **210** (2012) 26
16. Dj. Stojaković, J. Milenković, N. Daneu, N. Rajić, *Clay. Clay. Miner.* **59** (2011) 277
17. M. H. Stanić, B. Kalajdžić, M. Kules, N. Velić, *Desalination* **229** (2008) 1
18. Z. H. Wang, D. Y. Geng, Y. J. Zhang, Z. D. Zhang, *J. Cryst. Growth* **310** (2008) 4148
19. J. Zielinski, I. Zglinicka, L. Znak, Z. Kaszkur, *Appl. Catal., A* **381** (2010) 191
20. E. Alvarado, L. M. T. Martinez, A. F. Fuentes, P. Quintana, *Polyhedron* **19** (2000) 2345
21. O. Korkuna, R. Leboda, J. Z. Skubiszewska-Zieba, T. Vrublevs'ka, V. M. Gun'ko, J. Ryczkowski, *Micropor. Mesopor. Mat.* **87** (2006) 243
22. M. Islam, R. Patel, *J. Hazard. Mater.* **169** (2009) 524
23. M. Falk, *Vib. Spetrosc.* **1** (1990) 69
24. S. Lagergren, K. Sven. Vetenskapsakad. Handl. **24** (1898) 1
25. Y.-S. Ho, *J. Hazard. Mater.* **136** (2006) 681.



Adaptive-network-based fuzzy inference system (ANFIS) model-based prediction of the surface ozone concentration

MARIJA SAVIĆ, IVAN MIHAJLOVIĆ*, MILICA ARSIĆ and ŽIVAN ŽIVKOVIĆ

University of Belgrade, Technical Faculty in Bor, Management Department,
Vojske Jugoslavije 12, 19210 Bor, Serbia

(Received 26 January, revised 8 April, accepted 9 April 2014)

Abstract: This paper presents the results of modeling the tropospheric concentration of ozone in dependence on volatile organic compounds - VOCs (benzene, toluene, *m*- and *p*-xylene, *o*-xylene and ethylbenzene) and inorganic compounds – NO_x (NO and NO₂) CO, H₂S, SO₂, and particulate matter (PM₁₀) in the ambient air, in parallel with meteorological parameters, *i.e.*, temperature, solar radiation, relative humidity, and wind speed and direction. The modeling was based on measured results obtained during the year 2009. The measurements were performed at the measuring station located within an agricultural area, near the city of Zrenjanin (Serbian Banat, Serbia). Statistical analysis of obtained data, based on bivariate correlation analysis, indicated that accurate modeling could not be performed using the linear statistics approach. Moreover, considering that almost all the input variables have wide ranges of relative change (ratio of variance compared to range), the nonlinear statistic analysis method based on only one rule describing the behavior of the input variable most certainly would not present sufficiently accurate results. For these reason, the employed modeling approach was based on Adaptive-Network-Based Fuzzy Inference System (ANFIS). The model obtained using the ANFIS methodology resulted in high accuracy, with a prediction potential of above 80 %, considering that obtained determination coefficient for the final model was $R^2 = 0.802$.

Keywords: ANFIS; modeling; NO_x; ozone; VOCs.

INTRODUCTION

Ozone plays an important role in controlling the chemistry and chemical composition of the troposphere. On the other hand, tropospheric ozone is a unique pollutant in that it is not emitted directly into the ambient air. Ozone enters the troposphere from the stratosphere.¹ A major part of tropospheric

* Corresponding author. E-mail: imihajlovic@tf.bor.ac.rs

Serbian Chemical Society member.

doi: 10.2298/SC140126039S

ozone, however, is also produced and destroyed in the troposphere by chemical reactions with different organic and/or inorganic compounds, catalyzed by solar radiation.^{2–5}

Tropospheric ozone may have a negative impact on the environment and public health when present in the lower atmosphere in excess quantities. Human health, terrestrial ecosystems, and the degradation of materials are impacted by poor air quality resulting from high ozone levels caused by photochemical ozone production of human-emitted precursors. In establishing the quality of ambient air standards, regulations were introduced to set limits on the emissions of pollutants in such a way that they may not exceed the prescribed maximum values. Due to its harmful impact on human health and on vegetation in rural areas, the new European Directive 2008/50/EC limits the ozone concentration in ambient air according to the AOT40 index.^{6–8} The AOT40 index could be used to evaluate the potential risk that ozone could pose to the vegetation in an investigated area during the period of plant growth.

According to available literature, most authors calculate that the tropospheric production of ozone by photochemistry is much larger than the ozone influx from the stratosphere.¹ This was also confirmed by NASAs “Global Tropospheric Experiment”, which was facilitated during February–March 1994.¹ As a result of this experiment, the column O₃ photochemical production rate at subtropical latitudes determined for the western Pacific was found to be nearly 12 times larger than the nominal average Northern Hemispheric flux of O₃ from the stratosphere.⁹

Local changes in tropospheric ozone concentrations, such as stagnation episodes or altered transport patterns, could also be the result of climate changes and *vice versa*. The potential influence on climatic changes, as well as the oxidizing impact of tropospheric ozone, is significant through the entire depth of the troposphere. On the other hand, near ground levels of the troposphere have an important influence on the air quality.¹⁰

A deficit of representative observation locations in some parts of the world, with observational records of 15 years or more, is hampering the determination of long-term changes in tropospheric ozone concentrations on a global scale. This is especially a case in under developed and transitional countries, where organized measurement of the tropospheric concentration only commenced during the first decade of the 21st century.

Accordingly, measurements of the ozone concentration in the ambient air started in Serbia a few years ago. However, a comprehensive study concerning its genesis, level of concentration and possible risks that it presents to human health has not yet been performed because information on ozone dependences in this region of Europe is limited. The aim of this study was to obtain an insight into ground-level ozone concentrations in the medium region of the Serbian Banat, a

major agro-industrial region in Serbia, and to explore the possibility of determining dependencies between ozone concentration and important predictors.

According to literature investigations, the ozone concentration is either NO_x or VOCs sensitive, where NO_x stands for inorganic components and VOCs stands for volatile organic components.^{11–14} For this reason, in parallel with the ozone concentration, for investigations presented in this paper, measurements of NO_x (NO , NO_2), SO_2 , CO , H_2S , particulate matter (PM_{10}) and VOCs (benzene, toluene, *m*- and *p*-xylene, *o*-xylene and ethylbenzene) was facilitated. In addition, it was decided to investigate the correlation of the concentration of each gaseous pollutant to meteorological parameters, as suggested by different authors.^{12,15–17} Accordingly, the meteorological parameters (wind direction, wind speed, air temperature, solar radiation and relative air humidity) were also measured.

EXPERIMENTAL

The locality where the measurements were facilitated, Banat, is a region in southeastern Europe divided among three countries: the eastern part belongs to Romania, the western part to Serbia (the Serbian Banat, mostly included in Vojvodina except for the small part, which is included in Central Serbia) and a small northern part belongs to Hungary.

Air quality monitoring and meteorological data

Continuous measurement of the air pollutants investigated in this study was facilitated using an automatic measuring station, located in the urban part of Zrenjanin city, center of the region. This station was originally assigned for acquisition of air pollution levels in the residential – business zone of the city, originating from exhaust gasses and other sources of pollution. The following air pollutants are continually measured at this location: BTEX (benzene, toluene, ethylbenzene and xylene) according to the EN 14662 method; Ozone according to the EN 14625 method, ISO 13964; carbon monoxide according to the EN 14626, ISO 4224:2000 method; PM_{10} (Particulate matter) according to the EN 12341 method; $\text{NO}/\text{NO}_2/\text{NO}_x$ (nitrogen oxides) according to the EN 14211 method and $\text{H}_2\text{S}/\text{SO}_2$ (sulfur compounds) according to the EN 14212, ISO 10498:2004 method.

Data collection

For modeling the dependence of ozone concentration on different predictors, the data obtained from the automated measuring station were used. The data were collected during the year 2009 in the period January–December. Measurement of the seventeen input parameters (X_i) and the one output (Y) parameter was enabled using the above-described measuring station, with data acquisition in the database at one-hour intervals. Before the model building phase, all the data points were examined for potential outliers. The measurement intervals, during which some of investigated input parameters were not recorded, for different reasons, were eliminated. After this, 1477 data sets remained for further analysis.

Specific details connected with Experimental are given in Supplementary material to this paper.

RESULTS AND DISCUSSION

The values of the measured input parameters (X_i) and the air quality indicator investigated in this work – output of the process (Y) in the form of des-

criptive statistics results – are presented in Table I. According to the results presented in Table I, potential risk of the ozone pollution in the air is obvious in this region, considering that measured hourly ozone concentration was in the range up to $162 \text{ } \mu\text{g m}^{-3}$, which is above prescribed maximal value.

TABLE I. Values of the input (X_i) and the output (Y) variables of the model – descriptive statistics of 1477 data sets

Measured parameter	Unit	Model symbol	Range	Min.	Max.	Mean		SD	Var.
						Statistic	SE		
SO ₂	$\mu\text{g m}^{-3}$	$X_{1.1}$	220.4	0.0	220.4	17.651	0.5962	22.9147	525.082
CO	$\mu\text{g m}^{-3}$	$X_{1.2}$	3937	0	3937	738.89	12.928	496.835	246845.423
H ₂ S	$\mu\text{g m}^{-3}$	$X_{1.3}$	73.91	0.00	73.91	1.9636	0.16270	6.25268	39.096
NO	$\mu\text{g m}^{-3}$	$X_{1.4}$	232.4	0.7	233.1	28.495	0.7208	27.7018	767.388
NO ₂	$\mu\text{g m}^{-3}$	$X_{1.5}$	125.8	4.0	129.8	32.967	0.5473	21.0322	442.354
NOx	$\mu\text{g m}^{-3}$	$X_{1.6}$	446.3	5.5	451.8	76.516	1.5230	58.5321	3426.008
PM ₁₀	$\mu\text{g m}^{-3}$	$X_{1.7}$	378.9	0.0	378.9	42.078	0.9161	35.2083	1239.627
Benzene	$\mu\text{g m}^{-3}$	$X_{2.1}$	14.40	0.00	14.40	1.6015	0.05703	2.19180	4.804
Toluene	$\mu\text{g m}^{-3}$	$X_{2.2}$	29.33	0.00	29.33	2.4257	0.07458	2.86618	8.215
<i>m</i> -, <i>p</i> -Xylene	$\mu\text{g m}^{-3}$	$X_{2.3}$	20	0	20	1.47	0.058	2.233	4.987
<i>o</i> -Xylene	$\mu\text{g m}^{-3}$	$X_{2.4}$	9.55	0.00	9.55	0.4682	0.03126	1.20120	1.443
Ethylbenzene	$\mu\text{g m}^{-3}$	$X_{2.5}$	10	0	10	0.42	0.030	1.143	1.306
Wind direction	°	$X_{3.1}$	344	10	354	188.11	1.837	70.605	4985.082
Wind speed	m s^{-1}	$X_{3.2}$	5.39	0.18	5.57	1.6843	0.02270	.87241	0.761
Air temperature	°C	$X_{3.3}$	47.6	-12.5	35.1	15.136	0.2498	9.5989	92.140
Solar radiation	W m^{-2}	$X_{3.4}$	844	4	848	136.36	5.452	209.518	43897.918
Relative humidity	%	$X_{3.5}$	75	17	92	64.96	0.434	16.688	278.491
Ozone	$\mu\text{g m}^{-3}$	Y	160.7	1.3	162.0	70.111	0.8850	34.0110	1156.750

Defining the linear correlation dependence between the output and the input parameters with a significant value of the coefficient of correlation (R^2) provides the possibility of predicting a potential excess O₃ concentration in the air in the investigated area using linear statistical analysis methods, such as multiple linear regression analysis (MLRA). MLRA is one of the most widely used methodologies for expressing the dependence of a response variable on several independent variables.²¹ For defining the linear correlation dependence in the form: output of the model $Y = f(\text{input})$ of the model ($X_{1.1}$ – $X_{3.5}$), a bivariate correlation analysis was performed. As the result of this analysis, the Pearson correlation (PC) coefficients with the corresponding statistical significance were calculated (Table S-I). In cases where the values of the PC coefficients of the output and most of the input variables are above a value of 0.5 with a high statistical significance ($p < 0.05$), the linear modeling approach should be taken into consideration.

However, according to values presented in Table S-I of the Supplementary material to this paper, it could be concluded that there was not a high linear dependence between the ozone concentration in the air (Y) and the input variables, with the exceptions of the correlations $Y-X_{3.3}$ ($r = 0.647$; $p < 0.01$) and $Y-X_{3.5}$ ($r = -0.496$; $p < 0.01$), although statistical significance was recorded for most of the correlated pairs. According to these values, it was decided that using MLRA to obtain dependence between the ozone concentration and the investigated predictors would not result in a high accuracy.

A low value of correlation between two variables does not automatically mean that interdependence of their behavior does not exist. This is only an indicator that the linear modeling approach cannot describe their intercorrelation. This is usually good indicator that further modeling should be based on the dynamic behavior of the variables.¹⁹ In such cases, modeling could be facilitated using a nonlinear statistic approach, such as Artificial Neural Networks (ANNs) – in cases where the input variables do not have wide range during the complete time interval of observation,^{15,18,20} or an Adaptive-Network-Based Fuzzy Inference System for variables with a wide range of change.^{21,22}

Modeling approach based on an adaptive-network-based fuzzy inference system

In recent years, artificial intelligence (AI) based methods have been proposed as alternatives to traditional linear statistical ones in many scientific disciplines. The literature demonstrates that AI models such as ANN and neuro-fuzzy techniques are successfully used for air pollution modeling and forecasting.^{22–28}

According to the measurement series for the variables presented in Table I, it can be concluded that almost all have a wide range of relative change (ratio of variance compared to range). For example, the relative change of variables ranges from 37.64 for H₂S to 5.32 in case of CO. Accordingly, a modeling approach based on one rule describing the dynamic changes of the input variables, belonging to a group of nonlinear statistic analysis methods (such as ANNs), probably would not result with a sufficiently accurate prediction.²⁵ For this reason, the further modeling approach was based on an Adaptive-Network-Based Fuzzy Inference System (ANFIS).

As a basis for the construction of a set of fuzzy if–then rules, the ANFIS system based on selected membership functions can be used. The ANFIS structure is obtained by embedding the fuzzy interference system into the framework of adaptive networks.²⁹ An adaptive network is a network structure consisting of a number of nodes connected through directional links. The outputs of these adaptive nodes depend on modifiable parameters pertaining to these nodes.³⁰ The pattern in which these parameters should be iteratively varied, aimed at minimizing the final error, is specified by the learning rule. Moreover, according to Takagi

and Sugeno, the fuzzy inference system (FIS) is a framework based on fuzzy set theory and fuzzy if–then rules.³¹ The three main components of a FIS structure are: a rule base, a database and a reasoning mechanism. The appropriate number of if – then rules for levels of ranges of the input variables is located in the rule base. An example of a rule used in the investigations presented in this paper might be “registered ozone concentration in the air will be high if the wind speed is low”, where items such as low and high represent linguistic variables. The database defines the membership functions applied in the fuzzy rules and the reasoning mechanism performs the inference procedure.³²

In this way, for example, if there are two input variables (X_1 and X_2), and assuming that their ranges can be divided into two levels, there would be the rule base with two rules for modeling the value of the output variable Y :

Rule 1. If X_1 is in the range A_1 and X_2 is in the range B_1 , then:

$$f_1 = p_1x_1 + q_1x_2 + r_1;$$

Rule 2. If X_1 is in the range A_2 and X_2 is in the range B_2 , then:

$$f_2 = p_2x_1 + q_2x_2 + r_2.$$

In the case when $f(x_1, x_2)$ is a first-order polynomial, the model is called a first-order Sugeno fuzzy model.

The graphical presentation of a general ANFIS network is presented in Fig. 1. The procedure for the construction of such an ANFIS structure is described in details in the literature,²⁵ where a similar modeling approach was used to predict the potential increase in the SO₂ concentration in the ambient air near a copper smelter. The ANFIS architecture can be presented with five layers, in which X_1 and X_2 are inputs to the nodes in layer 1, A_i and B_i are the linguistic labels of the ranges of the input variables (small, large, *etc.*) associated with the node function. Membership functions of the nodes located in layer 1 ($O_i^1 = \mu A_i(X_i)$ or $O_i^2 = \mu B_i(X_i)$) specify the degree to which the given X_i satisfies the quantifier A_i , B_i , *etc.* Usually, membership functions are either bell-shaped with a maximum equal to 1 and a minimum equal to 0, or a Gaussian function. Nodes located in layer 2 are multipliers, which are multiplying the signals exiting the layer 1 nodes. For example $O_i^2 = W_i = \mu A_i(X_i) \times \mu B_i(X_i)$, $i = 1, 2, \dots$ etc. The output of each node represents the firing strength of a rule. The i -th node of layer 3 calculates the ratio of the firing strength of the i -th rule to the sum of the firing strengths of all rules. In this way, $O_i^3 = W_i = W_i / (W_1 + W_2 + \dots)$, $i = 1, 2, \dots$ Every node i in layer 4 has a node function of following type: $O_i^4 = \bar{W}_i \cdot f_1 = \bar{W}_i(p_i x_1 + q_i x_2 + r_i)$, where p_i , q_i and r_i will be referred to as consequent parameters. The single node of layer 5 is the node that computes the overall output as the summation of all incoming signals, *i.e.*:

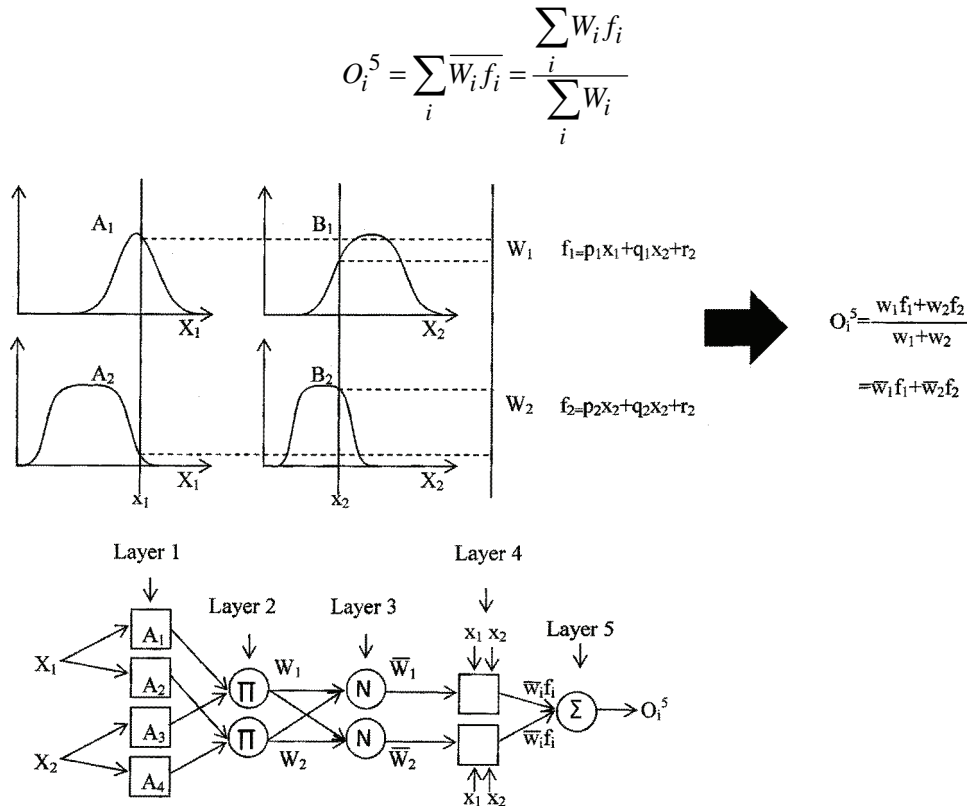


Fig. 1. Graphical presentation of the ANFIS.

The training of the parameters in the ANFIS structure is accommodated according to the hybrid learning rule algorithm, which is an integration of the gradient descent method and least square methods. In the forward pass of the algorithm, the functional signals advance until layer 4 and the consequent parameters are identified by the least squares method to minimize the measured error. In the back propagation pass, the premise parameters are updated by the gradient descent method.³²

According to the number of input variables, their ranges and the variations, presented in Table I, it was decided that a two-rule ANFIS network should be applied. A Gaussian function was selected as the membership function. There were 17 input variables ($X_{1.1}$ to $X_{3.5}$) with one output variable (Y).

To apply the ANFIS methodology, the assembly of 1477 input and output samples was divided into two groups. The first group consisted of 1067 ($\approx 70\%$) randomly selected samples, and this group was used to train the model, whereas the second group consisted of the 410 ($\approx 30\%$) remaining samples from the starting data set, and this group was used to test the model. The selection of the

variables for these two stages was realized using a random number generator, which was based on a Bernoulli distribution. During the training phase, correction of the weighted parameters (p_i , q_i , r_i , etc.) of the connections was achieved through the necessary number of iterations, until the mean squared error between the calculated and measured outputs of the ANFIS network was minimal. During the second phase, the remaining 30 % of the data was used for testing the “trained” network. In this phase, the network used the weighted parameters determined during the first phase. These new data, excluded during the network training stage, were incorporated as new input values (X_i), which were then transformed into a new output (Y). Matlab ANFIS editor was used for the calculations realized in this study.

Accordingly, the network-training phase was performed iteratively until the moment when the error between measured and calculated values of output variable (the O₃ concentration in the air – Y) was not minimized and remained constant. In the case of the investigation presented in this paper, the optimal number of iterations (epochs) was 10. The obtained results from the training stage could be evaluated by comparison of the calculated values of Y with the measured ones (Fig. 2).

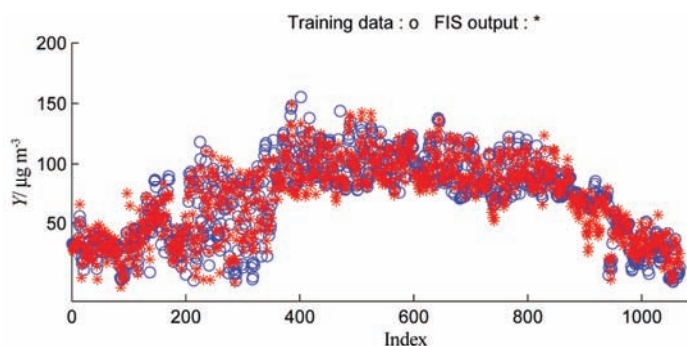


Fig. 2. Dependences between the calculated and measured values for the ozone concentration in the training stage (measured – ○; model predicted – *).

The test set (total 410 vectors), which examined the fidelity of the model, showed that the model could be used to estimate the O₃ concentration quite satisfactorily. A comparison of the measured and ANFIS model calculated values for the testing stage are presented in Fig. 3. It could be concluded that excellent fitting was obtained.

In the training stage, the ANFIS modeling approach predicted the ozone concentration in the air with a determination coefficient $R^2 = 0.92$ (Fig. 4), which does represent a large significance. The value of the determination coefficient (R^2) for the test set was smaller to some extent 0.802 (Fig. 5), however, the results showed that the ANFIS modeling methodology led to acceptable funct-

ional dependencies between the selected variables and the O_3 concentration. Accordingly, using the model described in this paper, the O_3 concentration in the air could be predicted as the function of investigated input variables, with an accuracy of above 80 %.

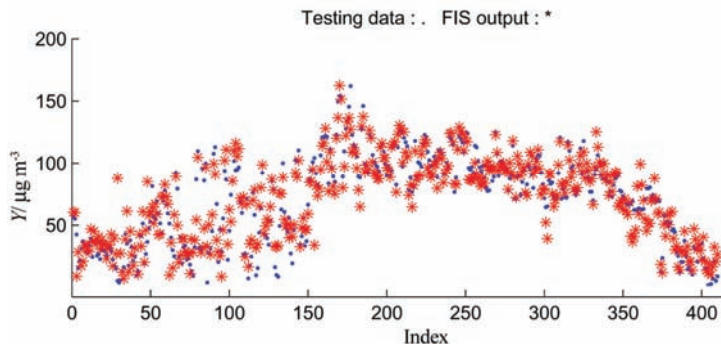


Fig. 3. Dependences between the calculated and measured values for the ozone concentration in the testing stage (measured – ○; model predicted – *).

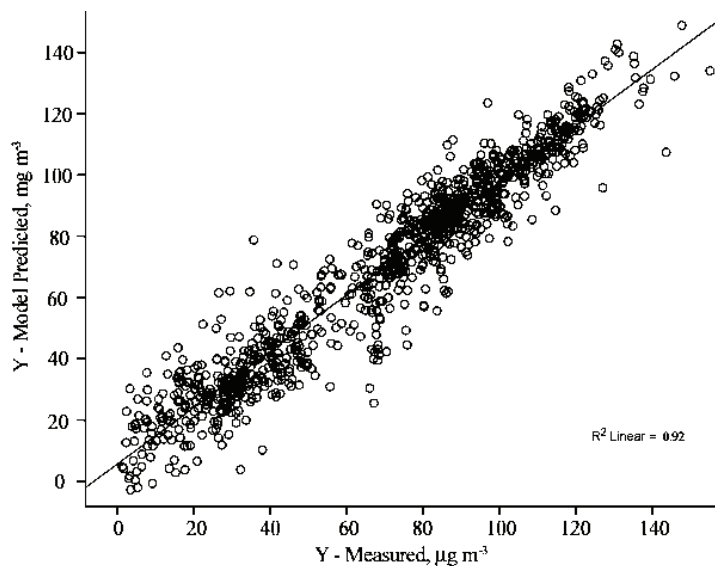


Fig. 4. Coefficient of determination between the measured and model predicted O_3 concentration in the training stage.

Final validation of the model accuracy was performed on data collected during two months of 2012. The data were collected during August and December to assess predictability of the model in different seasons. The obtained coefficients of determination were $R^2 = 0.782$ and 0.764 for August and December, respectively. These values indicated that the developed ANFIS model could be

used for a sufficiently accurate prediction of the dependence of the ozone concentration on the investigated input parameters in the investigated region.

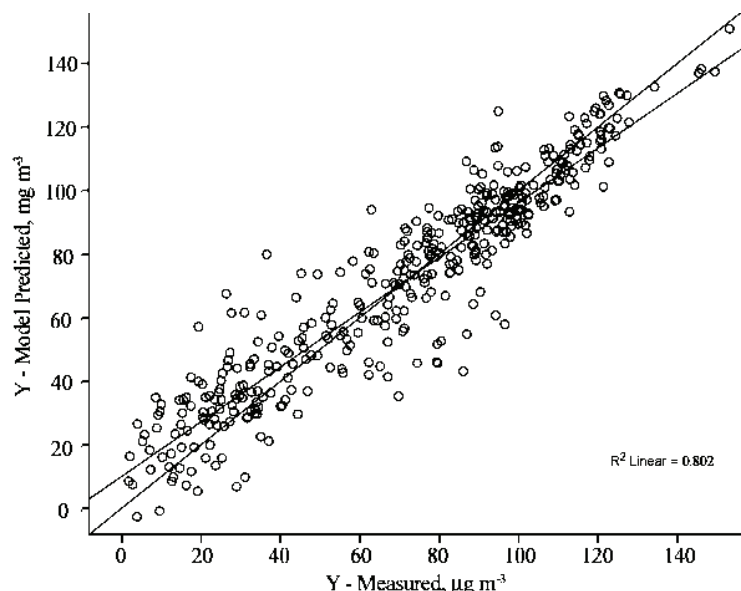


Fig. 5. Coefficient of determination between the measured and model predicted O_3 concentration in the testing stage.

CONCLUSIONS

Considering the importance of the daily O_3 concentrations in the atmosphere of urban regions, this research was aimed at developing proper prediction models using the ANFIS model. Since input selection is a significant step in modeling, it was decided to measure both VOCs and NO_x as potential predictors. Additionally, meteorological parameters were recorded. The goodness of final model fit was evaluated using R^2 values. The obtained values of 0.92 and 0.802 in training and testing stage, respectively, demonstrated that an accurate prediction model for ozone could be obtained using the ANFIS model. The obtained results could be used for further analysis of investigated problem. Further analysis would include the sensitivity of the model to the separate influence of VOCs and NO_x . In this way, it is planned to obtain a model that would be able to determine the origin of daily O_3 concentration changes, *e.g.*, is the ambient O_3 concentration VOCs or NO_x sensitive. This is of importance for determining the reasons for O_3 concentrations in excess of the limiting values in this region.

SUPPLEMENTARY MATERIAL

Details of geography, air quality monitoring and meteorological data as well as correlation matrix for the input and the output variables are available electronically from <http://www.shd.org.rs/JSCS/>, or from the corresponding author on request.

И З В О Д
ПРЕДВИЂАЊЕ КОНЦЕНТРАЦИЈЕ ПОВРШИНСКОГ ОЗОНА НА ОСНОВУ ANFIS
МОДЕЛА

МАРИЈА САВИЋ, ИВАН МИХАЈЛОВИЋ, МИЛИЦА АРСИЋ и ЖИВАН ЖИВКОВИЋ
Универзитет у Београду, Технички Факултет у Бору, Одсек за менаџмент,
Бојске Југославије 12, 19210 Бор

У раду су приказани резултати моделовања концентрације тропосферског озона као зависност од испарљивих органских једињења – VOCs (бензен, толуен, *m*-, *p*-ксилен, *o*-ксилен и етилбензен); неорганских једињења – NO_x (NO и NO₂), CO, H₂S, SO₂ и PM₁₀ (*particulate matter*)) у ваздуху паралелно са метеоролошким параметрима: температура, сунчево зрачење, релативна влажност, брзина и правац ветра. Моделовање се заснива на измереним резултатима добијеним у току 2009. године. Мерења су обављена на мерној станици која се налази у пољопривредном подручју, у близини града Зрењанина. Статистичка анализа добијених података, на основу биваријантне корелационе анализе, показује да прецизно моделовање не може бити изведеном помоћу приступа линеарне статистике. Такође, с обзиром на то да скоро све улазне варијабле имају широк спектар релативне промене (однос варијансе у односу на опсег), метод нелинеарне статистичке анализе заснован на само једном правилу за описивање понашања улазне варијабле, највећим делом не би могао да представи довољно прецизне резултате. Из тог разлога, моделовање је засновано на ANFIS приступу. Модел добијен коришћењем методологије ANFIS резултирао је високом прецизношћу, уз потенцијално предвиђање изнад 80 %, с обзиром на то да је добијени коефицијент детерминације за коначни модел био R² = 0,802.

(Примљено 26 јануара, ревидирано 8. априла, прихваћено 9. априла 2014)

REFERENCES

1. R. Guicherit, M. Roemer, *Chemosphere* **2** (2000) 167
2. J. Fishman, S. Solomon, P. J. Crutzen, *Tellus* **31** (1979) 432
3. R. Guicherit, in: *Climate Change Research: Evaluation and Policy Implications*, S. Zwart, R. S. A. R. van Rompaey, M. T. J. Kok, M. M. Berk, Eds., Elsevier, Amsterdam, 1995, pp. 155–279
4. J. A. Logan, M. J. Prather, S. C. Wofsy, M. B. McElroy, *J. Geophys. Res.* **86** (1981) 7210
5. J. F. Muller, G. Brasseur, *J. Geophys. Res.* **100** (1995) 16445
6. WHO, *Air quality guidelines for Europe*, European Series, No. 91, 2nd ed., WHO Regional Publications, Copenhagen, 2000
7. Directive EU 2008/50/EC, *On ambient air quality and cleaner air for Europe*, Official Journal of the European Union, 2008
8. J. D. Jacob, *Atmos. Environ.* **34** (2000) 2131
9. J. H. Crawford, D. Davis, G. Chen, J. Bradshaw, S. Sandholm, Y. Kondo, S. Liu, E. Browell, G. Gregory, B. Anderson, G. Sachse, J. Collins, J. Barrick, D. Blake, R. Talbot, H. Singh, *J. Geophys. Res.* **102** (1997) 28469

10. S. J. Oltmans, A. S. Lefohn, J. M. Harris, I. Galbally, H. E. Scheel, G. Bodeker, E. Brunke, H. Claude, D. Tarasick, B. J. Johnson, P. Simmonds, D. Shadwick, K. Anlauf, K. Hayden, F. Schmidlin, T. Fujimoto, K. Akagi, C. Meyer, S. Nichol, J. Davies, A. Redondas, E. Cuevas, *Atmos. Environ.* **40** (2006) 3156
11. J. Duan, J. Tan, L. Yang, S. Wu, J. Hao, *Atmos. Res.* **88** (2008) 25
12. A. Lengyel, K. Heberger, L. Paksy, O. Banhidi, R. Rajko, *Chemosphere* **57** (2004) 889
13. M. T. Odman, Y. Hu, A. G. Russell, A. Hanedar, J. W. Boylan, P. F. Brewer, *J. Environ. Manage.* **90** (2009) 3155
14. M. Shao, Y. Zhang, L. Zeng, X. Tang, J. Zhang, L. Zhong, B. Wang, *J. Environ. Manage.* **90** (2009) 512
15. S. A. Abdul-Wahab, S. M. Al-Alawi, *Environ. Modell. Software* **17** (2002) 219
16. D. Kley, A. Volz, F. Mulhiems, in *Regional and Global Scale Interactions*, I. S. A. Isaksen, Ed., NATO ASI Series C, 227, Reidel, Norwell, MA, 1988, p. 63
17. D. E. Linvill, W. J. Hooker, B. Olson, *Mon. Weather Rev.* **108** (1980) 1883
18. S. M. Al-Alawi, S. A. Abdul-Wahab, C. S. Bakheit, *Environ. Modell. Software* **23** (2008) 396
19. P. Đorđević, I. Mihajlović, Ž. Živković, *Serb. J. Manage.* **5** (2010) 189
20. H. Ozdemir, G. Demir, G. Altay, S. Albayrak, C. Bayat, *Environ. Eng. Sci.* **25** (2008) 1249
21. Z. C. Joihanyak, J. Kovacs, *Acta Technica Jaurinensis* **4** (2011) 113
22. R. Noori, G. Hoshyaripour, K. Ashrafi, B. N. Araabi, *Atmos. Environ.* **44** (2010) 476
23. G. Nunnari, S. Dorling, U. Schlink, G. Cawley, R. Foxall, T. Chatterton, *Environ. Modell. Software* **19** (2004) 887
24. R. Perez-Roaa, J. Castroa, H. Jorqueraa, J. R. Perez-Correaa, V. Vesovic, *Atmos. Environ.* **40** (2006) 109
25. M. Savić, I. Mihajlović, Ž. Živković, *Serb. J. Manage.* **8** (2013) 25
26. A. K. Gautam, A. B. Chelani, V. K. Jain, S. Devotta, *Atmos. Environ.* **42** (2008) 4409
27. P. Perez, A. Trier, J. Reyes, *Atmos. Environ.* **34** (2000) 1189
28. Y. Yildirim, M. Bayramogly, *Chemosphere* **63** (2006) 1575
29. J. S. R. Jang, *IEEE Trans. Syst. Man. Cybern.* **23** (1993) 665
30. A. F. Guneri, T. Ertay, A. Yucel, *Expert Syst. Appl.* **38** (2011) 14907
31. T. Takagi, M. Sugeno, *IEEE Trans. Syst. Man. Cybern.* **15**(1) (1985) 116
32. J. S. R. Jang, C. T. Sun, E. Mizutani, *Neuro-fuzzy and soft computing: A computational approach to learning and machine intelligence*, Matlab Curriculum Series, Prentice Hall, Upper Saddle River, NJ, 1997.



SUPPLEMENTARY MATERIAL TO
Adaptive-network-based fuzzy inference system (ANFIS) model-based prediction of the surface ozone concentration

MARIJA SAVIĆ, IVAN MIHAJLOVIĆ*, MILICA ARSIĆ and ŽIVAN ŽIVKOVIĆ

University of Belgrade, Technical Faculty in Bor, Management Department, Vojiske Jugoslavije 12, 19210 Bor, Serbia

J. Serb. Chem. Soc. 79 (10) (2014) 1323–1334

EXPERIMENTAL DETAILS

Geography

Banat is the part of the Pannonia Plain bordered by the Danube to the south, the Theiss to the west, the Mures to the north and the southern Carpathians to the east (Fig. S-1). The Serbian part of Banat is an area of 8.997 square kilometers located at the northeast of Serbian. The city of Zrenjanin is the center of this region, occupying 1326 km², with a population of about 80.000. From the whole territory that belongs to this municipality, 82.5 % is covered by large-scale farmlands. This area is part of a region with a humid continental climate; the average annual temperature is 11.2 °C and rainfall per year is 622 mm. The wind direction is mostly east, southeast or northwest. The average number of sunny hours in the area is 2,000 to 2,200 per year.¹ The Banat is one of the most fertile regions in Europe. All types of wheat and corn are the main agricultural crops of this region. This region is also convenient for the growth of sugar beet and tobacco. Large-scale industrial facilities include agro industry, milling, brewing industry, sugar production, textile industry, and brick production. Furthermore, oil and natural gas are exploited in the region. Most of the agricultural sorts that are grown in Banat are vulnerable to the ozone air pollution.²

Air quality monitoring and meteorological data and data collection

The coordinates of the measurement station are 45° 23' 0.80" and 20° 23' 24.53" at the altitude of 75 m above sea level. The measurements are repeated at 2 min intervals, with calculation of the hourly average value for each hour in the 0–24 interval. The results of the measurements are publicly available at <http://www.eko.vojvodina.gov.rs/?q=node/272>. The measurements, calibration of the equipment, quality control and standardization are organized by the Regional Committee for Environmental Protection and Sustainable Development, located in Novi Sad, the administrative capital of the Vojvodina Province. The meteorological parameters: wind speed and wind direction, air temperature and humidity, rainfall per year and solar radiation intensity are measured at the same measuring station as the air pollutants. The limiting value of O₃ in the air prescribed by EU is 80 µg m⁻³ using the 1-h values measured between 08.00 and 20.00 hours Central European Time (CET) each day.³

*Corresponding author. E-mail: imihajlovic@tf.bor.ac.rs



Fig. S-1. The investigated Serbian Banat region and its position in Europe.

The main motive of the investigations presented in this article was to draw conclusions about the possibilities of predicting the O₃ concentration in the ambient air under different environmental conditions and based on the influence of different input parameters. These input parameters were divided in three groups: the first group consisted of only inorganic compounds (SO₂, NO, NO₂, NO_x, CO, H₂S and PM₁₀); the second group contained the volatile organic compounds (benzene, toluene, *m*- and *p*-xylene, *o*-xylene and ethylbenzene) and the third group consisted only of the meteorological parameters (wind direction, wind speed, air temperature, solar radiation and relative humidity). Constituents of the first group (NO_x) were labeled as X_{1,1} to X_{1,7}, respectively. In same manner, constituents of the second group (VOCs) were labeled as X_{2,1} to X_{2,5}, respectively. Constituents of the third group (meteorological parameters) were labeled as X_{3,1} to X_{3,5}, respectively. The output parameter (labeled Y), the predictability of which was analyzed, is the ozone concentration in the ambient air surrounding the rural area near the city of Zrenjanin (Banat, Serbia).

TABLE S-1. Correlation matrix for the input ($X_{1,1}$ - $X_{3,6}$) and the output (Y) variables of the investigated occurrence (the number of data points for each variable was 1477) ; correlations in bold are significant at the 0.01 level (2-tailed); correlations in italic are significant at the 0.05 level (2-tailed)

Y	$X_{1,1}$	$X_{1,2}$	$X_{1,3}$	$X_{1,4}$	$X_{1,5}$	$X_{1,6}$	$X_{1,7}$	$X_{2,1}$	$X_{2,2}$	$X_{2,3}$	$X_{2,4}$	$X_{2,5}$	$X_{3,1}$	$X_{3,2}$	$X_{3,3}$	$X_{3,4}$	$X_{3,5}$
$X_{1,1}$ -0.042	1																
$X_{1,2}$ - 0.159	0.109	1															
$X_{1,3}$ -0.006	0.635	-0.045	1														
$X_{1,4}$ - 0.197	0.264	0.764	0.173	1													
$X_{1,5}$ -0.066	0.231	0.746	0.041	0.655	1												
$X_{1,6}$ - 0.166	0.276	0.823	0.140	0.963	0.835	1											
$X_{1,7}$ - 0.059	0.120	0.273	-0.035	0.266	0.410	0.341	1										
$X_{2,1}$ -0.362	0.006	0.018	-0.112	-0.010	0.225	0.072	0.299	1									
$X_{2,2}$ -0.211	-0.014	0.082	-0.109	0.026	0.303	0.126	0.258	0.884	1								
$X_{2,3}$ -0.227	0.009	0.133	-0.074	0.080	0.333	0.176	0.244	0.824	0.977	1							
$X_{2,4}$ -0.355	0.033	0.144	-0.029	0.097	0.307	0.178	0.224	0.829	0.927	0.956	1						
$X_{2,5}$ -0.339	0.044	0.160	-0.026	0.111	0.328	0.197	0.231	0.821	0.929	0.966	0.968	1					
$X_{3,1}$ -0.033	-0.150	0.052	-0.018	-0.093	0.088	-0.100	-0.050	-0.038	-0.050	-0.040	-0.001	-0.014	1				
$X_{3,2}$ -0.124	0.257	-0.237	0.012	-0.137	-0.293	-0.205	-0.172	0.073	0.030	0.017	0.027	0.011	-0.07	1			
$X_{3,3}$ - 0.647	0.030	0.073	0.221	0.016	0.181	0.075	0.076	-0.302	-0.057	-0.024	-0.108	-0.101	-0.023	-0.227	1		
$X_{3,4}$ - 0.359	0.128	0.006	0.154	-0.009	0.004	-0.007	-0.041	-0.042	0.031	0.052	0.040	0.041	-0.001	0.183	0.512	1	
$X_{3,5}$ - 0.496	-0.209	-0.070	-0.180	-0.005	-0.287	-0.105	-0.034	0.023	-0.143	-0.165	-0.111	-0.114	0.142	-0.042	-0.692	-0.613	1

REFERENCES

1. Republic Hydrometeorological Service of Serbia, <http://www.hidmet.gov.rs/eng/osmotreni/index.php> (accessed in January 2014)
2. I. Fumagalli, B. S. Gimeno, D. Velissariou, L. de Temmerman, G. Mills, *Atmos. Environ.* **35** (2001) 2583
3. Directive EU 2002/3/EC, *Relating to ozone in ambient air*, Official Journal of the European Union, 2002.



Erratum (printed version only)

Issue No. 8 (2014), Vol. 79:

– Back Cover, Contents, instead of *J. Serb. Chem. Soc.* Vol. 79, No. 7 (2014),
should be: *J. Serb. Chem. Soc.* Vol. 79, No. 8 (2014).